A retrospective analysis of ozone formation in the Lower Fraser Valley, B. C.

D. G. Steyn[1] and B. D. Ainslie[1]

and C. Reuten[2] and P. L. Jackson[3]

[1]*Atmospheric Science Programme*

The University of British Columbia

Vancouver, B.C., Canada, V6T 1Z4

[2]*RWDI Calgary, Suite 1000*

736 - 8th Avenue SW

Calgary, Alberta, Canada T2P 1H4

[3]*Environmental Science and Engineering Program*

The University of Northern British Columbia

Prince George, B.C., Canada, V2N 4Z9

Report Submitted to:

Fraser Valley Regional District

Fraser Basin Council

Metro Vancouver

May 31, 2011

1. Executive Summary

In order to understand ozone formation in the Lower Fraser Valley (LFV), B.C., a retrospective modeling study was performed. The motivation for this study was the observed differences in trends in summertime episodic ozone concentrations recorded at various monitoring stations within the valley: over the last 20 years, stations in the western part of the valley have generally shown noticeable reduction in episodic ozone concentrations, whereas stations in the eastern part of the valley have shown little or no improvement (as measured by the 8-hr CWS). The idea of investigating this question through a retrospective numerical modeling study of summertime ground level ozone formation over the last 20 years was motivated by the following considerations:

- The LFV has undergone a sizable and well documented reduction in ozone precursor emissions.
- The extensive fixed pollution monitoring network in the LFV operated by Metro Vancouver has likely captured any changes in the spatio-temporal patterns of ozone.
- There appears to be little or no impact from precursor emissions upwind of the LFV.
- The background concentrations of ozone and its precursors are generally from the North Pacific and are quite low.
- There have been two large scale field campaigns and numerous smaller field experiments undertaken within the regions aimed at studying both the meteorological and chemical processes that control ozone formation.

These considerations, and various analyses of ozone pollution lead to the conclusion that summertime ozone formation in the LFV is almost entirely due to local emissions and the observed change in behaviour of ozone formation must therefore arise from the observed changes in precursor emissions. In essence, an unintended natural experiment has taken place within the region, and the premise of this work is that, if through a modeling study, one can capture the observed changes in ozone stemming from the local emission reductions, then in principle it should be possible to determine why one part of the region has seen an improvement in summertime episodic ozone concentrations while another part has not. Complicating this analysis are the following two factors:

- There has been an observed shift in the population patterns within the valley over the last 25 years
- There has been a small but documented change in the tropospheric background concentration of ozone.

Within a numerical modeling framework it is not possible to simulate every ozone episode that has occurred over the past two decades. As a result, 7 episodes, which both capture the observed changes in ozone reduction and capture the different meteorological regimes that occur during LFV events, were selected for study. This group of episodes, summarized in Table 2 has the following desirable attributes:

- Two of the events (July 1985 and June 2006) provide test points at both the beginning and end of the 20 year retrospective timeframe.
- The August 1993 and August 2001 events occurred during the two large scale field campaigns

- All four meso-scale circulation regimes identified by Ainslie and Steyn (2007) are represented within the selected episodes.

- The July 1985 and August 1993 events were previously modeled by the NRC (Hedley et al. (1997) and Smyth et al. (2006)).

- The 1995 event has supplemental ozone data observed from an aircraft over parts of the region outside of the fixed monitoring network.

Ozone formation for each episode was investigated using a modeling system having the following three major components: the Weather Research and Forecasting (WRF v3.1) meso-scale numerical weather prediction system; the Sparse Matrix Operator Kernel Emissions modeling system (SMOKE v2.5); and the Community Multi-scale Air Quality modeling System (CMAQ v4.7.1). Model evaluation of each episode was performed in a number of ways:

- Output from the WRF meteorological model was compared against observations from Environment Canada weather stations; sounding data taken during the 1985 episode; and boundary layer depth data taken during the Pacific 1993 field campaign.

- Output from the CMAQ air quality model was compared against observations from the fixed monitoring network; VOC samples taken from the NAPS network; and aircraft observations taken during the July 1995 event.

- Output from the CMAQ air quality model was compared with results from previous modeling studies. These studies provide a local benchmark for the model evaluation.

For four of the episodes (June 2006, August 2001, July 1995 and July 1985) additional exploration runs were performed. These four episodes were singled out because they showed the best agreement with observations, and the meteorology for these episodes included all four of the meso-scale circulation patterns associated with high ozone concentrations in the LFV. For each of these episodes, two additional simulations were performed: one with 1985 level emissions and one with 2005 level emissions. These simulations were intended to isolate the effects of emission changes from meteorological changes.

In order to provide realistic simulations of past events, the emission inventory (as implemented by the SMOKE model) was adjusted to account for both changes in the amount of emissions and the location of emission sources. The SMOKE modeling system was set-up to produce separate emission inventories for: light and heavy duty vehicles (through the MOBILE 6.2 and MOBILE 6.2C modeling framework), off-road vehicles, railroads, aircraft, marine, other mobile sources, biogenic emissions, point sources, and area sources. Total annual emission rates of CO, NH3, NOx, PM10, PM2.5, SO2 and VOCs within the LFV, and for each of these 9 sources, were taken from the Metro Vancouver forecast and backcast emission inventories. Biogenic emissions were modeled using the MEGAN modeling framework (Guenther et al. 2006) and were assumed to remain fixed over the 20 year retrospective timeframe. The spatial distribution of emissions was adjusted based on observed changes in the spatial distribution of population density over the 20 year timeframe. Thus, the emission inventory was set-up to capture the changes in both the magnitude and spatial distribution of emissions within the LFV over the 20 year timeframe.

Based on analysis of the modeling, observational data and emissions inventories we conclude:

- The WRF-SMOKE-CMAQ modeling system produces ozone fields over the 20 year retrospective period which are responsive to the estimated changes in local precursor emissions and are in general agreement with observations. Some of the modeled episodes show better comparisons with observations than others, and this, in part, can be traced back to weaknesses in the meteorological modeling.

- Many of the simulations show highest ozone concentrations occur outside of the area sampled by the fixed monitoring network and within the LFV's numerous tributary valleys.

- Precursor emission reduction within the LFV have generally moved the ozone ridgeline boundary westward from the Agassiz-Chilliwack area to the Abbotsford-Langley area and southward from the ridges of the North Shore Mountains to the valley floor near Port Moody, Coquitlam and Pitt Meadows. However, the ozone ridgeline is sensitive to meteorology (mainly wind direction and wind speed) and shows a great deal of variability within and between ozone episodes.

- Based on the current modeling and consistent with previous studies, we find the Port Moody (T09) station has been and remains a VOC-sensitive location. Based on the current modeling and observational data, we infer that the large VOC emission reductions that have occurred within the LFV over the 1985-2005 period, stemming largely from the LDV and petroleum refining sectors, have been effective in reducing ozone concentrations at T09. Some of the benefits of the VOC emissions reductions have likely been offset by the concomitant NOx emission within the LFV. Nonetheless, the local NOx and VOC emissions reductions have been responsible for the decreasing 1-hr and 8-hr episodic ozone concentrations seen at this station. Although there is not the observation data to confirm this, the modeling suggests the western areas of the LFV surrounding Port Moody (Coquitlam, Port Coquitlam and Pitt Meadows) have likely responded to these same precursor emissions changes in a similar fashion.

- Based on the modeling, we find the eastern part of the LFV around Chilliwack has generally gone from being VOC-limited to NOx-limited over the last 20 years, although the ozone ridgeline shows a lot of variability with meteorological conditions. It is possible that presently this region has a mixed-sensitivity. Additionally, we suspect that VOC reductions (largely from the LDV VOC emission controls with the petroleum refining emissions not being as greatly influential here as at Port Moody) and NOx emission reductions, appear to have offset one another in terms of ozone production in this part of the LFV. Furthermore, based on the observational data, ozone production efficiency as a function of NO has increased noticeably at Chilliwack (T12) and likely in the other eastern parts of the valley. This efficiency increase has likely offset some of the benefits resulting from NOx emission reductions. The change in ozone sensitivity, along with the increased ozone production efficiency have changed the shape of the diurnal ozone profile to one that is less peaked around the daily maximum. As a result of this broadening, for a fixed peak ozone level, 8-hour averaged concentrations calculated around the peak concentration are increased. Finally, changes in population and economic activity over the 1985-2005 period have likely had a greater impact at T12 than T09. However, compared to the absolute changes in precursor emissions seen over the LFV during this period, the effects of this differential growth are likely small.

- In the easternmost part of the LFV, around Hope, the CMAQ modeling has difficulties capturing ozone formation. It is believed that this difficulty is due to the narrow valley and steep topography near the station; deficient modeled NOx sources upwind of T29 and deficient modeled NOx sources around the station. Nonetheless, based on the modeling, it is fairly evident that Hope has been and remains a NOx-limited region and based on the observational data at Chilliwack, that ozone production efficiency with respect to NO has likely increased here as well. Such an increase would have offset some, and perhaps all of the NOx emissions reductions achieved in the LFV. Due to its NOx-sensitive conditions, VOC emission reductions within the LFV have likely had negligible impact on ozone concentrations at T29.

- The modeling suggests that for every 10 ppb increase in background ozone concentration a roughly 3.0 ppb increase in 8-hour ozone concentrations would be observed in the LFV, with slightly higher increases expected in the western parts (3.7 ppb) of the LFV than the eastern parts (2.3 ppb). Based on recent studies showing increasing background ozone concentrations over Western North America (Vingarzan (2004), Jaffe and Ray (2007), Chan and Vet (2010)), over the next 20 years and within the LFV, a 3.0 ppb increase in episodic 8-hour averaged ozone concentrations could be expected, independent of local air quality management planning.

- The model consistently over-predicts ozone at a number of stations within the city of Vancouver (T04, T06) and under-predicts daytime NOx concentrations there. Both results are consistent with a deficiency in NOx emissions. Given the dominant role that marine, off-road and LDV emissions play as a local NOx sources, episodic emission rates from these sources need to be investigated further. Additionally, the model tends to under-predict ozone concentrations at Hope, also suggesting deficient modeled NOx sources within the LFV. The model shows a changing bias over time which implies uncertainties in the emissions backcasting.

- Trajectory modeling suggests that emissions and ozone from the Puget Sound region do not directly impact LFV air quality during summertime ozone episodes.

List of Acronyms

ACM2 Asymmetric Convective Model version 2

ASL Above Sea-Level

AURAMS Environment Canadas Unified Regional Air quality Modelling System

BELD3 Biogenic Emissions Landuse Database version 3

BEIS Biogenic Emissions Inventory System

CAP Criteria Air Pollution

CAPMON Canadian Air and Precipitation Monitoring Network

CB5 Carbon bond version 5

CMAQ Community Multiscale Air Quality modeling system

CTM Chemical Transport Model

CWS Canada Wide Standard

FVRD Fraser Valley Regional District

HYSPLIT HYbrid Single-Particle Lagrangian

IER Integrated Empirical Rate

IPR Integrated Process Rate

IRR Integrated Reaction Rate

LAI Leaf Area Index

LFV Lower Fraser Valley

LIDAR LIght Detection And Ranging

MCIP Meteorology-Chemistry Interface Processor

MC2 Mesoscale Compressible Community

MEGAN Model of Emissions of Gases and Aerosols from Nature

MODIS Moderate Resolution Imaging Spectroradiometer

MLD Mixed Layer Depth

MV Metro Vancouver

NAPS National Air Pollution Surveillance

NARR North American Regional Re-analysis

NRC National Research Council

OZIPR Ozone Isopleth Plotting Program Revised

PA Process Analysis

PBL Planetary Boundary Layer

PM Particulate Matter

PST Pacific Standard Time

RAMS	Regional Atmospheric Modeling System
RETRO	REanalysis of the TROpospheric chemical composition
SMOKE	Sparse Matrix Operator Kernel Emissions
SST	Sea Surface Temperature
TKE	Turbulent Kinetic Energy
UAM-V	Urban Airshed Model version V
VKMT	Vehicle KiloMeters Traveled
VOC	Volatile Organic Compounds
WRF	Weather Research and Forecasting

Contents

2. Introduction

The Lower Fraser Valley (LFV) of B.C. is a roughly triangular shaped valley having a population of 2 million people, the majority living in the city of Vancouver and its satellite communities in the western-most part of the valley (Figure 1). While the region has generally very good air quality (Steyn et al. 1997), it does experience occasional episodes of degraded air quality during the summer months. These events are generally associated with development of a low level thermal trough in combination with an upper level ridge (McKendry (1994); Pryor and Steyn (1995)) and at the meso-scale are associated with sea breezes and slope winds (Ainslie and Steyn 2007). These events tend to be of short duration (1 to 3 days) and often culminate in a cool surge of marine air from the Pacific. There are on average 2-3 such events each summer (Ainslie and Steyn 2007) with a fair amount of year to year variability. While the frequency of the meteorological conditions conducive to these events has shown no temporal changes (Ainslie and Steyn 2007), the frequency and intensity of the observed ground level ozone concentrations during these events has shown a marked decrease over the last 25 years (Vingarzan and Taylor 2003). It is generally believed that this decrease can be attributed to a marked reduction in local precursor emissions which have been driven by local air quality management plans (Greater Vancouver Regional District (1994); Greater Vancouver Regional District (2005)). One puzzling aspect of the changes is that the observed reductions in ozone concentrations during the events has not been uniform across the valley.

An important means of quantifying ozone air quality is the Canada Wide Standard (CWS; Canadian Council of Ministers of the Environment (2000)). For ozone, the CWS standard is set at a threshold of 65 ppb as determined by the 4th highest annual measurement of daily maxima of eight-hour running averages, averaged over three consecutive years. Loosely, achievement of the CWS therefore requires that, averaged over many years, fewer than four days per year have measured 8-hour ozone concentrations above 65 ppb. By this standard, locations in the western part of the valley (Port Moody, Surrey East, Langley) have shown statistically significant reductions in their calculated CWS values of over 20 ppb. These reductions have led several of these stations to move from out of- to in- CWS compliance. However, locations in the eastern part of the valley, namely Chilliwack and Hope have shown either modest reductions (Chilliwack) or no reductions (Hope) in their reported CWS values with present CWS values at or near the 65 ppb threshold. Figure 2 shows timeseries plots of the 3-year average of the 4th highest 8-hour average ozone concentrations at Port Moody (T09), Surrey (T15), Chilliwack (T12) and Hope (T29) between 1985 and 2005.

Given the context provided above, the overall objective of this study is to provide a policy relevant understanding of the relationship between ambient ozone and emissions of ozone precursors in the LFV. To be policy-relevant, the work must be scientifically credible, must be based on methods appropriate to the tasks, and must be presented in ways that lead directly into the policy-making and regulatory realms. In order to be scientifically credible, the work must be based on appropriate tools at the forefront of air pollution research. These tools are combinations of emissions -, meteorological - and air pollution chemistry models, all models being numerical in nature. As the work is to be policy relevant, all models must be evaluated by comparison with observations to demonstrate that model results are a fair reflection of reality. Specifically, the model evaluation must demonstrate that the models are responsive to emissions changes (gross reductions in NOx and volatile organic compounds

(VOC), changes in chemical speciation and spatial and temporal shifts in emissions) that have occurred in the past, and are likely in future scenarios. Given these methods, the investigation is directed by a set of research questions that can be summarized as:

- What has caused the relative decline in ozone air quality in the upper part of the Lower Fraser Valley (Abbotsford to Hope) over the past decades?
- What is the relative importance of changes in emissions (reactivities as well as amounts) as compared to spatial shifts in emissions densities in governing the noted spatio-temporal changes in LFV air quality over the past two decades?
- What is the effect of decadal changes in particular emissions sectors on ozone in LFV?

In order to address these questions, models will be evaluated by demonstrating that they can successfully capture the decadal evolution of photochemical pollution in the LFV in relation to changes in emissions and meteorology.

A particular research challenge arises because the research questions explicitly address air quality changes occurring over decades. An obvious, though extraordinarily expensive strategy to understand the decadal trends would be to run the models over 20 years, or possibly over 20 consecutive summers. Rather than undertake this 'brute force' approach, Steyn et al. (2005) propose an alternate strategy:

i. Simulate all four meteorological regimes discovered by Ainslie and Steyn (2007) by conducting model runs over episodes from the past, selected as representative of the four mesoscale circulation regimes.

ii. Perform runs of each for the inventory years 1985, 1990, 1995, 2000, 2005. Prioritize the runs as follows: 2005 1985 1995 1990 2000 in an attempt to maximize our ability to resolve air quality response to changing emissions.

iii. Do not attempt to provide a composite picture of the ozone climatology of the LFV by performing runs with the regimes weighted in terms of their frequency of occurrence. Rather simply, assume that any effect that is shown to occur in all clusters in the same direction will be representative of that effect as it would be seen in a full year of data (or a full years model run).

iv. Movement eastward of the ozone plume will be analyzed by quantifying the plume movement within each meteorological cluster.

The strategy in essentially this form was employed in the study, although in order to limit the computational load, only exploratory runs using the 1985 and 2005 were performed. While the questions addressed in this study have substantial interest in the scientific realm, they are also potentially interesting in the realm of regional air pollution management. In order to maximize the possibility that the results of the study were policy-relevant, the project was closely associated (especially in the early stages) with a multi-stakeholder steering committee. Members of that committee (and their affiliations) were:

- Peter Jackson (UNBC)
- Markus Kellerhals (BC Min. H, L & S.),
- Martin Mullan (Env. Can.),
- Roger Quan (Metro. Van.),

- Ken Reid (Metro. Van.),
- Peter Schwarzhoff (Env. Can.),
- Hugh Sloan (FVRD),
- Bob Smith (FVRD),
- Douw Steyn (UBC)
- Roxanne Vingarzan (Env. Can.).

The research was conducted at UBC and UNBC by Bruce Ainslie and Christian Reuten, under the supervision of Douw Steyn and Peter Jackson.

3. The Physical Setting

The LFV is flanked to the north by the southern Coast Mountains Ranges (rising to over 2000 m ASL), to the south by the Cascade Ranges (rising to over 1200 m ASL) and to the west by the Pacific Ocean. The valley floor is relatively flat rising to an elevation of only 10 m above sea-level at the town of Chilliwack, 100 km inland. In the East-West direction, the valley narrows from a width of 100 km at its western edge to a few kilometers at is eastern boundary some 90 km inland. Cutting across the valley in an east-west direction is the Canadian-US international border which separates Whatcom county, Washington from the districts of Metro Vancouver and the Fraser Valley Regional District (FVRD) in BC. Several major tributary valleys intersect the LFV, including Indian Arm, the Pitt River valley, Chilliwack Lake, Harrison Lake, the Fraser Canyon and the Chilliwack River/Cultus Lake

Valley. Figure 1 shows some of the important urban areas, geographic features and Metro Vancouver (MV) monitoring station locations. The presence of these tributary valleys plays an important role in the transport of ozone and its precursors during summertime episodic ozone conditions. Ocean waters offshore from the LFV are sheltered from the North Pacific Ocean by the presence of Vancouver Island. Vancouver Island in turn is separated from the mainland of BC by the Georgia strait to the north and the strait of Juan de Fuca to the south. These straits channel any offshore winds approaching the LFV and play a crucial role in determining where morning rush hour emissions from Vancouver are carried during the day.

4. Previous investigations into ozone formation in the LFV

There have been numerous modeling, observational and experimental studies investigating either directly or indirectly ozone formation in the LFV over the last 20 years. Taken together, and along with the extensive hourly observations from the fixed monitoring network, an impressive body of scientific findings has been collected in this region. Given this, one might question why another modeling exercise is needed. Our belief is that, while these individual studies are important in their own right, none have tried to piece together a comprehensive picture of how ozone forms in the LFV that takes into account the full interplay of emissions, meteorological variability and geography. This being said, one of the goals of the project was to rely extensively on the past studies to help evaluate the modeling system and to help ‘tell the story’. That is, we want to make sure that conclusions drawn from this study are consistent and supported by findings in these previous studies. Below is a brief overview of the some of the more important studies.

a. Observational studies

While ozone and other pollutants have been regularly monitored within the region since the late 1970s, special field studies designed to enhance the understanding of the meteorological and chemical influences on ozone pollution are relatively recent. In some sense, the first of such studies was the Pacific 1993 observational field campaign (Steyn et al. 1997). Its objectives were to provide data that could be used to enhance confidence in numerical modeling studies. While there were a significant number of studies published from Pacific 1993, a few are noteworthy. Banta et al. (1997) use a Light Detection and Ranging (LIDAR) to study daytime and nighttime flows up the Pitt River tributary valley. They showed that during the day, polluted air is drawn up the Pitt River Valley but during the night, air moving out of the valley is noticeably cleaner. The significance of this study is that it shows tributary valleys are important pathway for daytime ozone transport and that these valleys may not be acting as reservoirs for ozone and its precursors - in fact they may act to clean the air mass through the process of deposition along valley sidewalls during katabatic (downslope) flows. Up to this point, the main focus on ozone transport was with land/sea breezes and valley breezes within the LFV (Steyn and Faulkner (1986), Miao and Steyn (1994) and Steyn and McKendry (1988)) but this study shows the importance of including the role of tributary flows in controlling the spatial extent of ozone formation within the LFV.

McKendry et al. (1998a) followed this study up with a more detailed analysis of the August 1993 Pitt River Valley tributary flows using back-trajectories to identify emission source regions; tethered balloons to measure vertical profiles of ozone within the Pitt River Valley; and aircraft measurements along the valley to record the spatial extent of polluted air within the Pitt River valley. Among their findings were:

- The tethersonde observations recorded the highest ozone concentrations measured during the Pacific 1993 field campaign - 111 ppb observed 300m above ground level within the Pitt River Valley.

- Back-trajectory calculations show the likely source region for this polluted air was the Surrey, Delta and Port Coquitlam regions.

- Aircraft-based observations show pollutant levels generally increasing further up-valley with pollutants, held over from the previous day, likely contributing to some of this gradient.

This study clearly spells out the central importance of tributary valleys flows in determining the spatial extent of ground level ozone in the LFV; the possibility of higher ozone concentrations being observed outside of the fixed monitoring network; and the source region for these high pollutant levels being the urbanized areas around the city of Vancouver.

In an attempt to extend these findings to other tributary valleys, McKendry et al. (1998b) instrumented an aircraft to measure mixed layer ozone concentrations while flying up the Pitt River and Harrison Lake tributary valleys. This study found that the polluted tributary flows seen during Pacific 1993 were likely not an isolated event as again, higher concentrations were seen in the tributary valleys rather than in the LFV itself; and that tributary valley pollutant transport is not restricted to the Pitt River Valley and likely occurs in many other such valleys including the Harrison Lake valley.

A second major field campaign (Pacific 2001;Li (2004)) took place in the LFV during August 2001 with objectives more geared to understanding the evolution and formation of particulate matter (PM). Nonetheless, this campaign provided a rich dataset of observations suitable for model evaluation. Also, aircraft flights equipped with a downward looking LIDAR (Strawbridge and Snyder 2004) provided additional insight into pollutant circulation patterns within the LFV, namely: high nighttime PM concentrations were observed up both Harrison and Stave Lake valleys; daytime upslope flows were seen advecting pollutants aloft; and nighttime drainage flows appearing to carry PM seaward.

Ozone monitoring at the UBC forest site over two summer periods (Krzyzanowski et al. 2006) showed high ozone concentrations on south facing sides of the North Shore mountains along with evidence of ozone-caused injury to native plants. The implication of this study is that ozone is being also carried up the LFV side walls by daytime slope flows, a finding also observed by Reuten et al. (2005). In this study, they also find that pollutants within the slope flow are not necessarily vented to the free atmosphere at mountain top but can be re-circulated within the convective boundary layer.

Taken together, these observational studies show that pollutant circulation occurs at many scales and paint a picture of the overvall advection of pollutants being governed by the interaction of the large-scale seabreeze/valley flow with the smaller tributary valley and slope flows. Obviously, such a situation presents a very challenging task for numerical modeling studies.

b. Modeling studies

The first major attempt to model ozone formation using a grid-based chemical transport model was undertaken by Hedley and Singleton (1997) and Hedley et al. (1997) using Environment Canada's mesoscale compressible community (MC2) meso-scale meteorological model with the CALGRID photochemical model. With a grid spacing of 5km, they studied a five day (July 17-21) 1985 event. Because of the complex terrain and the interacting scales of motion, they devote a fair bit of effort in their papers to evaluating both their modeled meteorology and modeled concentrations against observations. Their model produced ozone fields showing higher ozone concentrations outside of the LFV (specifically, over the north shore mountains and the cascade mountains to be specific) with lower but still elevated concentrations mid-valley. They also conclude that their emissions inventory likely underestimates VOC emissions within the urban areas.

In a follow up study Hedley et al. (1998) examine the effects of emission control strategies on future summertime air quality in the LFV. They model the 1985 July 17-21 episode with both a forecasted 2005 emissions inventory using a business-as-usual change in vehicle fleet composition and with an emission inventory reflecting a large shift of vehicles to natural and propane gas technologies. They also perform two VOC- and NOx-sensitivity studies with the business-as-usual inventory. This study, and in particular the business-as-usual simulations, is relevant here for a number of reasons. To start, they compare the influence of 1985- and 2005-based emissions on local ozone concentrations under a fixed set of meteorological conditions. This is precisely what has been undertaken in this report, however, we are using estimates of *present* day 2005 emissions and *backcast* 1985 emissions, while they used *present* day 1985 emissions and *forecast* 2005 emissions[1]. Next, the VOC- and NOx-sensitivity studies provide information on the spatial extent of the VOC- and NOx-limited regions within the LFV. Based on their modeling, they determine that reducing VOC emissions should be a priority in a LFV ozone control strategy (from a 1985 perspective). That is, they estimate, that in 1985, the urban Vancouver area, the mid-valley region and parts of the North Shore mountains were VOC-limited. In addition, they show that the effects of VOC emission reductions would not be felt uniformly across the valley, with rural and suburban areas likely to experience greater reductions than the urban regions. Observations show that this has not come to pass, but to be fair, the region has also been influenced by simultaneous and significant NOx reductions. To this matter, they anticipate that if NOx reductions do occur (in addition to VOC reductions), then parts of the urban plume will then become NOx-limited. This present study confirms that many of these predictions and shows they hold under a wide range of meteorological conditions.

Jiang et al. (1997) use the 1985 episode to test ozone sensitivities to VOC and NOx emissions using the Ozone Isopleth Plotting Program Revised (OZIPR) box model and a single trajectory constrained to pass over the downtown core at 0800 Pacific Standard Time (PST) on July 18th. They find that ozone formation along this trajectory, which ends up passing over the Stave Lake area en-route to Harrison Lake to be VOC-limited. They identify a VOC species, whose major source is from vehicle emissions, as being the most important emitted ozone precursor.

The 1985 episode was also modeled by Suzuki (1997) using the Urban Airshed Model

[1] It should be noted that the use of present and backcast emissions should in principle lead to a more robust picture of the change in ozone behaviour than with the use of present and forecasted emissions

(UAM). The UAM-modeled ozone plume showing peak concentrations away from the valley. In particular, the model produces ozone maxima at the head of the Pitt River valley and southeast of Abbotsford in Washington state. Analysis of model output using indicator species showed western part of the valley (Burnaby and Port Moody) to be VOC-limited but sites in the eastern part of the valley (Surrey, Abbotsford and Chilliwack) were NOx-limited. The modeling work also suggests that the downwind location of the afternoon ozone plume is sensitive to the strength of the modeled wind fields around the North Shore mountains.

Barna et al. (2000) use MM5/CALMET and CALGRID to model ozone formation over the Pacific Northwest (including the LFV, Puget Sound and the Portland, Oregon regions) at a 5km resolution. Spatial plots of modeled ozone fields for July 14th 1996 show highest ozone concentrations in the LFV over the north shore mountains (although it is difficult to accurately place the maxima due to the scale of plot). A secondary maximum is seen around the Bellingham area with generally elevated concentrations extending from the Seattle area along the I5 corridor. Ozone concentrations are only compared locally to the Custer Wa. station. These are found to be below 70 ppb for the entire 4 day simulation while maximum ozone concentrations in the Puget Sound area reach 130 ppb and in the Portland Oregon area reach 170 ppb. What is most relevant to this study are the findings that:

- There is no widespread build up of ozone over the episode, with ozone maxima occurring downwind of the major urban areas.
- There is no evidence for pollutant recirculation from one day to the next within the urban areas.

- There is no evidence of observed emissions from one urban area influencing neighbouring downwind urban areas.

In an effort to improve air quality modeling in the LFV, Yin et al. (2004) make modifications to the LFV biogenic emissions inventory. They improve the local landuse database through the examination of Canadian forest and crop data as well as make modifications to the methods used to calculate shortwave radiation and soil temperatures. They test their modifications using the Community Multiscale Air Quality (CMAQ) modeling system at a 5km resolution over an episode from the Pacific 1993 field campaign. Their main research focus is PM modeling and no ozone results are given. This study highlights the local deficiencies found in some of the biogenic emission databases (prepared for use mainly in the US).

Pottier et al. (2000) make use of a UAM model output of the Pacific 1993 field campaign to explore ozone control strategies using indicator species and process analysis. They too find that western locations within the valley tend to be VOC-limited with eastern stations more likely to be NOx-limited. They find that the ratio of $[O_3]/[NOy]$ is a good indicator of ozone sensitivity with values below 5 indicating VOC-limited conditions and above 10 NOx-limited conditions. They also find high rates of ozone production above the surface and that vertical and horizontal mixing play a vital in determining local ozone concentrations.

Smyth et al. (2006) used CMAQ at a 4km resolution to model a 12-day period during the Pacific 2001 field campaign. The main focus of the paper is assessing the model's ability to reproduce observed pollutant concentrations, especially PM values. The study provides a benchmark for measuring model agreement with observations and provides daily emission totals which are also useful for comparison purposes. They do not provide statistical results on a per station basis, so it is hard to tell how well their modeling effort does at capturing ozone concentrations at key stations like Port Moody, Chilliwack and Hope. They do, however, compare observed and predicted ozone concentrations averaged over both the entire episode and just daytime hours (0600-0900). There, they find that the Chilliwack and Hope mean values are significantly over-predicted by CMAQ. They suggest that this over-prediction may arise in part from improper setting of the minimum vertical eddy diffusivity.

Jiang et al. (2006) and ONeill et al. (2006) both model ozone formation in Pacific Northwest but neither of their inner domains extends to LFV. Jiang et al. (2006) show the sensitivity of model output to weekday/weekend emissions estimates around the Seattle area. They also make use of back-trajectories to identify air mass transport paths. ONeill et al. (2006) look at the effects of different estimates of emission rates on modeled ozone and PM concentrations.

Qiu et al. (2004) model the Pacific 2001 field campaign using Environment Canada's MC2 numerical weather prediction model along with Sparse Matrix Operator Kernel Emissions (SMOKE) based emissions and the CMAQ chemical transport model. They find that modeled nighttime ozone concentrations are too high using a 12km resolution but much of this over-prediction is removed when a 4km resolution is used. However, they find that the increased model resolution did not improve predictions of the daytime maxima at the Vancouver International Airport station. The ozone spatial distribution for August 12th at 2300 shows highest ozone concentrations mid-valley near Chilliwack, around Harrison Lake and around Stave Lake. High concentrations are also produced along the North Shore mountains.

Herron-Thorpe et al. (2010) perform a model evaluation exercise on the 12km resolution

AIRPACT-3 air quality forecast system using satellite observed tropospheric NO_2 concentrations. They find the AIRPACT model systematically underestimates NO_2 concentrations around the Vancouver region while over predicting NO2 concentrations in the Seattle area. They suggest that the Vancouver underestimation arises from the AIRPACT-3 emission inventory lacking sufficient NOx sources. It is not known how the AIRPACT-3 emission inventory compares with the inventory used in this project, but many of the components and datasets are likely the same.

Finally, Cai and Steyn (2000) and Cai et al. (2000) perform numerical modeling of the meteorology for the 1985 and Pacific 1993 events. They do not use the model fields to drive chemical transport model. Both studies produce afternoon wind fields having a sea-breeze/valley flow interacting with smaller tributary valley flows and slope flows. These two studies provide additional benchmarks for our model evaluation.

c. Other studies

In addition to the modeling studies, numerous statistical and semi-empirical studies have been undertaken locally. While not having the same physics-based foundation as the numerical modeling studies, these data-driven studies can be a very powerful tool for exploring certain aspects of ozone formation. For example, Pryor and Steyn (1995) examined observed ozone concentrations between 1984 and 1991 and find that summertime ozone concentrations were typically higher on weekends than weekdays while NOx concentrations were higher weekdays than weekends. The latter they attribute to a greatly reduce weekend morning rush hour. They also find the magnitude of the above hebdomadal cycles to be spatially varying and to have increased over the 1984-1991 period. They conclude that the shift is not likely caused by meteorological variability but more likely from changes in precursor emissions.

In a follow on study, Pryor (1998) suggests that, after controlling for the influence of meteorology on observed ozone concentrations, there was a decrease in ozone concentrations outside of the urban core between 1984 and 1991. They suggest that this arises from enhanced NOx-titration stemming from a shift in precursor emissions. Various lines of reasoning lead them to conclude that the region (in 1991) was VOC-limited.

Joe et al. (1996), in a statistical study of observed ozone concentrations at two fixed monitoring stations between 1978 and 1990, find a statistically significant decreasing ozone trend at Port Moody and an increasing trend at Abbotsford. They speculate that these differing trends have arisen due to an eastward shift in the centroid of precursors, likely due to more rapid population growth up-valley. Another statistical analysis, using more recent data from 1985 to 2000 (Vingarzan and Taylor 2003), find decreasing meteorologically-adjusted summertime ozone trends at all 5 stations studied. They also find increasing annual trends at stations in the western part of the valley which they speculate is caused by increasing hemispheric background ozone concentrations.

Steyn et al. (1996) use two data-driven prognostic models, the Integrated Empirical Rate (IER) equations (Johnson 1984) and Sillman indicator ratios (Sillman 1995) to study the sensitivity of LFV ozone formation to NOx and VOC emissions over 4 episodes during the years 1985, 1988, 1993 and 1994. Two of these episodes have been modeled in this study. For the 1985 episode, they find the western-most monitoring stations to be VOC-limited with the eastern stations of Surrey and Chilliwack showing NOx-sensitive conditions in the late afternoon. Analysis of the Pacific 1993 data show VOC-limited conditions early in the episode with a transition to NOx-limited conditions at some stations as the episode progressed. Based on the analysis of the 4 events, they conclude an increased propensity to NOx-limited conditions over the 1985-1994 period, with stations in the eastern part of the valley becoming more NOx-limited. Also, as an episode progresses, they find a westward movement of the NOx-VOC transition line.

Finally, Ainslie (2004) used a scaling-level model of ozone formation in the LFV to show that the region is likely VOC-limited and that under these conditions, the competing effects of both NOx and VOC emissions reductions on ozone formation may not lead to noticeable changes on peak summertime ozone concentrations.

Taken together, a general picture emerges from the observational, modeling and semi-empirical studies. The LFV, a largely de-industrialized region with emissions dominated by the transportation sector, has experienced large reduction in precursor emissions over the last 20 years with these reductions resulting in concomitant changes in summertime ambient ozone concentrations. But these changes have not been uniform across the region, with the long term behaviour differing noticeably between Port Moody and Chilliwack. Concurrent with the observed changes in ozone and emissions is a change in the region's population distribution (with increased development up-valley); and changes in the hemispheric background ozone concentration.

The advection and ultimately the formation of ozone in the LFV results from a set of processes acting at a range of spatial scales and that numerical modeling at a resolution at least as fine as 5km is likely needed to capture these processes. As a result of interactions between these scale dependent processes, ozone concentrations in the Lower Mainland is likely to be found outside of the region sampled by the fixed monitoring network.

Ozone formation was likely VOC-limited in late 1980s, but the effect of both NOx and VOC emissions reductions over the last 20 years has lead to the potential for some parts of the region to be NOx-limited. Finally, meteorologically adjusted hourly averaged summertime ozone concentrations have not necessarily shown the same trends as CWS-based trends which leads to the possibility of 'peak shaving' whereby emissions controls have been effective at reducing the highest (peak) hourly values but not in reducing the mid-level concentrations (Lefohn et al. 1998).

5. LFV Emission Inventory

In many respects, the core of this study is a model sensitivity study, i.e. we are exploring the changes in ozone that stem from changes in emissions under a fixed set of meteorological conditions. What is notably different about this study is that the modeled emissions changes are based on what has actually occurred, rather than ones that are hypothesized to occur, or are fabricated to test model performance. Most importantly, we require that the spatio-temporal structure of modeled ambient ozone fields match those observed over time. Once this is achieved, we will use process analysis on model output to develop an understanding of the underlying causes of changes spatio-temporal patterns and levels of ambient ozone in the LFV. Clearly this research strategy demands that the emissions inventory and its changes through time be known as realistically as possible.

a. Metro Vancouver Emissions Inventory

Metro Vancouver, through its Air Quality Policy & Management Division maintains an emissions inventory for all of the physical (rather than just political) LFV. The inventory is used for a variety of purposes, but in the present context, provides the bulk of basic data needed for constructing the emissions inventory required by CMAQ. The inventory is updated every five years, with backcasts being performed in order to ensure consistency between individual inventory years. Inventory years relevant to the present study are 1985, 1990, 1995, 2000 and 2005. The MV inventory covers emissions of pollutants from various source sectors and sources as indicated in Table 3. Table 4 shows average daily emission rates (metric tones/day) within the LFV based on the Metro Vancouver emission inventories (Greater Vancouver Regional District (2003), Greater Vancouver Regional District (2007)) for 1985 and 2005. Figure 3 shows a plot of the temporal evolution of VOC and NOx emissions in the LFV. In this plot both the NOx and VOC emissions totals have been scaled so that their 1985 values equal 100. It is evident from this figure and from Table 3 large changes in VOC and NOx emissions have occurred since 1990.

In addition to emissions estimates from the MV emissions inventory, we were also able to access data and analyses pertinent to light duty mobile sector emissions from the AirCare emissions testing program operated under contract for the British Columbia Ministry of Attorney General (`http://www.aircare.ca/`). While these data and analyses do not provide direct emissions estimates, they are invaluable in validating emissions estimates from the all-important mobile sector.

Between the MV inventory produced in 2002 and the one produced in 2007, it was discovered by MV (in collaboration with the Port of Vancouver) that their estimates of marine NOx emissions were substantially high, so revisions were made to this portion of the inventory (The Chamber of Shipping (2007), Greater Vancouver Regional District (2007)). These revised emissions estimates were incorporated into our emissions inventory.

b. SMOKE-based Emissions inventory

In order to provide realistic simulations of past events, the SMOKE-based inventory was adjusted to account for both changes in the amount of emissions and the location of emission sources. The SMOKE modeling system was set-up to produce separate emission inventories for: light and heavy duty vehicles (through the MOBILE 6.2 and MOBILE 6.2C modeling framework), off-road vehicles, railroads, aircraft, marine, other mobile sources, biogenic emissions, point sources, and area sources. Total annual emission rates of NOx, VOCs, CO, SO2, PM10, PM25 and NH3 within the LFV, and for each of these 9 sources, were taken from the Metro Vancouver forecast and backcast emission inventories. Biogenic emissions were modeled using the Model of Emissions of Gases and Aerosols from Nature (MEGAN; Guenther et al. (2006)) modeling framework and were assumed to remain fixed over the 20 retrospective timeframe.

The spatial distribution of emissions was achieved through the use of 38 different spatial surrogates. These are maps of physical or geographic features used to indirectly estimate the intensity of a polluting activity that occurs at a given location. For instance, roadway maps are often used to estimate where mobile source emissions occur. These maps were gridded to the 36, 12 and 4km domains and each give the fraction of a specific surrogate that occurs in each gridcell. For instance, one of the spatial surrogates gives the fraction of the total MV population living within each of our 4x4 km gridcells. All of the spatial surrogate maps were based on datasets valid for 2001, and since an important component of the present study is to represent as precisely as possible the response of the ozone plume to spatial shifts in emissions densities resulting from changing population and economic activity in the LFV, the spatial surrogate maps had to be adjusted for the different time periods. In order to do this, the spatial surrogates valid in any particular year were adjusted based on observed changes in the local population density:

$$S_{ij}^{y} = S_{ij}^{2001}\left[\left(\frac{P_{ij}^{y}}{\sum P_{ij}^{y}}\right)\Big/\left(\frac{P_{ij}^{2001}}{\sum P_{ij}^{2001}}\right)\right] \tag{1}$$

where S_{ij}^{y} represents that fraction of spatial surrogate S in year y and at grid cell ij and P_{ij}^{y} represents the fraction of population in gridcell ij at year y. LFV total population densities in each of our 4x4 km grid squares at 5 year intervals (1980-2010) were obtained from MV. As a result of this population-scaling of the spatial surrogates, our emission inventory was set-up to capture the changes in both the magnitude (through the MV backcasting) and spatial distribution of emissions within the LFV over the 20 year timeframe.

6. Synoptic and meso-scale meteorology during summertime ozone episodes

As mentioned earlier, summertime ozone episodes occur under fair weather anticyclonic conditions. Such conditions tend to be synoptically slack resulting in light winds. Marked thermal inversions, arising from dry air descending in the anticyclone, are usually observed.

The presence of the thermal inversion allows temperatures to rise and also tends to limit daytime thermal convection allowing for abundant solar insolation. With mountains limiting horizontal dispersion and the thermal inversion limiting vertical mixing, under the clear skies and warm temperatures the stage is set for photochemically driven reactions to convert hydrocarbon and nitrogen oxide emissions into ozone and other by-products typically found in smog.

In addition to summertime, photochemically dominated ozone production, near surface ozone can periodically be elevated due to intrusions of stratospheric ozone through meteorological conditions which lead to stratosphere-troposphere exchange of air. The phenomenon occurs worldwide (Seinfeld and Pandis 1998) and has been investigated in the LFV by Bovis (2003). This study does not address ozone of stratospheric origin directly.

The relationship between synoptic meteorological conditions and ozone formation in the LFV have been investigated by McKendry (1994). He finds that LFV summertime ozone episodes are usually characterized by a surface thermal trough coupled with an upper-level ridge. These synoptic features provide the large-scale meteorological context within which the observed thermal inversion, strong insolation, light mesoscale winds and dominant thermally driven circulations occur.

Pryor et al. (1995) use principal component analysis rather than the synoptic typing to assess the relationship between surface ozone concentrations and synoptic-scale weather patterns. This work finds that some ozone episodes can be predicted solely on the basis of synoptic meteorology, but that in some cases the prediction is poor. The interpretation of this result is that mesoscale meteorological features in the LFV are important in determining the occurrence and strength of an ozone episode, and that these features are not uniquely determined by synoptic fields alone.

With the bulk of the population living in and around the City of Vancouver, the main ozone precursor emission sources are released in the western part of the valley. It appears that the emissions arising from the morning commute are the key source of ozone precursors. While it is typically held that these morning emissions are then carried inland by a sea-breeze circulation, this is not strictly true. Ainslie and Steyn (2007) show that most ozone events do not have well developed sea-breeze circulations, but nonetheless, ozone events do typically have onshore flow which carries precursor emissions inland and away from Vancouver. It appears that the fate of these emissions is governed by a delicate balance between the onshore flow, the topography of the North Shore mountains and the presence of secondary thermally driven circulations around the mountains (slope flows) and tributary valleys (valley flows).

In the preceding paragraph it was mentioned that the LFV is roughly a triangular shaped valley. While this description is basically correct, the actual valley shape differs crucially from this description in at least one way: the northern boundary of the valley dips southward to form a convex border with the most southern excursion around the city of Mission. As a result, the City of Abbotsford, typically considered to be mid-valley, is actually both south and east of downtown Vancouver. Additionally, the City of Chilliwack, which we will consider to be close to the eastern most extension of the LFV [2], is both east and north of Abbotsford (and continuing east, the City of Hope is actually north of Chilliwack and even

[2] While many consider Hope to be at the eastern most point of the valley, from the point of view of the transport of ozone and its precursors, the topographic relief of the valley suggests that at a point midway between Chilliwack and Hope, the broad nature of the valley ends, and that Hope is found to be part way up what amounts to another (and actually somewhat minor) tributary valley.

north of Vancouver). In essence, for ozone and its precursors to impact the eastern part of the valley, the air mass carrying these pollutants must follow a dogleg trajectory. While not impossible, it turns out that the meteorological conditions necessary to produce such a trajectory are quite restricted. While we will discuss this in greater detail in the following sections, essentially, if the onshore winds do not have a sufficient northerly component, the morning emissions will not be able to get around the bend in the valley. If the air mass gets too close to the North Shore Mountains, it tends to get caught in the slope and valley flows and redirected northward out of the valley. If the precursors can make it to Abbotsford, then the usual up-valley flows from this location will guide the precursors northeastward to Chilliwack. From Chilliwack, the modeling suggests that the air mass tends to continue northward and head up Harrison Lake and to a lesser extent continue on to Hope. It must be mentioned here, that not all of the episodes modeled follow this general description.

The likelihood of precursor emissions being advected up-valley, rather than being carried over the North Shore mountains or flushed into Georgia Strait is partially captured in the mesoscale circulation analysis of Ainslie and Steyn (2007). This analysis, based on daily average hodographs at YVR, YXX and BLI, identifies four dominant, independent circulation regimes that set-up during summer fair weather conditions in the LFV: two characterized by morning YVR winds from the northwest direction, and two with southerly YVR morning winds (Figure 4). The typical circulation patterns within each regime show characteristically different capacities to carry morning emissions away from the downtown core and up the Fraser valley. However, because of the averaging used to identify the circulation patterns, it is generally not quite enough to know a day's circulation regime in order to pinpoint where it's ozone plume will develop. Nonetheless, the identification of circulation regimes provides an excellent framework for conducting the retrospective investigation.

Finally, it must be stressed that the McKendry (1994) synoptic analysis represents one end of a long arc of meteorological analysis that continues through to the meso-scale (Ainslie and Steyn 2007) and logically ends at the surface spatial ozone distribution. This analysis train involves processes linked across a wide range of scales: the type and positioning of synoptic-scale weather systems influences meso-scale circulations; these circulations interact with topography and thermally driven flows to drive the transport of precursor emissions which ultimately determines the local ozone spatial distribution. One of the major goals of this research is to tie together the considerable body of research, which has largely independently explored many of the facets influencing local ozone formation, into a common narrative of ozone formation, through the use of numerical models.

7. Model Set-up

In order to simulate summertime ozone formation in the LFV a combination of numerical models was used: the Weather Research and Forecast (WRF) model was used to simulate the meteorological conditions; the SMOKE model to model the precursor emission rates; and the CMAQ model to handle the chemical and dispersive evolution of the precursors. While biogenic modeling is supported within the SMOKE framework, a separate model, MEGAN, was used for the biogenic modeling instead. Finally, the SMOKE, MEGAN and CMAQ models cannot handle the WRF meteorological fields directly, so the Meteorological-Chemistry Interface Processor (MCIP) model was used as both a meteorological post-processor (for CMAQ) and a pre-processor (for SMOKE and MEGAN). Figure 5 gives a flowchart showing the sub-models used in the modeling system, described in more detail in the following sections.

a. WRF Meteorological Modeling

WRF(version 3.1;Skamarock et al. (2008)) was used to create time-varying 3D meteorological fields for each of the seven episodes. Three two-way nested domains with grid cell resolutions of 36, 12 and 4 km were used to produce high-resolution meteorological fields over the LFV and surrounding regions. Each WRF run was 96 hours long and was initialized at 1800Z using North American Regional Re-analysis (NARR) fields at a 32-km resolution. Because of the complex terrain and the potential for pollutant carry-over in elevated layers (McKendry and Lundgren 2000), the model was run with 48 vertical eta-levels. In the horizontal, the 36 km domain had 100x100 gridcells, the 12km 76x97 and the 4km 178x109 gridcells. Figure 6 shows the boundaries of the nested domains. The model simulations in the 36 and 12km domains were nudged to the analysis fields outside of the boundary layer. No nudging was applied to the inner 4km domain. The Kain-Fritsch convective parametrization (Kain 2004) was used to emulate the effects of unresolved cloud updraft and downdraft processes while the Asymmetric Convective Model version 2 (ACM2) scheme was used to capture unresolved planetary boundary layer (PBL) processes (Pleim (2007a), Pleim (2007b)). Data from the Moderate Resolution Imaging Spectroradiometer (MODIS), onboard the Terra/Aqua satellites, were used to initialize the model sea surface temperatures. Weekly averaged values used were possible, otherwise weekly climatological values, centered around the episode date, were used. A single sensitivity run was performed for the 2006 event using a very high resolution 1.3km domain. This domain used the same 48 vertical levels along with 130x79 1.33km resolution gridcells centered over the LFV.

b. MCIP meteorological processor

The MCIP (version 3.4.1; Otte and Pliem (2010)) model was used as a meteorological preprocessor for the SMOKE and MEGAN models and as a meteorological post-processor of the WRF output. The MCIP post-processing of the WRF output results in a slightly smaller computational domain: 93x95 for the 36 km domain, 70x89 for the 12km and 172x103 for the 4km domain. This is the domain size used by the SMOKE, MEGAN and CMAQ modeling.

c. SMOKE emissions modeling

Non-biogenic hourly precursor emissions were simulated by SMOKE (version 2.5; Houyoux and Vukovich (1999)). Annual emission inventories for the 12 and 4km domains were obtained from Environment Canada (Boulton et al. 2009). This consisted of annual emission totals, at the municipal district level, valid for 2001 over the extent of the 12km domain. A set of 38 surrogate files, used to spatially allocate the emissions, were also supplied. For the 36km domain, emission data from the 2001-based Criteria Air Pollution (CAP) inventory (ftp://ftp.epa.gov/EmisInventory/2001v2CAP/) were used. The 12 and 4km inventories were set-up to handle area, mobile, point emissions separately. Further modifications were made to the mobile inventories so that light duty, heavy duty, off road, marine, rail, air and other mobile sources could be modeled separately. Outside of the LFV, light duty (LDV) and heavy duty vehicle (HDV) emissions were calculated from regional annual totals, while inside the LFV, the MOBILE6.2C (MV and FVRD) and MOBILE6.2 (Whatcom Co.) models were used to calculate emissions based on driving rates and fleet characteristics. Input data files for MOBILE6.2C were supplied by MV and for MOBILE6.2 by the Washington Department of Ecology.

Backcast emission totals (Greater Vancouver Regional District 2007) within Metro Vancouver, the FVRD and Whatcom Co., Wa were used in the preparation of the 4km, non-2001, point, area, off-road, marine, air and rail emission inventories. The MOBILE6.2 and MOBILE6.2C models used backcasted Vehicle Kilometers Traveled (VKMT) values for the estimation of LFV mobile emission rates. No year specific adjustments were made to the 12 and 36km inventories.

Evolution of the spatial distribution of emissions over the 20 year period was handled using LFV population density data. Population density datasets at 5 year intervals (from 1985 to 2010) were gridded to the inner 4km domain. For each year modeled, each 4km grid cell's surrogate weight (for each of the non-marine spatial surrogates) was adjusted based on the change in population density (with respect to the 2000 population density) in that gridcell. The spatial distribution of the marine surrogate weights was not changed since there was no reason to believe that the spatial[3] behaviour of marine emissions has changed over the 20 year retrospective period.

[3]Changes in the marine *emissions*, as for the other sources, was handled through the emissions inventory backcasting.

d. Biogenic emissions modeling

In the 4km domain, biogenic emissions were calculated using the MEGAN (version 2.04) emissions model. It was found that the maps of Leaf Area Index (LAI) supplied with the MEGAN model were showing abnormally high values over parts of the local North Shore Mountains. These were manually corrected based on a small set of field measurements. In the 36 and 12 km domains, the Biogenic Emissions Inventory System (BEIS v3.09) model using landuse tiles from the Biogenic Emission Landuse Database version 3 (BELD3) was used to model biogenic emissions. Local adjustments to BELD3 tiles made by the Yin et al. (2004) were used in the 12 km domain and by Stroud et al. (2008) in the 36km domain. We did not make any adjustments to the biogenic landuse databases to reflect changes that may have occurred over the 1985-2005 period. Temperature and radiation data used to calculate biogenic emissions were taken from the from the MCIP-processed WRF fields.

e. CMAQ Chemical transport model

The EPA Models-3 CMAQ modeling system (Byun and Schere 2006) version 4.7.1 was used for the photochemical modeling. Using the SMOKE-based emissions and the MCIP-processed WRF fields, CMAQ simulates the transport, deposition, and chemical evolution of ozone, particulate matter, as well as photochemical precursors and other oxidants using its Chemical Transport Model (CTM). Each of the 7 evaluation simulations was 96 hours long. Allowing for a 12 hour spin up-period, this provided in excess of 3 full days of modeling for each episode. For the four subsequent investigation simulations (which used 1985 and 2005 inventories but with fixed meteorology characteristic of one of the four meso-scale circulation regimes) the run lengths were shortened to 84 hours, which still allowed for 3 days of modeling (less the 12-hour spin up period). All runs used 48 vertical levels.

Background ozone, CO and NOx were obtained from the Reanalysis of the TROpospheric chemical composition (RETRO; Pozzoli et al. (2011)) monthly average output fields created from the ECHAM5-MOZ coupled GCM/chemical and aerosol model. The carbon bond version 5 (CB5) gas phase chemical mechanism with chlorine (Yarwood et al. 2005) using the AE-5 aerosol module was used. The CTM used ACM2 PBL physics module, to calculate stability and vertical mixing as recommended by Otte and Pliem (2010).

The Process Analysis (PA) explanatory tool was used to provide quantitative information on the relative importance of chemical reactions and other atmospheric processes that are being simulated by the CTM. The integrated process rate (IPR) tool used to show relative importance of deposition, chemical production and transport in the observed change in ozone concentrations at each gridcell. Integrated reaction rate analysis (IRR) used to explore relative importance of chemical pathways in simulated ozone formation. These tools were used to determine VOC/NOx sensitive regions.

f. HYSPLIT trajectory analysis

Finally, the HYbrid Single-Particle Lagrangian (HYSPLIT) model (Draxler and Hess 1997) was used as an exploratory tool to determine ozone source regions and emission receptor regions via forward and backward particle releases. The particle releases were driven using the WRF meteorological fields. Forward particle releases were used to examine the fate of morning emissions from the downtown Vancouver area. Neutrally buoyant particles were seeded into the WRF wind field continuously from 0700 to 1000 (PST) at an elevation of 10 m agl and were followed until 1600 PST. The areal particle density at 1600 PST was calculated and contoured over a landsat image in order to identify the morning emission receptor regions. The backward releases were used to identify the source regions of air traveling throughout the day and arriving at known ozone 'hot-spots' (and other areas of interest) in late afternoon. These hot-spot regions included: Hope, Chilliwack, Abbotsford, Pitt River, Harrison Lake, Slave Lake, Squamish, Saturna Island and the Strait of Juan de Fuca. In these simulations, particles were released for a single hour (1600-1700 PST) and followed back in time for between 1 and 9 hours, for a total of 9 runs per day at each hot-spot. The final particle positions from all 9 runs where then plotted over a landsat image and the cloud of points was used to delineate each hot-spot's daily source region. Both forward and backward releases where performed on 3 days during each of the 7 modeled episodes.

8. Description of the Episodes used in the Model Evaluation

To test the fitness of the WRF-SMOKE-CMAQ modeling system, it was exercised over 7 different ozone episodes spanning the retrospective timeframe. Episodes were selected based on their meso-scale circulation type; whether the episode had previously been studied or had observational data above and beyond the hourly data collected by the fixed monitoring network; and so as to provide a roughly uniform distribution of events over the 20 year retrospective period. Below is a description of meteorology and modeled ozone concentrations for each episode. Table 2 list the dates, circulation regimes and special characteristics of each of the seven episodes. The results of a detailed evaluation of the model performance over each episode, discussed at length in the the Meteorological and Chemical Transport Model Evaluation appendices, are summarized in Section 9.

a. 1985 Episode

Chronologically, the earliest episode modeled was from Thursday July 18th to Monday July 22nd, 1985[4]. This episode was selected for three reasons:

i. On the last two days (July 20 and 21) it has type IV meso-scale circulation regimes.

ii. It has been previously modeled (Hedley and Singleton (1997). Hedley et al. (1997), Suzuki (1997), and Jiang et al. (1998)).

iii. It provides a test for the modeling system at the earliest point in the retrospective period.

This episode's large scale synoptic pattern was characterized by a weak 500 hPa ridge to the west of the coast on the 19th which shifted eastward and weakened by the 21st (Figure 7). At the surface, the synoptic pattern was quite slack with little pressure gradient over the region during the 3 days (Figure 8). On the 19th, a weak thermal trough can be seen

[4]Although the modeling spans 5 days, only 96 hours were modeled and only 3 days (July 19, 20 and 21) had all 24 hours (0000-23000 PST) simulated (the other 96-72=24 hours fall on the 18th and 22nd). This temporal coverage is the same for all the modeled episodes, and when discussing the the meteorology of each episode, only the 3 fully covered days are considered. However, the statistical analyses given in later sections consider all 96 simulated hours.

over and south of the region which fades away by the 21st. The center of a weak high pressure system, positioned off the coast, drops south during these 3 days as well. Surface temperatures at YXX peak on the 19th at 33^{o}C and remain above 30 on the 20th before dropping on the 21st (Figure 9). Measured wind speeds are low at YVR (< 4 m/s) and YXX (< 5 m/s) throughout the event.

The average morning/early afternoon (0700-1500 PST) surface flow pattern on the 19th was characterized by northwesterly flow down Georgia strait (Figure 10) with the YVR hodographs showing northwesterly winds (Figure 11). On the 20th and 21st, westerly flows through Juan de Fuca appear (likely in response to the shift in the location of the offshore high) and these flows penetrate into the LFV leading to a more SW flow at YVR and giving rise to type IV meso-scale circulation regimes. A small re-circulation zone appears to form over the southern Gulf islands on the 20th.

It is interesting to compare the location of peak 1-hr modeled ozone concentrations (Figure 12) with the general circulation patterns. On the 19th, the modeled ozone plume has its maximum concentration (> 102 ppb) over the Stave Lake area, with high (> 82 ppb) concentrations extending southward into the U.S. along the I5 corridor. A secondary peak is seen in the strait of Juan de Fuca. The flow pattern in Figure 10 would suggest that this last ozone maxima is from Victoria area precursors. On the 20th, the highest concentrations (> 102 ppb) are found over Howe Sound, consistent with the southerly flow regime seen in the streamlines (Figure 10) and in the YVR hodograph (Figure 11). Additionally, this day's streamlines suggest that the secondary ozone maximum seen over southern Vancouver Island is also from Victoria area precursor emissions. Finally, on the 21st, the severity of the episode has decreased, with peak ozone concentrations reaching 92 ppb north of the Stave

Lake area. The modeled YVR hodograph for this day shows a more westerly flow than shown on the 20th which is conducive to up-valley advection of Vancouver's urban area precursor emissions.

b. August 1987 Episode

The next episode in chronological order was the August 24-28 1987 episode. This episode was chosen because each of the 3 fully modeled days (Tuesday August 25th to Thursday August 27th) showed type IV circulation patterns. Originally, the meteorology from this episode was to be used as the canonical type IV circulation patterns in the retrospective study, but the model evaluation from this episode was not very satisfactory (Section 22 and below), and the 1985 episode was used in its place. Nonetheless, this episode was still used to evaluate the modeling system.

The synoptic pattern for this event was characterized by a slack surface pressure gradient on the 25th and 26th with an offshore surface high building on the 27th (Figure 13). The upper-level pattern was characterized on the 25-26 by a pronounced 500 hPa ridge positioned over the coast with a upper level low to the west. By the 27th, the ridge has flattened and the upper-level low has started to fill and moved over the Queen Charlotte Islands (Figure 14).

Throughout the episode, the YXX surface temperatures were relatively cool with daytime maxima dropping from 28 on the 25th to 21^{o}C on the 27th (Figure 15). Winds were generally light at both YXX (< 3 m/s) and YVR (< 4 m/s) throughout the episode. The surface streamlines (Figure 16) show southerly flow up Juan de Fuca on all days with the southerly flow extending into Georgia strait on the 25th and 26th leading to southeasterly flow at YVR (Figure 17). On the 27th, the surface streamlines show northwesterly flow down Georgia strait, which when coupled with the southerly flow up Juan de Fuca, forces the flow over the Vancouver urban region to head in a northeasterly direction towards the North Shore mountains. This day's streamlines also show a small recirculation region over the southern Gulf Island. It is important to note that the modeled YVR hodograph shows northwesterly flow (blue circles and lines), while the observed flow (red circles and lines) is from the southwest with morning southeasterly outflow (Figure 17). It is believed that this mis-characterization of the flow incorrectly leads to advection of the Vancouver morning emissions up-valley resulting in over prediction at many inland stations (e.g. T09 in Figure 84) and significantly contributing to this episode's poor model performance.

Given the strong southerly circulation patterns on the 25th and 26th, it is not surprising that the modeled ozone plume (Figure 18) shows a maximum ($>$ 82 ppb) over Howe Sound and up along the sunshine coast on the 25th and up Georgia Strait on the 26th. It appears that the return of NW flow down Georgia Strait on the 27th leads to onshore advection of the Vancouver precursor towards the North Shore mountains, with the model producing peak ozone concentrations above 72 ppb over the Pitt River and Stave Lake areas. Although, as mentioned above, it is likely the placement of the ozone plume on this day is in error given the difficulties reproducing this day's YVR hodograph.

c. August 1993 Episode

The third modeled episode covers part (August 1-5) of the Pacific 1993 field campaign (Steyn et al. 1997). Each of the 3 fully modeled days (Monday August 2nd-Wednesday August 4th) was characterized by a weak 500 hPa ridge centered along the coast (Figure 19). On the 3rd and 4th, the ridge weakens and shortwave troughs can be seen moving down the lee side. At the surface, a weak surface thermal trough extended south of the coastal sections of BC with a surface high pressure to the northwest (Figure 20). This synoptic configuration resulted in 3 days of type I meso-scale circulation patterns. The shortwave trough passage on the 4th lead to unstable afternoon conditions with thunderstorm activity reported along the northern edge of the LFV (McKendry et al. 1998a). The weak ridging plus shortwave passage, conditions not characteristic of classic LFV ozone episodes, made this a difficult episode to model.

Surface temperatures at YXX exceeded 30^oC each day with August 4th being the warmest at close to 34^0C (Figure 21). Unlike the 1985 and 1987 episodes, observed wind speeds at YVR were moderately strong on the 2nd and 3rd (> 7 m/s) before dying down on the 4th (Figure 21).

The surface circulation patterns show northwesterly flow down Georgia Strait and easterly flow through Juan de Fuca on all three days (Figure 22). In the eastern part of the LFV, outflow conditions are modeled throughout the episode. Northwesterly flow is also observed in the YVR hodographs (Figure 23) which also shows no (August 2 and 3) or very weak (August 4) night time off-shore land-breeze. At YXX the flow is mainly down-valley on the 2nd and 3rd, with up- and down-valley flow occurring on the 4th. These features, all consistent with the type I circulation regime found on these days, appear to be reasonably well captured by WRF.

The surface ozone plot for August 2nd shows a single area of high (> 62 ppb) ozone at the western edge of Juan de Fuca (Figure 24). The absence of high ozone concentrations over the LFV likely arises from the strong northwesterly winds at YVR and northeasterly winds at YXX (Figure 23) flushing precursor emissions from the valley. A similar ozone pattern is produced on the 3rd, with the exception of a small region of 62+ ppb around the Bellingham, Wa. area. The ozone pattern on August 4th shows a LFV peak (> 92 ppb) east of Bellingham with additional > 82 ppb peaks along the I5 corridor and throughout Juan de Fuca. HYSPLIT particle releases from Bellingham on the 4th (not shown) reveal onshore flow. It is likely that northwesterly flow over the Vancouver area, onshore flow along the coast, and weak morning down-valley flow turning to afternoon weak up-valley flow at YXX, has impeded the usual up-valley precursor advection and led to the modeled Bellingham ozone peak.

d. July 1995 Episode

The 1995 episode was chosen because of the additional spatial ozone data available for model evaluation from the McKendry et al. (1998b) aircraft measurements. Additionally, it has 3 days of type III circulation patterns.

The upper-level synoptic pattern was characterized by a ridge over the coast on Monday July 17th which shifts westward on the 18th before amplifying and shifting northward on the 19th (Figure 25). At the surface, on all 3 days, a weak surface high pressure was positioned offshore with thermal a trough positioned along the south coast (Figure 26).

On the 17th and 18th, the surface circulation very much similar to that on the 1993 event with northwest flow down Georgia Strait, easterly flow out of Juan de Fuca, and outflow conditions in the LFV (Figure 27). On the 19th, WRF produces westerly flow through Juan de Fuca and up-valley flow at YXX (Figure 28). Notice that on the 17th (and to a lesser extent on the 18th), WRF produces outflow at YXX while the observations show up-valley flow. At YVR, WRF does a good job of reproducing the observed northwesterly flow on the 17th and 18th but has a more westerly flow on the 19th than is observed. All of these discrepancies likely lead to incorrect positioning of the ozone plume and lowered statistical agreement at the monitoring stations.

YXX temperatures exceed 32^{o}C on all three days, with WRF reproducing the high temperatures on the first 2 days but being about 4^{o}C too cool on the 19th (Figure 29). Daily maximum temperatures at YVR increase throughout the 3 days with WRF doing at an excellent job at reproducing this trend. Concomitant with the increasing temperatures is a decreasing wind speed trend at YVR which WRF captures but with speeds consistently light by about 2 m/s (Figure 29).

The modeled ozone plume on July 17th, 1995 (Figure 30A), shows a North-South oriented finger of moderate ($>$ 62ppb) ozone over the central portion of the LFV and along the I5 corridor in Washington State with another ozone maxima at the western edge of Juan de Fuca Strait. This spatial ozone distribution over the LFV is similar to the modeled plume on July 19th, 1985 (Figure 12C). This finger-like plume orientation likely results from a balance between precursors being advected up-valley by the northwesterly (onshore) flow seen at YVR and being carried down-valley by the the modeled northeasterly (outflow) at

YXX (Figure 27). On the 18th, ozone concentrations over the LFV have increased with maxima > 92 ppb predicted around the Cultus Lake area and > 82 ppb over Harrison Lake. Concentrations exceeding 72 ppb are also seen along the I5 corridor and at the western edge of Juan de Fuca. There is much less modeled outflow at YXX on this day (Figure 28) and this likely allows CMAQ to move the ozone plume further up-valley on this day. By the 19th, the daytime modeled flow is entirely up-valley at YXX but the modeled winds at YVR are due west (onshore) with some morning easterly outflow (Figure 28). The flow through Juan de Fuca is from the west (Figure 27). Thus there appears to be a meso-scale flow regime shift on this day, with flow from Juan de Fuca and up through the Southern Gulf islands working its way to the LFV. This appears to influence the trajectory of flow over the urban Vancouver area – directing it towards the North Shore mountains. This flow change is consistent with the subtle shift in surface pressure patterns seen between the 18th and 19th (Figure 26). On the 18th (and 17th), the surface pressure gradient is aligned with Vancouver Island, with higher pressure over Port Hardy than over Vancouver. This generates the northerly flow down Georgia Strait. On the 19th, the Vancouver Island pressure gradient relaxes, and the driving synoptic gradient appears to in an east-west direction allowing the westerly flow through Juan de Fuca and more a westerly flow at YVR. It must be noted that while WRF produces the westerly flow at YVR, the observations still show north-westerlies (Figure 28) and this day's resulting ozone plume, showing peak concentrations exceeding 122 ppb over the Pitt River Valley (Figure 30C), may be misplaced.

e. July 1998 Episode

The 1998 episode was originally chosen because it shows 2 days of type II circulation patterns (July 25th and 27th). Because the 2001 episode (next subsection) also exhibits type II circulations, has additional supplemental model evaluation data, and showed higher statistical evaluation scores, the 1998 meteorology was not used in the retrospective analysis.

This event is typical of summer ozone events with high YXX temperatures (28, 33 and 34^{o}C) and low YXX and YVR winds (generally below 2 m/s; Figure 31). The surface synoptic pattern (Figure 32) showed dominant high pressure over Eastern Pacific on Saturday July 25th, with a thermal trough developing on the 26th and a general weakening of the pressure gradient on the 27th. The upper-level pattern (Figure 33) was relatively static with a high pressure ridge positioned along the coast on all 3 days.

The resulting surface circulation patterns (Figure 34 and Figure 35) shows northwesterly flow down Georgia strait, westerly flow down Juan de Fuca and up-valley flow within the LFV on the 25th. On the 26th, a day characterized by type III meso-scale circulation, the southerly Juan de Fuca flow exerts more influence in the LFV, with winds over the coast having a more southerly direction. By the 27th, the northwesterly flow in Georgia Strait flow eases and southerly flow from Juan de Fuca penetrates to the LFV. The modeled ozone fields show peak concentrations mid-valley, with maximum values exceeding 102 ppb over the Stave Lake area on the 25th (Figure 36). On the 26th, peak ozone concentrations ($>$ 102 ppb) are seen along an east-west running line over the North Shore mountains. By the 27th, ozone concentrations exceeding 72 ppb cover almost the entire LFV region, much of the Gulf Islands and southern Vancouver Island. Concentrations exceeding 112 ppb are seen in a broad region over the Pitt River area, over the sunshine coast, over Boundary Bay and north of Victoria.

f. August 2001 Episode

The August 9-13 2001 episode was chosen to coincide with the highest ozone concentrations measured during Pacific 2001 field campaign (Li 2004). It also provided three days (Friday August 10th, Saturday August 11th and Sunday August 12th) of type II circulations. This episode began (August 10th) with a 500 hPa ridge over the coast coupled with a upper-level low over the Gulf of Alaska (Figure 37). The upper-level low dug southward on 11th and 12th leading to an amplification of the ridge and eastward displacement of the ridge axis towards the interior of B.C. At the surface, a weak thermal trough over the coast with high pressure offshore was seen on the 10th (Figure 38). The offshore high pressure weakened and by the 12th the pressure gradient over the south coast was quite slack. The modeled surface streamlines (Figure 39) show northwesterly flow down the Georgia Strait on all three days but with this flow extending into Juan de Fuca only on the 10th. By the 11th, westerly flow through Juan de Fuca is shown and a slight recirculation region is seen over the southern Gulf Islands. The flow pattern on the 12th is similar to the 11th but with a slightly more pronounced southerly flow.

Observed temperatures at YXX were slightly cooler than for some of the other episodes with temperature just reaching 30^{o}C on the 10th and dropping to the high 20s on the other 2 days (Figure 40). Wind speeds observed at YXX were generally light ($<$ 3m/s) and from the southwest (Figure 41). At YVR, the winds were also light and from the northwest on the 10th, from the west on the 11th and from the southwest on the 12th (which the WRF model did not quite reproduce; Figure 41).

The modeled ozone plumes show ozone concentrations above 82 ppb over the Mission area on the 10th, with other maxima east of Bellingham, and south of Victoria (Figure 42). On the 11th and 12th, the maximum modeled concentrations exceed 92 ppb and are seen over the North Shore mountains.

g. June 2006 Episode

The final modeled episode was chosen because it provides a test of the modeling system at the end of the retrospective period and because it exhibits type I circulation on the first 2 fully modeled days (Saturday June 24th and Sunday 25th, 2006). The upper-level pressure pattern for this event starts off like the 2001 event with a ridge of high pressure over the coast with an upper-level low to the northwest (Figure 43). However, in this event, the upper-level ridge is a bit stronger and positioned further inland. As the event progresses, geopotential heights rise, the ridge strengthens and the low moves northward while filling. At the surface, a thermal trough aligned with the south coast deepens over the course of the event with a building high pressure center offshore and a weakening low pressure center over the Gulf of Alaska (Figure 44). The surface streamlines show northwesterly flow down Georgia Strait and easterly flow through Juan de Fuca on all three days (Figure 45). The streamlines show the flow passing over the Vancouver urban area and penetrating far up-valley. At YXX, surface temperatures exceeded 30°C on the 25th and 26th, with generally light (< 3 m/s) winds (Figure 46). At YVR, daytime winds speeds were surprisingly strong, rising from nearly 5 m/s on the 24th, to 7 on the 25th and near 9 m/s on the 26th (Figure 46 and Figure 47). The strengthening winds on the 26th push this day into a type II circulation regime from the type I patterns seen on the 24th and 25th.

The highest modeled ozone concentrations are found between Abbotsford and Hope on all three days, and within the valley and not along the tributary valleys (Figure 48). High ozone concentrations are also seen extending along, and east of, the I5 corridor and in Juan de Fuca.

9. Model Evaluation

The model evaluation is conducted not so much to measure how well the model reproduces observations but to determine whether the model is fit enough for the task of exploring the response of ozone formation to the observed decadal scale changes in local precursor emissions. As mentioned before, we have chosen to assess model fitness by exercising it over seven episodes that span the retrospective period and include all of the meso-scale circulation regimes identified by Ainslie and Steyn (2007).

Because of the importance of pollution transport and dispersion in ozone formation, evaluation of the meteorological modeling has been performed separately from that of the chemical transport model. It is a two-stage evaluation, where first WRF output interpolated to meteorological station locations is compared against point observations. Next, various other meteorological data, not routinely available, are used to assess model performance. The statistically based levels of agreement ('scores') used to assess the present WRF modeling are then benchmarked against statistical scores from other LFV modeling efforts. Table 6 list the names, acronyms and formula of the various statistical metrics commonly use to evaluate model performance. A similar evaluation methodology has been used with the CMAQ model output. Owing to the lengthy and detailed nature of the model evaluation methodology, we have placed the full results in two appendices and summarize the findings here.

a. Meteorological Model Evaluation

1) Surface Temperature

Surface temperature is an indirect measure of the surface energy budget and hence the net effects of incoming short wave radiation, surface sensible heat flux, soil moisture, and mixed layer depth are reflected in the observed and modeled surface (2 m) temperatures. On this front, the most relevant comparison between model and observations is at the inland Abbotsford (YXX) station far from the ocean where the complex coastline of the LFV makes temperature comparisons problematic. For the present WRF simulations, root mean square errors (RMSE) at YXX were highest for the 1995 simulation (3.1^{o}C) and lowest for the 1993 simulation (1.9^{o}C). The NRC's (Hedley and Singleton 1997) simulation of the 1985 event produced a YXX RMSE of 2.0^{o}C which is only slightly better than the 2.2^{o}C produced by the present WRF simulations. At Hope, WRF tends to produce higher RMSE errors where the model's relatively smooth topography leads to unrealistically smooth modeled temperature fields in the complex terrain surrounding the station. It also tends to produce higher errors at coastal locations, like YVR, where the marine influence is highly variable and difficult to reproduce with 4km X 4km volume averaged temperatures. The poorer statistical scores at both coastal and mountainous stations is consistent with similar studies (Hedley and

Singleton (1997), Mass et al. (2003)).

2) Surface Winds

As a measure of the model's ability to capture pollutant advection, surface (10 m) wind speed RMSE errors at YVR range from 1.4 (1998) to 2.4 m/s (1995) and from 0.9 (1998) to 2.0 m/s (1993) at YXX. These can be compared with RMSE of 2.95 m/s (YVR) and 1.97 m/s (YXX) produced by the NRC from their 1985 simulation. A RAMS-based simulation of the 1985 event (Cai and Steyn 2000) produced LFV averaged RMSE values between 1 and 2 m/s, in line with present WRF simulations. The Cai et al. (2000) Pacific 1993 RAMS simulation does not reproduce the surface wind fields as closely as the 1985 event, with domain averaged RMSE values generally between 3 and 4 m/s. Cai et al. (2000) argue that the occurrence of local weather systems, such as thunderstorms degraded the overall model performance. The present WRF simulation also shows generally lower statistical agreement during the 1993 than 1985 event. It is found that the overall level of agreement of surface winds at Hope is generally in line with that seen at YVR and YXX despite the considerably narrower valley at this location. However, all seven simulations systematically underestimate wind speeds there with average biases ranging from 1.2 m/s (2001) to 1.5 m/s (1985). This underestimation likely affects how CMAQ handles up-valley pollutant transport and ozone formation here.

3) Other meteorological comparisons

Vertical measurements of temperature, wind speed and direction, taken during the 1985 episode, have been used to compare both the present WRF and the Cai and Steyn (2000) RAMS modeling against observations (Figure 49). In general, the WRF-based profiles are: cooler than the observed or RAMS output; reproduce the dominant afternoon westerly wind direction; and reproduce the vertical wind speeds in the lower 500 m while tending to over-predict winds above this height.

A spatial comparison of modeled afternoon surface (10m) wind fields from the Hedley and Singleton (1997) MC2, the Cai and Steyn (2000) RAMS and the present WRF 1985 simulations over the LFV (Figure 50) shows that the present WRF simulation (Fig. 50C), and the RAMS simulation (Fig. 50B) produce wind fields with small scale up-slope flows interacting with the larger scale up-valley flow. The Hedley and Singleton (1997) MC2 afternoon windfields (Fig. 50A) do not resolve the important up-slope flows.

Finally, for the 1993 episode, MLD over the LFV were gathered from an aircraft equipped LIDAR during the Pacific 1993 field campaign (Hoff et al. 1997). WRF predicted MLD along three of the flight paths (Figure 51A) have been extracted and plotted along with the observed MLD. Over Leg 1 (Figure 51B) WRF diagnosed MLD over the ocean are too low but WRF does a good job of capturing the quick MLD rise over land. Further north, the diagnosed heights are too low when the leg passes over Burrard Inlet. Over Leg 2 (Figure 51C) WRF over estimates heights when approaching the North Shore mountains. For Leg 3 (Figure 51D) good agreement is seen over portions of the flight path near coast, but away from coast, the diagnosed MLD again is too high. Not shown in the figures are the MLD diagnosed from the Cai et al. (2000) RAMS simulations which generally does a much better job at reproducing the observations. The RAMS MLD were extracted from the RAMS output using a more sophisticated turbulent kinetic energy (TKE) based procedure Batchvarova et al. (1999), than the WRF-based Richardson number approach, which may be better suited at diagnosing MLD with an internal thermal boundary layer. It is not clear what effect, if any, these higher diagnosed MLD values will have on the photochemical modeling.

b. Chemical Transport Model Evaluation

1) NOx

As for the CTM model evaluation, we find daytime NOx predictions to be in-line with those found in Hedley et al. (1997) with all but two station (T07 and T14) have index of agreement (IOA), a broad measure of statistical agreement with IOA=1 for perfect agreement and IOA=0 for absolutely no agreement, above 0.50 with the worst agreement at T07 (0.26) and best at T03 (0.94). The RMSE errors are slightly larger than Hedley et al. (1997) with values at T04, T05, T10, T14, T15 and T16 exceeding 20 ppb. The spatial distribution of mean bias errors (MBE), averaged over all seven episodes (Figure 52), shows the model tends to consistently under-predict NOx concentrations within the Vancouver urban area with the largest average errors at the T06 (29 ppb), T09 (16.8 ppb) and T01 (11.2 ppb) stations. On average, the model tends to slightly over-predict daytime NOx concentrations just outside of the main urban areas in Richmond (T17), Surrey (T15), Langely(T27) and Maple Ridge (T30).

2) VOC

Modeled VOC concentrations have also been compared with observed concentrations using data collected from the National Air Pollution Surveillance (NAPS) network. Through this network, 24-hr averaged VOC concentrations, of up to 176 compounds, are collected from a number of sites within the LFV every third or sixth day depending on a national schedule. Because of the irregularity of the sampling times, only a limited number (12) of NAPS measurements occurred during the seven modeled episodes (with none occurring prior to 1993) and only at six different locations (T09, T15, T17, T18, T22 and T24). In order to compare the NAPS data with the CMAQ output, observed VOC concentrations were mapped onto eight CB05 VOC classes: OLE (terminal olefin carbon bond), PAR (paraffin carbon bond), TOL (toluene and other monoalkyl aromatics), XYL (xylene and other polyalkyl aromatics), FORM (formaldehyde), ALD2 (acetaldehyde), ETHA (ethane) and ISOP (isoprene). The mapping performs a weighted-allocation of each NAPS VOC species onto one or more of the CB5 classes based on the VOC's chemical structure (Table 1).

The comparison by CB5 class shows that CMAQ produces OLE and PAR concentrations that are, on average, 4.0 and 5.3 times larger than is observed (Figure 53) [5]. The present level of agreement, while not great, is comparable with results seen over the Northeastern US (Doraiswamy et al. 2009). Figure 54A shows a comparison of the average relative composition of each CB5 class to the total VOC concentration. The plot shows that both the

[5] The most extreme over prediction of 17.8 is for the ALD2 class which, in many of the analyzed NAPS samples, was found in very low concentrations ($<$ 0.1 ppb)

CMAQ and NAPS speciations have PAR making up almost 75% of the VOC mixture with all the other classes contributing a much smaller amount. Because PAR is associated with many slower reacting VOC compounds, it is more meaningful to examine the VOC composition when each class' concentration has been scaled by its affinity for reacting with the hydroxyl radical. When this OH-reactivity scaling is performed, the PAR dominance on the composition is removed (Figure 54B) and the OH-weighted speciation shows the NAPS speciation is weighted towards the heavier aromatic class (XYL) while the CMAQ profile is weighted toward ALD2 class. Both the CMAQ and NAPS OH-weighted speciations show similar breakdowns for OLE and PAR and neither show the ISOP class to be dominant.

3) Ozone

A detailed examination of the results from the each episode along with comparisons against other modeling efforts and special field studies is presented in the Chemical Transport Model Evaluation appendix. Here we present only the average level of agreement, for a range of statistical measures, between CMAQ and the MV measured ozone concentrations, and for all seven episodes (Table 7). As a means of benchmarking the present results, we have also included in the table are statistical scores from the NRC's CMAQ simulation of the 2001 episode (Smyth et al. 2006). The table shows the model, with the exception of 1985 (and to a lesser extent 1987) has a persistent positive mean bias (MB), suggesting the model consistently over-estimates ozone concentrations. The WRF-CMAQ mean error (ME) statistics are generally closer to the NRC's ME than the MB statistics suggesting the main difference between the two modeling efforts is the larger bias seen in the WRF-

CMAQ results. Based on the these statistics, it would appear that the 2006, 2001 and 1985 simulations achieve the best agreement with the observations and are on par with the Smyth et al. (2006) results. The 1993 and 1995 simulations appear to be significantly worse while the 1987 is somewhere in-between. As noticed in the episode description section, the 1987 and 1995 episodes showed difficulties reproducing the observed circulation patterns which likely contributes to their poorer model evaluation scores. Model success for both the 2006 and 1985 events is encouraging because the retrospective analysis is based on comparisons of model output driven by 2005 and 1985 emissions and fixed meteorology. It appears that the inventory at these two timepoints is well modeled. It is also noteworthy that the nature of the model bias changes over the 20 year timeframe: WRF-CMAQ overestimates in 2006 and 2001 while it underestimates in 1985. Finally, while the model bias is significant, its effects on the retrospective analysis can be mitigated by looking at the differences between simulations with 2005 and 1985 emissions.

c. Model Evaluation Summary

The WRF-SMOKE-CMAQ modeling looks to be an improvement over some of the earlier local modeling efforts and is on par with the recent NRC modeling and modeling performed by other groups over the Pacific Northwest. The level of model agreement,in terms of statistical measures, is surprisingly similar across the various modeling efforts. This hints at a limit to which a volumed average model output can be expected to match a point observation (Galmarini et al. 2010). Some episodes show better comparisons with observations than others, and this, in part, can be traced back to errors in the meteorological modeling.

The persistent bias in modeling suggests there are still some unresolved error in emissions modeling. The change in this bias over time also suggests uncertainties in the emissions backcasting. Finally, based on the model evaluation, we select the 2006 event as representative of the type I meso-scale meteorology; the 2001 event for type II; 1995 for type III (recognizing its shortcomings on July 19th – see the Chemical Transport Model Validation appendix); and 1985 for type IV.

10. VOC/NOx sensitivity runs

A series of 4 additional sensitivity runs were made with the August 2001 event. In these runs, the first fully modeled day (August 11th), preceded by a 12 hour spin-up (for a total of 36 hours), was run first with 15% more and then 15% less anthropogenic VOC and NOx emissions. The 8-hour averaged (1300-1800 PST) ozone fields from the baseline and 4 sensitivity runs were then used to explore the region's ozone sensitivity to changing VOC and NOx emissions. Figure 55 gives the baseline (100% VOC and NOx emissions) 8-hour average ozone concentrations which shows highest concentrations (> 80 ppb) over the North Shore mountains and high (> 60 ppb) values throughout the LFV and into Harrison Lake.

Figure 56A shows the spatial distribution of ozone sensitivity to changing anthropogenic VOC emissions (E_{VOC}) as a percent change in $[O_3]$ to a percent change in E_{VOC}:

$$\begin{aligned}\frac{d[O_3]}{dVOC} &= \frac{[O_3]_{+VOC} - [O_3]_{-VOC}}{[O_3]_{base}} \Big/ \frac{1.15E_{VOC} - 0.85E_{VOC}}{E_{VOC}} \\ &= \frac{[O_3]_{+VOC} - [O_3]_{-VOC}}{0.3[O_3]_{base}} \qquad (2)\end{aligned}$$

This plot shows most of the Vancouver urban area, parts of Howe Sound and the area around Bellingham can experience up to a 0.5% increase (decrease) in ozone concentration for every percent increase (decrease) in anthropogenic VOC emissions. East of Abbotsford and outside of the valley itself, ozone shows very little (> 0.1%) sensitivity to changing VOC emissions. This behaviour can be understood in terms of an ozone isopleth diagram which has been schematically reproduced in Figure 56B. Such a diagram shows the response surface (blue lines) of ozone concentrations to varying amounts of NOx and VOC emissions and can be divided into 2 regions by a ridgeline (green line). The blue lines are lines of constant ozone concentration (ozone isopleths) and increase in magnitude away from the origin. Above the ridgeline, ozone concentrations increase with increasing VOC emissions and decrease with decreasing VOC emissions (with NOx emissions being held constant). This region of the response surface is called the VOC-sensitive region and the large red arrow above the ridgeline illustrates the positive sensitivity of ozone to VOC emissions. We have highlighted one of the warm coloured regions in (Figure 56A) and have drawn a line connecting it to a location above the ridgeline to illustrate that the model is finding this region of the LFV to be VOC-sensitive. Below the ridgeline, the isopleths are nearly parallel to the VOC axis, and as shown by the lower red arrow, changing VOC emissions has little effect on ozone concentrations. The behaviour of the cool coloured points in (Figure 56A) is consistent with ozone sensitivity in this region which we have illustrate by joining a line from the highlighted gridcells over the Cascade mountains in (Figure 56A) to the lower red arrow.

This analysis has allowed us to qualitatively classify gridcells based on their ozone sensitivity to changing anthropogenic VOC emissions. Before we repeat the analysis for NOx sensitivity we must point out that:

- The above analysis is only representative of a single day from one of the episodes; and
- Performing this type of brute force sensitivity analysis is quite time consuming.

As a result, it is desirable to look for chemical species or combinations of chemical species, whose absolute concentrations or magnitudes can be used to distinguish VOC (and NOx) sensitive gridcells *without having to perform additional sensitivity simulations* (Sillman (1995), Tonnesen and Dennis (2000)). While there are many such indicator species suggested in the literature (Sillman and He 2002), over the LFV, Pottier et al. (2000) found the ratio of $[O_3]/[NOy]$ was successful in characterizing the sensitivity of their UAM-V model output to changing emissions [6]. This indicator is also amenable to field measurement (Arnold et al. (2003), Pottier et al. (2000)) which makes it useful for diagnostic model evaluation. In Figure 56C, we have extracted model predicted $[O_3]/[NOy]$ at each LFV grid point and plotted the modeled $d[O_3]/dVOC$ as a function of this ratio (blue crosses). Regardless of spatial location, the $d[O_3]/dVOC$ – $[O_3]/[NOy]$ relationship is monotonically decreasing confirming the indicators suitability at diagnosing VOC sensitivity. Another way of looking at this is that if a gridcell's $[O_3]/[NOy]$ ratio is less than 5, ozone concentrations at that gridcell are strongly sensitive to changing VOC emissions. Likewise, if the gridcell's ratio is greater than 10, it shows little sensitivity. This relationship is illustrated by the lines connecting the two highlighted regions in (Figure 56A) to the highlighted regions in (Figure 56C).

In Figure 57 three plots showing the spatial pattern of ozone sensitivity to NOx emissions (Figure 57A), the general behaviour of ozone to changing NOx emissions on an isopleth dia-

[6] where $[NOy]$ represents the oxidized nitrogen species ($NOy = NO + NO2$+nitrate radical+nitric acid+nitrous acid + peroxyacetyl nitrate + other organic nitrates)

gram (Figure 57B) and the relationship between the modeled ozone sensitivity ($d[O_3]/dNOx$ in this case) and $[O_3]/[NOy]$ (Figure 57C) are given. In Figure 57A most of the urban core, and the waters off of the LFV show a negative sensitivity of changing ozone concentrations. This behaviour is consistent with emission mixtures lying above the ridgeline on an isopleth diagram where the red arrow in (B) indicates *decreasing* ozone concentrations in response to *increasing* NOx emissions and vice versa. Again, east of Abbotsford and outside of the valley itself, the modeled sensitivity is positive, indicative of emission mixtures below the ridgeline. In this region of an isopleth diagram, called the NOx-sensitive region, ozone concentrations *increase* with increasing NOx emissions and *decrease* with decreasing NOx emissions. The relationship between $d[O_3]/dNOx$ and $[O_3]/[NOy]$ shows a monotonically increasing relationship (purple circles) which in this case, crosses the $d[O_3]/dNOx = 0$ axis (small circled area in (Figure 57C)). This zero-crossing corresponds to the ridgeline on the isopleth diagram. We find that 95% of the purple circles associated with negative sensitivities ($d[O_3]/dNOx < 0$) have $[O_3]/[NOy]$ ratios less than 6.7 and 95% of the circles associated with positive sensitivities ($d[O_3]/dNOx > 0$) have $[O_3]/[NOy]$ ratios greater than 7.3. The value of the line of best fit passing through the circles (purple line) at zero sensitivity is 7.0. Thus, it appears that the $[O_3]/[NOy]$ ratio can be used to indicate a gridcell's ozone sensitivity with a VOC-NOx transition value of $[O_3]/[NOy] \approx 7.0$. As a consequence, we can now located the ridgeline over the LFV in all of our simulated episodes by simply plotting the $[O_3]/[NOy] = 7$ contour [7]. This contour, plotted as the thin purple line in (Figure 57A), closely tracks the zero-sensitivity region (green shading) in this figure.

[7] Along with $[O_3]$, $[NOy]$ is easily calculated from the CMAQ output and does not require running additional sensitivity simulations.

11. CMAQ exploration runs

Having presented results from seven evaluation runs, meant to evaluate the model's fitness at capturing ozone formation in the LFV, as well as documenting a means of diagnosing the ozone ridgeline from the model output, we now present results from a 4x2 matrix of simulations comprised of meteorological conditions from each of the 4 meso-scale circulation regimes and emission levels consistent with 1985 and 2005.

Figures 58 to 69 consist of 12 plots showing modeled maximum 8-hr average ozone exposure contours (in 5 ppb increments) over each day of the three fully modeled days for each of the four mesoscale meteorological regimes are given using (A) 1985 emissions and (B) 2005 emissions. These plots, showing each gridcell's daily maximum 8-hour averaged concentrations, should not be confused with plots showing modeled ozone plume averaged over a fixed 8-hr period. In these plots, each gridcell's maximum modeled 8-hr averaged concentration can occur over any period within the day and this period can be different for different gridcells. In this sense, these figures show the expected 8-hr ozone exposure throughout the region, and are easier to reconcile with CWS reporting or epidemiological studies. Also shown in each plot is the predicted VOC/NOx ridgeline based on the $[O_3]/[NOy]$ ratio (green line) and the fixed monitoring network station locations (+).

a. Cluster I simulations (June 2006 meteorology)

On the first day of the Cluster I simulations (i.e. June 24th, 2006 meteorology) the 1985 emission-based ozone exposure footprint has almost the entire valley between Langley and Hope experiencing 8-hr exposures above 60 ppb with large areas around Chilliwack, Agassiz and the Cultus Lake area reaching exposures above 75 ppb (Figure 58A). With 2005-level emissions, no regions above 60 ppb are predicted (Figure 58B). Within the valley, the VOC-NOx boundary is also predicted to shift from the Mission area westward to between Chilliwack and Abbotsford. This boundary also moves down from the ridges along the North Shore Mountains to almost the valley floor and retreating down the Pitt River Valley to the Port Coquitlam area. On the second day, similar changes are predicted but with the VOC-NOx boundary retreating west of the Langley and Maple Ridge areas under the 2005 emissions. Only on the 3rd day is a small 60+ ppb region southwest of Chilliwack and Agassiz expected under the 2005 emissions. which, under the 1985 emissions, sees > 80 ppb exposures. The change in VOC-NOx boundary under this day is similar to the first with the boundary generally shifting to lie between Chilliwack and Abbotsford but with a fair degree of spatial variability south of Abbotsford.

The model has Chilliwack switching between VOC- and NOx-sensitive conditions on all 3 days while Hope is always NOx-sensitive and Port Moody (i.e. T09) is always VOC-sensitive.

b. Cluster II simulations (August 2001 meteorology)

The first day of the Cluster II simulations (August 10th, 2001 meteorology) produces a 1985-based exposure footprint similar to the Cluster I footprints with high (> 60) ppb concentrations in the eastern part of the valley (Figure 61A). For this day though, the high concentrations also extend to Hope, the Bellingham area and parts of southern Vancouver Island. Under the 2005 emissions, (Figure 61B) only a small region around Bellingham continues to experience exposures above 60 ppb. The VOC-NOx boundary moves from the

Mission area to the Langley area within the valley and down the North Shore Mountains to the valley floor.

On the second day (Figure 62A), the 1985-based footprint of 60+ ppb exposures covers the entire LFV, most of Harrison lake, much of the North Shore mountains and most of the Gulf Islands. Under the 2005 emissions (Figure 62B), up-valley, only the southeastern edges of the LFV have 60+ ppb exposures and along the north Shore mountains, high concentrations are seen only in and around the Pitt River and the Coquitlam lake areas. Between the two timeframes, peak 8-hr average exposures drop by up to 25 ppb. Interestingly, the VOC-NOx boundary shows little east-west displacement over the 20 year period, but shows a large north-south retreat over the North Shore mountains. The third day (Figure 63) shows many similarities with the second day in terms of both the change in the exposure footprint and VOC-NOx boundary. It is not surprising the exposure footprint for these last two days differs from the first given the shift in flow patterns through Juan de Fuca between the first and second days.

Only on the last two days does the Hope station change sensitivity (going from VOC- to NOx-sensitive on the second day) while all of the remaining stations showing VOC-sensitive conditions throughout. The different behaviour of VOC-NOx boundary to the emission changes seen in days two and three versus day one highlights the important role local circulation patterns have in influencing ozone sensitivity.

c. Cluster III simulations (July 1995 meteorology)

The first day of the Cluster III simulations (July 17th, 1995 meteorology) is interesting in that neither the 1985 nor the 2005 based emissions show regions with 8-hour averaged ozone concentrations exceeding 60 ppb (Figure 64). However, the VOC-NOx boundary responds to the emission changes by moving westward from its 1985 location between Langely and Abbotsford to the Surrey east (T15) area in 2005. The Pitt Meadows and Maple ridge stations also shift from VOC to NOx-sensitive conditions under this meteorology.

On the second Cluster III day, the 1985 emissions produce high (> 60 ppb) ozone exposures throughout much of the eastern part of the valley and over parts of the North Shore mountains (Figure 65A) Peak concentrations exceed 80 ppb south of Chilliwack over the Cascade mountains. Under 2005 emission levels (Figure 65B), no 60+ ppb regions are predicted and the VOC-NOx boundary is seen to shift from the Mission area to around the Surrey area (within the valley) and move down the North Shore mountains (in the western part of the LFV).

The behaviour of the third Cluster III day is different from the two previous days: high exposures (80+ ppb) are seen along a line running from the North Shore mountains through the Boundary Bay area and over to southern Vancouver Island with 60+ ppb exposures over much of the LFV west of Hope. With 2005-level emissions, only a thin finger of 60+ ppb exposures stretches across the western LFV, with another 60+ region east of Bellingham and a 65+ region over parts of the Gulf Islands. Under this meteorological pattern, the VOC-NOx boundary shows little east-west displacement but retreats southward from well over the North Shore mountains to almost the valley floor in the western LFV.

d. Cluster IIII simulations (July 1985 meteorology)

Finally, for the Cluster IIII simulations, the July 19th, 1985 meteorology (the first day) with the 1985-level emissions, produces its highest exposures (> 70 ppb) at the northern end of Pitt Lake with 60+ ppb concentrations mid-valley and 65+ ppb concentrations in the southeastern LFV along the northern flanks of the Cascade mountains (Figure 67A). Under 2005 emission levels (Figure 67B), all of the 60+ ppb regions disappear. The VOC-NOx boundary retreats westward as well, moving from around the Mission area to west of Abbotsford and down the coast mountains to almost valley bottom.

Before continuing on with days 2 and 3, it is interesting to compare predicted changes in exposure from the Hedley et al. (1998) CALGRID simulations with those predicted by the present CMAQ simulations (Figure 70). In these plots, the difference arising from 2005- and 1985-level emissions on the 1-hr average exposure have been plotted using the July 19, 1985 meteorology. It must be remembered that the Hedley et al. (1998) simulations are based on backcasted 1985 emissions and forecasted 2005 emissions while the present modeling uses backcasted emissions estimates for both 1985 and 2005, and that the latest backcasted inventories have substantially changed emission estimates from the late 1980's (Greater Vancouver Regional District 2007). Both plots are surprisingly similar with both showing the differences to be entirely negative (i.e. 2005 concentrations are lower than 1985 concentrations) and with the region with greatest change to lie between Pitt Lake and Harrison Lake. However, the present CMAQ modeling shows a much larger region with significant differences which extends south of Bellingham and over Juan de Fuca.

Using meteorology for the 20th (day two), the highest 1985-based exposures are over the Howe Sound and southern Vancouver Island areas (> 80 ppb); over the Boundary Bay area (> 75 ppb) and the North Shore mountains (> 70 ppb) (Figure 68A). Under 2005 emission levels (Figure 68B) the Howe Sound and North Shore regions drop below 60 ppb; the Vancouver Island region is reduced in size and concentration level; and only a thin 60+ region extends from Boundary Bay over Georgia Strait. Surprisingly, the VOC-NOx boundary does not dramatically change positions over the Howe Sound area, but does move down the North Shore mountains and westward within the valley.

On the third and final day, the 1985 exposure footprint shows peak concentrations well up Harrison Lake and along the very eastern part of the LFV, with additional high (> 60 ppb) regions over the Stave and Coquitlam lake areas (Figure 69A). A small part of southern Vancouver Island also has high concentrations, which is the only region that remains above 60 ppb under the 2005 emissions (Figure 69B). Finally, the VOC-NOx boundary retreats to the ridges along the North Shore Mountains (in the western part of the LFV) while along the valley floor in the eastern part of the LFV, it moves to around the Abbotsford area. It appears that Chilliwack changes sensitivity under this meteorology.

In summary, the ozone ridgeline in the eastern part of the LFV, appears to have moved westward during the 1985-2005 timeframe. For many of the modeled days, this shift has seen the ridgeline move from the Agassiz area to west of Abbotsford. In the western part of the LFV, the ridgeline has moved south, from the top of the North Shore Mountains to the edge of the urban areas. It has also moved south down Pitt Lake to the lake entrance. The ridgeline along the Cascade mountains in southeastern part of the LFV does not appear to have shifted much. Additionally, it appears that the VOC and NOx boundary is strongly influenced by local meteorological circulation.

By averaging the change of the modeled ozone exposure fields (between 1985 and 2005) over each day from each of the four exploration runs, a spatial picture of the evolution of the local ozone plume can be gained (Figure 71). This figure shows the greatest change (> 16 ppb) in 8-hr concentrations has been over the in the western part of the LFV, around the Pitt Lake region and north of Mission. The region of next greatest change (12 ppb) includes much of the North Shore Mountains, parts of Harrison Lake, and much of the eastern part of the valley from Abbotsford to just west of Hope. There is a noteable gap in the 12 ppb contour around Chilliwack. Locations near the downtown core see only a modest (< 8 ppb) change while the locations further east, including Port Moody, Pitt Meadows, and Surrey show changes between 8 to 12 ppb. While the magnitude of the changes in 8-hr averaged concentrations are reasonable, the spatial pattern does not quite mesh with the observed CWS trends. For example, the 12 ppb boundary should include the Port Moody area, and probably not extend into Abbotsford and the eastern part of the valley. One reason the modeled spatial distribution of the response of 8-hour averaged ozone concentrations to long term changes in precursor emissions is not entirely consistent with the observed CWS trends could be the averaging procedure. As the modeling has shown, the ozone plume is sensitive to meteorological conditions and so to be fair to the observational record, the averaging used to create this long term composite should have weighted each day by the frequency of that days' meso-scale meteorology.

12. Background sensitivity runs

To explore the influence of remote background ozone levels on maximum 8-hour averaged ozone concentrations within the LFV, a set of two additional runs using the 2001 episode were performed: one with background ozone set 10 ppb higher; and one set 10 ppb lower. This was achieved by adjusting the initial and boundary ozone concentrations as calculated from the RETRO analysis and used by the 36km runs. No other changes were made to the 36km runs, and the influence of the changed background ozone levels was passed on to the inner domains through the nesting processes. Generally, the effects of changing background ozone levels on maximum 8-hour ozone concentrations was uniformly felt across the LFV, with changes at most MV monitoring station locations being about 3.1 ppb change in the 8-hour average concentration for a 10 ppb change in background ozone. The maximum change was 3.7 ppb (T09) and minimum was 2.3 ppb (T12 and T29). It is interesting to note that, with respect to the 2001 emissions and meteorology, T12 and T29 were the most NOx-limited stations and were the least sensitive to changing background ozone. On the other hand, the two most sensitive stations T09 and T32 (3.6 ppb increase per 10 ppb background) were both VOC-limited yet a little downwind of the Vancouver downtown core. The spatial sensitivity to changing background concentrations can be explained as follows: tropospheric ozone formation involves a complex set of photochemical reactions which are dependent on intermediate species called radicals. The radical life cycle, and consequently the efficiency at which ozone can be produced, is dependent on reactions with VOC species in what are called propagation reactions (Jeffries 1995). In addition, radicals are readily produced by the photolysis of certain VOC species (e.g. formaldehyde) in what are called initiation reactions.

Thus the efficiency at which ozone can be produced via radical assisted reactions is closely tied to VOC concentrations. As a result, when a region is called VOC-sensitive, it should more properly be called radical-sensitive. But the important point to make is that ozone formation is also auto-catalytic, in that it can photolyze to produce to hydroxyl radicals itself. These newly created radical can react with VOCs to produce ozone, and as a result, ozone can act as a seed for its own production. Thus, at T09, an increase in background ozone concentration will lead to an increase in the radical pool – the factor limiting ozone production at this location – and hence a greater increase in ozone concentrations, than at a NOx-limited region (like T29) whose ozone production is not being limited by radical availability.

Several studies have recently shown increasing background ozone concentrations over Western North America (Vingarzan 2004) with summertime (JJA) estimates of between 0.43 ± 0.50 (Jaffe and Ray 2007) and 0.72 ± 0.55 (Chan and Vet 2010) ppb per year. Using a rough increase of 0.5 ppb/year over a 20 year period gives a 10 ppb background increase which would translate into a 3.0 ppb increase in 8-hour averaged ozone concentrations observed during an ozone episode.

13. Evolution of ozone sensitivity in the LFV

We now proceed to use the CMAQ predicted VOC-sensitivity, the yearly CWS values, and the observed ambient ozone, VOC and NOx concentrations to assemble a picture of the evolution of ozone sensitivity at three key MV monitoring stations in the LFV: T09 (Rocky Point Park), T12 (Chilliwack) and T29 (Hope).

a. T09

Figure 72 provides a schematic of an ozone response surface. Overlaid is an estimate of how the ozone response to VOC and NOx concentrations at T09 has changed over the 1985-2005 period (dashed red lines). For convenience, the T09 CWS ozone timeseries (upper left), a scaled timeseries plot of VOC and NOx emissions (upper left), and the yearly mean 8-average summertime (June 1 - August 31) VOC and NOx concentrations (restricted to days with VOC measurements) observed at T09 (lower left) have also been included.

The CMAQ retrospective simulations suggest that ozone concentration at T09 were VOC sensitive in both 1985 and in 2005, but with the ozone ridgeline migrating south towards the station over these 20 years, T09's sensitivity has likely moved closer to the ridgeline. The yearly CWS values show little change between 1985 and 1990 but shows a sustained drop between 1990 and 2000. Since 2000, the CWS value has been roughly constant. The yearly mean of the summertime observed VOC concentrations (restricted to those summer days which have both VOC and NOx measurements), shows a generally steady drop in ambient VOC concentrations from 1990 to the early 2000s with a slight decrease thereafter. Finally, the observed NOx concentrations show a decreasing trend from 1990 to 2000 with a slightly increasing trend from 2000 to 2005.

We have used all of the above information (the CMAQ predicted VOC-sensitivity, the yearly CWS values and the observed ambient VOC and NOx concentrations) to piece together an estimate of how T09's sensitivity to precursor emissions has likely changed over the 1985-2005 period. We have placed T09's 1985 sensitivity above the ridgeline with 1990's sensitivity located slightly to the right and lying on pretty much the same isopleth as 1985's.

This requires that ambient VOC concentrations increased only a little during this 5 year period while NOx concentrations remained roughly constant. While there are no NAPS VOC data to support this conclusion, the estimated VOC emissions from MV over this period show only slight increases, while the NOx emissions remain constant. We have located the sensitivity in 2000 much closer to the ridgeline (based on the CMAQ runs), to the left (in an area with lower VOCs as guided by the NAPS data), and below (in an area with lower NOx as inferred from the observed NOx concentrations) its estimated 1985 position. This transition, which crosses several isopleths, puts T09 in a region of lower ozone concentration which is consistent with the CWS trends. From 2000 to 2005, the observations suggest that T09 has moved slightly away from the ridgeline (due to the observed increases in VOC and decreases NOx in concentrations), but in order to be consistent with the observed unchanging CWS values, such a transition must have followed an isopleth. There is probably a lot of uncertainty in the evolution of T09's ozone sensitivity and the influence of meteorology on the idealized picture presented here would tend to make the description less straightforward.

Additional insight into the evolution of T09's ozone sensitivity can be gleaned from the observed diurnal ozone concentrations. In Figure 73, the average diurnal ozone concentrations from the 1985-1990 (red) and 2000-2006 (blue) periods is shown. The curves, derived from MV measurements, have been calculated by finding the seven days from each year with the highest hourly ozone concentration and then averaging those days' hourly concentrations together to get a single diurnal ozone profile for each year. Finally, the resulting six yearly profiles within each period were averaged together to get single, period-averaged, profiles and each period-profile has been normalized by its peak value to facilitate inter-period comparisons. This figure shows that, on average, the morning onset, afternoon peak and evening decay of ozone concentrations at T09 has been delayed by about an hour over the last 20 years. This temporal shift is consistent with slower chemical production, likely in response to a decrease in the reactivity (VOC/NOx ratio) of the air mass. Also evident in the figure is the incomplete nighttime titration in the 2000-2006 profile which is consistent with the reduction in ambient NOx concentrations seen over the 20 year interval. Diurnal profiles at T09 based on the CMAQ simulations using 1985 and 2005 emissions and averaged over the cluster I-IV simulations (not shown) do not reproduce the ≈ 1 hour delay in ozone formation but do reproduce the trend in the reduction of nighttime titration.

b. T12

A slightly different picture can be pieced together at T12 (Figure 74). There, the CMAQ modeling shows T12 has likely crossed over from VOC- to NOx-sensitive conditions (with the 2005 conditions close to the ridgeline). Again, with no VOC or NOx data between 1985 and 1990 to guide us, we have used the estimated LFV emissions to place the 1985 and 1990 sensitivities close to one another (with 1990 slight to the right) and above the ridgeline. Given the 1990-2000 emission changes, the CMAQ predicted shift in sensitivity, and the almost uniform observed CWS values, we infer a transition that follows an isopleth while moving towards the origin (i.e. to lower VOC and NOx concentrations) and crossing the ridgeline. It would appear that little change in sensitivity has occurred between 2000 and 2005. It is hard to interpret the big spike in NOx concentrations in 1998, but again with T12 being fairly far downwind of the major emission sources, local observed concentrations may only be loosely correlated with the actual upwind emissions driving ozone formation that is eventually observed at T12. Another point is that while emissions totals show decreasing VOC and NOx emissions between 2000 and 2005, these are total annual values averaged over the entire LFV. It is possible that emissions sources which impact T12 have not shown such a decrease, especially given the relative growth in the eastern part of the valley since the 1980s.

The evolution of the episodic diurnal ozone profile at T12 (Figure 75) also differs from what was observed at T09. The timing of ozone build up and peak concentrations has not noticeably changed, but the timing of the afternoon decline has slowed with relatively higher concentrations lingering into the late afternoon. As a consequence of this broadening of the diurnal profile, ozone metrics based on 8-hr averaging will increase even if the peak (hourly) concentration does not.

Finally, declining NOx concentrations can impact the efficiency at which ozone is produced. Ozone can be produced via the radical assisted oxidation of NO emissions ('new' NO) or via radical assisted oxidation of NO re-cycled from NO_2 photolysis ('old' NO). While NOx emission reductions always lower the mass of 'new' NO available in the photochemical reactions, the number of times an NO molecule can participate in the ozone oxidation cycle and hence the mass of 'old' NO typically increases as NOx emissions decrease. Thus the mass of NO reacting ('old' + 'new') does not necessarily decrease with decreasing NOx emissions and can be estimated through the ratio of ambient $[O_3]$ to ambient $[NOx]$ (Reynolds et al. 2003). Figure 76 shows a plot of mean yearly $[O_3]/[NOx]$ (blue dots) where each year's ratio has been calculated using ozone and NOx observations from the 7 days having the highest peak ozone concentration. For each day, 8-hour (1100-1800 PST) averages of both the NOx and ozone were first taken before calculating the day's $[O_3]/[NOx]$ ratio. Also included in the figure is the (statistically significant) linear regression through the data. The figure clearly shows an increase in the $[O_3]/[NOx]$ ratio between 1984 and 2006 suggesting an increase in ozone efficiency and hence the mass of NO reacting. While this estimate of ozone production efficiency does not take into account the effects of deposition or changing background levels, it does suggest that at T12, part of the benefits associated with NOx emission reductions have likely been offset by an increase in ozone efficiency. This effect is likely part of the reason that T12 has not experienced declining CWS values. The observational record also shows a increase in the episodic $[O_3]/[NOx]$ ratio at T09 (not shown) albeit with a much smaller increase. This suggests that there has only been a modest increase in ozone production efficiency at T09. The CMAQ-based diurnal timeseries at T12 (not shown) reproduce the trend towards a broadening of the diurnal ozone profiles around the peak, but with the broadening occurring equally before and after the peak. The CMAQ profiles also reproduce the trend towards less nighttime titration (not shown).

c. T29

A much different picture emerges at Hope (T29). Reconstructing Hope's behaviour is more difficult due to the shorter measurement period and CMAQ's difficulty reproducing T29's ozone concentrations throughout the model evaluation simulations. Nonetheless, CMAQ suggests that T29 was and still is NOx-limited (Figure 77. The nearly uniform CWS trend suggest emissions changes relevant to Hope have moved its sensitivity along an isopleth. The limited NAPS and concurrent MV measurements show decreasing VOC and NOx concentrations[8] which suggest a trajectory moving towards the origin. With the isopleth orientation in this region, it would appear that any reductions in ambient VOC concentrations would have had little influence on observed ozone concentrations. The lack of long term measurement data at T29 prevents an analysis of the change in the diurnal ozone profile or the change in ozone production efficiency but it is suspected that the lowering of ambient NOx concentrations in the LFV has lead to increased ozone efficiency at this site and likely a broadening of its diurnal ozone profile. The increase in ozone efficiency would counteract NOx emissions reductions and the change in diurnal profile would tend to boost 8-hr averages (relative to 1-hr averages).

14. VOC-NOx boundary and uncertainty

Generally, the VOC/NOx sensitivity of a location changes throughout day and is not a fixed geographic entity. For instance, at most locations, morning rush hour emissions create an excess of NOx leading to VOC-limited conditions. As the day progress and temperatures warm, there is increased evaporative VOC emissions. Also, biogenic VOC emissions tend to peak near mid-day. Finally, NOx is readily removed from an air mass through deposition and other chemical processes. As a result, many locations, especially those downwind of urban areas, tend to evolve from VOC-limited to NOx-limited in the afternoon. In Figure 78 timeseries plots of $[O_3]/[NOy]$ throughout the 2001 simulation at the T01, T09, T12 and T29 stations are shown (blue lines). The timeseries have only been plotted between the hours

[8] Again, these measurements may not be indicative of the actual upstream VOC and NOx emissions driving the observed ozone concentrations at Hope given its distance from the urbanized parts of the LFV.

of 1000 and 2000 PST because the early morning and nighttime values of $[O_3]$ and $[NOy]$ are indicative of local ozone titration and NOx emissions and not ozone production under fair weather conditions. Also shown in each plot is the critical $[O_3]/NOy$ threshold (red line) indicating VOC-limited conditions below and NOx-limited conditions above the red line.[9] At T01, because of the presence of large NOx sources, the timeseries always shows VOC-limited conditions with very little change in the indicator ratio throughout the day. At T09, the timeseries still shows, despite the large $[O_3]/NOy]$ variability, VOC-limited conditions at all times except at the very beginning. It is likely that this excursion into NOx-limited conditions is an artifact of the model spin-up period. At T12, the timeseries suggests the station becomes NOx-limited in the afternoon on the 10th and 11th but not on the 12th or 13th. At Hope, NOx-limited conditions are predicted every afternoon with VOC-limited conditions only in the morning and late evening.

Finally, as many of the spatial plots showing the VOC/NOx boundary indicate, on any given day, meteorology has a strong influence on the location of VOC and NOx-limited areas. With the VOC/NOx boundary being diagnosed using the $[O_3]/[NOy]$ ratio and not through actual sensitivity runs, this leads to additional uncertainty in the actual ozone sensitivity at a given station.

[9]It must be mentioned here that the critical threshold identifies the ridgeline on an isopleth diagram and that the region just below the ridgeline on an isopleth diagram is more properly called a region of mixed- rather than NOx-sensitivity. The region of true NOx-sensitivity occurs below and to the right of the ridgeline where the isopleths become parallel to the x-axis. In the region just below the ridgeline, both NOx and VOC controls will be effective in reducing ozone concentrations. This mixed-sensitivity region is usually quite narrow and a little subjective in defining. Nonetheless, indicator values only slightly greater than the critical threshold would indicate mixed-sensitivity conditions.

15. 1.33km Resolution Simulations

One of the main concerns with using the CMAQ model to answer the research questions is its difficulties in reproducing the observed ozone concentrations at Hope (T29). A clear example of these shortcomings is evident in the simulation of the 2006 episode. In Figure 79 the observed (red) and CMAQ 4km (blue) T29 ozone timeseries have been re-plotted (upper panel). The plot clearly shows ozone concentrations at T29 building during the event (peak afternoon concentrations increase each day) while nighttime low concentrations fall to near zero values each night. The modeled ozone concentrations show a much more muted build up and have nighttime values not dropping below 40 ppb. It was believed that one of the causes for this poor behaviour was the model's inability to reproduce the steep topography and narrow valleys at this end of the LFV. It was hoped that by increasing the model resolution, CMAQ would have a better handle on the horizontal advection and vertical hand-over processes in and around this part of the LFV. To test this, the 2006 event was re-run at a 1.33km resolution over a small (73x124) domain covering the LFV and parts of Georgia Strait. No changes were made to the emissions inventory other than re-gridding the 4km fields to the 1.33km domain. The resulting ozone timeseries at T29 (green) has been plotted with the original 4km and observations in Figure 79. The difference between the 4 and 1.33 km runs is given in the lower plot. The results show that during the daytime, the 1.33km ozone concentrations are slightly higher than the 4km runs (negative differences) although, with the exception of the 27th, nighttime values are also slightly higher to. In general, the increased model resolution has made little difference to ozone concentrations at Hope. It appears that inadequate model resolution is not the factor holding the model back at this location and it is a bit of a puzzle as too what is contributing to poor model performance here. Due to Hope's NOx-limited nature, a lack of NOx emission sources upwind of T29 might be the cause of the low daytime predictions and a lack of local NOx sources might be the cause of the nighttime over-predictions.

16. Ozone production above the surface and role of day-to-day carryover

The modeled ozone concentration produced at a station only tells part of the story. The final concentration represents a balance between various competing processes like transport (both advection and turbulent diffusion), chemistry and deposition. Furthermore, the surface concentrations are intimately tied to ozone production above the surface through vertical exchange processes (McKendry and Lundgren 2000). The IPR facility in the CMAQ model, allows extraction of the relative importance of the major processes contributing to a modeled concentration at each timestep. In Figures 80 and 81, the net contribution of chemistry, transport (from advection and turbulent dispersion in both the horizontal and vertical) and deposition, over the 8-hr leading up to peak modeled ozone concentrations at the downtown T01 station and at the entrance to Pitt Lake, during the 2001 simulation are given at all the model vertical levels in the lowest 750 m of the PBL.

At the downtown T01 station, the modeled ozone timeseries shows that leading up to the 71 ppb peak observed on the 11th, local modeled surface concentrations rose a little over 60 ppb (the red segment in the timeseries plot). That 60 ppb gain was caused by a nearly 250 ppb gain from transport which was partially offset by 47 ppb loss by deposition (not shown) and and a 140 ppb loss due to chemistry (likely ozone titration stemming from abundant local NOx emissions). Above the surface, the story is a little different: ozone production due to chemical processes becomes positive above 100m, likely due to the lack of elevated NOx sources, but transport is almost zero and becomes negative above 300 m. The overall effect is for net ozone production to rise just above the surface (likely due to absence of depositional and chemical losses) and then decline to under 40 ppb at 750 m agl. Likely, the lack of upper-level production from transport arises from low ozone air being advected into T01 from either upwind downtown areas or from Georgia Strait. The high transport at the surface likely arises from vertical transport of relatively rich ozone air aloft down to the surface through convection. Conversely, convection of surface NOx-rich air aloft likely causes the negative chemical production rates seen above the surface.

At Pitt Lake, net surface ozone production is somewhat less (≈ 50 ppb) with both chemistry (≈ 80 ppb) and transport (≈ 140 ppb) leading to positive production while deposition at -170 ppb (not shown) offsets most of the production. At this location, chemical production is positive at all levels while transportation is negative except at the surface. Ozone production steadily decreases with height to a minimum of ≈ 25 ppb at 800 m.

The process analysis at both these sites highlight how ozone production occurs throughout the mixed layer and how upper-level production influences surface concentrations through transport processes. These findings are consistent with the Pottier et al. (2000) process analysis of UAM-V model output and the many upper air ozone field studies (McKendry (1997), Pisano et al. (1997), McKendry et al. (1998b), McKendry et al. (1998a) and Salmond and McKendry (2002)).

17. Relative importance of changing spatial surrogates and emissions levels on ozone formation

The last model runs performed were designed to test the relative importance of changing emission levels versus changing spatial surrogates on the modeled 2005-1985 differences in ozone concentrations. This was achieved with two additional runs: one with 1985 emission levels but spatial surrogates appropriate for 2005; and the other with 2005 emission levels but with 1985 spatial surrogates. These runs were performed using the 2006 (cluster I) meteorology. These simulations produced ozone maxima over the eastern part of the valley (Figure 48).

Figure 82 shows timeseries plots of the difference in modeled average diurnal ozone concentrations (in ppb) at T01, T09, T12 and T29 between the runs with: 1985 emissions/1985 spatial surrogates and 2005 emissions/2005 spatial surrogates (red curves); 1985 emissions/2005 spatial surrogates and 2005 emissions/2005 spatial surrogates (blue curves); 2005 emissions/1985 spatial surrogates and 2005 emissions/2005 spatial surrogates (green curves). The red curves represent the difference in ozone concentrations arising from both emission and spatial surrogate changes, the blue curves from emissions changes only and the green curves from changing spatial surrogates only. In principle, at any time, the differences due to emissions only (blue curve) and to spatial surrogate changes only (green curve) should equal the differences due to changes in both (red curve), but they often do not because of the non-linearity in ozone formation.

At the downtown T01 station, changing the spatial distribution of emissions (green line) has a generally small negative effect on ozone concentrations, that is, ozone concentrations are slightly higher using the 2005 spatial distribution than when using the 1985 distribution. Likely, under the 2005 distribution, while the total precursor emission rates are unchanged, they are more spread out resulting in less NOx titration around the downtown core. Changing the emission levels (blue curve) also has a generally small negative influence, again implying ozone concentrations are generally slightly higher under 2005 emission levels, except during the afternoon (time of peak concentrations here; not show) where the blue curve is slightly positive.

At T09, the differences arising from changes to spatial surrogates (green line) peak in the early morning and late afternoon but are generally small (less than 5 ppb) and are generally much less than differences due to emissions (blue curve). These changes are negative throughout the nighttime and until around noon when they become positive. The negative nighttime differences (i.e. higher nighttime ozone concentrations under the 2005 emission scenario) likely, reflect lower nighttime titration under 2005 emission levels. After noon, the differences are positive are larger, and this can be attributed to the higher 1985 precursor emissions rates facilitating more ozone production. From the figure, from the maximum difference of 6 ppb (seen at 1600 and coincident with time of peak concentration; not shown), 4 ppb can be attributed to changes in emissions levels and 2 ppb to changes in the spatial distribution of these emissions.

At T12, the effect of spatial surrogate changes is positive and generally small (green) until around 1600 when it becomes as important as emissions changes (2000) which is after the 1800 time of average modeled peak ozone (not shown). Until 1600, almost all of the difference in ozone concentrations (red) can be attributed to changes in emission levels (blue). At the time of peak concentration, the 28 ppb difference can be divided into an 18 ppb stemming from emission changes and a 10 ppb due to spatial surrogate changes. Notice that the positive nature of the differences due to the spatial surrogate (green curve) implies the changes in landuse and population between 1985 and 2005 have resulted in *decreasing* ozone concentrations (with emission levels being held fixed). The only explanation we have at the present time is that under the 2005 spatial distribution, precursors emissions from the Vancouver urban area are being released over a larger area with proportionally less released within those upstream areas impacting Chilliwack.

At Hope (T29), a picture similar to T12 is observed: the influence of spatial surrogate changes is important only in the afternoon and during the day it is essentially negligible. At the time of modeled average peak concentration (2100; not shown) the 21 ppb reduction in ozone concentration (red curve) can be partitioned into a 13 ppb reduction from emission level changes (blue) and a 8 ppb reduction from changes to the spatial distribution (green). At T29 and T12, the higher precursor emission rates under the 1985 levels (blue curves) do not influence the morning ozone concentrations to the same extent as they do at T09 (where they fall by up to 10 ppb). This suggests that at T12 and T29, it is upwind precursor emissions that influence ozone at these stations with the local influence of changing emission rates having little direct impact of modeled ozone concentrations.

In general, modeled ozone is sensitive to both absolute level of emissions as well as their spatial distribution. The shift from the 1985 to 2005 spatial distribution seems to allow ozone concentrations up-valley to remain higher later in the day, perhaps in response to a more diffuse upwind plume of precursors. Also at these up-valley locations, it is the afternoon ozone concentrations that are most effected by changing emission rates. These results are only for one meteorological pattern – one that is conducive to highest ozone concentrations in the eastern part of the valley. Additional runs using the other meteorological regimes need to be performed to see how robust these findings are.

18. Research Questions Revisited

We return now to a discussion of the original research questions in light of our modeling results:

What has caused the relative decline in ozone air quality in the upper part of the Lower Fraser Valley (Abbotsford to Hope) over the past decades?

and

What is the relative importance of changes in emissions (reactivities as well as amounts) as compared to spatial shifts in emissions densities in governing the noted spatio-temporal changes in LFV air quality over the past two decades?

We answer these questions by contrasting both model results and observations at T09 with those at T12. Both stations have long and mostly complete observational records, are reasonably well modeled by the present CMAQ analysis and can be considered representative of air quality in the western and eastern parts of the LFV.

Based on the current modeling, and consistent with previous studies (Steyn et al. (1996), Jiang et al. (1997), Suzuki (1997), Pryor (1998), Hedley et al. (1998), Pottier et al. (2000) and Ainslie (2004)), T09 has been and remains a VOC-sensitive location. Based on the preceding analyses, we infer that the large VOC emission reductions, stemming from LDV and petroleum refining emission controls, have been effective in reducing ozone concentrations at T09. Part of the benefits of the VOC emissions reductions have likely been offset by the concomitant NOx emission reductions that have occurred in and around the Vancouver urbanized area. Nonetheless, these precursor emissions reductions have led to decreasing 1-hr and 8-hr episodic ozone concentrations.

At T12, it appears the station has gone from being VOC-limited to NOx-limited over the last 20 years. It is possible that the station's present sensitivity lies only slightly below the ridgeline on an isopleth diagram and as such it is sensitive to both NOx and VOC emissions. The true extent of T12's present NOx-sensitivity is difficult to asses given the modeling uncertainties and the variability of the ridgeline with respect to meteorological conditions. Additionally, VOC reductions (largely from the LDV VOC emission controls with the petroleum refining emissions not being greatly influential here) along with NOx emission reductions, appear to have offset one another in terms of ozone production at this part of the LFV. Furthermore, ozone production efficiency as a function of NO, has increased noticeably in this part of the valley. This efficiency increase has likely offset some of the benefits resulting from NOx emission reductions. The change in ozone sensitivity, along with the increased ozone production efficiency have changed the shape of the diurnal ozone profile to one that is less peaked around the daily maximum. As a result of this broadening, for a fixed peak ozone level, 8-hour averaged concentrations calculated around the peak concentration are increased. Finally, changes in population and economic activity over the 1985-2005 period have likely had a greater impact at T12 than T09. However, compared to the absolute changes in precursor emissions seen over the LFV during this period, the effects of this differential growth are likely small. The net effects of these changes has been a modest decline in peak 1-hr ozone concentrations (mainly since the late 1980's and early 1990's) with a weakly (and not statistically significant) declining trend in 8-hour averaged concentrations.

It is difficult to comment on the observed ozone trends at Hope due to its more limited observational record and the difficulties the CMAQ modeling had capturing ozone formation there. Nonetheless, it is fairly evident that Hope has been and remains a NOx-limited region and that ozone production efficiency with respect to NO has likely increased here as well. Such an increase would have offset some, and perhaps all of the NOx emissions reductions achieved in the LFV. VOC emission reductions have likely had negligible impact on ozone concentrations at T29. Increased growth in the eastern part of the LFV has also likely negatively affected air quality at Hope, but it is difficult to quantify this effect without better modeling abilities in this part of the LFV.

19. Conclusions

- The WRF-SMOKE-CMAQ modeling system produces ozone fields over the 20 year retrospective period which are responsive to the estimated changes in local precursor emissions and are in generally good agreement with observations taken by the MV monitoring network. Some of the modeled episodes show better comparisons with observations than others, and this, in part, can be traced back to errors in the meteorological modeling.

- Many of the simulations show the highest ozone concentrations to occur outside of the area sampled by the fixed monitoring network and within the LFV's numerous tributary valleys. These findings are consistent with previous observational studies

(McKendry et al. (1998b), McKendry et al. (1998a)).

- Precursor emission reduction within the LFV have generally move the ozone ridgeline boundary westward from the Agassiz-Chilliwack area to the Abbotsford-Langley area and southward from the ridges of the North Shore Mountains to the valley floor near Port Moody, Coquitlam and Pitt Meadows. However, the ozone ridgeline is sensitive to meteorology (mainly wind direction and wind speed) and shows a great deal of variability within and between ozone episodes.

- Based on the current modeling and consistent with previous studies, we find the Port Moody (T09) station has been and remains a VOC-sensitive location. Based on the current modeling and observational data, we infer that the large VOC emission reductions that have occurred within the LFV over the 1985-2005 period, stemming largely from the LDV and petroleum refining sectors, have been effective in reducing ozone concentrations at T09. Some of the benefits of the VOC emissions reductions have likely been offset by the concomitant NOx emission within the LFV. Nonetheless, the local NOx and VOC emissions reductions have been responsible for the decreasing 1-hr and 8-hr episodic ozone concentrations seen at this station. Although there is not the observation data to confirm this, the modeling suggests the western areas of the LFV surrounding Port Moody (Coquitlam, Port Coquitlam and Pitt Meadows) have likely responded to these same precursor emissions changes in a similar fashion.

- Based on the modeling, we find in the eastern part of the LFV around Chilliwack, has generally gone from being VOC-limited to NOx-limited over the last 20 years, although the ozone ridgeline shows a lot of variability with meteorological conditions. It is possible that presently this region has a mixed-sensitivity. Additionally, we suspect that VOC reductions (largely from the LDV VOC emission controls with the petroleum refining emissions not being as greatly influential here as at Port Moody) and NOx emission reductions, appear to have offset one another in terms of ozone production in this part of the LFV. Furthermore, based on the observational data, ozone production efficiency as a function of NO has increased noticeably at T12 and likely in the other eastern parts of the valley. This efficiency increase has likely offset some of the benefits resulting from NOx emission reductions. The change in ozone sensitivity, along with the increased ozone production efficiency have changed the shape of the diurnal ozone profile to one that is less peaked around the daily maximum. As a result of this broadening, for a fixed peak ozone level, 8-hour averaged concentrations calculated around the peak concentration are increased. Finally, changes in population and economic activity over the 1985-2005 period have likely had a greater impact at T12 than T09. However, compared to the absolute changes in precursor emissions seen over the LFV during this period, the effects of this differential growth are likely small. At Chilliwack and the surrounding areas, the net effects of these changes has been a modest decline in peak 1-hr ozone concentrations (mainly since the late 1980's and early 1990's) with a weakly (and not statistically significant) declining trend in 8-hour averaged concentrations.

- In the easternmost part of the LFV, around Hope, the CMAQ modeling has difficulties capturing ozone formation. It is believed that this difficulty is due to narrow valley and steep topography near the station; deficient modeled NOx sources upwind of T29 and deficient modeled NOx sources around the station. Nonetheless, based on the modeling, it is fairly evident that Hope has been and remains a NOx-limited region and based on the observational data at Chilliwack, that ozone production efficiency with respect to NO has likely increased here as well. Such an increase would have offset some, and perhaps all of the NOx emissions reductions achieved in the LFV. Due to its NOx-sensitive conditions, VOC emission reductions within the LFV have likely had negligible impact on ozone concentrations at T29. Increased growth in the eastern part of the LFV has also likely negatively affected air quality at Hope, but it is difficult to quantify this effect without better modeling abilities in this part of the LFV.

- The model suggests that the Saturna Island CAPMON station is regularly subjected to high summertime ozone levels originating in the Vancouver and Victoria regions, consistent with the findings of Vingarzan and Thomson (2004). Care must be taken when using data from this station to study background air pollution trends.

- The modeling suggests that for every 10 ppb increase in background ozone concentration a roughly 3.0 ppb increase in 8-hour ozone concentrations would be observed in the LFV, with slightly higher increases expected in the western parts (3.7 ppb) of the LFV than the eastern parts (2.3 ppb). Based on recent studies showing increasing background ozone concentrations over Western North America (Vingarzan (2004), Jaffe and Ray (2007), Chan and Vet (2010)), over the next 20 years and within the LFV, a 3.0 ppb increase in episodic 8-hour averaged ozone concentrations could be expected, independent of local air quality management planning.

- The model consistently over-predicts ozone at a number of stations within the city of Vancouver (T04, T06) and under-predicts daytime NOx concentrations there. Both results are consistent with a deficiency in NOx emissions. Given the dominant role that marine, off-road and LDV emissions play as a local NOx sources, episodic emission rates from these sources need to be investigated further. Additionally, the model tends to under-predict ozone concentrations at Hope, also suggesting deficient modeled NOx sources within the LFV. The model shows a changing bias over time which also suggests uncertainties in the emissions backcasting.

- Trajectory modeling suggests that emissions and ozone from the Puget Sound region do not directly impact LFV air quality during summertime ozone episodes.

20. Recommendations

Here we present a few recommendations for relatively limited measurement and modeling programmes designed to increase confidence in the mechanistic interpretations of our modeling results from the preceding sections.

- The model consistently shows T09 to be VOC-sensitive while T12 to have changed from VOC- to NOx-sensitivity (or possibly mixed-sensitivity) over the two decades spanned by our study. Because of the different behaviour of VOC- and NOx-sensitive conditions to emission reductions, it is important to test these model results experimentally. Measurements of $[O_3]/[NOy]$ taken along transects running from downtown Vancouver to both T09 and T12, on an ozone episode day, should be compared with model simulations. A categorical evaluation of the observations and model output, in terms of $[O_3]/[NOy]$ being below or above the ridgeline threshold, would be helpful in this regard (Arnold et al. 2003). The Metro Vancouver mobile air monitoring units might be suitable for such a test.

- Many of the simulations show high ozone levels outside of the area sampled by the fixed monitoring network. Such behaviour is consistent with the few measurements taken outside of the valley (McKendry et al. (1998b), McKendry et al. (1998a)). The use of remote sensing data would be helpful in further validating this behaviour (Herron-Thorpe et al. 2010).

- The SMOKE-generated emissions inventory is a key component of the modeling study yet it is difficult to directly test its veracity through observations. In order to strengthen our confidence in the inventory in particular and the modeling in general, the development of daily, episode specific emissions should be undertaken with a closer collaboration with the Metro Vancouver air emissions group. This would be especially useful in the speciation of VOC emissions, where the present inventory seems to over-predict alkanes and under-predict aromatics. Additionally, the model persistently under-predicts NOx concentrations in the in urbanized Vancouver area. Given the important role that marine, off-road and LDV emissions play as a local NOx sources in this area, and given that annual NOx emissions estimates from the marine source have been recently revised (The Chamber of Shipping (2007), Greater Vancouver Regional District (2007)), more effort is likely needed to accurately represent marine, off-road and LDV NOx emissions in the summertime episodic emissions inventory.

- Additional CMAQ runs with the IRR process analysis configured to track the mass of NO reacted and the cycling of NO within the photochemical system would be useful for comparisons with the observed increase (with respect to the 1985-2005 period) in ozone production efficiency (as diagnosed from the $[O_3]/[NOx]$ ratio)

Acknowledgments.

Funding for this work was provided by NSERC (in the form of grants to D.G. Steyn and P.L. Jackson), with two years of support from the BC Clean Air Research fund (BC CLEAR), two years of support from the Fraser Valley Regional District, and one year of support from Metro Vancouver. Hugh Sloan and Bob Smith provided valuable encouragement and support throughout. We wish to also thank Trudi Trask at the Metro Vancouver Policy and Planning Department – Air Quality Policy and Management for the MOBILE6.2C inputs and help in implementing model. Brett Taylor at Environment Canada for MOBILE6.2C source code. Derek Jennejohn at Metro Vancouver for help with emissions inventory. Sally Otterson at the Washington State Department of Ecology for the MOBILE6.2 inputs. Roxanne Vingargan at Environment Canada for NAPS data. Lori Neary York University with help converting data files. Craig Stroud at Environment Canada for his BELD3 adjusted landuse tiles. Gail Tonnesen University of California (Riverside) for help with the CMAQ process analysis modeling. Ken Reid, Gerald Chen and Richard Visser for the LFV population data. Brian Klinkenburg in the UBC Geography Department for GIS work with the population data. Weimin Jiang at the National Research Center (NRC) for model output.

REFERENCES

Ainslie, B., C. Reuten, D. G. Steyn, N. D. Le, and J. V. Zidek, 2009: Application of an entropy-based Bayesian optimization technique to the redesign of an existing monitoring network for a single air pollutant. *Journal of Environmental Management*, **90**, 2715-2729.

Ainslie, B. and D. G. Steyn, 2007: Spatiotemporal trends in episodic ozone pollution in the Lower Fraser Valley, British Columbia, in relation to mesoscale atmospheric circulation patterns and emissions. *Journal of Applied Meteorology and Climatology*, **46**, 1631-1644.

Ainslie, B. D., 2004: A photochemical model based on a scaling analysis of ozone photochemistry. Ph.D. thesis, University of British Columbia, Vancouver, B.C., Canada, 311 pp.

Arnold, J. R., R. L. Dennis, and G. S. Tonnesen, 2003: Diagnostic evaluation of numerical air quality models with specialized ambient observations: testing the Community Multiscale Air Quality modeling system (CMAQ) at selected SOS 95 ground sites. *Atmospheric Environment*, **37**, 1185–1198.

Banta, R. M., et al., 1997: Nocturnal cleansing flows in a tributary valley. *Atmospheric Environment*, **31**, 2147–2162.

Barna, M., B. Lamb, S. O'Neil, H. Westberg, C. Figueroa-Kaminsky, S. Otterson, C. Bowman, and J. DeMay, 2000: Modeling ozone formation and transport in the cascadia region of the Pacific Northwest. *Journal of Applied Meteorology*, **39**, 349–366.

Batchvarova, E., X.Cai, S.-E. Gryning, and D. G. Steyn, 1999: Modelling internal boundary-layer development in a region with a complex coastline. *Boundary-Layer Meteorology*, **90**, 1–20.

Boulton, J. W., M. Gauthier, X. Qiu, M. Lepage, and C. d. Cenzo, 2009: Emission inventory preparation and air quality modelling in the Pacific Northwest. URL `http://www.epa.gov/ttnchie1/conference/ei12/modeling/boulton.pdf`.

Bovis, P. E., 2003: Stratosphere troposphere exchange and its influence on surface ozone concentrations in the Lower Fraser Valley. M.S. thesis, University of British Columbia, Vancouver, B.C., Canada, 120 pp.

Byun, D. and K. L. Schere, 2006: Review of the governing equations, computational algorithms, and other components of the models-3 community multiscale air quality (CMAQ) modeling system. *Applied Mechanics Reviews*, **59**, 51–77.

Cai, X. M., R. A. S. Hourston, and D. G. Steyn, 2000: A numerical study of meteorological conditions during Pacific 93. *Atmosphere-Ocean*, **38**, 457–479.

Cai, X. M. and D. G. Steyn, 2000: Modelling study of sea breezes in a complex coastal environment. *Atmospheric Environment*, **34**, 2873–2885.

Canadian Council of Ministers of the Environment, 2000: Canada-wide stantards for particulate matter (PM) and ozone. Tech. rep., CCME, Quebec City, PQ.

Chan, E. and R. J. Vet, 2010: Baseline levels and trends of ground level ozone in Canada and the United States. *Atmospheric Chemistry and Physics*, **10**, 8629–8647.

Doraiswamy, P., et al., 2009: A diagnostic comparison of measured and model-predicted speciated VOC concentrations. *Atmospheric Environment*, **43**, 5759–5770.

Draxler, R. and G. Hess, 1997: Description of the hysplit 4 modeling system. Tech. rep., NOAA Tech Memo ERL ARL-224, 24 pp pp. URL `http://www.arl.noaa.gov/documents/reports/arl-224.pdf`.

Galmarini, S., D. G. Steyn, K. L. Schere, and M. D. Moran, 2010: Advancing the evaluation of regional-scale air quality models. Tech. Rep. 2010JRC56481, Office for Official Publications of the European Communities.

Gilliam, R. C., C. Hogrefe, and S. T. Rao, 2006: New methods for evaluating meteorological models used in air quality applications. *Atmospheric Environment*, **40**, 5073–5086.

Greater Vancouver Regional District, 1994: GVRD Air Quality Management Plan. Tech. rep., GVRD Policy and Planning Department, Burnaby, B.C.

Greater Vancouver Regional District, 2003: Forecast and backcast of the 2000 emissions inventory for the Lower Fraser Valley airshed 1985-2025. Tech. rep., GVRD Policy and Planning Department, Burnaby, B.C.

Greater Vancouver Regional District, 2005: GVRD Air Quality Management Plan. Tech. rep., GVRD Policy and Planning Department, Burnaby, B.C.

Greater Vancouver Regional District, 2007: 2005 Lower Fraser Valley air emissions inventory & forecast and backcast. Tech. rep., GVRD Policy and Planning Department, Burnaby, B.C.

Guenther, A., T. Karl, P. Harley, C. Wiedinmyer, P. I. Palmer, and C. Geron, 2006: Estimates of global terrestrial isoprene emissions using MEGAN (Model of Emissions of Gases and Aerosols from Nature). *Atmospheric Chemistry and Physics*, **6**, 3181–3210.

Hedley, M., W. Jiang, R. McLaren, and D. L. Singleton, 1998: Modeling of future-year emissions control scenarios for the Lower Fraser Valley: Impacts of natural gas and propane vehicle technologies. *Journal of Applied Meteorology*, **37**, 1190–1204.

Hedley, M., R. McLaren, W. Jiang, and D. L. Singleton, 1997: Evaluation of an air quality simulation of the Lower Fraser Valley - II. Photochemistry. *Atmospheric Environment*, **31**, 1617–1630.

Hedley, M. and D. L. Singleton, 1997: Evaluation of an air quality simulation of the Lower Fraser Valley - I. Meteorology. *Atmospheric Environment*, **31**, 1605–1615.

Herron-Thorpe, F. L., B. K. Lamb, G. H. Mount, and J. K. Vaughan, 2010: Evaluation of a regional air quality forecast model for tropospheric NO2 columns using the OMI/Aura satellite tropospheric NO2 product. *Atmospheric Chemistry and Physics*, **10**, 8839–8854.

Hoff, R. M., M. Harwood, A. Sheppard, F. Froude, J. B. Martin, and W. Strapp, 1997: Use of airborne lidar to determine aerosol sources and movement in the Lower Fraser Valley (LFV), BC. *Atmospheric Environment*, **31**, 2123–2134.

Houyoux, M. R. and J. M. Vukovich, 1999: Updates to the sparse matrix operator kernel emissions modeling system (SMOKE) and integration with Models-3. *The Emissions Inventory: Regional Strategies for the Future*, Raleigh, NC, Air and Waste Management Association.

Jaffe, D. and J. Ray, 2007: Increase in surface ozone at rural sites in the Western US. *Atmospheric Environment*, **41**, 5452–5463.

Jeffries, H. E., 1995: *Composition, Chemistry & Climate*, chap. 9. Photochemical Air Pollution, 308–348. Van Nostand-Reinhold.

Jiang, G., B. Lamb, and H. Westberg, 2006: Using back trajectory and process analysis to investigate photochemical ozone production in the Puget Sound region. *Atmospheric Environment*, **37**, 1489–1502.

Jiang, W., M. Hedley, and D. L. Singelton, 1998: Comparison of the MC2/CALGRID and SAIMM/UAM-V photochemical modelling systems in the Lower Fraser Valley, British Columbia. *Atmospheric Environment*, **32**, 2969–2980.

Jiang, W., D. L. Singelton, M. Hedley, and R. McLaren, 1997: Sensitivity of ozone concentrations to VOC and NOx emissions in the Canadian Lower Fraser Valley. *Atmospheric Environment*, **31**, 627–638.

Joe, H., D. G. Steyn, and E. Susko, 1996: Analysis of trends in tropospheric ozone in the Lower Fraser Valley, British Columbia. *Atmospheric Environment*, **30**, 3413–3421.

Johnson, G. M., 1984: A simple model for predicting ozone concentration of ambient air. *Proceedings of the Eighth International Clean Air Conference*, Melbourne Australia, 716–731.

Kain, J. S., 2004: The Kain-Fritsch convective parametrization: an update. *Journal of Applied Meteorology*, **43**, 170–181.

Krzyzanowski, J., I. G. McKendry, and J. L. Innes, 2006: Evidence of elevated ozone concentrations on forested slopes of the Lower Fraser Valley, British Columbia,Canada. *Water, Air and Soil Pollution*, **173**, 273–287.

Le, N. D. and J. V. Zidek, 2006: *Statistical analysis of environmental space-time processes*. Springer, New York, NY.,USA.

Lefohn, A. S., D. S. Shadwick, and S. D. Ziman, 1998: The difficult challenge of attaining EPA's new ozone standard. *Environmental Science & Technology*, **32**, 276A–282A.

Li, S. M., 2004: A concerted effort to understand the ambient particulate matter in the Lower Fraser Valley: The Pacific 2001 Air Quality Study. *Atmospheric Environment*, in press.

Mass, C. F., et al., 2003: Regional environmental prediction over the Pacific Northwest. *Bulletin of the American Meteorological Society*, **84**, 1353–1366.

McKendry, I. G., 1994: Synoptic circulation and summertime ground-level ozone concentration at Vancouver, British Columbia. *Journal of Applied Meteorology*, **33**, 627–641.

McKendry, I. G., 1997: Elevated ozone layers and vertical down-mixing over the Lower Fraser Valley, B.C. *Atmospheric Environment*, **31**, 2135–2146.

McKendry, I. G. and J. Lundgren, 2000: Tropospheric layering of ozone in regions of urbanized complex and/or coastal terrain: a review. *Progress in Physical Geography*, **24**, 329–354.

McKendry, I. G., D. G. Steyn, R. M. Banta, W. Strapp, K. Anlauf, and J. Pottier, 1998a:

Daytime photochemical pollutant transport over a tributary valley lake in Southwestern British Columbia. *Journal of Applied Meteorology*, **37**, 393–404.

McKendry, I. G., D. G. Steyn, S. O'Kane, P. Zewar-Reza, and D. Hueff, 1998b: Lower tropospheric ozone measurements by light aircraft equipped with chemiluminescent sonde. *Journal of Atmospheric and Oceanic Technology*, **15**, 136–143.

Miao, Y. and D. G. Steyn, 1994: Mesometeorological modelling and trajectory analysis during an air pollution episode in the Lower Fraser Valley, BC. *Transactions of Regional Photochemical Measurement and Modelling Studies Conference*, 249–281.

Otte, T. L. and J. E. Pliem, 2010: The Meteorology-Chemistry Interface Processor (MCIP) for the CMAQ modeling system: updates through MCIPv3.4.1. *Geoscientific Model Development*, **3**, 243–256.

ONeill, S. M., et al., 2006: Modeling ozone and aerosol formation and transport in the Pacific Northwest with the Community Multi-scale Air Quality (CMAQ) modeling system. *Environmental Science and Technology*, **40**, 1286–1299.

Pielke, R. A., et al., 1992: A comprehensive meteorological modeling system–rams. *Meteorology and Atmospheric Physics*, **49**, 69–91.

Pisano, J. T., I. McKendry, D. G. Steyn, and D. R. Hastie, 1997: Vertical nitrogen dioxide and ozone concentrations measured from a tethered balloon in the Lower Fraser Valley. *Atmospheric Environment*, **31**, 2071–2078.

Pleim, J. E., 2007a: A combined local and nonlocal closure model for the atmospheric boundary layer. Part I: Model description and testing. *Journal of Applied Meteorology and Climatology*, **46**, 1383–1395.

Pleim, J. E., 2007b: A combined local and nonlocal closure model for the atmospheric boundary layer. Part II: Application and evaluation in a mesoscale meteorological model. *Journal of Applied Meteorology and Climatology*, **46**, 1396–1409.

Pottier, J. L., H. P. Deuel, and S. C. Pryor, 2000: Application of the UAM-V and use of indicator species to assess control strategies for ozone reductions in the Lower Fraser Valley of British Columbia. *Environmental Monitoring and Assessment*, **65**, 459–467.

Pozzoli, L., G. Janssens-Maenhout, T. Diehl, I. Bey, M. G. Schultz, J. Feichter, E. Vignati, and F. Dentener, 2011: Reanalysis of tropospheric sulphate aerosol and ozone for the period 1980-2005 using the aerosol-chemistry-climate model ECHAM5-HAMMOZ. *Atmospheric Chemistry and Physics Discussions*, **11**, 10 191–10 263.

Pryor, S. C., 1998: A case study of emission changes and ozone responses. *Atmospheric Environment*, **32**, 123–131.

Pryor, S. C., I. G. McKendry, and D. G. Steyn, 1995: Synoptic scale meteorological variability and surface ozone concentrations in Vancouver, British Columbia. *Journal of Applied Meteorology*, **34**, 1824–1833.

Pryor, S. C. and D. G. Steyn, 1995: Hebdomadal and diurnal cycles in ozone time series from the Lower Fraser Valley, B. C. *Atmospheric Environment*, **29**, 1007–1019.

Qiu, X. M., Lepage, J. W. Boulton, and M. Gauthier, 2004: Urban and regional air quality modelling in the Pacific Northwest. 38^{th} *Annual CMOS Congress*, Edmonton, Alberta.

Reuten, C., D. G. Steyn, K. B. Strawbridge, and P. Bovis, 2005: Observations of the relation between upslope flows and the convective boundary layer in steep terrain. *Boundary Layer Meteorology*, **116**, 37–61.

Reynolds, S. D., C. L. Blanchard, and S. D. Ziman, 2003: Understanding the effectiveness of precursor reductions in lowering 8-hr ozone concentrations. *Journal of the Air and Waste Management Association*, **53**, 195–2005.

SAI, 1995: User's guide to the Systems Applications International Model (UAM-V) (Version 3.0). Tech. Rep. SYSAPP-95/027, Systems Applications International, San Rafeal, USA.

Salmond, J. A. and I. G. McKendry, 2002: Secondary ozone maxima in a very stable nocturnal boundary layer: observations from the Lower Fraser Valley, BC. *Atmospheric Environment*, **36**, 5771–5782.

Seinfeld, J. H. and S. N. Pandis, 1998: *Atmospheric Chemistry and Physics*. John Wiley and sons, New York, USA, 1326 pp.

Sillman, S., 1995: The use of NO_y, H_2O_2 and HNO_3 as indicators for ozone-NOx-hydrocarbon sensitivity in urban locations. *Journal of Geophysical Research*, **100**, 14 175–14 188.

Sillman, S. and D. He, 2002: Some theoretical results concerning O3-NOx-VOC chemistry and NOx-VOC indicators. *Journal of Geophysical Research*, **107**, doi:10.1029/2001JD001 123.

Skamarock, W. C., et al., 2008: A description of the Advanced Research WRF Version 3. Tech. Rep. NCAR/TN-475+STR, National Center for Atmospheric Research. 113 pp.

Smyth, S. C., W. Jiang, D. Yin, H. Roth, and E. Giroux, 2006: Evaluation of CMAQ O3 and PM2.5 performance using Pacific 2001 measurement data. *Atmospheric Environment*, **40**, 2735–2749.

Steyn, D., B. Ainslie, and I. McKendry, 2005: Air pollution in the Lower Fraser Valley, B.C.: Evolution, measurement, modelling and management. 39^{th} *Canadian Meteorological and Oceanographic Society Congress*, Richmond, British Columbia, Canada.

Steyn, D. G., M. Baldi, and K. Stephens, 1996: Observation based analysis of photochemical smog in the Lower Fraser Valley using two analytical schemes. Tech. Rep. Occasional Paper no. 41, Department of Geography, The University of British Columbia.

Steyn, D. G., J. W. Bottehnheim, and R. B. Thomson, 1997: Overview of tropospheric ozone in the Lower Fraser Valley, and the Pacific '93 Field Study. *Atmospheric Environment*, **31**, 2025–2035.

Steyn, D. G. and D. A. Faulkner, 1986: The climatology of sea breezes in the Lower Fraser Valley, B.C. *Climatological Bulletin*, **20**, 21–39.

Steyn, D. G. and I. G. McKendry, 1988: Quantitative and qualitative evaluation of a three dimensional mesoscale numerical model of a sea breeze in complex terrain. *Monthly Weather Review*, **116**, 1914–1926.

Stockwell, W. R. and F. W. Lurmann, 1989: Intercomparison of the ADOM and RADM gas-phase chemical mechanisms. Tech. rep., Electric Power Research Institute, Palo Alto, CA.

Strawbridge, K. B. and B. J. Snyder, 2004: Daytime and nighttime aircraft lidar measurements showing evidence of particulate matter transport into the Northeastern valleys of the Lower Fraser Valley, BC. *Atmospheric Environment*, **38**, 5873–5886.

Stroud, C. A., et al., 2008: OH-reactivity of volatile organic compounds at urban and rural sites across Canada: evaluation of air quality model predictions using speciated VOC measurements. *Atmospheric Environment*, **42**, 7746–7756.

Suzuki, N. M., 1997: Application of the Urban Airshed Model in the Lower Fraser Valley, British Columbia. M.S. thesis, University of British Columbia, Vancouver, B.C., Canada, 111 pp.

The Chamber of Shipping, 2007: 2005-2006 BC ocean-going vessel emissions inventory. Tech. rep., The Chamber of Shipping, Vancouver, B.C. 126 pp.

Tonnesen, G. S. and R. L. Dennis, 2000: Analysis of radical propagation efficiency to assess ozone sensitivity to hydrocarbons and NOx 2. Long-lived species as indicators of ozone concentration sensitivity. *Journal of Geophysical Research*, **105**, 9227–9241.

Vingarzan, R., 2004: A review of surface ozone background levels and trends. *Atmospheric Environment*, **38**, 3431–3442.

Vingarzan, R. and B. Taylor, 2003: Trend analysis of ground level ozone in the greater Vancouver/Fraser Valley area of British Columbia. *Atmospheric Environment*, **37**, 2159–2171.

Vingarzan, R. and B. Thomson, 2004: Temporal variation in daily concentrations of ozone and acid-related substances at Saturna Island, British Columbia. *Journal of the Air and Waste Management Association*, **54**, 459–472.

Yarwood, G. C., S. L. C. Tran, and E. Fujita, 2003: Impact of updates to on-road mobile source emission factor models (EMFAC) for the Los Angeles Region:ozone model sensitivity and ambient/inventory reconciliation. Tech. rep., Environ International Corporation, Novato, CA, USA. 128 pp.

Yarwood, G. C., S. Rao, M. Yocke, and G. Whitten, 2005: Updates to the carbon bond chemical mechanism: CB05. Tech. Rep. RT-0400675, U.S. Environmental Protection Agency (EPA). Available at `http://www.camx.com/publ/pdfs/CB05_Final_Report_120805.pdf`.

Yin, D., W. Jiang, H. Roth, and E. Giroux, 2004: Improvement of biogenic emissions estimation in the Canadian Lower Fraser Valley and its implication on particulate matter modeling results. *Atmospheric Environment*, **38**, 507–521.

APPENDIX

21. Appendix – Meteorological Model Evaluation

The meteorological modeling is the first step towards modeling of an ozone episode as it establishes how pollutant transport is handled in the chemical transport model. Here we perform a two-stage meteorological model evaluation, where first WRF output interpolated to meteorological station locations is compared against point observations. Next, various other meteorological data, not routinely available, are used to assess model performance. We compare the WRF model not only against observations but against other modeling efforts. In the Chemical Transport Model Evaluation appendix, we undertake a similar two-stage evaluation of the CMAQ output.

a. Meteorological timeseries analysis

We begin with a comparison of observed and predicted temperature, wind speed and wind direction using data from up to 23 meteorological stations located within the inner 4km domain and administered by both Environment Canada and the US National Weather Service (Table 8). Also, in order to get a feel for the model results, for each episode, wind speed, wind direction and temperature timeseries plots at YVR and YXX, arguably the two stations most indicative of the local pollutant transport and episodic meteorological conditions, are presented in Figures 9 to 46. Each figure has 4 plots showing observed (red) and predicted (blue) wind speed and direction at YVR (upper panels) and YXX wind speed and temperature (lower panels).

In comparing the WRF output against both observations and other modeling efforts, various statistical metrics have been considered. Each statistical measure, while not independent, provides a different assessment into the model's ability to reproduce the observations. Unfortunately, there are no absolute pass/fail threshold values which are associated with each metric (Gilliam et al. 2006). As a result, where possible, we will judge the fitness of our modeling results by comparing statistical scores against previous simulations of the same events by other groups against other Pacific Northwest studies with similar meteorological conditions. Raw station-level statistical results from each episode are presented in Tables 9 to 29. Table 6 list names, acronyms and formula of the various statistical metrics used to evaluate the model.

1) Temperature

While ambient temperatures directly influence chemical reaction rates, the main importance of analyzing the modeled surface temperature field lies in the fact that 2m temperatures reflect the integrative effects of many boundary layer processes including: the amount of shortwave radiation incident at surface, surface sensible heat flux density, surface moisture, boundary layer depth. As a result, correctly predicting 2m temperature is a good indication that other boundary layer processes are being well simulated.

To start, using the National Research Council's (NRC) evaluation of the MC2 modeling of the 1985 simulation (Hedley and Singleton 1997), we can directly compare temperature and wind timeseries statistics with the present WRF modeling of the same episode[10]. For

[10]This is not quite a direct comparison since their simulation ran from 0400 (PST) July 17th to 0000

temperature, the most relevant comparison is at the inland Abbotsford (YXX) station far from the ocean where the region's complex coastline makes temperature comparisons problematic. The NRC-MC2 simulations at YXX show a RMSE of 2.0^{o}C, which they consider excellent, whereas the present WRF simulations produce a similar error of 2.2^{o}C. Both modeling efforts show identical and high index of agreement (IOA) statistics of 0.97. Further up-valley, at Hope the NRC modeling produces RMSE and IOA statistics of 4.3^{o}C and 0.83 while the present WRF modeling shows values of 5.0^{o}C and 0.84. The poorer MC2 and WRF results at this inland station most likely arise from each model's relatively smooth topography contributing to unrealistically smooth modeled temperature fields in the complex terrain surrounding the station. Both models underestimate the mean temperature at this location.

In another comprehensive model evaluation exercise, Cai and Steyn (2000) use up to 10 meteorological stations within the western part of the LFV to evaluate a Regional Atmospheric Modeling System (RAMS;Pielke et al. (1992)) simulation of the same 1985 episode. The domain average RMSE temperature statistic appears to be around 2.0^{o}C (their figure 3c) although the unsystematic component of RMSE (RMSEu) appears to be a much lower 1.0^{o}C. The present WRF RMSE and RMSEu, averaged over YVR and YXX (the two Environment Canada stations within the Cai and Steyn (2000) observational network), is a similar 2.3 and 1.5^{o}C. Cai and Steyn (2000) also show that the temperature RMSE is low and IOA high during day but with the model having difficulty at night due to subgrid scale temperature variations caused by unresolved effects in the surface radiation inversion. Inspection of the daily YXX timeseries show that for many episodes (1987,1995,1998 and

(PST) July 22, 1985 whereas the present WRF simulation ran 1000 (PST) July 18th to 1000 (PST) July 22.

2006) WRF also has problems getting the nighttime low temperatures correct but for other episodes (1985,1987,1995 and 1998) it has some difficulties getting the daytime maximum correct. Looking at the other 6 modeled episodes, the YXX RMSE errors do not show a great deal of variability, ranging from 1.9 (1993) to 3.1^{o}C (1995) while the IOA statistics range from 0.98 (1993) to 0.93 (2001).

For their RAMS Pacific 1993 simulations, Cai et al. (2000) find poorer domain average RMSE temperature statistics – varying between 2 and 4^{o}C, although, the higher RMSE values are seen typically in the early morning and also at the end of their simulation which featured an upper-level shortwave disturbance producing rain and thunderstorms. The WRF 2-m temperature RMSE for the Pacific 1993 simulations are 1.9 (YXX), 2.4 (YVR) and 3.3^{o}C (YHE) which is inline with Cai et al. (2000).

The meteorological analysis of the Smyth et al. (2006) Pacific 2001 study reveals mean absolute errors (MAE) of 2.3^{o}C for stations within the LFV. The average of the 2001 MAE from the YVR, YXX and YHE stations for the WRF modeling is 2.4^{o}C. Again, the comparison is not quite a direct one since the Smyth et al. (2006) simulations were 7 days longer than the present 4 day simulation.

From two simulations outside of the LFV but over the Pacific Northwest, Barna et al. (2000) find 2m temperature RMSE between 1.5 and 3.0^o and IOA statistics between 0.90 and 0.98 while ONeill et al. (2006) find IOA values between 0.76 and 0.82 with MAE ranging from 2.8 to 3.4^{o}C. Again, these levels of statistical agreement are consistent with the present WRF values.

2) Wind speed and direction

The Hedley and Singleton (1997) MC2 evaluation finds MC2 over-predicts YVR wind speeds and rotate them clockwise (i.e. modeled u wind component too high while modeled v-component too low). The present WRF simulations has the same deficiencies, although the WRF wind speed RMSE at YVR is noticeably smaller at 1.6 m/s versus the 2.95 for MC2 while the IOA is better at 0.66 versus MC2's 0.58. Hedley and Singleton (1997) also find MC2 under-predicts sea-breeze (onshore flow) during the day while over-predicting the nighttime land-breeze. The present WRF simulation also tends to under-predict the daytime YXX wind speeds but does a good job of producing the observed calm nighttime conditions (Figure 9). At YXX, the MC2 simulation shows an IOA of 0.65, which is deemed acceptable, and a RMSE of 1.97 m/s, while the present simulation shows a much higher level of agreement (0.86) and lower RMSE (1.0 m/s). WRF also does a very good job at capturing the east-west (mean of 1.34 m/s versus observed 1.28) and north-south (mean 0.71 versus 0.71 m/s) wind speeds.

Only one episode has a YVR wind speed IOA below the MC2 standard of 0.58 (it is 0.36 in 1987) and all YVR wind speed RMSEs are below the MC2 benchmark of 2.95 m/s. At YXX, all episodes have RMSEs below the MC2 1.97 m/s benchmark but only 2 exceed the 0.65 IOA benchmark (1985 and 1998). Agreement statistics are close for 1987 (0.61), 2001 (0.64) and 2006 (0.62) while they are relatively worse for 1993 (0.46) and 1995 (0.57). From their RAMS 1985 simulations, Cai and Steyn (2000) consider wind speed IOA statistics below 0.5 to be poor and above 0.5 to be good. They find that generally poor agreement occurs during the nighttime hours and good agreement during the daytime. They also find domain averaged RMSE values to be generally between 1 and 2 m/s which is consistent with all of the events simulated here.

The Cai et al. (2000) Pacific 1993 RAMS simulation does not reproduce the surface wind fields for that episode as closely as the Cai and Steyn (2000) 1985 RAMS simulations with domain averaged RMSE values generally between 3 and 4 m/s. They argue that the occurrence of local weather systems, such as thunderstorms degraded the overall model performance. The present WRF simulations also show lower statistical agreement during the 1993 than 1985 events.

The Smyth et al. (2006) Pacific 2001 simulations find domain and episode averaged wind speed MAE of 1.2 m/s and IOA statistics of 0.42. The WRF simulation of Pacific 2001 (with its shorter modeling time) has MAE of 1.1, 1.3 and 1.5 m/s at YVR, YXX and YHE and IOA values of 0.64, 0.66 and 0.68. It is likely that the NRC's lower agreement levels stem from their evaluation against MV ozone monitoring stations which are not as well sited for meteorological measurements as the Environment Canada stations.

It is interesting to note that overall level of agreement at Hope is generally in line with that seen at YVR and YXX despite the considerably narrower valley at this location. However, all simulations systematically underestimate wind speeds at Hope with average errors ranging from 1.2 m/s (2001) to 1.5 m/s (1985). This underestimation likely affects how CMAQ handles up-valley pollutant transport and ozone formation here.

For gauging how well the flow within Georgia Strait is being reproduced, the Entrance Island station (WEL) is well sited but data exists for only the 1995 and later year episodes. Over these 4 episodes, RMSE values are 2.1 (1995), 2.7 (1998), 3.2 (2001) and 2.2 m/s (2006) while agreement indices are 0.90, 0.78, 0.63 and 0.89. The high agreement indices along with the moderate RMSE errors are indicative of the generally higher wind speeds observed at WEL (mean values often exceeding 8.0 m/s) and the less variable wind directions observed in the strait. WRF does not seem to systematically over or underestimate wind speeds at this location which suggests flow field within the Georgia strait is generally well captured.

There does not appear to be a similarly well sited station for characterizing the offshore flow field south of the LFV. The Saturna island station (WEZ) appears to be strongly influenced by local flows around the gulf islands. South of the gulf islands, the Discovery Island (DIS) station appears to be better sited for characterizing Juan de Fuca and Haro strait flow but this station has only observations for the 1998, 2001 and 2006 episodes. For these 3 events, the DIS RMSE and IOA statistics are: 1.4 m/s and 0.83; 1.6 m/s and 0.67; 2.0 m/s and 0.57. The corresponding WEZ values are: 2.6 m/s and 0.45; 3.1 m/s and 0.16; 4.4 m/s and 0.26. The large discrepancy in statistics between DIS and WEZ, two relatively close and well maintained stations south of the LFV, gives a good indication of the complex nature of the flow and the difficult (and somewhat subjective) nature of model evaluation (at least via model comparisons with point measurements).

Finally, Barna et al. (2000) find surface wind speed RMSE values between 1.3 and 1.8 m/s and IOA statistics between 0.56 and 0.78 and ONeill et al. (2006) find IOA values between 0.59 and 0.70 with MAE ranging from 1.8 to 2.0 m/s over their Pacific Northwest modeling domains.

Generally, the WRF's level of statistical agreement is comparable with other studies, although some of events achieve higher statistical agreement than others. We must keep in mind that errors in the emission inventories or deficiencies in the representation of ozone photochemistry will be added to shortcomings of meteorological modeling and it is possible for some episodes to end up with poorly reproduced of ozone fields, even if their meteorological fields are well modeled. Finally, it is interesting that generally the same level of agreement exists across the different models despite WRF and some of the other current models arguably using more advanced physical parametrization. Much of the observed discrepancies must stem from the models' similar spatial resolution and the difficulty in comparing point observations with volume averaged model output. Perhaps model evaluation using other datasets will reveal more intra-model differences.

b. Other meteorological comparisons

Starting with the 1985 episode, observed vertical profiles of temperature, wind speed and direction as well as the Cai and Steyn (2000) RAMS predictions of these profiles are available to compare against the WRF model. In addition, spatial plots of the RAMS, WRF and MC2 modeled wind fields can also be compared. Finally, aircraft based observations of mixed layer depth (MLD) during the 1993 field campaign can be compared with MLD diagnosed from the WRF model.

Figure 49 shows vertical profiles of temperature (A), wind speed (B) and wind direction (C) for the present WRF modeling (blue), the Cai and Steyn (2000) RAMS modeling (green) and tethersonde observations (red) on July 17th 1985. Each plot has results from 0930, 1330 and 1730 PST. The observations and RAMS data have been manually extracted from Figures 6-8 in Cai and Steyn (2000) and appear smoother here than in the original figures. The vertical elevations are with respect to sea-level. The 3 plots in Figure 49A show that WRF is noticeably cooler than both the observations and the RAMS output above 500 m at

0930 and 1330 and cooler above 200 m at 1730 (PST) although at the surface the modeled temperatures are close to the observed. Cai and Steyn (2000) speculate that the observed temperature inversion above 400 m at 1730 is possibly caused by a thermal layer, shed from a fully developed convective boundary layer and then advected over the sounding site by mid-afternoon. Whatever source of this warm layer, it is not being captured by WRF. It is possible that the colder WRF upper-level temperatures arise from initialized sea-surface temperatures (SST) being too cold. For this episode, SST was initialized using climatological MODIS SST and not the actual observed SST.

For wind direction (Figure 49B) at 0930 (PST), WRF, RAMS and observations all show westerly winds below 400m. Above this level, the observed winds back to easterlies while WRF veers to the NW. These direction discrepancies are probably not significant because of the low modeled wind speeds at these heights (Figure 49C). At 1330 and 1730 PST, the major feature of the observed wind field, namely the westerly wind direction, is well captured by both models.

Wind speed profiles are given in Figure 49C. At 0930 the observed winds are light (generally below 2 m/s) with the WRF model in excellent agreement throughout the measured 1000 m depth. By 1330 PST, the sea-breeze is fully developed and the WRF model reproduces the observed wind speeds up to a depth of about 500 m. Above this height, both the observations and RAMS winds become light, while the WRF winds remain close to 5 m/s. At 1730, observations show a jet at 500 m which WRF does a good job at capturing but keeps the winds too strong above this level. The proximity of the Queen Elizabeth Park site to the coast and the higher than observed WRF wind speeds may be leading to too much cold air advection at this site. This might also explain some of the cooler upper-level WRF temperatures seen in Figure 49A.

Figure 50 shows a comparison of modeled afternoon surface (10m) wind fields from the Hedley and Singleton (1997) MC2, the Cai and Steyn (2000) RAMS and the present WRF 1985 simulations over the LFV. Cai and Steyn (2000) argue that the the Hedley and Singleton (1997) MC2 afternoon windfields (Fig. 50A) do not resolve up-slope flows which are evident in their RAMS simulation (Fig. 50B). In the present WRF simulation (Fig. 50C), up-slope flows are clearly seen interacting with the larger scale up-valley flow.

Finally, during the Pacific 1993 field campaign, MLD over the LFV were gathered using a downward looking LIDAR operated from an aircraft flown at roughly 3500 m above sea-level (Hoff et al. 1997). From this study, 3 flight tracks capturing the coastline-to-valley floor MLD transition were studied by Batchvarova et al. (1999) using a variety of models. WRF predicted MLD along these same 3 flight paths (Figure 51A) have been extracted and plotted along with the observed MLD. MLD is a derived variable from the WRF output using Richardson number. Over Leg 1 (Figure 51B) WRF diagnosed MLD over ocean are too low but WRF does a good job of capturing the quick MLD rise over land. Continuing on, the diagnosed heights are too low when the leg passes over Burrard Inlet. Over Leg 2 (Figure 51C) WRF over estimates heights when approaching the North Shore mountains. For Leg 3 (Figure 51D) good agreement is seen over portions of the flight path near coast, but away from coast, the diagnosed MLD again is too high. Not shown in the figures are the RAMS diagnosed MLD, which generally does a much better job at reproducing the observations. The RAMS MLD were extracted from the RAMS output using a more sophisticated turbulent kinetic energy (TKE) based procedure, which may be better suited to diagnosing MLD from an internal boundary layer than the WRF Richardson based method.

It is not clear what effect, if any, these higher diagnosed MLD values will have on the photochemical modeling, since CMAQ does not directly use MLD in its calculations.

These few additional model evaluation tests do not really provide much additional insight into whether the WRF modeling is any better than the previous modeling efforts or, more importantly, whether the fields it produces reach a level of agreement necessary to drive the retrospective analysis. Perhaps the best way to explore this question is to examine the CMAQ ozone and precursor fields themselves.

22. Appendix – Chemical Transport Model Validation

The methods used to evaluate the CMAQ ozone output is similar to the WRF evaluation – through point comparisons against station data and through additional datasets gathered from various scientific studies. Again our purpose is see if the model is fit for purposes of this study and we test that fitness by exercising it over a representative set of events characteristic of LFV ozone episodes.

a. Concentration timeseries analysis

Exemplary ozone timeseries plots from each episode are presented in Figures 83 to 89. Each figure has 4 plots showing observed (red) and predicted (blue) ozone concentrations at T01, T09, T15 and T12. These 4 stations were selected from the network to highlight the model results because they have been operating over the entire 1985-2006 period and give results at downtown (T01), urban (T09, T15) and up-valley (T12) locations. Within the 4km domain, observations are available from up to 21 air quality stations administered by Metro Vancouver, the BC Ministry of Environment and Environment Canada (Table 30). As with the meteorological model evaluation, various metrics have been proposed to compare concentration timeseries against observations and again, there is no one best test with universally agreed upon pass/fail threshold value. As a result, where possible, we will judge the fitness of our modeling results by comparing against previous simulations of the same events (ideally) or from other studies within the Pacific Northwest under similar meteorological conditions. Complete listings of station-level statistical results for each of the episodes can be found in Tables 31 to 51. Finally, the CMAQ produced ozone fields are inherently dependent on WRF meteorological fields and SMOKE emission rates, so the ozone comparisons are an evaluation of the entire modeling chain. And, as we will see, for many of the simulated days, the modeled ozone maxima lie outside of the region sampled by the fixed monitoring network, making model evaluation very difficult. But, if the model does a good job of reproducing observed concentrations within the network footprint, this then increases its credibility when assessing the validity of predictions lying outside of the network footprint.

From the Hedley et al. (1997) CALGRID 1985 simulation, an extensive model evaluation is presented which can be used to benchmark our own efforts. Table 90 is a copy of station-level statistical results from the CALGRID simulation (Table 4 from Hedley et al. (1997)) and Table 51 list the present CMAQ statistical results at these same stations. In general, the CMAQ results have higher IOA, lower RMSE and least square regression slopes closer to unity than the corresponding CALGRID results.

Jiang et al. (1998) further evaluate the MC2/CALGRID model results through an intercomparison with Urban Airshed Model version V (UAM-V;SAI (1995)) model simulations of the same episode. We have used those results, along with the present simulations to extend the model-inter comparison to include the CMAQ output. This WRF/CMAQ, MC2/CALGRID and UAM-V comparison is performed at 4 stations between July 18th 0400 PST through July 20 2300 (PST) 1985 (which includes the CMAQ spin-up time). The CALGRID and UAM results have been taken from Figure 2 of Jiang et al. (1998). Figures 91 to 92 show timeseries plots of observations along with each model's output at T02 (Kitslano), T07 (Anmore), T11 (Abbotsford) and the T12 (Chilliwack) stations. Table 52 gives RMSE and IOA for each model at each station over the 68 hour inter-comparison. The CMAQ model results show marked improvement over the earlier CALGRID and UAM modeling especially at stations T07 and T11. A large part of the higher IOA values for the CMAQ model likely arises from CMAQ's better handling of the overnight low ozone concentrations (Figures 91 to 92). All of the models tend to under-predict the peak daytime concentrations, especially at Chilliwack on July 18 and 19. Jiang et al. (1998) find the agreement between CALGRID and UAM is closer to one another than the agreement with observations, with both models tending to under-predict peak ozone concentrations and over-predict nighttime concentrations, and both showing similar sensitivities to modeled precursor emission reductions. It appears that the results from the present CMAQ modeling are different enough from the CALGRID and UAM to say that CMAQ has improved upon these earlier results but still shows some of the same shortcomings.

Continuing with the 1985 episode, we can compare the present simulation with results from the Suzuki (1997) July 17-19, 1985 simulation. There Suzuki (1997) reports NMB of 29.1, 31.3 and 28.5% and NME of 35.6, 37.5 and 36.9 % over the July 17, 18 and 19th when restricting the analysis to times when the observations exceed 20 ppb. Using the same criteria but calculated over our entire 97 CMAQ simulation hours, the present modeling produces an improved NMB of -15.5% and a similar NME of 36.2%. Figure 93 shows scatter plots of predicted versus observed ozone concentrations based on the Suzuki (1997) RAMS/UAM-V (A) and the present WRF/CMAQ simulations (B) [11]. The RAMS/UAM-V scatter plot shows the Suzuki (1997) simulations tend to over-predict at low concentrations and under-predict at higher (> 40 ppb)concentrations. The WRF/CMAQ simulations tends to under-predict at low (< 20 ppb) concentrations and above 80 ppb, but tends to do a better job than the RAMS/UAM-V between 40 and 80 ppb.

While not a quantitative means of evaluating models, it is interesting to compare the afternoon ozone plumes (valid 1500 (PST) July 19th, 1985) based on the MC2/CALGRID (A), WRF/CMAQ (B and D) and RAMS/UAM-V (C) in Figure 94. The MC2/CALGRID field shows peak concentration of 106 ppb south of Chilliwack on the American side of the border with another region with concentrations exceeding 100 ppb west of Harrison Lake. High concentrations are also seen south of Gulf Islands. The CMAQ plume (B) shows a region with concentrations exceeding 102 ppb southeast of the Pitt River. A secondary maximum is produced over Strait of Juan de Fuca. Both show a north-south oriented region of high concentrations along the I5 corridor south of the border. The RAMS/UAM-V plume (C) shows a region with concentrations above 100 ppb northwest of the Pitt River valley and a larger 80+ ppb region over the Chilliwack area and extending north up what is likely the Stave Lake area. The corresponding CMAQ field (D but which is the same as B but

[11] The RAMS/UAM-V simulations span the July 17-19, 1985 time period while the WRF/CMAQ span July 18-22, 1985 timeframe.

contoured to match the presentation style of C), has generally lower concentrations which are closer to the Vancouver urban core and confined to the valley.

For the 2001 episode, Smyth et al. (2006) present timeseries plots of observed and predicted surface ozone concentrations at Kitslano (T02) and Burnaby South (T18), which we have reproduced here along with results from the present analysis (Figures 95 and 96). The present WRF-CMAQ model results at T02 clearly show a greater ability at reproducing both the extent and the timing of the daytime maxima as well as the nighttime minima when compared with the MM5-CMAQ. At T18, the present modeling greatly overestimates the daytime peak on the 11th and 12th which the MM5-CMAQ model captures nicely. Both models do a good job reproducing the nighttime ozone titration at this station.

Smyth et al. (2006) also present evaluation statistics, not at the individual station level, but for the whole domain and over the entire simulation period. These statistics (their Table 3) as well as the corresponding statistics from the present simulation of the 2001 episode are presented in Tables 7 and 53. Table 7 provides statistics for all model-observational data pairs while Table 53 provides statistics based daily observed and predicted peak values. Finally, in order to compare the level of agreement across all episodes, the statistics for all 7 simulations have also been included in the tables. It must be stressed that while both models simulated the August 2001 event, the NRC simulation was 12 days long while the present was only 4 days. Starting with the 2001 simulations, it appears that the two models reach roughly the same level of agreement with the NRC's showing slightly better statistics but with the present modeling shows a higher MB (5.7 versus 2.6 ppb). However, the 4 days modeled in the present WRF/CMAQ simulation was a period that saw higher ozone concentrations than the 8 additional days modeled by the NRC. It could be argued that simulating the rapid daytime peaks to nighttime low ozone transition during the high ozone days is a tougher task than simulating the more uniform diurnal ozone trends seen during the lower ozone period that followed. This situation would tend to penalize the WRF/CMAQ statistical scores relative to the NRC's. Examination of the results from the other simulations in Table 7 shows the model, with the exception of 1985 (and to a lesser extent 1987) has a persistent positive MB, suggesting the model consistently over-estimates ozone concentrations. This trend is especially evident in the modeled daily peak concentrations (Table 53). The WRF-CMAQ ME statistics in both tables are generally closer to the NRC's ME values suggesting the main difference between the models is the larger bias seen in the WRF-CMAQ results. Based on the these tables, it would appear that the 2006, 2001 and 1985 simulations achieve the best agreement with the observations and are on par with the Smyth et al. (2006) results. The 1993 and 1995 simulations appear to be significantly worse while the 1987 is somewhere in-between. As noticed in the episode description section, the 1987 and 1995 episodes showed difficulties reproducing the observed circulation patterns which likely contributes to their poorer model evaluation scores. Model success for both the 2006 and 1985 events is encouraging because the retrospective analysis is based on comparisons of model output driven by 2005 and 1985 emissions and fixed meteorology. It appears that the inventory at these two timepoints is well modeled. It is also noteworthy that the nature of the model bias changes over the 20 year timeframe: WRF-CMAQ overestimates in 2006 and 2001 while it underestimates in 1985. Finally, while the model bias is significant, its effects on the retrospective analysis can be mitigated by looking at the differences between simulations with 2005 and 1985 emissions.

It is interesting to speculate on the nature of the varied model results. Specifically, the simulations of the earliest and latest events score noticeable higher than the simulations in the middle of the 20 year timeframe. It was during the middle part of the timeframe that the greatest emissions reductions occurred and perhaps the inventory has had difficulties capturing the rapid emission changes. For instance, at the start and end of the timeframe, the local vehicle fleet might have had a more homogeneous composition of vehicles with similar emission standards, than during the transition period, where there would have been a large mixture of both the newer, cleaner, Tier I and the older, less regulated, cars, potentially leading to large uncertainties in the daily LDV emission rates. Another factor may be how the episodes themselves evolved. The 1987, 1993 and 1995 episodes do not have especially high concentrations (the 1987 episode was chosen more for its type IV circulation; the 1993 episode was chosen to coincide with Pacific 1993; and the 1995 episode was chosen because of the McKendry et al. (1998b) aircraft measurements). Both the 1985 and 2006 events had relatively high observed ozone concentrations. Thus, it is possible that the modeling system has difficulties reproducing all but the most pronounced ozone episodes.

Finally, we can compare statistical results against simulations performed elsewhere in the Pacific Northwest. The ONeill et al. (2006) Pacific Northwest simulations over a 2 week period during July 1996, report normalized bias (NB) and normalized error (NE) Because normalized error statistics can become large when the observations are small, they exclude all data points when the observations are less than 40 ppb. The station level NE values fall between a low of 15% to a high of 40 % with a majority of stations showing errors between 20 and 30%. In the present simulations, in chronological order from 2006 to 1985, the NE statistics (in %) are: 15.1, 26.4, 33.3, 32.8, 23.1, 30.8 and 28.6 – consistent with the ONeill et al. (2006) results. The ONeill et al. (2006) NB values range from -7 to 45% with most stations showing NB values between 15 and 30%. For the WRF-CMAQ simulations we find (in %): 3.9, 4.6, 27.2, 14.6, -5.7, -25.9 and -21.4%, again well within the range of values reported by ONeill et al. (2006).

The Jiang et al. (2006) MM5/CALGRID July 1996 simulation over the Puget Sound region reports station-level ozone IOA and RMSE (ppb) values ranging from 0.65 to 0.95 (IOA) and 9.3 to 18.3 (RMSE). Again, the present simulations are consistently within these ranges. Finally, the Barna et al. (2000) MM5-CALGRID simulation for the same time period but over a large portion of the coastal Pacific Northwest reports IOA values ranging from 0.34 to 0.92 and RMSE values from 12.7 to 29.7 (ppb). Statistics from the present simulations easily fall into these ranges as they do for a number of other statistics reported by Barna et al. (2000) including slope, intercept,NE and NB.

b. Other comparisons

The first additional test involves evaluating how well the model reproduces the ozone concentration field away from the monitoring stations but still within the area spanned by the network. The next comparison will look at the more demanding task of reproducing the ozone field away from the network. This first evaluation makes use observational data from the monitoring stations which is interpolated over the valley portions of the LFV. This purely data-driven means of establishing ozone field uses both the spatial and temporal correlations within the data in order to perform a entropy-based Bayesian interpolation (Le and Zidek 2006). Using this technique, observed 8-hr maximum ozone concentration on August 12th, 2001 were interpolated onto a 10x30 4km resolution grid over the LFV. and used by Ainslie et al. (2009). The CMAQ output for this day was regridded to same the 10x30 domain and the resulting ozone fields (in ppb) from both methods have been contoured over valley portion of the LFV in Figure 97A (interpolated data) and 97B (CMAQ output). A scatter plot of the data points used in creating the ozone isopleths is given in Figure 97C. The agreement between the two 8-hr ozone concentration fields is quite good with both showing concentrations increasing up valley with strong ozone titration around the Vancouver urban area. The biggest discrepancy between the plots is the extension of the 40 ppb isopleth in the CMAQ plot extending from the central Burnaby area into Surrey. The statistical agreement between the two fields is also quite good with RMSE of 5.9 ppb; IOA of 0.90; ME of 4.5 (ppb); NME of 8.9%; MB of 1.3 ppb;and NMB of 2.5%.

A second and more demanding comparison involves examining how well the model reproduces observed ozone concentrations away from the valley – namely along the Pitt River and Harrison Lake tributary valleys – using aircraft measurements collected by McKendry et al. (1998b). In this field study, McKendry et al. (1998b) measured lower tropospheric ozone concentrations along a flight path (Figure 98A) having 3 legs within the LFV and 3 over the complex forested terrain north of the LFV (including the Pitt River and Harrison Lake tributary valleys). Observations were taken between 1200-1500 (PST) on July 19th, 1995 at 500 m agl for most of the flight except for the flight leg which took the aircraft from the northern end of the Pitt River valley over to the northern end of Harrison Lake where the aircraft ascended to approximately 2500 m (Figure 3c in McKendry et al. (1998b)). Because this event was also modeled, CMAQ based concentrations along the McKendry flight path have been extracted and plotted with the observed concentrations. In order to determine the correct CMAQ gridcells to extract model output from, each leg of the flight was broken into between 10 and 4 intervals. By assuming a uniform flight speed along each leg, and using the flight height/time data given in their Figure 3C, it was possible to create a table of latitude, longitude, elevation and time coordinates along each flight leg. These coordinates were then used determine the corresponding CMAQ ozone concentrations through a bi-linear interpolation process. In Figure 98B, curves of observed and modeled ozone concentrations along the 6 flight legs are given. In general the fit is not very good, with CMAQ concentrations tending to be much lower along legs BC (Pitt Lake) and CD (Pitt Lake to Harrison Lake). The model produces the correct concentrations at the northern most section of the Harrison Lake leg, but does not reproduce the observed high concentrations along the southern part of Harrison Lake. The model shows good agreement with the observations along the Harrison-Boundary Bay return leg (FA). If model output over the 1500-1800 (PST) time period is used instead of output from the 1200-1500 period (but using the same latitude, longitude and elevation coordinates), a much better fit to the observations is found (Figure 98C) along the Harrison Lake legs (DE and EF). Along the return flight within the LFV (FA) the model over-predicts close to the Boundary Bay airport. The model also over-predicts along the legs leading to the Pitt River (AB and BC) but under-predicts along the flight between the two tributary valleys (CD). As discussed above, this episode is not well captured with the model showing a large mean bias of 10.8 ppb. The YVR hodograph comparison for this day (Figure 28) shows the observed flow was mainly from the northwest while the modeled flow was from the west. What can be taken from this comparison, is that the modeled high ozone concentrations along Harrison Lake are a realistic feature but that the model is too slow at putting them there. Also, the modeled ozone concentrations along the LFV legs are too high, consistent with the statistical evaluation using the station data.

The third and final comparison is a process-based evaluation. McKendry et al. (1998a) observed daytime up-valley transport of polluted air with nighttime return flow of cleaner air using a combination of tethersonde, lidar, aircraft and surface chemistry measurements. Time-height cross-sectional plots showing modeled up- and down-valley winds along with ozone concentrations at the mouth of the Pitt River valley for both Pacific 1993 and the June 2006 episode are given in Figures 99 and 100. We begin with the June 2006 model results which are easier to interpret. The top panel, showing modeled wind speeds in the lowest 1000 m above ground level, reveals, in the lowest 200m, a diurnal pattern of upvalley winds (yellow/orange) during day (i.e. before noon) followed by strong outflow (blue colours) starting around midnight each day. Between 200 m and 600 m agl, the winds are consistently upvalley while above this, the winds are consistently downvalley. Also given on the plot is the modeled MLD (solid red line) which shows diurnal variation with daytime peaks between 400 and 300 m and nighttime heights about 50 m. The accompanying time-height plot of ozone concentrations (lower panel) shows the daytime upvalley flows below 200 m are associated with high ozone concentrations, while the low level nighttime flows are associated with relatively cleaner air – exactly as observed in McKendry et al. (1998a). The model also shows a layer of high ozone concentration between 200 m and 600 m agl much of it above the modeled mixed layer (red line). The high daytime concentrations are almost certainly as a result of photochemical production as seen by the HYSPLIT back-trajectories arriving at the Pitt River on the 24th, 25th and 26th at 1700 (PST) (Figure 101) which shows the urban Vancouver area as the source region for this airmass. That the model can reproduce such an important process in the LFV photochemical lifecycle is an important indicator that model meteorology, its spatial resolution and emissions inventory are suitably matched and well simulated.

This daily pattern of ozone transport was originally observed by McKendry et al. (1998a) and Banta et al. (1997) at the entrance to the Pitt River valley during the Pacific 1993 field campaign. Unfortunately, the model does not produce such a clear picture of polluted daytime up-valley flow with cleaner nighttime down-valley flow for this event (Figure 99) For this simulation, the modeled up-valley flows appearing after noon are much weaker and are limited to around 100 m (with the exception of August 4th). Above 100 m, the simulated winds are strongly down-valley for all days except the 4th. The corresponding ozone concentrations show little diurnal variation and little vertical variation until late in the day on the 4th. The corresponding HYSPLIT back-trajectory particle releases arriving at Pitt River in the late afternoon, show daytime source regions to the northeast on the 2nd and 3rd, with only the 4th showing a weak daytime source region passing over the Vancouver urban area (Figure 102). Both the 2006 and 1993 events have cluster I type meso-scale circulation patterns, so it is surprising that the 2006 simulation exhibits many of the meso-scale processes observed at Pitt River during Pacific 1993. That the 1993 simulation does not reproduce these features is a good indicator that this set of runs is not suitable for use in the exploration analysis. Perhaps it is not surprising that the 1993 simulation shows some of the lowest ozone performance statistics (Table 7) as well as some of the lowest measures of statistical agreement for wind speed and direction at YVR (Table 22 and 23).

c. NAPS-VOC evaluation

Modeled VOC concentrations have also been compared with observed concentrations using data collected from the National Air Pollution Surveillance (NAPS) network. Through this network, 24-hr averaged VOC concentrations, of up to 176 compounds, are collected from a number of sites within the LFV every third or sixth day depending on a national schedule. Canister contents are analyzed by Environment Canada in Ottawa. Because of the irregularity of the sampling times, only a limited number (12) of NAPS measurements occurred during the 7 modeled episodes (with none occurring prior to 1993) and only at 6 different locations (T09, T15, T17, T18, T22 and T24). In order to compare the NAPS data with the CMAQ output, the observed VOC concentrations were mapped onto the 8 CB05 VOC classes (OLE, PAR, TOL, XYL, FORM, ALD2, ETH and ISOP). The mapping, based on a similar scheme developed by Yarwood et al. (2003) for mapping CB4 classes to US-based PAMS data, performs a weighted-allocation of each NAPS VOC species onto one or more of the CB5 classes (Table 1). The allocation and weighting of each VOC with respect to the CB5 classes is based on the VOC's chemical structure.

Figure 53 is a box and whisker plot showing the distribution of the ratio of CMAQ-predicted to NAPS-observed VOC concentrations for the 8 CB5 VOC classes. The lines in the box show the 25th, 50th and 75th percentile while the whisker give the 1.5×IQR above and below the 75th and 25th percentiles. Generally, CMAQ over-predicts VOC concentrations with mean ratios of 4.0, 5.3, 1.2, 0.8, 2.2, 17.8, 1.8 and 1.2. The most extreme over prediction of 17.8 is for the ALD2 class which has been omitted from Figure 53 because of its large size relative to the others. In many of the profiles, the NAPS canisters show very little

ALD2 concentrations (0.1 ppb) while CMAQ shows moderate (5 ppb) amounts and these low ALD2 cases lead to huge over-predictions. Even without the ALD2 values, the model still greatly over-predicts the amount of single bonded one-carbon surrogate (PAR) and the double bonded two-carbon OLE surrogate. These discrepancies are in line with comparisons of CMAQ output against hourly VOC data over the Northeastern US (Doraiswamy et al. 2009)

Figure 54A shows a comparison of the average relative composition of each CB5 class to the total VOC concentration. The plot shows that both the CMAQ and NAPS speciations find that PAR makes up almost 75% of the VOC mixture with all the other classes contributing a uniformly much smaller amount. Because the PAR class is associated with many slower reacting VOC compounds, it is more meaningful to examine the VOC composition when each class' concentration has been scaled by its affinity for reacting with the hydroxyl radical (k_{OH} rate constant). When the OH-reactivity scaling is performed, the PAR dominance on the composition is removed (Figure 54B). The OH-weighted speciation shows for the NAPS speciation that the heavier aromatic class (XYL) is now the most influential component, while for CMAQ, it is the ALD2 class. It is interesting to note that the CMAQ speciation is heavier on the carbonyl classes (FORM and ALD2) while the NAPS observations are more weighted towards the aromatics (TOL and XYL).

Summarizing, both the CMAQ and NAPS show similar breakdown of VOC composition along the CB5 classes with PAR being dominant. When concentrations from each CB5 class are weighted by their OH-reactivity, both the CMAQ and NAPS speciations show similar breakdowns for OLE and PAR but differ in their aromatic and carbonyl make up. Of course, it must be kept in mind that CMAQ is producing concentrations of OLE and PAR that are, on average, 4.0 and 5.3 times larger than is observed. Neither the NAPS or CMAQ weighted speciations show the ISOP class to be dominant with the CMAQ ISOP make-up being about half of what NAPS shows it to be. Stroud et al. (2008) compare modeled VOC concentrations from the AURAMS model using the ADOM-II chemical mechanism (Stockwell and Lurmann 1989) to NAPS data over the summer of 2005 at Vancouver, Surrey and Hope/Chilliwack. Also find little ISOP contribution in their observations and find different VOC breakdowns between Vancouver, Surrey and Hope/Chilliwack with high aromatic compositions from the Vancouver samples. AURAMS tended to under-predict the aromatic composition in Vancouver and Hope/Chilliwack.

Total VOC concentrations, weighted by the OH-reactivity of propene, shows that CMAQ tends to greatly overestimate (4-8 times) the propene weighted total VOC concentration at the sites (T15, T18 and T22) with low (¡3 ppb) propene weighted total VOC concentration while at the T24 Eton North Burnaby site, with the highest weighted average concentration (¿45 ppb) CMAQ underestimates total VOC concentrations by about one half. At the T09 station, with average weighted VOC concentration of 13.3 ppb, CMAQ overestimates by a factor of 1.8.

d. NOx model evaluation

We have also compared CMAQ's ability to reproduce daytime NOx concentrations at the MV measurement stations. As suggested by Hedley et al. (1997), we have excluded nighttime values because of the possibility of local (sub-grid scale) emissions source, within the nocturnal stable layer, unduly impacting the measurements. Also, as with Hedley et al.

(1997) no adjustments were made to the NOx observations to correct for possible nitrate interference, an effect that can lead to a 10% NOx overestimation. Comparing present CMAQ NOx predictions against those reported by Hedley et al. (1997) a similar level of agreement is achieved. As with Hedley et al. (1997) all but 2 station (T07 and T14) have index of agreement above 0.50 with the worst agreement at T07 (0.26) and best at T03 (0.94). The RMSE are slightly larger with values at T04, T05, T10, T14, T15 and T16 being larger than 20 ppb. In general, the mean bias errors are positive (with the exception of T14) suggesting the model under-predicts daytime NOx concentrations. The comparisons with the other episodes show similar results with some event performing generally better (1995) and some generally worse (1993). Looking at the 2006 event, the model has poor levels of agreement at T01 (0.26), T04 (0.36), T06 (-0.04), T09 (-0.10), T12 (0.25), T13 (0.07), T18 (0.37), T30 (0.24) and T32 (0.25) although the RMSE errors are greater than 20 ppb only at T06 (37.1), T09 (28.1) and T32 (21.4). It is interesting to note that the T04, T06, T09 and T32 stations are in close proximity, suggesting the model has problems with NOx emissions in East Vancouver and the Coquitlam/Port Coquitlam/Port Moody areas. Looking at the spatial distribution of MBE, averaged over all 7 episodes (Figure 52), we find that the model tends to consistently under-predict NOx concentrations within the Vancouver urban area with the largest average errors at the T06 (29 ppb), T09 (16.8 ppb) and T01 (11.2 ppb) stations. On average, the model tends to slightly over-predict daytime NOx concentrations just outside of the main urban areas in Richmond (T17), Surrey (T15), Langely (T27) and Maple Ridge (T30).

Table 1: Mapping factors to convert NAPS VOC species to the 8 CB5 VOC classes.

NAPS VOC species	OLE	PAR	TOL	XYL	FORM	ALD2	ETH	ISOP
Ethane	0.00	0.30	0.00	0.00	0.00	0.00	0.00	0.00
Ethylene	0.00	0.00	0.00	0.00	0.00	0.00	1.00	0.00
Acetylene	0.00	1.00	0.00	0.00	0.00	0.00	0.00	0.00
Propylene	0.67	0.33	0.00	0.00	0.00	0.00	0.00	0.00
Propane	0.00	1.00	0.00	0.00	0.00	0.00	0.00	0.00
1-Propyne	0.00	1.00	0.00	0.00	0.00	0.00	0.00	0.00
Isobutane	0.00	1.00	0.00	0.00	0.00	0.00	0.00	0.00
1-Butene/Isobutene	0.50	0.50	0.00	0.00	0.00	0.00	0.00	0.00
1,3-Butadiene	0.50	0.00	0.00	0.00	0.00	0.50	0.00	0.00
Butane	0.00	1.00	0.00	0.00	0.00	0.00	0.00	0.00
trans-2-Butene	0.00	0.00	0.00	0.00	0.00	1.00	0.00	0.00
2,2-Dimethylpropane	0.00	1.00	0.00	0.00	0.00	0.00	0.00	0.00
1-Butyne	0.00	1.00	0.00	0.00	0.00	0.00	0.00	0.00
cis-2-Butene	0.00	0.00	0.00	0.00	0.00	1.00	0.00	0.00
Isopentane	0.00	1.00	0.00	0.00	0.00	0.00	0.00	0.00
1-Pentene	0.40	0.60	0.00	0.00	0.00	0.00	0.00	0.00
2-Methyl-1-Pentene	0.33	0.67	0.00	0.00	0.00	0.00	0.00	0.00
2-Methyl-1-butene	0.40	0.60	0.00	0.00	0.00	0.00	0.00	0.00
3-Methyl-1-butene	0.40	0.60	0.00	0.00	0.00	0.00	0.00	0.00
Pentane	0.00	1.00	0.00	0.00	0.00	0.00	0.00	0.00
Isoprene	0.00	0.00	0.00	0.00	0.00	0.00	0.00	1.00

Continued on Next Page...

Table 1 – Continued

NAPS VOC species	OLE	PAR	TOL	XYL	FORM	ALD2	ETH	ISOP
trans-2-Pentene	0.00	0.20	0.00	0.00	0.00	0.80	0.00	0.00
cis-2-Pentene	0.00	0.20	0.00	0.00	0.00	0.80	0.00	0.00
2-Methyl-2-butene	0.00	0.60	0.00	0.00	0.00	0.40	0.00	0.00
2,2-Dimethylbutane	0.00	1.00	0.00	0.00	0.00	0.00	0.00	0.00
Cyclopentene	0.00	0.60	0.00	0.00	0.00	0.40	0.00	0.00
4-Methyl-1-pentene	0.33	0.67	0.00	0.00	0.00	0.00	0.00	0.00
3-Methyl-1-pentene	0.33	0.67	0.00	0.00	0.00	0.00	0.00	0.00
Cyclopentane	0.00	1.00	0.00	0.00	0.00	0.00	0.00	0.00
2,3-Dimethylbutane	0.00	0.83	0.00	0.00	0.00	0.00	0.00	0.00
trans-4-Methyl-2-pentene	0.00	0.67	0.00	0.00	0.00	0.33	0.00	0.00
2-Methylpentane	0.00	1.00	0.00	0.00	0.00	0.00	0.00	0.00
cis-4-Methyl-2-pentene	0.00	0.67	0.00	0.00	0.00	0.33	0.00	0.00
3-Methylpentane	0.00	1.00	0.00	0.00	0.00	0.00	0.00	0.00
1-Hexene	0.33	0.67	0.00	0.00	0.00	0.00	0.00	0.00
Hexane	0.00	1.00	0.00	0.00	0.00	0.00	0.00	0.00
trans-2-Hexene	0.00	0.67	0.00	0.00	0.00	0.33	0.00	0.00
2-methyl-2-Pentene	0.00	0.67	0.00	0.00	0.00	0.33	0.00	0.00
2-Ethyl-1-Butene	0.40	0.60	0.00	0.00	0.00	0.00	0.00	0.00
trans-3-Methyl-2-pentene	0.00	0.67	0.00	0.00	0.00	0.33	0.00	0.00
cis-2-Hexene	0.00	0.67	0.00	0.00	0.00	0.33	0.00	0.00
cis-3-Methyl-2-pentene	0.00	0.67	0.00	0.00	0.00	0.33	0.00	0.00
2,2-Dimethylpentane	0.00	1.00	0.00	0.00	0.00	0.00	0.00	0.00
Methylcyclopentane	0.00	1.00	0.00	0.00	0.00	0.00	0.00	0.00

Continued on Next Page...

Table 1 – Continued

NAPS VOC species	OLE	PAR	TOL	XYL	FORM	ALD2	ETH	ISOP
2,4-Dimethylpentane	0.00	1.00	0.00	0.00	0.00	0.00	0.00	0.00
2,2,3-Trimethylbutane	0.00	1.00	0.00	0.00	0.00	0.00	0.00	0.00
1-Methylcyclopentene	0.00	0.60	0.00	0.00	0.00	0.40	0.00	0.00
Benzene	0.00	0.17	0.00	0.00	0.00	0.00	0.00	0.00
Cyclohexane	0.00	1.00	0.00	0.00	0.00	0.00	0.00	0.00
2-Methylhexane	0.00	1.00	0.00	0.00	0.00	0.00	0.00	0.00
2,3-Dimethylpentane	0.00	1.00	0.00	0.00	0.00	0.00	0.00	0.00
Cyclohexene	0.33	0.67	0.00	0.00	0.00	0.00	0.00	0.00
3-Methylhexane	0.00	1.00	0.00	0.00	0.00	0.00	0.00	0.00
1-Heptene	0.33	0.67	0.00	0.00	0.00	0.00	0.00	0.00
2,2,4-Trimethylpentane	0.00	1.00	0.00	0.00	0.00	0.00	0.00	0.00
trans-3-Heptene	0.33	0.67	0.00	0.00	0.00	0.00	0.00	0.00
cis-3-Heptene	0.33	0.67	0.00	0.00	0.00	0.00	0.00	0.00
Heptane	0.00	1.00	0.00	0.00	0.00	0.00	0.00	0.00
trans-2-Heptene	0.33	0.67	0.00	0.00	0.00	0.00	0.00	0.00
cis-2-Heptene	0.33	0.67	0.00	0.00	0.00	0.00	0.00	0.00
2,2-Dimethylhexane	0.00	1.00	0.00	0.00	0.00	0.00	0.00	0.00
Methylcyclohexane	0.00	1.00	0.00	0.00	0.00	0.00	0.00	0.00
2,5-Dimethylhexane	0.00	1.00	0.00	0.00	0.00	0.00	0.00	0.00
2,4-Dimethylhexane	0.00	1.00	0.00	0.00	0.00	0.00	0.00	0.00
2,3,4-Trimethylpentane	0.00	1.00	0.00	0.00	0.00	0.00	0.00	0.00
Toluene	0.00	0.00	1.00	0.00	0.00	0.00	0.00	0.00
2-Methylheptane	0.00	1.00	0.00	0.00	0.00	0.00	0.00	0.00

Continued on Next Page…

Table 1 – Continued

NAPS VOC species	OLE	PAR	TOL	XYL	FORM	ALD2	ETH	ISOP
1-Methylcyclohexene	0.00	1.00	0.00	0.00	0.00	0.00	0.00	0.00
4-Methylheptane	0.00	1.00	0.00	0.00	0.00	0.00	0.00	0.00
3-Methylheptane	0.00	1.00	0.00	0.00	0.00	0.00	0.00	0.00
cis-1,3-Dimethylcyclohexane	0.00	1.00	0.00	0.00	0.00	0.00	0.00	0.00
trans-1,4-Dimethylcyclohexane	0.00	1.00	0.00	0.00	0.00	0.00	0.00	0.00
2,2,5-Trimethylhexane	0.00	1.00	0.00	0.00	0.00	0.00	0.00	0.00
1-Octene	0.33	0.67	0.00	0.00	0.00	0.00	0.00	0.00
Octane	0.00	1.00	0.00	0.00	0.00	0.00	0.00	0.00
trans-1,2-Dimethylcyclohexane	0.00	1.00	0.00	0.00	0.00	0.00	0.00	0.00
trans-2-Octene	0.33	0.67	0.00	0.00	0.00	0.00	0.00	0.00
cis-1,4/t-1,3-Dimethylcyclohexane	0.00	1.00	0.00	0.00	0.00	0.00	0.00	0.00
cis-2-Octene	0.33	0.67	0.00	0.00	0.00	0.00	0.00	0.00
cis-1,2-Dimethylcyclohexane	0.00	1.00	0.00	0.00	0.00	0.00	0.00	0.00
Ethylbenzene	0.00	0.13	0.87	0.00	0.00	0.00	0.00	0.00
2,5-Dimethylheptane	0.00	1.00	0.00	0.00	0.00	0.00	0.00	0.00
m and p-Xylene	0.00	0.00	0.00	1.00	0.00	0.00	0.00	0.00
4-Methyloctane	0.00	1.00	0.00	0.00	0.00	0.00	0.00	0.00
3-Methyloctane	0.00	1.00	0.00	0.00	0.00	0.00	0.00	0.00
Styrene	0.13	0.00	0.87	0.00	0.00	0.00	0.00	0.00
o-Xylene	0.00	0.00	0.00	1.00	0.00	0.00	0.00	0.00
1-Nonene	0.33	0.67	0.00	0.00	0.00	0.00	0.00	0.00
Nonane	0.00	1.00	0.00	0.00	0.00	0.00	0.00	0.00
iso-Propylbenzene	0.00	0.22	0.78	0.00	0.00	0.00	0.00	0.00

Continued on Next Page...

Table 1 – Continued

NAPS VOC species	OLE	PAR	TOL	XYL	FORM	ALD2	ETH	ISOP
3,6-Dimethyloctane	0.00	1.00	0.00	0.00	0.00	0.00	0.00	0.00
n-Propylbenzene	0.00	0.22	0.78	0.00	0.00	0.00	0.00	0.00
3-Ethyltoluene	0.00	0.11	0.00	0.89	0.00	0.00	0.00	0.00
4-Ethyltoluene	0.00	0.11	0.00	0.89	0.00	0.00	0.00	0.00
1,3,5-Trimethylbenzene	0.00	0.11	0.00	0.89	0.00	0.00	0.00	0.00
2-Ethyltoluene	0.00	0.11	0.00	0.89	0.00	0.00	0.00	0.00
1-Decene	0.33	0.67	0.00	0.00	0.00	0.00	0.00	0.00
tert-butylbenzene	0.00	0.22	0.78	0.00	0.00	0.00	0.00	0.00
1,2,4-Trimethylbenzene	0.00	0.11	0.00	0.89	0.00	0.00	0.00	0.00
Decane	0.00	1.00	0.00	0.00	0.00	0.00	0.00	0.00
iso-butylbenzene	0.00	0.22	0.78	0.00	0.00	0.00	0.00	0.00
sec-butylbenzene	0.00	0.22	0.78	0.00	0.00	0.00	0.00	0.00
1,2,3-Trimethylbenzene	0.00	0.11	0.00	0.89	0.00	0.00	0.00	0.00
p-Cymene	0.00	0.22	0.78	0.00	0.00	0.00	0.00	0.00
Indane	0.00	1.00	0.00	0.00	0.00	0.00	0.00	0.00
1-Undecene	0.33	0.67	0.00	0.00	0.00	0.00	0.00	0.00
1,3-Diethylbenzene	0.00	0.20	0.00	0.80	0.00	0.00	0.00	0.00
1,4-Diethylbenzene	0.00	0.20	0.00	0.80	0.00	0.00	0.00	0.00
n-Butylbenzene	0.00	0.22	0.78	0.00	0.00	0.00	0.00	0.00
1,2-Diethylbenzene	0.00	0.22	0.78	0.00	0.00	0.00	0.00	0.00
Undecane	0.00	1.00	0.00	0.00	0.00	0.00	0.00	0.00
Naphthalene	0.00	0.17	0.00	0.00	0.00	0.00	0.00	0.00
Dodecane	0.00	1.00	0.00	0.00	0.00	0.00	0.00	0.00

Continued on Next Page...

Table 1 – Continued

NAPS VOC species	OLE	PAR	TOL	XYL	FORM	ALD2	ETH	ISOP
Hexylbenzene	0.00	0.17	0.00	0.00	0.00	0.00	0.00	0.00
MTBE	0.00	0.80	0.00	0.00	0.00	0.00	0.00	0.00
a-pinene	0.00	0.60	0.00	0.00	0.00	0.40	0.00	0.00
b-pinene	0.00	0.60	0.00	0.00	0.00	0.40	0.00	0.00
d-Limonene	0.00	0.60	0.00	0.00	0.00	0.40	0.00	0.00
camphene	0.00	0.60	0.00	0.00	0.00	0.40	0.00	0.00
Freon22	0.00	0.00	0.00	0.00	0.00	0.00	0.00	0.00
Chloromethane	0.00	0.00	0.00	0.00	0.00	0.00	0.00	0.00
Freon114	0.00	0.00	0.00	0.00	0.00	0.00	0.00	0.00
Freon113	0.00	0.00	0.00	0.00	0.00	0.00	0.00	0.00
Vinylchloride	0.00	0.00	0.00	0.00	0.00	0.00	1.00	0.00
Bromomethane	0.00	0.00	0.00	0.00	0.00	0.00	0.00	0.00
Chloroethane	0.00	0.30	0.00	0.00	0.00	0.00	0.00	0.00
Freon11	0.00	0.00	0.00	0.00	0.00	0.00	0.00	0.00
Freon12	0.00	0.00	0.00	0.00	0.00	0.00	0.00	0.00
Ethylbromide	0.00	0.30	0.00	0.00	0.00	0.00	0.00	0.00
1,1-Dichloroethylene	0.00	0.00	0.00	0.00	0.00	0.00	1.00	0.00
Dichloromethane	0.00	0.00	0.00	0.00	0.00	0.00	0.00	0.00
trans-1,2-Dichloroethylene	0.00	0.00	0.00	0.00	0.00	0.00	1.00	0.00
1,1-Dichloroethane	0.00	0.30	0.00	0.00	0.00	0.00	0.00	0.00
cis-1,2-Dichloroethylene	0.00	0.00	0.00	0.00	0.00	0.00	1.00	0.00
Bromochloromethane	0.00	0.00	0.00	0.00	0.00	0.00	0.00	0.00
Chloroform	0.00	0.00	0.00	0.00	0.00	0.00	0.00	0.00

Continued on Next Page...

Table 1 – Continued

NAPS VOC species	OLE	PAR	TOL	XYL	FORM	ALD2	ETH	ISOP
1,2-Dichloroethane	0.00	0.30	0.00	0.00	0.00	0.00	0.00	0.00
1,1,1-Trichloroethane	0.00	0.30	0.00	0.00	0.00	0.00	0.00	0.00
Carbontetrachloride	0.00	0.00	0.00	0.00	0.00	0.00	0.00	0.00
Dibromomethane	0.00	0.30	0.00	0.00	0.00	0.00	0.00	0.00
1,2-Dichloropropane	0.00	1.00	0.00	0.00	0.00	0.00	0.00	0.00
Bromodichloromethane	0.00	0.00	0.00	0.00	0.00	0.00	0.00	0.00
Trichloroethylene	0.00	0.00	0.00	0.00	0.00	0.00	1.00	0.00
cis-1,3-Dichloropropene	0.67	0.33	0.00	0.00	0.00	0.00	0.00	0.00
trans-1,3-Dichloropropene	0.67	0.33	0.00	0.00	0.00	0.00	0.00	0.00
1,1,2-Trichloroethane	0.00	0.00	0.00	0.00	0.00	0.00	1.00	0.00
Bromotrichloromethane	0.00	0.00	0.00	0.00	0.00	0.00	0.00	0.00
Dibromochloromethane	0.00	0.00	0.00	0.00	0.00	0.00	0.00	0.00
EDB	0.00	0.30	0.00	0.00	0.00	0.00	0.00	0.00
Tetrachloroethylene	0.00	0.00	0.00	0.00	0.00	0.00	1.00	0.00
Chlorobenzene	0.00	0.17	0.00	0.00	0.00	0.00	0.00	0.00
Benzylchloride	0.00	0.17	0.00	0.00	0.00	0.00	0.00	0.00
Bromoform	0.00	0.00	0.00	0.00	0.00	0.00	0.00	0.00
1,4-Dichlorobutane	0.00	1.00	0.00	0.00	0.00	0.00	0.00	0.00
1,1,2,2-Tetrachloroethane	0.00	0.30	0.00	0.00	0.00	0.00	0.00	0.00
1,3-Dichlorobenzene	0.00	0.17	0.00	0.00	0.00	0.00	0.00	0.00
1,4-Dichlorobenzene	0.00	0.17	0.00	0.00	0.00	0.00	0.00	0.00
1,2-Dichlorobenzene	0.00	0.17	0.00	0.00	0.00	0.00	0.00	0.00
1,2,4-Trichlorobenzene	0.00	0.17	0.00	0.00	0.00	0.00	0.00	0.00

Continued on Next Page...

Table 1 – Continued

NAPS VOC species	OLE	PAR	TOL	XYL	FORM	ALD2	ETH	ISOP
Hexachlorobutadiene	0.50	0.00	0.00	0.00	0.00	0.50	0.00	0.00
Formaldehyde	0.00	0.00	0.00	0.00	1.00	0.00	0.00	0.00
Acetaldehyde	0.00	0.00	0.00	0.00	0.00	2.00	0.00	0.00
Acrolein	0.00	3.00	0.00	0.00	0.00	0.00	0.00	0.00
Acetone	0.00	3.00	0.00	0.00	0.00	0.00	0.00	0.00
Propionaldehyde	0.00	1.00	0.00	0.00	0.00	2.00	0.00	0.00
Crotonaldehyde	0.00	0.00	0.00	0.00	0.00	4.00	0.00	0.00
MEK (=Methyethylketone)	0.00	4.00	0.00	0.00	0.00	0.00	0.00	0.00
Benzaldehyde	0.00	5.00	0.00	0.00	0.00	2.00	0.00	0.00
2-Pentanone/Isovaleraldehyde	0.00	3.00	0.00	0.00	0.00	2.00	0.00	0.00
Valeraldehyde	0.00	3.00	0.00	0.00	0.00	2.00	0.00	0.00
o-Tolualdehyde	0.00	6.00	0.00	0.00	0.00	2.00	0.00	0.00
m-Tolualdehyde	0.00	6.00	0.00	0.00	0.00	2.00	0.00	0.00
p-Tolualdehyde	0.00	6.00	0.00	0.00	0.00	2.00	0.00	0.00
MIBK	0.00	4.00	0.00	0.00	0.00	2.00	0.00	0.00
Hexanal	0.00	4.00	0.00	0.00	0.00	2.00	0.00	0.00
2,5-Dimethylbenzaldehyde	0.00	5.00	0.00	0.00	0.00	2.00	0.00	0.00

List of Tables

Table 2. List of model ozone episodes given dates, meso-scale circulation regimes and additional characteristics of each episode. The circulation regimes are for the 3-fully modeled days within each episode. See text for details.

Year	Dates	Circulation Regimes	Notes
1985	July 19-22	I-IV-IV	Event modeled by NRC and SAI
1987	August 24-28	IV-IV-IV	Type IV circulation
1993	August 1-5	I-I-I	Pacific 1993 field campaign
1995	July 16-20	III-III-III	Aircraft based observations
1998	July 24-28	II-III-II	
2001	August 9-13	II-II-II	Pacific 2001 field campaign
2006	June 23-27	I-I-I	Type I circulation

Table 3. List of inventoried source sectors and sources in the MV emissions inventory.

Source Sector	Source
Point	Bulk Shipping Terminals
	Chemical Manufacturing
	Electric Power Generation
	Metal Foundries and Metal Fabrication
	Municipal Solid Waste Incineration
	Non-metallic Mineral Processing Industries
	Paper and Allied Products
	Petroleum Products
	Primary Metal Industries
	Wood Products
	Misc. Point Sources
Area	Agricultural
	Burning
	Gasoline Marketing
	Landfills
	Natural Sources
	Solvent Evaporation
	Space Heating
	Misc. Area Sources
Mobile	Light Duty Vehicles
	Heavy Duty Vehicles
	Aircraft
	Rail
	Marine
	Non-road

Table 4. Average daily emission rates (metric tones/day) within the Lower Fraser Valley based on the Metro Vancouver emission inventories (Greater Vancouver Regional District (2003), Greater Vancouver Regional District (2007)).

	1985			2005		
Source	CO	NOx	VOC	CO	NOx	VOC
Point	111	32	44	43	24	14
Area	56	9	107	53	17	96
Biogenic	0	2	100	0	2	97
LDV+HDV	1768	182	150	639	59	51
Marine	2	16	1	3	23	1
Rail	2	14	0	1	10	1
Air	14	2	2	18	3	3
Non-road+other	304	20	34	447	29	34
Total	2256	277	439	1207	167	296

Table 5. Average daily emission rates (metric tones/day) within the Lower Fraser Valley based on the SMOKE emissions model during an ozone episode.

		1985			2005	
Source	CO	NOx	VOC	CO	NOx	VOC
Point	108	28	109	43	21	35
Area	21	3	258	6	1	83
Biogenic	56	0	128	56	0	128
LDV+HDV	2514	176	426	651	53	127
Marine	13	24	10	17	35	14
Rail	2	18	1	2	13	1
Air	12	2	4	16	3	5
Non-road+other	353	37	125	130	16	38
Total	3079	288	1061	921	142	431

TABLE 6. Names, abbreviations and formulae of the various statistical metrics used in the report. P_i is the i^{th} predicted value, O_i is the i^{th} observed value, N is the number of observations, $P_i^{'}$ is the deviation of the i^{th} predicted value from the mean predicted value and $O_i^{'}$ is the deviation of the i^{th} observed value from the mean observed value. Note that some of the metrics are referred to by multiple names.

Abbreviation	Name	Formula
RMSE	Root Mean Square Error	$\left[\frac{1}{N}\sum(P_i - O_i)^2\right]^{1/2}$
IOA	Index of Agreement	$1 - \left[\sum(P_i - O_i)^2 / \sum(\lvert P_i^{'}\rvert + \lvert O_i^{'}\rvert)^2\right]$
MBE	Mean Bias Error	$\frac{1}{N}\sum(P_i - O_i)$
MB	Mean Bias	$\frac{1}{N}\sum(P_i - O_i)$
ME	Mean Error	$\frac{1}{N}\sum\lvert P_i - O_i\rvert$
MAE	Mean Absolute Error	$\frac{1}{N}\sum\lvert P_i - O_i\rvert$
NMB	Normalized Mean Bias	$\frac{\sum(P_i - O_i)}{\sum O_i} * 100\%$
NMBE	Normalized Mean Bias Error	$\frac{\sum(P_i - O_i)}{\sum O_i} * 100\%$
NME	Normalized Mean Error	$\frac{\sum\lvert P_i - O_i\rvert}{\sum O_i} * 100\%$
NMAE	Normalized Mean Absolute Error	$\frac{\sum\lvert P_i - O_i\rvert}{\sum O_i} * 100\%$
NE	Normalized Error	$\frac{\sum\lvert P_i - O_i\rvert}{\sum O_i} * 100\%$
MNB	Mean Normalized Bias	$\frac{1}{N}\sum\frac{(P_i - O_i)}{O_i} * 100\%$
MNAE	Mean Normalized Absolute Error	$\frac{1}{N}\sum\frac{\lvert P_i - O_i\rvert}{O_i} * 100\%$

TABLE 7. Domain-wide overall ozone performance statistics for all WRF/CMAQ simulations and for the NRC (Smyth et al. 2006) MM5/CMAQ 2001 simulation.

Statistic	2006	2001	1998	1995	1993	1987	1985	NRC
n (data points)	1660	1717	1543	1319	1098	650	644	5948
Model mean (ppb)	27.6	26.8	36.1	27.6	25.1	16.8	24.5	21.8
Obs mean (ppb)	21.1	21.1	23.6	16.8	14.3	17.6	27.7	19.2
MB (ppb)	6.5	5.7	12.5	10.8	10.1	-0.9	-3.2	2.6
NMB (%)	30.7	27.0	53.2	64.3	70.6	-4.9	-11.5	13.3
ME (ppb)	10.0	11.5	15.3	13.2	13.1	10.4	12.0	9.8
NME (%)	47.0	54.4	65.0	78.9	91.7	59.1	43.2	51.2
% within factor of 2	67.9	54.9	55.2	52.0	44.1	42.3	53.9	58.6

Table 8. Meteorological evaluation stations within the 4km modeling domain.

Station Abbreviation	Location	Latitude	Longitude	Elevation (ft asl)
YXX	Abbotsford, B. C. Can.	49.03333	-122.36667	177
YVR	Vancouver Int'l, Can.	49.18333	-123.16667	10
YHE	Hope, B. C. Can.	49.36667	-121.48333	128
WEZ	Saturna Island Can.	48.78333	-123.05	79
YYJ	Victoria Int. Airport, B. C. Can.	48.65	-123.43333	66
YQQ	Comox, B. C. Can.	49.71667	-124.9	79
WEL	Entrance Island Can.	49.21667	-123.80	16
WQC	Port Alberni, B. C. Can.	49.25	-124.83333	7
WSP	Sheringham Point Can.	48.38333	-123.91667	69
WGP	Pemberton Automatic Can.	50.3	-122.73333	669
YDC	Princeton Airport Can.	49.46667	-120.51667	2297
YPW	Powell River Airport Can.	49.83333	-124.5	427
YAZ	Tofino Airport Can.	49.08333	-125.76667	79
WDR	Discovery Island Can.	48.42	-123.23	49
YBL	Campbell River Airport Can.	49.95	-125.26667	348
WLY	Lytton, B. C. Can.	50.23333	-121.58333	751
YZT	Port Hardy, B. C. Can.	50.68333	-127.36667	72
WEB	Estevan Point, B. C. Can.	49.38333	-126.55	23
WVF	Sand Heads CS, B. C. Can.	49.1	-123.3	43
BEL	Bellingham Wa. USA	48.80000	-122.53330	000
PAE	Evrett Paine Wa. USA	47.90000	-122.28330	000
QUI	Quillayute Wa. USA	47.95000	-124.55000	000
SEA	Seattle Int'l Wa. USA	47.45000	-122.30000	000

TABLE 9. Temperature time series statistics at meteorological stations within the 4km domain for the 2006 episode.

Stn	N	$< Obs >$	$< WRF >$	δObs	δWRF	slope	int	RMSE	RMSEs	RMSEu	Index	MAE	NMAE	MBE	NMBE
-	#	^{o}C	^{o}C	^{o}C	^{o}C	-	^{o}C	^{o}C	^{o}C	^{o}C	-	^{o}C	^{o}C	^{o}C	^{o}C
YXX	97	21.4	19.4	6.0	7.2	1.16	-5.4	3.0	2.2	1.9	0.95	2.4	0.8	2.0	0.7
YVR	97	19.4	18.1	2.7	3.2	1.06	-2.5	2.0	1.4	1.5	0.88	1.5	0.5	1.4	0.5
YHE	97	22.3	19.0	5.6	7.1	1.21	-8.1	4.1	3.5	2.0	0.90	3.4	1.2	3.3	1.1
WEZ	97	21.4	16.5	3.8	1.0	0.18	12.6	5.9	5.8	0.7	0.50	5.1	1.7	5.0	1.7
YYJ	97	20.2	19.0	5.5	4.3	0.76	3.6	2.1	1.8	1.1	0.96	1.7	0.6	1.2	0.4
YQQ	97	20.4	18.3	4.6	3.9	0.71	3.9	3.2	2.4	2.1	0.86	2.4	0.8	2.0	0.7
WEL	97	20.4	18.2	2.3	1.2	0.42	9.6	2.7	2.6	0.8	0.64	2.2	0.8	2.2	0.7
WQC	97	20.8	20.5	7.9	6.4	0.79	4.1	2.2	1.7	1.4	0.98	1.7	0.6	0.2	0.1
WSP	97	15.7	15.8	3.7	2.0	0.37	10.1	2.7	2.3	1.4	0.75	2.2	0.8	-0.2	-0.1
WGP	97	20.3	18.2	8.5	7.4	0.85	0.9	3.1	2.5	1.8	0.96	2.4	0.8	2.1	0.7
YDC	97	22.3	18.2	7.8	7.0	0.87	-1.1	4.6	4.3	1.8	0.91	4.1	1.4	4.1	1.4
YPW	57	20.3	18.4	4.7	4.1	0.75	5.1	1.8	1.2	1.4	0.95	1.4	0.5	-0.2	-0.1
YAZ	53	19.0	15.5	4.5	1.2	0.18	12.2	5.0	4.9	0.9	0.55	4.4	1.5	3.3	1.1
DIS	97	19.1	14.9	4.0	1.2	0.25	10.2	5.2	5.1	0.8	0.57	4.4	1.5	4.2	1.4
YBL	65	22.8	19.4	5.5	5.2	0.80	3.4	2.1	1.5	1.5	0.96	1.6	0.5	1.1	0.4
WLY	97	24.5	19.9	7.5	6.8	0.84	-0.6	5.3	4.7	2.5	0.87	4.7	1.6	4.6	1.5
YZT	97	14.0	13.5	2.6	1.3	0.35	8.7	2.0	1.7	1.0	0.70	1.6	0.5	0.5	0.2
WEB	97	14.5	14.0	1.9	1.4	-0.09	15.4	2.5	2.1	1.3	0.36	2.1	0.7	0.5	0.2
WVF	97	18.3	17.7	2.2	1.0	0.41	10.2	1.5	1.4	0.4	0.78	1.2	0.4	0.6	0.2

Table 10. Windspeed time series statistics at various stations within the 4km domain for the 2006 event.

Stn	N	$< Obs >$	$< WRF >$	δObs	δWRF	slope	int	RMSE	RMSEs	RMSEu	Index	MAE	NMAE	MBE	NMBE
-	#	m/s	m/s	m/s	m/s	-	m/s	m/s	m/s	m/s	-	m/s	m/s	m/s	m/s
YVR	97	5.70	4.79	2.63	2.01	0.68	0.93	1.5	1.2	0.9	0.89	1.3	22.3	0.9	15.9
YHE	97	3.51	2.37	1.86	1.22	0.39	1.01	1.9	1.6	1.0	0.68	1.6	44.2	1.1	32.6
WEZ	97	2.09	5.63	0.94	2.84	0.93	3.69	4.4	3.5	2.7	0.26	3.7	178.6	-3.5	-169.0
YYJ	97	2.02	2.18	1.20	1.17	0.11	1.95	1.6	1.1	1.2	0.43	1.2	61.3	-0.2	-7.8
YQQ	97	4.59	3.89	2.35	1.63	0.53	1.45	1.7	1.3	1.0	0.82	1.3	27.6	0.7	15.2
WEL	97	8.51	8.88	3.36	3.53	0.83	1.80	2.2	0.7	2.1	0.89	1.7	19.8	-0.4	-4.4
WQC	97	0.94	2.48	0.68	0.93	0.31	2.19	1.8	1.6	0.9	0.40	1.6	173.2	-1.5	-164.4
WSP	97	3.76	3.14	2.76	1.85	0.41	1.60	2.3	1.7	1.5	0.73	1.9	51.1	0.6	16.7
WGP	97	0.91	0.86	0.61	0.62	0.61	0.31	0.6	0.2	0.5	0.77	0.4	48.1	0.0	5.1
YDC	97	1.00	1.23	1.18	0.74	0.11	1.12	1.3	1.1	0.7	0.45	1.0	102.8	-0.2	-22.7
YPW	97	2.78	3.37	2.03	1.45	0.51	1.95	1.5	1.1	1.0	0.79	1.2	44.2	-0.6	-21.2
YAZ	53	3.41	3.15	2.13	2.49	0.74	0.18	1.9	0.9	1.7	0.80	1.6	45.9	0.7	20.3
DIS	97	3.10	3.16	1.79	1.62	0.25	2.39	2.0	1.3	1.5	0.57	1.7	53.9	-0.1	-1.9
YBL	65	3.87	2.80	2.26	0.87	0.30	1.50	2.1	2.0	0.7	0.63	1.6	41.4	1.2	31.1
WLY	97	1.89	1.94	1.75	1.95	0.15	1.65	2.4	1.5	1.9	0.45	1.8	96.9	-0.0	-2.6
YZT	97	3.34	6.23	1.93	2.66	0.72	3.81	3.7	2.9	2.3	0.54	3.1	93.6	-2.9	-86.7
WEB	97	8.96	6.20	2.41	3.54	1.13	-3.89	3.6	2.8	2.3	0.68	3.0	33.1	2.8	30.8
WVF	97	7.18	7.35	3.83	3.30	0.77	1.79	1.7	0.9	1.4	0.94	1.2	16.8	-0.2	-2.3

TABLE 11. Wind direction time series statistics at various stations within the 4km domain for the 2006 event.

Stn	N	$< ObsU >$	$< WRFU >$	$< ObsV >$	$< WRFV >$	$\delta ObsU$	$\delta WRFU$	$\delta ObsV$	$\delta WRFV$	Vector Correlation
-	#	m/s	m/s	m/s	m/s	m/s	m/s	m/s	m/s	-
YXX	97	0.94	1.31	0.70	0.31	1.49	0.91	1.74	1.21	0.60
YVR	97	4.04	3.95	-3.09	-2.10	2.64	2.22	2.59	1.44	0.71
YHE	97	0.63	0.71	-0.27	0.37	3.75	2.24	1.19	0.89	0.65
WEZ	97	1.28	3.33	-0.56	-3.82	1.14	2.02	1.43	3.16	0.38
YYJ	97	-0.67	0.64	0.19	-1.11	1.97	1.09	1.08	1.72	0.51
YQQ	97	1.59	1.14	-3.94	-3.49	1.68	0.96	2.41	1.85	0.70
WEL	97	7.13	7.71	-4.09	-4.30	3.08	3.29	2.60	1.54	0.76
WQC	97	-0.15	-1.70	0.19	-0.50	0.83	1.11	0.78	1.18	0.14
WSP	97	1.39	1.38	-1.12	-0.91	4.01	2.90	1.63	1.34	0.70
WGP	97	0.50	-0.07	-0.03	-0.39	0.88	0.42	0.42	0.73	0.41
YDC	97	0.20	0.13	-0.04	-0.33	1.21	0.77	0.94	0.70	0.20
YPW	97	2.72	2.54	-0.37	-1.86	1.98	1.46	0.63	1.05	0.58
YAZ	53	2.48	2.66	-0.00	-1.49	2.65	2.12	1.76	1.51	0.65
DIS	97	1.40	1.22	-1.09	-0.71	2.06	1.84	2.35	2.70	0.61
YBL	65	1.22	1.42	-2.30	-1.69	3.02	1.51	2.07	1.18	0.71
WLY	97	-0.73	0.14	1.33	1.44	0.66	0.61	1.98	2.21	0.19
YZT	97	1.54	4.78	-1.99	-3.87	1.98	2.29	2.15	1.63	0.51
WEB	97	8.18	4.45	-3.47	-4.11	2.28	2.90	1.39	2.39	0.55
WVF	97	5.80	5.98	-3.03	-3.61	4.21	3.10	2.43	2.54	0.78

Table 12. Temperature time series statistics at various stations within the 4km domain for the 2001 event.

Stn	N	$<Obs>$	$<WRF>$	δObs	δWRF	slope	int	RMSE	RMSEs	RMSEu	Index	MAE	NMAE	MBE	NMBE
-	#	^{o}C	^{o}C	^{o}C	^{o}C	-	^{o}C	^{o}C	^{o}C	^{o}C	-	^{o}C	^{o}C	^{o}C	^{o}C
YXX	97	21.2	21.1	6.1	5.7	0.82	3.6	3.0	1.1	2.8	0.93	2.3	0.8	0.2	0.1
YVR	97	19.8	20.1	2.8	2.6	0.77	4.8	1.6	0.7	1.4	0.91	1.2	0.4	-0.4	-0.1
YHE	97	23.1	20.6	5.2	4.1	0.65	5.5	3.8	3.1	2.2	0.84	3.1	1.1	2.5	0.8
WEZ	97	20.8	17.0	4.0	1.0	0.14	14.1	5.2	5.1	0.8	0.54	4.1	1.4	3.8	1.3
YYJ	97	19.2	20.0	5.6	3.3	0.49	10.6	3.5	2.9	1.8	0.84	2.9	1.0	-0.8	-0.3
YQQ	97	20.7	20.8	4.2	3.9	0.74	5.5	2.6	1.1	2.3	0.89	2.0	0.7	-0.1	-0.0
WEL	97	19.7	19.0	1.5	1.0	0.30	13.1	1.5	1.3	0.9	0.61	1.1	0.4	0.7	0.2
WQC	96	20.8	23.9	7.5	4.1	0.53	12.9	4.9	4.7	1.2	0.84	4.1	1.4	-3.1	-1.1
WSP	97	14.5	15.6	4.7	2.8	0.39	10.0	3.7	3.0	2.1	0.73	2.8	1.0	-1.1	-0.4
WGP	97	20.8	19.9	7.8	4.3	0.52	9.0	4.0	3.8	1.2	0.89	3.4	1.1	0.9	0.3
YDC	96	23.4	20.0	7.9	5.0	0.58	6.4	5.3	4.8	2.1	0.84	4.4	1.5	3.5	1.2
YPW	57	21.0	19.9	4.6	3.5	0.61	8.8	2.4	1.9	1.4	0.90	2.0	0.7	-0.7	-0.3
YAZ	53	15.6	15.0	4.2	2.7	0.45	8.0	2.8	2.3	1.6	0.81	1.8	0.6	0.5	0.2
DIS	97	17.0	15.4	4.2	1.1	0.15	12.8	4.0	3.9	0.8	0.49	2.8	1.0	1.6	0.5
YBL	65	23.0	21.6	5.6	4.7	0.65	8.5	2.8	2.0	1.9	0.92	2.1	0.7	-0.6	-0.2
WLY	97	26.0	22.2	6.8	3.8	0.47	10.1	5.6	5.2	2.1	0.75	4.8	1.6	3.8	1.3
YZT	97	13.2	14.0	2.3	1.8	0.36	9.2	2.3	1.7	1.5	0.67	1.6	0.6	-0.8	-0.3
WEB	97	14.3	15.1	3.0	2.5	0.42	9.1	2.9	1.9	2.2	0.68	2.2	0.8	-0.8	-0.3
BLI	91	18.6	18.3	5.0	3.9	0.65	6.3	2.7	1.8	2.0	0.90	2.1	0.7	0.3	0.1
PAE	91	19.8	18.3	4.6	3.5	0.67	4.9	2.6	2.2	1.5	0.89	2.2	0.8	1.6	0.5
UIL	93	15.1	16.1	4.3	5.2	1.03	0.6	2.7	1.0	2.5	0.92	1.9	0.7	-1.0	-0.3
SEA	92	21.3	22.2	5.6	4.6	0.80	5.3	1.9	1.5	1.1	0.97	1.4	0.5	-1.0	-0.3

Table 13. Windspeed time series statistics at various stations within the 4km domain for the 2001 event.

Stn	N	$< Obs >$	$< WRF >$	δObs	δWRF	slope	int	RMSE	RMSEs	RMSEu	Index	MAE	NMAE	MBE	NMBE
-	#	m/s	m/s	m/s	m/s	-	m/s	m/s	m/s	m/s	-	m/s	m/s	m/s	m/s
YXX	97	1.71	1.78	1.48	1.01	0.28	1.31	1.4	1.1	0.9	0.64	1.1	65.1	-0.1	-4.5
YVR	97	2.20	2.22	1.80	1.41	0.33	1.50	1.7	1.2	1.3	0.66	1.3	59.3	-0.0	-1.0
YHE	97	3.11	1.92	1.76	1.14	0.42	0.61	1.8	1.6	0.9	0.68	1.5	48.1	1.2	38.3
WEZ	97	2.89	3.18	1.68	2.10	-0.47	4.54	3.1	2.5	1.9	0.16	2.5	87.3	-0.3	-10.0
YYJ	97	1.74	2.38	1.23	1.43	0.44	1.62	1.6	0.9	1.3	0.61	1.2	68.0	-0.6	-36.9
YQQ	97	2.55	2.85	1.41	1.21	0.19	2.36	1.7	1.2	1.2	0.55	1.3	50.5	-0.3	-11.7
WEL	97	3.65	5.61	2.45	2.47	0.49	3.83	3.2	2.3	2.1	0.63	2.5	68.8	-2.0	-53.6
WQC	95	1.56	1.76	1.28	1.13	0.12	1.54	1.6	1.1	1.1	0.45	1.1	68.4	-0.2	-11.1
WSP	97	6.13	3.95	3.57	2.07	0.45	1.20	3.2	2.9	1.3	0.72	2.7	44.2	2.2	35.6
WGP	97	0.65	1.04	0.63	0.57	0.56	0.67	0.6	0.5	0.4	0.71	0.5	83.7	-0.4	-59.4
YDC	96	1.39	1.16	1.72	0.83	0.19	0.90	1.6	1.4	0.8	0.57	1.2	85.4	0.2	16.4
YPW	97	0.81	1.58	0.92	0.86	0.38	1.27	1.2	1.0	0.8	0.60	0.9	113.5	-0.8	-94.9
YAZ	53	2.14	2.14	1.33	1.09	0.24	1.88	1.5	1.0	1.1	0.55	1.2	56.3	-0.2	-11.6
DIS	97	3.70	3.18	1.59	1.41	0.42	1.62	1.6	1.1	1.2	0.67	1.3	35.9	0.5	14.0
YBL	65	2.20	2.21	1.22	0.89	0.03	1.93	1.3	1.2	0.6	0.37	1.0	46.7	0.2	9.4
WLY	97	3.56	2.82	2.69	1.85	0.45	1.22	2.2	1.7	1.4	0.75	1.7	48.7	0.7	20.9
YZT	97	1.90	4.53	1.86	1.99	0.54	3.50	3.2	2.8	1.7	0.56	2.7	143.8	-2.6	-138.1
WEB	97	1.63	2.91	2.65	1.57	0.37	2.30	2.4	2.1	1.2	0.70	2.0	122.9	-1.3	-78.7
WVF	96	3.32	3.86	2.07	2.27	0.62	1.76	2.1	0.9	1.8	0.75	1.6	48.6	-0.5	-15.1
BLI	77	1.81	1.72	0.73	1.11	-0.18	2.13	1.4	0.9	1.1	0.35	1.2	65.4	-0.0	-0.4
PAE	73	1.57	1.92	0.66	0.81	0.22	1.63	0.9	0.7	0.7	0.48	0.8	48.5	-0.4	-26.1
UIL	57	1.27	1.65	0.78	1.13	0.93	0.77	1.1	0.7	0.8	0.71	0.8	65.9	-0.7	-53.2
SEA	75	1.47	1.90	0.60	0.91	0.72	0.93	0.8	0.5	0.6	0.64	0.7	45.3	-0.5	-35.2

TABLE 14. Wind direction time series statistics at various stations within the 4km domain for the 2001 event.

Stn	N	$< ObsU >$	$< WRFU >$	$< ObsV >$	$< WRFV >$	$\delta ObsU$	$\delta WRFU$	$\delta ObsV$	$\delta WRFV$	Vector Correlation
-	#	m/s	m/s	m/s	m/s	m/s	m/s	m/s	m/s	-
YXX	97	1.11	0.24	0.62	0.32	1.34	1.53	1.32	1.31	0.53
YVR	97	0.95	1.73	-0.23	-0.60	2.18	1.49	1.55	1.12	0.64
YHE	97	0.37	0.41	-0.15	-0.15	3.34	1.95	1.25	0.75	0.58
WEZ	97	1.53	1.45	1.56	-1.55	1.39	1.47	2.12	2.80	0.55
YYJ	97	-0.48	-0.21	0.17	-1.48	1.80	1.64	1.04	1.61	0.47
YQQ	97	0.50	0.84	-2.10	-2.53	1.18	0.90	1.56	1.29	0.57
WEL	97	2.66	4.31	-1.57	-2.98	2.43	2.69	2.00	1.67	0.42
WQC	95	-0.16	-0.71	-0.03	0.25	1.54	0.93	1.29	1.54	0.43
WSP	97	4.69	2.56	-2.55	-0.72	4.31	3.26	1.84	1.26	0.67
WGP	97	0.45	0.12	0.01	-0.31	0.69	0.59	0.37	0.76	0.46
YDC	96	0.40	0.22	0.00	-0.41	1.82	0.84	1.20	0.90	0.51
YPW	97	0.77	1.16	-0.15	-0.66	0.91	1.02	0.26	0.55	0.55
YAZ	53	0.55	0.92	1.13	0.21	1.43	1.52	1.67	1.58	0.56
DIS	97	2.28	1.83	0.21	0.00	2.57	1.63	2.11	2.47	0.65
YBL	65	-0.40	0.68	-0.85	-1.35	2.00	1.70	1.22	0.70	0.54
WLY	97	0.09	0.21	2.85	2.19	1.19	0.45	3.23	2.46	0.53
YZT	97	-0.28	3.72	-1.29	-2.39	0.94	1.92	2.12	1.11	0.45
WEB	97	0.91	1.06	-0.84	-0.76	1.94	2.23	2.09	2.06	0.48
WVF	96	0.43	2.31	-0.75	-2.06	2.86	2.43	2.54	2.14	0.57
BLI	77	0.45	0.55	1.48	0.97	0.72	0.71	1.18	1.54	0.38
PAE	73	0.46	0.49	-1.27	-1.18	0.94	0.89	1.02	1.35	0.53
UIL	57	0.64	0.41	0.73	0.18	0.69	1.37	1.03	1.38	0.71
SEA	75	0.47	0.52	-0.49	-0.80	0.80	1.08	1.34	1.52	0.75

TABLE 15. Temperature time series statistics at various stations within the 4km domain for the 1998 event.

Stn	N	$<Obs>$	$<WRF>$	δObs	δWRF	slope	int	RMSE	RMSEs	RMSEu	Index	MAE	NMAE	MBE	NMBE
-	#	^{o}C	^{o}C	^{o}C	^{o}C	-	^{o}C	^{o}C	^{o}C	^{o}C	-	^{o}C	^{o}C	^{o}C	^{o}C
YXX	96	23.1	21.2	5.7	5.9	0.97	-1.1	2.7	1.8	2.0	0.95	2.3	0.8	1.8	0.6
YVR	97	22.3	19.8	3.5	3.9	0.90	-0.2	3.4	2.5	2.3	0.81	2.7	0.9	2.5	0.8
YHE	97	24.4	20.6	4.6	6.2	1.26	-10.3	4.6	4.0	2.2	0.83	4.1	1.4	3.9	1.3
YYJ	97	19.9	19.9	4.7	3.1	0.63	7.3	1.9	1.7	0.9	0.94	1.6	0.5	0.1	0.0
YQQ	97	22.7	20.6	4.1	3.7	0.79	2.8	3.0	2.3	2.0	0.86	2.5	0.8	2.1	0.7
WEL	97	22.0	18.0	2.7	0.7	0.16	14.4	4.6	4.6	0.5	0.48	4.1	1.4	4.0	1.4
WQC	97	23.9	22.8	6.9	5.8	0.81	3.4	2.5	1.8	1.7	0.96	1.8	0.6	1.2	0.4
WSP	97	15.1	16.6	2.6	1.8	0.49	9.2	2.3	1.9	1.3	0.73	1.9	0.7	-1.4	-0.5
WGP	97	25.5	20.8	7.7	6.2	0.78	1.0	5.3	5.0	1.5	0.87	4.7	1.6	4.7	1.6
YDC	97	26.2	20.2	7.4	6.2	0.80	-0.8	6.5	6.2	1.9	0.81	6.0	2.0	6.0	2.0
YPW	57	23.3	20.4	4.7	3.7	0.67	6.7	2.5	1.9	1.7	0.90	1.9	0.7	1.0	0.3
YAZ	53	18.0	14.8	4.3	1.3	0.17	11.7	4.8	4.7	1.0	0.54	3.6	1.2	3.2	1.1
DIS	97	17.1	15.9	3.3	1.2	0.24	11.7	2.9	2.7	0.9	0.60	2.2	0.8	1.2	0.4
YBL	65	25.1	21.9	5.3	4.3	0.69	6.5	2.4	2.0	1.3	0.93	2.0	0.7	1.3	0.4
WLY	97	30.0	22.4	6.3	5.1	0.73	0.5	8.0	7.7	2.2	0.68	7.5	2.5	7.5	2.5
YZT	97	16.3	15.2	3.3	1.9	0.40	8.7	2.6	2.2	1.4	0.73	2.1	0.7	1.1	0.4
WEB	97	17.2	14.1	2.7	1.4	-0.03	14.5	4.4	4.2	1.4	0.40	3.6	1.3	3.1	1.1
WVF	97	20.7	18.6	2.7	0.6	0.16	15.3	3.1	3.1	0.4	0.53	2.5	0.8	2.1	0.7

TABLE 16. Windspeed time series statistics at various stations within the 4km domain for the 1998 event.

Stn	N	$<Obs>$	$<WRF>$	δObs	δWRF	slope	int	RMSE	RMSEs	RMSEu	Index	MAE	NMAE	MBE	NMBE
-	#	m/s	m/s	m/s	m/s	-	m/s	m/s	m/s	m/s	-	m/s	m/s	m/s	m/s
YXX	96	1.22	1.39	1.17	1.01	0.57	0.70	0.9	0.5	0.7	0.81	0.7	57.1	-0.2	-15.1
YVR	97	2.34	1.98	1.43	1.36	0.47	0.88	1.4	0.8	1.2	0.69	1.2	49.3	0.4	15.7
YHE	97	3.55	2.10	2.08	1.50	0.51	0.31	2.1	1.8	1.1	0.72	1.7	47.2	1.4	40.6
WEZ	97	3.18	1.98	1.80	1.44	0.02	1.91	2.6	2.1	1.4	0.45	2.0	63.9	1.2	37.5
YYJ	97	1.60	1.01	1.32	0.81	0.38	0.40	1.2	1.0	0.6	0.71	0.9	57.5	0.6	36.6
YQQ	97	2.51	1.91	1.51	1.24	0.47	0.73	1.4	1.0	1.0	0.72	1.2	47.0	0.6	23.9
WEL	97	4.03	4.10	2.92	3.16	0.66	1.45	2.7	1.0	2.5	0.78	2.1	53.2	-0.1	-1.8
WQC	97	0.73	1.54	0.94	1.08	0.61	1.10	1.3	0.9	0.9	0.66	1.0	132.7	-0.8	-111.7
WSP	97	4.69	3.52	3.40	1.89	0.48	1.25	2.3	2.1	0.9	0.82	1.9	40.1	1.2	25.0
WGP	97	0.98	0.74	1.05	0.59	0.23	0.51	1.0	0.8	0.5	0.58	0.6	63.0	0.2	24.7
YDC	97	1.69	1.42	1.39	1.10	0.30	0.91	1.4	1.0	1.0	0.61	1.1	64.0	0.3	16.4
YPW	97	1.03	1.74	0.98	1.18	0.42	1.31	1.4	0.9	1.1	0.58	1.1	106.9	-0.7	-69.8
YAZ	53	1.97	1.89	1.63	1.09	0.23	1.24	1.6	1.3	0.9	0.57	1.3	68.1	0.3	13.7
DIS	97	3.12	2.62	1.75	1.88	0.78	0.20	1.4	0.6	1.3	0.83	1.2	38.9	0.5	15.9
YBL	65	1.84	2.11	1.11	0.82	0.27	1.39	1.1	0.8	0.8	0.61	0.9	46.5	-0.0	-2.3
WLY	97	4.47	2.41	3.31	2.28	0.46	0.35	3.2	2.7	1.7	0.70	2.6	57.1	2.1	46.1
YZT	97	2.07	3.63	1.75	2.22	0.55	2.48	2.6	1.7	2.0	0.58	2.2	106.1	-1.6	-75.3
WEB	97	3.12	2.87	1.78	1.88	0.79	0.40	1.3	0.4	1.2	0.86	1.1	33.9	0.2	7.9
WVF	97	3.02	2.89	1.56	2.20	0.37	1.77	2.3	1.0	2.1	0.53	1.9	63.6	0.1	4.3

TABLE 17. Wind direction time series statistics at various stations within the 4km domain for the 1998 event.

Stn	N	$< ObsU >$	$< WRFU >$	$< ObsV >$	$< WRFV >$	$\delta ObsU$	$\delta WRFU$	$\delta ObsV$	$\delta WRFV$	Vector Correlation
-	#	m/s	m/s	m/s	m/s	m/s	m/s	m/s	m/s	-
YXX	96	0.85	1.06	0.70	0.63	0.98	0.97	0.82	0.70	0.45
YVR	97	0.54	1.39	0.50	-0.34	2.24	1.46	1.41	1.20	0.65
YHE	97	1.24	0.75	-0.36	0.15	3.73	2.26	1.20	0.70	0.61
WEZ	97	2.11	0.98	1.60	-0.18	1.49	1.04	2.03	1.98	0.37
YYJ	97	-1.30	-0.40	0.20	-0.27	1.46	0.95	0.66	0.63	0.52
YQQ	97	0.53	0.48	-1.86	-1.55	1.37	0.92	1.73	1.31	0.62
WEL	97	1.11	3.27	-0.97	-1.97	3.42	2.95	3.32	1.86	0.56
WQC	97	-0.36	-0.58	0.31	0.36	0.91	0.95	0.61	1.27	0.43
WSP	97	3.98	2.99	-1.86	-0.91	3.46	2.17	1.51	0.55	0.65
WGP	97	0.34	0.04	-0.15	-0.28	1.24	0.44	0.63	0.57	0.33
YDC	97	0.39	0.59	-0.15	-0.47	1.88	1.22	1.06	0.83	0.36
YPW	97	0.78	1.26	-0.26	-0.71	1.04	1.16	0.50	0.92	0.40
YAZ	53	0.53	1.41	1.00	0.03	1.98	1.35	1.18	0.94	0.44
DIS	97	1.82	1.86	1.09	1.06	2.66	1.90	1.14	1.48	0.53
YBL	65	-0.36	0.92	-0.64	-0.93	1.69	1.58	1.12	0.93	0.61
WLY	97	-0.15	0.04	3.77	1.53	1.34	0.38	3.87	2.90	0.57
YZT	97	0.24	2.73	-1.29	-1.22	1.46	2.19	1.88	2.08	0.50
WEB	97	1.14	1.62	-0.63	-0.92	3.00	2.26	1.50	1.80	0.59
WVF	97	-0.56	1.88	0.54	-0.92	2.47	1.87	2.22	2.30	0.43

TABLE 18. Temperature time series statistics at various stations within the 4km domain for the 1995 event.

Stn	N	$< Obs >$	$< WRF >$	δObs	δWRF	slope	int	RMSE	RMSEs	RMSEu	Index	MAE	NMAE	MBE	NMBE
-	#	^{o}C	^{o}C	^{o}C	^{o}C	-	^{o}C	^{o}C	^{o}C	^{o}C	-	^{o}C	^{o}C	^{o}C	^{o}C
YXX	97	23.7	21.5	6.1	6.5	1.01	-2.4	3.1	2.2	2.2	0.94	2.5	0.8	2.2	0.7
YVR	97	20.5	19.5	2.7	3.5	1.15	-4.1	1.9	1.1	1.6	0.90	1.5	0.5	1.0	0.3
YHE	93	26.0	20.3	5.7	6.4	1.08	-8.2	6.3	6.0	1.9	0.79	6.0	2.0	6.0	2.0
WEZ	97	21.5	16.9	2.8	0.9	0.16	13.4	5.2	5.2	0.8	0.47	4.6	1.6	4.6	1.6
YYJ	97	21.6	20.6	5.2	3.2	0.58	8.1	2.7	2.4	1.1	0.90	2.3	0.8	1.1	0.4
YQQ	97	22.3	19.9	3.9	4.0	0.88	0.3	3.1	2.5	1.9	0.85	2.7	0.9	2.4	0.8
WEL	97	20.8	18.8	2.0	0.8	0.33	12.0	2.5	2.4	0.5	0.60	2.0	0.7	2.0	0.7
WQC	95	23.2	22.6	7.6	5.9	0.74	5.2	2.6	2.1	1.6	0.96	2.2	0.8	0.7	0.3
WSP	97	18.1	17.3	5.1	1.3	0.17	14.2	4.4	4.3	1.0	0.50	3.6	1.2	0.8	0.3
WGP	97	23.7	18.6	8.5	6.8	0.79	-0.2	5.5	5.4	1.1	0.88	5.1	1.7	5.1	1.7
YDC	97	22.5	17.8	6.8	6.5	0.91	-2.7	5.1	4.7	1.8	0.87	4.7	1.6	4.7	1.6
YPW	57	22.6	20.1	4.8	4.0	0.70	6.3	2.1	1.5	1.4	0.93	1.5	0.5	0.5	0.2
YAZ	52	20.2	15.9	5.8	2.1	0.22	11.5	6.2	6.0	1.4	0.58	5.0	1.7	4.1	1.4
YBL	65	25.1	21.7	4.9	4.8	0.76	5.1	2.1	1.6	1.4	0.94	1.6	0.5	1.0	0.3
WLY	97	27.0	19.2	5.9	6.1	0.98	-7.2	8.0	7.7	1.9	0.71	7.7	2.6	7.7	2.6
YZT	96	15.9	14.4	3.7	1.5	0.27	10.2	3.3	3.1	1.1	0.62	2.5	0.9	1.5	0.5
WEB	97	17.7	15.3	3.3	2.0	0.23	11.3	3.9	3.5	1.9	0.57	3.1	1.1	2.4	0.8
WVF	97	19.4	18.4	1.8	0.8	0.35	11.7	1.6	1.5	0.5	0.68	1.3	0.4	1.0	0.3

TABLE 19. Windspeed time series statistics at various stations within the 4km domain for the 1995 event.

Stn	N	$< Obs >$	$< WRF >$	δObs	δWRF	slope	int	RMSE	RMSEs	RMSEu	Index	MAE	NMAE	MBE	NMBE
-	#	m/s	m/s	m/s	m/s	-	m/s	m/s	m/s	m/s	-	m/s	m/s	m/s	m/s
YXX	97	1.67	2.04	1.43	1.12	0.22	1.67	1.6	1.2	1.1	0.57	1.1	68.2	-0.4	-22.7
YVR	97	5.91	3.94	2.17	1.76	0.63	0.24	2.4	2.1	1.1	0.71	2.1	34.9	2.0	33.3
YHE	93	3.80	2.54	2.14	0.97	0.24	1.60	2.2	2.1	0.8	0.62	1.8	48.5	1.3	33.5
WEZ	97	4.11	4.81	2.10	2.45	0.32	3.49	2.8	1.6	2.3	0.55	2.4	57.7	-0.7	-17.2
YYJ	97	1.47	2.23	1.20	1.58	-0.16	2.47	2.2	1.6	1.6	0.32	1.7	114.1	-0.8	-52.0
YQQ	97	4.51	2.70	1.85	1.25	0.49	0.50	2.2	2.0	0.9	0.66	1.9	41.7	1.8	40.0
WEL	97	8.07	6.76	3.25	3.21	0.86	-0.21	2.1	1.4	1.6	0.90	1.7	21.2	1.3	16.2
WQC	95	1.70	2.24	1.74	0.87	-0.03	2.29	2.1	1.9	0.9	0.37	1.7	102.9	-0.5	-32.1
WSP	97	4.24	2.85	3.83	1.88	0.34	1.40	3.2	2.9	1.3	0.67	2.6	60.7	1.4	32.8
WGP	97	1.06	1.17	0.65	0.69	0.45	0.69	0.7	0.4	0.6	0.67	0.6	54.3	-0.1	-10.6
YDC	97	1.72	1.58	1.30	0.82	0.15	1.33	1.4	1.1	0.8	0.52	1.1	65.8	0.1	8.2
YPW	97	2.31	2.41	1.38	1.14	0.45	1.37	1.2	0.8	0.9	0.73	1.0	43.6	-0.1	-4.3
YAZ	52	2.25	1.50	1.45	1.17	0.38	1.00	1.5	1.0	1.1	0.67	1.2	53.9	0.4	17.6
YBL	65	4.08	2.40	1.80	0.93	0.25	1.18	2.5	2.3	0.8	0.57	1.9	47.3	1.9	46.2
WLY	97	2.48	1.71	2.83	2.05	0.62	0.16	1.7	1.3	1.1	0.88	1.1	46.3	0.8	31.1
YZT	96	2.59	5.38	2.21	2.37	0.67	3.65	3.4	2.9	1.9	0.61	2.9	112.1	-2.8	-108.0
WEB	97	6.57	3.78	1.84	2.55	0.45	0.80	3.8	3.0	2.4	0.44	3.4	52.4	2.8	42.5
WVF	97	8.10	5.95	2.93	2.75	0.84	-0.89	2.5	2.2	1.2	0.83	2.2	27.3	2.1	26.5

TABLE 20. Wind direction time series statistics at various stations within the 4km domain for the 1995 event.

Stn	N	$< ObsU >$	$< WRFU >$	$< ObsV >$	$< WRFV >$	$\delta ObsU$	$\delta WRFU$	$\delta ObsV$	$\delta WRFV$	Vector Correlation
-	#	m/s	m/s	m/s	m/s	m/s	m/s	m/s	m/s	-
YXX	97	1.22	0.79	0.80	-0.03	1.24	1.36	1.07	1.73	0.42
YVR	97	3.36	2.47	-3.16	-1.66	3.45	2.77	2.57	1.47	0.70
YHE	93	0.00	-0.27	-0.98	-0.05	3.89	2.24	1.76	1.26	0.60
WEZ	97	2.75	2.51	-0.95	-2.41	1.51	1.86	3.26	3.69	0.65
YYJ	97	-0.98	0.73	0.22	-1.49	1.34	1.31	0.88	1.69	0.39
YQQ	97	1.49	0.71	-4.10	-2.41	1.10	0.73	1.88	1.42	0.62
WEL	97	6.23	5.16	-3.08	-3.21	4.44	3.84	2.81	2.07	0.78
WQC	95	-0.91	-1.37	0.79	0.07	1.23	1.13	1.73	1.13	0.53
WSP	97	1.95	0.59	-0.01	-0.60	5.34	2.95	0.69	1.40	0.64
WGP	97	0.65	0.15	-0.08	-0.39	0.87	0.67	0.61	0.82	0.42
YDC	97	0.22	0.52	-0.94	-0.93	0.92	0.77	1.70	1.00	0.27
YPW	97	1.86	1.38	-0.37	-0.92	1.75	1.56	0.80	1.32	0.52
YAZ	52	0.60	0.12	1.12	0.66	1.63	1.09	1.73	1.39	0.58
YBL	65	2.24	1.29	-2.48	-1.26	2.51	1.60	1.59	0.87	0.56
WLY	97	0.11	0.12	0.99	0.37	0.78	0.45	3.55	2.57	0.63
YZT	96	0.62	4.83	-1.31	-1.83	2.34	2.16	2.01	1.75	0.62
WEB	97	1.93	1.40	-3.43	-1.53	3.37	2.75	4.47	2.99	0.59
WVF	97	4.86	3.84	-4.36	-3.02	4.66	3.64	3.16	2.43	0.86

TABLE 21. Temperature time series statistics at various stations within the 4km domain for the 1993 event.

Stn	N	$< Obs >$	$< WRF >$	δObs	δWRF	slope	int	RMSE	RMSEs	RMSEu	Index	MAE	NMAE	MBE	NMBE
-	#	^{o}C	^{o}C	^{o}C	^{o}C	-	^{o}C	^{o}C	^{o}C	^{o}C	-	^{o}C	^{o}C	^{o}C	^{o}C
YXX	97	23.4	22.3	6.1	6.3	1.01	-1.3	1.9	1.1	1.5	0.98	1.5	0.5	1.1	0.4
YVR	97	21.2	19.9	3.0	3.4	0.93	0.1	2.4	1.4	1.9	0.86	1.8	0.6	1.3	0.5
YHE	45	25.0	19.8	5.3	6.6	1.18	-7.3	3.3	2.9	1.6	0.92	2.8	0.9	2.7	0.9
YYJ	97	21.7	21.0	5.3	3.2	0.58	8.5	2.5	2.4	0.9	0.91	2.2	0.7	0.7	0.2
YQQ	97	22.6	20.4	4.5	4.3	0.82	1.9	3.2	2.4	2.1	0.87	2.5	0.9	2.2	0.7
YDC	53	21.5	17.4	6.8	6.2	0.87	1.5	1.9	1.5	1.2	0.98	1.5	0.5	1.2	0.4
YPW	57	22.6	20.2	5.0	4.0	0.71	6.1	2.0	1.6	1.3	0.94	1.6	0.5	0.6	0.2
YAZ	53	21.3	17.8	5.0	1.4	0.23	13.0	5.2	5.1	1.0	0.59	4.6	1.6	3.4	1.2
YBL	65	25.0	22.0	5.0	4.5	0.76	5.3	2.0	1.5	1.3	0.95	1.6	0.5	0.8	0.3
YZT	97	16.3	16.0	3.8	1.7	0.31	11.0	2.9	2.6	1.3	0.68	2.3	0.8	0.3	0.1

TABLE 22. Windspeed time series statistics at various stations within the 4km domain for the 1993 event.

Stn	N	$< Obs >$	$< WRF >$	δObs	δWRF	slope	int	RMSE	RMSEs	RMSEu	Index	MAE	NMAE	MBE	NMBE
-	#	m/s	m/s	m/s	m/s	-	m/s	m/s	m/s	m/s	-	m/s	m/s	m/s	m/s
YXX	97	1.50	2.39	1.36	1.33	0.10	2.24	2.0	1.5	1.3	0.46	1.6	109.4	-0.9	-59.1
YVR	97	3.91	3.63	2.59	1.22	0.31	2.42	2.0	1.8	0.9	0.69	1.7	42.8	0.3	7.0
YHE	97	3.96	2.55	2.02	0.95	-0.04	2.73	2.7	2.5	0.9	0.37	2.3	58.0	1.4	35.6
YYJ	97	1.71	2.96	1.12	1.54	-0.22	3.34	2.4	1.9	1.5	0.28	1.9	111.7	-1.3	-73.1
YQQ	97	3.41	2.13	1.67	1.18	0.35	0.94	2.0	1.7	1.0	0.59	1.6	47.7	1.3	37.5
YDC	53	1.23	1.88	1.27	1.11	0.33	1.30	1.5	1.0	1.2	0.58	1.2	96.0	-0.5	-38.3
YPW	97	0.99	1.94	1.01	0.92	0.26	1.68	1.5	1.2	0.9	0.54	1.2	121.0	-0.9	-95.5
YAZ	53	1.65	2.01	2.07	1.65	0.59	1.38	1.7	1.1	1.3	0.79	1.5	89.0	-0.7	-43.0
YBL	97	2.27	2.58	1.69	1.06	0.12	2.31	1.8	1.5	1.0	0.49	1.5	66.1	-0.3	-13.3
YZT	97	1.82	3.35	1.58	2.19	0.59	2.29	2.6	1.7	2.0	0.56	2.0	109.9	-1.5	-84.5

TABLE 23. Wind direction time series statistics at various stations within the 4km domain for the 1993 event.

Stn	N	$< ObsU >$	$< WRFU >$	$< ObsV >$	$< WRFV >$	$\delta ObsU$	$\delta WRFU$	$\delta ObsV$	$\delta WRFV$	Vector Correlation
-	#	m/s	m/s	m/s	m/s	m/s	m/s	m/s	m/s	-
YXX	97	0.16	-0.60	-0.46	-0.80	1.40	1.91	1.39	1.69	0.36
YVR	97	3.15	2.57	-1.91	-1.65	2.33	1.99	1.74	1.18	0.52
YHE	97	-2.66	-1.39	-0.59	-0.64	3.25	1.37	1.38	1.52	0.37
YYJ	97	0.14	0.95	-0.26	-2.30	1.64	1.39	1.20	1.69	0.47
YQQ	97	1.68	0.78	-2.38	-1.78	1.33	0.83	2.06	1.21	0.57
YDC	53	-0.34	-0.20	-0.47	-1.12	0.97	1.34	1.37	1.08	0.27
YPW	97	0.93	1.09	-0.22	-0.88	1.00	1.31	0.30	0.87	0.40
YAZ	53	1.12	0.59	-0.29	-0.65	1.81	1.90	1.55	1.54	0.59
YBL	97	1.08	1.69	-1.45	-0.77	1.62	1.85	1.47	0.95	0.51
YZT	97	-0.12	2.19	-0.97	-1.08	1.33	2.64	1.77	1.77	0.39

TABLE 24. Temperature time series statistics at various stations within the 4km domain for the 1987 event.

tn	N	$< Obs >$	$< WRF >$	δObs	δWRF	slope	int	RMSE	RMSEs	RMSEu	Index	MAE	NMAE	MBE	NMBE
-	#	^{o}C	^{o}C	^{o}C	^{o}C	-	^{o}C	^{o}C	^{o}C	^{o}C	-	^{o}C	^{o}C	^{o}C	^{o}C
YXX	97	18.3	17.0	5.9	4.6	0.75	3.4	2.4	1.9	1.4	0.95	1.9	0.7	1.2	0.4
YVR	97	19.0	17.2	3.9	3.6	0.85	1.1	2.4	1.9	1.4	0.90	2.0	0.7	1.8	0.6
YYJ	97	15.8	16.4	3.9	2.8	0.61	6.8	2.2	1.6	1.5	0.88	1.8	0.6	-0.6	-0.2
YQQ	97	18.7	16.9	3.3	3.4	0.92	-0.3	2.2	1.7	1.4	0.89	1.9	0.6	1.7	0.6
YPW	57	20.1	17.4	4.0	3.5	0.79	3.4	1.7	1.2	1.1	0.95	1.3	0.4	0.9	0.3
YAZ	65	14.0	12.3	2.3	1.1	0.23	9.3	2.5	2.3	1.1	0.54	1.8	0.6	1.5	0.5
YBL	65	20.7	17.4	4.7	4.1	0.80	2.4	2.4	1.9	1.4	0.93	2.0	0.7	1.7	0.6
YZT	97	14.3	13.5	2.7	2.0	0.39	8.0	2.5	1.8	1.6	0.69	2.1	0.7	0.8	0.3

TABLE 25. Windspeed time series statistics at various stations within the 4km domain for the 1987 event.

Stn	N	$<Obs>$	$<WRF>$	δObs	δWRF	slope	int	RMSE	RMSEs	RMSEu	Index	MAE	NMAE	MBE	NMBE
-	#	m/s	m/s	m/s	m/s	-	m/s	m/s	m/s	m/s	-	m/s	m/s	m/s	m/s
YXX	97	1.71	1.57	1.48	0.82	0.25	1.13	1.3	1.1	0.7	0.61	1.1	61.8	0.1	8.4
YVR	97	2.35	2.27	1.54	0.84	-0.01	2.29	1.8	1.5	0.8	0.36	1.3	57.1	0.1	3.3
YYJ	97	1.60	1.51	1.44	0.78	0.14	1.28	1.4	1.2	0.7	0.51	1.2	74.3	0.1	5.5
YQQ	97	1.83	2.12	1.28	1.06	0.37	1.43	1.3	0.8	0.9	0.67	1.0	55.5	-0.3	-15.6
YPW	97	1.17	2.30	1.16	1.08	0.20	2.07	1.8	1.5	1.0	0.52	1.5	131.0	-1.1	-96.3
YAZ	65	2.65	1.35	1.56	1.07	0.43	0.38	1.7	1.4	0.9	0.68	1.4	52.6	1.1	42.9
YBL	91	1.49	1.86	1.49	0.80	0.13	1.60	1.5	1.3	0.8	0.52	1.2	82.4	-0.3	-20.5
YZT	97	1.82	3.38	1.60	1.76	0.33	2.78	2.5	1.9	1.7	0.52	2.1	118.3	-1.6	-86.1

TABLE 26. Wind direction time series statistics at various stations within the 4km domain for the 1987 event.

Stn	N	$< ObsU >$	$< WRFU >$	$< ObsV >$	$< WRFV >$	$\delta ObsU$	$\delta WRFU$	$\delta ObsV$	$\delta WRFV$	Vector Correlation
-	#	m/s	m/s	m/s	m/s	m/s	m/s	m/s	m/s	-
YXX	97	1.11	0.94	0.68	0.46	1.20	0.95	1.41	1.07	0.43
YVR	97	-0.89	-0.08	0.83	0.31	2.34	2.04	1.00	1.21	0.46
YYJ	97	-1.21	-0.57	0.63	-0.47	1.43	1.10	0.86	0.91	0.36
YQQ	97	0.10	0.32	-0.99	-1.33	1.36	1.11	1.48	1.59	0.61
YPW	97	0.64	0.10	-0.29	-0.09	1.28	1.99	0.76	1.54	0.53
YAZ	65	0.89	0.74	1.34	0.41	1.77	0.85	1.95	1.22	0.58
YBL	91	0.14	0.69	-0.28	-0.67	1.85	1.54	0.99	0.88	0.51
YZT	97	0.48	2.81	-1.01	-1.14	1.19	1.72	1.79	1.52	0.55

TABLE 27. Temperature time series statistics at various stations within the 4km domain for the 1985 event.

Stn	N	$< Obs >$	$< WRF >$	δObs	δWRF	slope	int	RMSE	RMSEs	RMSEu	Index	MAE	NMAE	MBE	NMBE
-	#	^oC	^oC	^oC	^oC	-	^oC	^oC	^oC	^oC	-	^oC	^oC	^oC	^oC
YXX	97	22.2	20.7	6.7	6.3	0.90	0.6	2.2	1.6	1.5	0.97	1.7	0.6	1.5	0.5
YVR	97	21.2	19.5	4.1	3.7	0.81	2.3	2.4	1.8	1.6	0.90	2.0	0.7	1.7	0.6
YHE	77	25.3	19.0	5.8	6.7	1.00	-4.5	5.0	4.5	2.3	0.84	4.5	1.5	4.5	1.5
YYJ	97	19.4	19.7	5.4	3.3	0.52	9.6	3.1	2.6	1.7	0.86	2.8	0.9	-0.3	-0.1
YQQ	97	22.4	19.9	4.5	3.7	0.73	3.5	3.3	2.8	1.7	0.85	2.7	0.9	2.5	0.9
YDC	65	25.5	19.0	7.4	6.8	0.76	3.0	4.1	3.7	1.9	0.91	3.4	1.1	3.2	1.1
YPW	65	23.4	19.7	5.0	3.4	0.55	8.5	3.4	3.1	1.4	0.83	2.7	0.9	2.1	0.7
YAZ	65	15.8	14.7	4.5	1.6	0.30	10.1	3.4	3.3	0.9	0.68	2.3	0.8	1.0	0.3
YBL	65	25.5	21.0	5.4	4.9	0.74	4.5	3.0	2.6	1.4	0.91	2.4	0.8	2.2	0.7
WLY	77	28.5	22.4	5.8	5.0	0.73	3.0	5.7	5.1	2.5	0.77	5.0	1.6	4.9	1.6
YZT	97	14.2	13.4	2.5	1.4	0.43	7.3	1.8	1.6	0.9	0.77	1.5	0.5	0.7	0.3

TABLE 28. Windspeed time series statistics at various stations within the 4km domain for the 1985 event.

Stn	N	$< Obs >$	$< WRF >$	δObs	δWRF	slope	int	RMSE	RMSEs	RMSEu	Index	MAE	NMAE	MBE	NMBE
-	#	m/s	m/s	m/s	m/s	-	m/s	m/s	m/s	m/s	-	m/s	m/s	m/s	m/s
YXX	97	1.68	1.82	1.65	1.20	0.58	0.86	1.0	0.7	0.7	0.86	0.8	48.9	-0.1	-8.7
YVR	97	2.16	2.28	1.43	1.37	0.37	1.48	1.6	0.9	1.3	0.66	1.1	53.0	-0.1	-5.4
YHE	97	4.14	2.58	2.83	1.90	0.57	0.24	2.2	2.0	1.0	0.80	1.8	44.3	1.6	37.6
YYJ	97	1.70	1.46	1.30	0.93	0.40	0.78	1.1	0.8	0.8	0.72	0.9	53.1	0.2	13.9
YQQ	97	3.26	2.73	1.82	1.11	0.42	1.36	1.4	1.2	0.8	0.75	1.2	35.3	0.5	16.3
YDC	97	1.92	1.59	1.86	1.30	0.50	0.62	1.3	1.0	0.9	0.81	1.0	52.4	0.3	17.5
YPW	97	1.92	2.50	1.62	1.37	0.45	1.63	1.6	1.1	1.2	0.71	1.3	66.4	-0.6	-30.2
YAZ	65	2.62	2.50	1.42	1.93	-0.11	2.61	2.3	1.6	1.7	0.34	1.9	70.9	0.3	11.6
YBL	97	2.97	2.04	1.56	0.85	0.22	1.39	1.7	1.5	0.8	0.57	1.3	44.6	0.9	31.2
WLY	77	4.90	5.26	2.56	2.09	0.33	3.68	2.7	1.7	2.1	0.64	2.1	43.1	-0.4	-8.1
YZT	97	1.99	4.73	1.66	1.52	0.33	4.07	3.3	3.0	1.4	0.49	2.8	139.4	-2.7	-137.5

TABLE 29. Wind direction time series statistics at various stations within the 4km domain for the 1985 event.

Stn	N	$<ObsU>$	$<WRFU>$	$<ObsV>$	$<WRFV>$	$\delta ObsU$	$\delta WRFU$	$\delta ObsV$	$\delta WRFV$	Vector Correlation
-	#	m/s	m/s	m/s	m/s	m/s	m/s	m/s	m/s	-
YXX	97	1.28	1.34	0.73	0.71	1.39	1.17	1.20	1.05	0.63
YVR	97	0.26	1.75	0.32	-0.55	2.43	1.45	0.84	1.24	0.53
YHE	97	2.36	2.03	-0.74	0.54	4.09	2.16	1.85	0.80	0.66
YYJ	97	-1.15	-0.51	0.51	-0.36	1.31	1.07	1.13	1.08	0.52
YQQ	97	1.10	0.76	-2.80	-2.51	1.37	0.66	1.74	1.17	0.66
YDC	97	0.93	0.78	-0.15	-0.31	2.19	1.55	1.23	0.80	0.55
YPW	97	1.87	1.87	-0.32	-1.21	1.58	1.37	0.46	1.04	0.44
YAZ	65	0.47	1.85	1.59	-0.27	1.36	1.93	2.08	1.63	0.58
YBL	97	1.27	0.67	-1.48	-1.40	2.28	1.32	1.51	0.84	0.60
WLY	77	1.26	-0.18	4.53	5.17	1.63	0.69	2.40	2.11	0.28
YZT	97	-0.32	4.07	-1.34	-2.29	1.23	1.40	1.83	0.95	0.54

Table 30. Air quality evaluation stations within the 4km modeling domain.

Station ID	Location	Latitude	Longitude
01	Robson Square	49.28222222	-123.1219400
02	Kitsilano	49.26167000	-123.1633333
04	Kensington Park	49.27944444	-122.9711111
06	North Vancouver	49.30167000	-123.0202800
09	Rocky Point Park	49.28083000	-122.8491700
12	Chilliwack	49.15611000	-121.9405600
13	North Delta	49.15833333	-122.9016700
15	Surrey East	49.13277778	-122.6941700
17	Richmond South	49.14139000	-123.1083300
18	Burnaby South	49.21528000	-122.9855600
20	Pitt Meadows	49.24527778	-122.7088900
26	Mahon Park	49.32388889	-123.0836100
27	Langley Central	49.09556000	-122.5669400
29	Hope Airport	49.36972222	-121.4994444
30	Maple Ridge	49.21500000	-122.5819444
31	Vancouver International Airport	49.18638889	-123.1522200
32	Coquitlam	49.28805556	-122.7913900
33	Central Abbotsford	49.04278000	-122.3097200
Vic	Victoria Topaz	48.4292	-123.3583
Nam	Nanaimo	49.0500	-123.8667
Sat	Saturna Island	48.7745	-123.1700

TABLE 31. CO time series statistics at various stations within the 4km domain for the 2006 event.

Stn	N	$< Obs >$	$< CMAQ >$	δObs	$\delta CMAQ$	slope	int	RMSE	RMSEs	RMSEu	Index	MAE	NMAE	MBE	NMBE
-	#	ppb	ppb	ppb	ppb	-	ppb	ppb	ppb	ppb	-	ppb	ppb	ppb	ppb
T01	44	411.4	260.4	78.4	226.6	-0.09	191.1	272.3	269.9	36.5	-1.65	256.3	62.3	256.3	62.3
T02	40	202.5	172.6	15.8	147.2	-0.12	145.5	87.5	83.1	27.6	-0.82	81.2	40.1	81.2	40.1
T04	45	257.8	384.0	65.7	328.0	1.20	-86.3	143.5	38.0	138.4	0.74	100.7	39.1	35.9	13.9
T06	45	555.6	344.0	99.0	297.1	-0.13	271.8	394.6	372.5	130.2	-1.06	369.1	66.4	355.7	64.0
T09	44	613.6	379.5	218.4	312.9	0.12	199.3	459.0	392.5	238.0	-0.01	395.7	64.5	342.9	55.9
T12	44	290.9	254.9	29.1	152.5	0.40	118.0	150.4	58.0	138.7	0.02	116.4	40.0	55.4	19.0
T15	45	295.6	400.8	60.1	363.7	2.84	-558.8	240.9	110.3	214.2	0.50	167.0	56.5	16.4	5.5
T18	44	372.7	299.8	84.5	269.2	0.37	35.3	227.6	207.8	92.9	0.04	213.2	57.2	200.9	53.9
T20	42	292.9	411.6	51.3	329.2	0.43	130.7	249.1	46.8	244.6	0.40	175.2	59.8	36.8	12.6
T26	45	322.2	289.7	59.9	212.2	0.29	95.0	177.4	139.1	110.2	0.19	162.4	50.4	132.7	41.2
T27	45	331.1	365.4	46.8	355.5	3.54	-855.2	300.6	118.4	276.3	0.31	212.8	64.3	14.5	4.4
T29	43	297.7	159.7	55.6	64.1	-0.01	137.6	181.7	173.4	54.2	-2.28	173.4	58.2	164.2	55.2
T30	42	335.7	356.6	69.2	292.2	0.81	48.3	309.5	19.0	308.9	0.27	212.4	63.3	14.2	4.2
T31	45	208.9	167.8	46.8	150.3	-0.15	152.0	105.8	103.1	23.4	-0.57	95.1	45.5	88.3	42.3
T32	45	311.1	317.8	80.4	237.0	0.97	-34.3	228.1	44.9	223.7	0.40	179.3	57.6	44.8	14.4
T33	19	231.6	294.5	58.2	186.1	-0.35	280.6	109.5	83.4	70.9	0.58	92.4	39.9	32.8	14.2
Vic	42	189.2	419.3	92.3	203.5	-0.03	288.6	175.7	132.9	115.0	0.53	116.7	61.7	-94.4	-49.9

TABLE 32. NOx time series statistics at various stations within the 4km domain for the 2006 event.

Stn	N	$< Obs >$	$< CMAQ >$	δObs	$\delta CMAQ$	slope	int	RMSE	RMSEs	RMSEu	Index	MAE	NMAE	MBE	NMBE
-	#	ppb	ppb	ppb	ppb	-	ppb	ppb	ppb	ppb	-	ppb	ppb	ppb	ppb
T01	44	23.0	22.8	7.3	14.6	-0.14	16.0	13.9	13.2	4.5	0.26	11.0	47.8	10.3	44.9
T02	40	6.1	17.1	1.7	12.1	0.42	7.7	5.0	4.3	2.6	0.66	4.4	73.2	-4.2	-68.4
T04	45	23.2	22.3	9.4	16.1	0.14	5.9	17.4	16.2	6.3	0.36	15.3	66.0	14.1	60.8
T06	45	37.3	21.0	27.2	14.9	0.14	3.6	37.1	36.8	4.9	-0.04	28.5	76.6	28.5	76.5
T09	44	32.9	19.2	16.8	13.6	0.18	3.3	28.1	27.3	6.9	-0.10	24.5	74.5	23.6	71.9
T12	44	10.6	9.9	4.3	6.5	-0.21	8.3	8.7	6.9	5.3	0.25	7.4	69.6	4.6	43.4
T13	45	20.8	14.7	8.4	11.5	0.23	1.4	16.6	16.0	4.3	0.07	14.7	70.5	14.7	70.5
T15	45	13.3	17.3	7.8	11.9	0.37	2.3	10.2	7.7	6.7	0.70	8.2	62.0	6.0	45.3
T17	45	4.2	10.5	1.9	9.9	0.58	1.7	1.7	0.8	1.5	0.96	1.2	29.2	0.1	2.4
T18	44	18.8	16.3	10.6	14.0	0.16	2.5	16.3	15.8	3.9	0.37	13.4	71.7	13.1	70.0
T20	40	16.1	20.5	6.2	14.7	0.06	5.9	12.8	11.0	6.7	0.61	10.8	67.1	9.3	57.8
T26	45	16.3	18.4	10.5	11.8	0.36	4.3	9.7	9.1	3.4	0.72	6.5	40.0	6.1	37.6
T27	45	10.3	13.4	4.2	10.4	0.96	-2.6	7.6	3.1	7.0	0.69	6.0	57.6	3.1	29.7
T29	43	4.8	4.7	1.5	3.6	1.13	-3.1	3.0	2.5	1.6	0.60	2.7	56.7	2.5	52.6
T30	45	18.9	15.7	7.2	11.0	0.09	6.2	15.3	12.8	8.5	0.24	13.2	69.8	11.0	58.3
T31	45	11.5	12.0	5.9	10.9	0.11	4.8	7.8	7.6	1.9	0.53	5.5	48.2	5.5	47.5
T32	43	20.8	14.4	18.3	10.6	0.12	5.5	21.4	20.5	6.0	0.25	14.2	68.2	12.9	61.8
T33	45	7.1	15.8	5.1	13.0	1.15	-1.5	5.4	0.9	5.3	0.89	3.6	50.4	0.5	6.5
Vic	42	22.9	20.7	20.4	15.5	-0.01	12.7	24.0	22.8	7.5	0.32	15.9	69.6	10.4	45.3

Table 33. Ozone time series statistics at various stations within the 4km domain for the 2006 event.

Stn	N	$< Obs >$	$< CMAQ >$	δObs	$\delta CMAQ$	slope	int	RMSE	RMSEs	RMSEu	Index	MAE	NMAE	MBE	NMBE
-	#	ppb	ppb	ppb	ppb	-	ppb	ppb	ppb	ppb	-	ppb	ppb	ppb	ppb
T01	95	12.4	19.1	7.7	12.9	1.42	1.6	10.2	7.6	6.8	0.77	8.0	64.2	-6.9	-55.4
T02	89	21.5	21.7	13.4	11.3	0.71	7.0	7.6	4.0	6.5	0.90	5.9	27.6	-0.8	-3.5
T04	96	18.7	21.6	11.3	17.3	1.22	-1.2	11.3	3.9	10.6	0.83	9.4	50.2	-3.0	-15.9
T06	96	11.8	23.3	9.6	15.7	1.35	7.4	15.0	12.0	8.9	0.70	12.8	108.1	-11.6	-97.6
T09	95	14.3	27.1	13.7	17.0	1.07	11.5	15.2	12.5	8.7	0.79	12.6	87.6	-12.4	-86.6
T12	95	32.3	39.1	24.2	16.1	0.59	20.0	14.2	11.9	7.6	0.88	10.8	33.4	-6.7	-20.8
T13	96	17.8	25.7	12.0	16.4	1.12	5.8	12.5	8.2	9.4	0.82	9.9	56.0	-8.0	-45.2
T15	96	23.2	26.4	14.1	19.7	1.21	-1.4	10.5	4.5	9.5	0.90	8.4	36.4	-3.4	-14.8
T17	96	22.1	25.6	11.4	12.0	0.61	12.3	11.3	5.7	9.8	0.75	8.2	37.1	-3.5	-15.9
T18	95	19.2	24.2	11.5	16.3	1.14	2.4	11.1	5.4	9.7	0.83	9.4	49.1	-5.1	-26.6
T20	92	20.0	25.5	18.4	20.6	1.06	4.4	9.3	5.8	7.3	0.94	7.7	38.3	-5.7	-28.5
T26	95	15.7	26.7	12.1	12.5	0.89	12.8	12.9	11.1	6.5	0.78	11.2	71.3	-11.1	-70.4
T27	96	22.4	31.0	18.8	18.7	0.77	14.0	15.1	9.9	11.4	0.84	11.5	51.3	-8.9	-39.8
T29	94	35.1	44.3	24.7	8.9	0.26	35.4	21.4	20.4	6.2	0.65	17.4	49.7	-9.5	-27.0
T30	96	28.8	29.7	18.3	19.4	0.90	3.7	10.5	2.0	10.3	0.92	8.3	28.7	-0.9	-3.1
T31	96	19.6	24.4	9.5	11.0	0.75	10.0	9.9	5.5	8.3	0.75	7.0	35.8	-4.9	-25.2
T32	96	21.8	32.1	17.2	15.4	0.75	15.7	14.0	11.1	8.5	0.84	11.1	50.8	-10.2	-46.9
T33	46	26.9	30.5	20.0	21.6	0.92	3.6	10.1	2.2	9.9	0.93	8.5	31.7	-1.5	-5.6
Vic	93	20.0	33.6	16.2	17.1	0.57	22.7	21.3	15.7	14.4	0.66	17.0	85.2	-14.2	-70.9
Nam	86	27.7	31.3	6.0	9.4	1.07	1.5	8.2	3.6	7.4	0.71	6.4	22.9	-3.6	-13.0
Sat	96	37.1	31.1	8.4	11.1	0.79	2.1	10.8	6.1	8.9	0.69	9.0	24.2	5.8	15.8

TABLE 34. CO time series statistics at various stations within the 4km domain for the 2001 event.

Stn	N	$< Obs >$	$< CMAQ >$	δObs	$\delta CMAQ$	slope	int	RMSE	RMSEs	RMSEu	Index	MAE	NMAE	MBE	NMBE
-	#	ppb	ppb	ppb	ppb	-	ppb	ppb	ppb	ppb	-	ppb	ppb	ppb	ppb
T01	45	673.3	851.7	199.3	717.0	1.01	-1.6	696.8	6.2	696.8	0.31	283.8	42.2	-5.8	-0.9
T02	44	456.8	605.0	140.4	686.9	1.73	-275.0	679.9	117.3	669.7	0.27	256.2	56.1	-58.9	-12.9
T04	45	753.3	933.6	117.9	707.1	-1.81	2183.0	845.7	334.2	776.8	0.11	547.8	72.7	-63.9	-8.5
T06	44	522.7	832.6	134.4	576.2	1.30	10.8	633.9	174.6	609.3	0.28	367.5	70.3	-169.9	-32.5
T09	44	843.2	776.3	326.6	603.6	0.25	523.3	713.4	262.4	663.4	0.34	539.9	64.0	104.9	12.4
T12	43	446.5	392.9	88.2	219.3	-0.51	576.0	272.1	165.9	215.6	0.06	212.8	47.7	100.4	22.5
T15	45	366.7	737.4	76.9	634.5	4.26	-959.4	686.5	341.1	595.8	0.17	334.4	91.2	-234.7	-64.0
T17	45	320.0	445.9	96.8	301.5	0.47	180.4	240.0	52.0	234.3	0.43	121.2	37.9	-9.2	-2.9
T18	45	460.0	746.2	86.3	646.6	3.23	-959.3	572.6	202.2	535.6	0.35	288.1	62.6	-67.6	-14.7
T20	45	502.2	746.0	75.3	595.0	0.60	375.2	660.0	179.1	635.2	0.06	394.5	78.6	-176.6	-35.2
T26	45	426.7	702.4	117.6	490.4	3.20	-755.2	498.6	316.4	385.4	0.38	275.6	64.6	-185.6	-43.5
T27	45	326.7	503.1	49.5	359.5	1.46	-71.5	307.7	81.8	296.6	0.26	173.4	53.1	-78.6	-24.1
T29	45	346.7	242.4	54.8	135.7	-0.93	534.1	204.9	169.6	115.0	-0.44	177.3	51.1	133.7	38.6
T30	45	551.1	712.9	62.6	557.6	-2.43	2005.8	628.6	241.1	580.5	0.06	412.5	74.8	-113.9	-20.7
T31	44	347.7	454.0	97.6	436.4	1.68	-217.0	381.4	68.6	375.2	0.38	170.7	49.1	-19.6	-5.6
T32	44	506.8	610.0	138.8	437.4	1.51	-107.7	506.9	168.1	478.2	0.33	344.4	67.9	-152.6	-30.1
T33	44	479.5	431.0	109.1	214.5	-0.64	653.5	287.5	222.6	182.1	0.07	243.1	50.7	134.6	28.1
Vic	45	265.9	512.8	152.3	244.8	0.28	309.9	263.3	161.0	208.3	0.49	194.8	73.3	-119.6	-45.0

Table 35. NOx time series statistics at various stations within the 4km domain for the 2001 event.

Stn	N	$< Obs >$	$< CMAQ >$	δObs	$\delta CMAQ$	slope	int	RMSE	RMSEs	RMSEu	Index	MAE	NMAE	MBE	NMBE
-	#	ppb	ppb	ppb	ppb	-	ppb	ppb	ppb	ppb	-	ppb	ppb	ppb	ppb
T01	45	45.3	60.6	32.2	34.7	0.49	15.8	27.1	17.7	20.5	0.78	16.8	37.1	7.2	15.9
T02	44	22.7	49.4	18.7	32.9	0.86	12.7	24.6	9.9	22.5	0.73	16.4	72.2	-9.6	-42.3
T04	45	40.0	55.8	16.6	38.5	0.94	-4.6	29.2	7.0	28.3	0.69	22.6	56.5	6.9	17.3
T06	44	62.8	50.6	29.2	35.7	0.39	4.1	45.9	38.8	24.6	0.41	39.2	62.5	34.5	54.9
T09	44	33.9	43.0	15.4	34.2	0.49	12.0	29.1	9.5	27.6	0.57	22.7	67.0	5.4	15.9
T13	45	22.8	40.5	11.7	27.5	0.74	3.4	20.0	4.0	19.6	0.75	15.0	65.6	2.6	11.4
T15	45	14.4	38.7	10.0	31.6	1.51	0.0	24.8	8.9	23.1	0.63	14.3	99.4	-7.3	-51.1
T17	45	12.9	30.6	10.3	20.1	0.45	8.5	12.8	5.8	11.5	0.77	7.6	59.0	-1.4	-10.5
T18	45	33.8	48.5	16.9	33.7	0.67	-1.6	25.3	13.9	21.2	0.74	20.9	61.9	12.8	37.8
T20	45	26.6	41.1	10.9	33.3	0.17	20.1	30.0	9.2	28.6	0.47	21.7	81.3	2.1	7.8
T26	45	31.5	42.2	21.5	30.0	0.87	0.2	13.4	4.9	12.5	0.91	10.2	32.4	4.0	12.6
T27	45	12.1	22.1	7.0	19.5	0.05	12.4	15.3	6.6	13.7	0.52	9.9	81.3	-0.9	-7.2
T29	45	8.2	9.4	4.2	7.6	0.94	-2.0	5.6	2.5	5.0	0.70	4.5	55.0	2.5	30.4
T30	45	18.3	38.6	9.7	28.8	0.48	15.6	28.4	7.9	27.3	0.47	18.3	99.8	-6.0	-33.0
T31	44	33.8	35.8	14.7	27.7	0.13	14.6	28.4	19.6	20.5	0.43	22.4	66.3	14.9	44.2
T32	44	30.0	29.7	12.4	24.6	1.16	-10.6	19.7	6.1	18.8	0.67	16.4	54.7	5.8	19.3
T33	44	19.4	22.9	10.8	16.5	0.50	1.1	14.1	10.0	9.9	0.66	11.2	57.8	8.5	44.1

TABLE 36. Ozone time series statistics at various stations within the 4km domain for the 2001 event.

Stn	N	$< Obs >$	$< CMAQ >$	δObs	$\delta CMAQ$	slope	int	RMSE	RMSEs	RMSEu	Index	MAE	NMAE	MBE	NMBE
-	#	ppb	ppb	ppb	ppb	-	ppb	ppb	ppb	ppb	-	ppb	ppb	ppb	ppb
T01	95	11.8	15.8	16.1	18.4	0.83	6.4	13.7	5.1	12.7	0.82	8.4	71.7	-4.3	-36.8
T02	95	15.3	16.6	17.8	16.7	0.80	4.5	9.8	3.8	9.0	0.91	5.9	38.3	-1.3	-8.7
T04	96	19.7	22.2	14.5	24.8	1.24	-2.0	17.8	4.4	17.2	0.77	13.2	67.4	-2.7	-13.7
T06	95	15.5	24.0	13.0	24.0	1.33	3.5	19.3	9.6	16.8	0.72	14.7	95.3	-8.6	-55.8
T09	95	19.0	27.3	19.3	23.8	1.02	7.7	16.0	8.2	13.7	0.86	12.1	63.7	-8.2	-42.9
T12	94	26.5	38.0	24.6	16.5	0.54	24.2	19.1	16.5	9.7	0.80	15.8	59.7	-12.0	-45.5
T13	96	17.7	23.5	14.2	22.9	1.27	1.1	15.8	7.1	14.0	0.81	11.4	64.7	-6.0	-33.9
T15	96	29.1	26.8	16.9	22.1	1.15	-6.4	10.7	3.3	10.2	0.92	8.4	28.9	2.0	6.9
T17	96	21.3	22.4	20.1	20.7	0.78	6.0	14.2	4.6	13.5	0.86	9.8	46.0	-1.4	-6.4
T18	95	20.3	21.4	14.2	24.6	1.29	-4.3	17.0	4.4	16.4	0.79	12.5	61.8	-1.6	-7.7
T20	96	19.8	26.1	20.2	24.8	1.10	4.5	12.9	6.8	10.9	0.92	9.4	47.3	-6.5	-32.8
T26	96	17.9	26.9	18.0	20.4	0.90	10.9	15.6	9.3	12.5	0.83	13.0	72.6	-9.1	-50.9
T27	96	27.0	34.9	23.4	20.1	0.66	17.1	17.1	11.2	13.0	0.85	12.9	47.8	-7.8	-28.9
T29	95	31.7	40.2	24.5	13.7	0.39	27.8	19.7	17.1	9.8	0.74	15.6	49.1	-8.4	-26.5
T30	96	27.4	27.3	20.7	24.3	1.07	-1.7	10.1	1.4	10.0	0.95	7.7	28.2	-0.2	-0.6
T31	95	14.1	20.4	13.4	20.8	1.06	5.6	16.6	6.5	15.3	0.74	11.0	77.7	-6.4	-45.4
T32	95	22.3	33.1	19.6	20.7	0.86	13.8	16.5	11.0	12.3	0.84	13.4	59.9	-10.7	-47.8
T33	95	24.1	33.6	22.8	19.7	0.76	15.5	14.7	11.1	9.6	0.88	11.8	49.0	-9.7	-40.2
Vic	93	15.9	25.9	12.8	17.9	1.01	10.3	16.4	10.4	12.7	0.73	12.7	79.8	-10.4	-65.3
Sat	95	42.1	32.6	12.5	14.9	0.87	-3.9	14.0	9.5	10.3	0.76	11.6	27.5	9.3	22.1

TABLE 37. CO time series statistics at various stations within the 4km domain for the 1998 event.

Stn	N	$< Obs >$	$< CMAQ >$	δObs	$\delta CMAQ$	slope	int	RMSE	RMSEs	RMSEu	Index	MAE	NMAE	MBE	NMBE
-	#	ppb	ppb	ppb	ppb	-	ppb	ppb	ppb	ppb	-	ppb	ppb	ppb	ppb
T01	41	795.1	1077.2	170.2	1043.9	3.07	-1808.3	568.5	384.0	419.1	0.64	359.6	45.2	162.3	20.4
T02	45	453.3	670.3	164.6	540.2	2.02	-426.6	261.6	169.2	199.5	0.79	141.3	31.2	-34.7	-7.7
T04	45	875.6	1258.6	257.7	1064.8	0.83	243.4	1100.2	102.1	1095.4	0.30	660.5	75.4	-92.1	-10.5
T06	43	590.7	1156.3	202.1	1053.7	1.27	-33.1	823.8	137.5	812.3	0.41	407.8	69.0	-126.5	-21.4
T09	45	1184.4	920.0	665.7	629.9	0.02	777.7	1041.5	749.3	723.4	0.27	801.3	67.6	382.1	32.3
T12	44	393.2	495.2	75.9	317.3	0.34	283.7	333.8	54.9	329.3	0.25	193.6	49.2	-23.3	-5.9
T15	45	382.2	795.0	119.3	708.2	4.51	-1048.0	702.4	507.8	485.3	0.27	349.9	91.5	-294.0	-76.9
T17	45	324.4	618.6	85.7	636.8	3.23	-618.5	507.1	216.3	458.7	0.34	216.2	66.6	-105.1	-32.4
T18	45	475.6	936.7	130.0	891.9	3.76	-1120.9	835.4	403.1	731.7	0.32	353.5	74.3	-191.6	-40.3
T20	45	422.2	924.6	99.7	614.5	1.66	44.5	712.5	328.6	632.2	0.08	364.9	86.4	-322.1	-76.3
T26	45	515.6	934.5	134.8	837.9	3.81	-1305.5	713.2	399.7	590.6	0.40	355.7	69.0	-141.2	-27.4
T27	42	347.6	578.5	96.9	495.9	2.24	-280.3	465.7	190.8	424.9	0.29	201.6	58.0	-149.6	-43.0
T29	45	324.4	257.3	85.7	123.7	-0.09	252.2	191.7	138.6	132.5	0.10	157.5	48.5	102.9	31.7
T30	45	520.0	800.3	112.0	556.8	1.72	-190.3	591.2	201.0	555.9	0.24	344.6	66.3	-184.5	-35.5
T31	44	393.2	560.4	106.5	508.0	2.43	-557.6	384.8	150.4	354.2	0.51	277.9	70.7	-3.8	-1.0
T33	44	931.8	473.1	255.0	298.8	0.22	156.9	657.0	605.2	255.6	-1.03	629.7	67.6	572.2	61.4
Vic	45	1387.5	614.9	259.5	355.7	0.69	-509.0	980.0	936.9	287.4	-1.80	944.4	68.1	933.6	67.3

TABLE 38. NOx time series statistics at various stations within the 4km domain for the 1998 event.

Stn	N	$< Obs >$	$< CMAQ >$	δObs	$\delta CMAQ$	slope	int	RMSE	RMSEs	RMSEu	Index	MAE	NMAE	MBE	NMBE
-	#	ppb	ppb	ppb	ppb	-	ppb	ppb	ppb	ppb	-	ppb	ppb	ppb	ppb
T01	40	39.8	67.1	26.0	48.4	1.08	-8.0	14.0	5.3	12.9	0.95	11.5	28.8	4.9	12.3
T02	45	25.3	48.7	23.2	33.6	0.81	9.9	16.6	6.7	15.2	0.89	11.7	46.3	-5.1	-20.1
T04	45	35.8	70.2	17.4	50.8	1.14	-3.4	41.5	3.1	41.4	0.62	22.8	63.6	-1.8	-5.1
T06	43	54.7	64.6	28.6	49.2	0.62	-5.9	40.7	28.6	28.9	0.69	32.7	59.7	26.5	48.5
T09	45	41.3	47.2	17.1	31.2	0.29	16.6	33.9	17.7	29.0	0.50	28.4	68.7	12.9	31.2
T12	44	16.8	19.8	5.3	14.3	1.97	-21.5	11.7	7.3	9.2	0.67	9.9	58.9	5.2	30.8
T13	45	22.0	40.5	10.3	32.3	1.28	-7.3	23.0	3.1	22.8	0.68	14.9	67.6	1.1	5.2
T15	45	12.7	37.3	7.3	31.4	2.33	-8.3	26.9	13.0	23.6	0.50	12.7	99.8	-8.6	-68.1
T17	45	9.7	34.8	5.3	30.4	3.41	-15.6	23.0	14.7	17.7	0.57	10.3	106.7	-7.6	-78.7
T18	45	26.1	52.7	15.1	42.6	2.08	-30.0	24.5	16.2	18.4	0.82	12.8	49.2	1.8	6.9
T20	45	19.4	49.5	7.2	34.8	0.97	5.0	27.3	4.4	27.0	0.60	16.0	82.8	-4.4	-22.6
T26	45	23.6	53.5	14.9	38.9	1.83	-13.2	23.6	13.8	19.1	0.80	12.8	54.1	-6.4	-27.0
T27	39	6.8	22.0	3.1	18.5	4.27	-15.4	17.6	12.1	12.9	0.38	8.2	120.1	-7.0	-101.6
T29	45	7.3	9.9	1.9	7.4	2.00	-9.0	5.9	2.5	5.4	0.59	4.9	67.7	1.7	22.9
T30	45	15.7	39.2	5.0	28.0	2.91	-23.6	24.6	11.4	21.8	0.51	13.7	87.5	-6.3	-40.4
T31	44	20.5	37.6	10.6	30.7	1.43	-11.1	19.1	5.1	18.4	0.77	12.5	61.2	2.2	10.9
T33	44	12.7	24.4	7.3	20.6	1.55	-9.7	10.4	4.8	9.2	0.84	7.7	60.9	2.8	21.9
Vic	45	53.3	28.6	27.3	20.8	0.43	0.1	38.6	34.2	17.9	0.27	33.7	63.1	30.5	57.2

TABLE 39. Ozone time series statistics at various stations within the 4km domain for the 1998 event.

Stn	N	$< Obs >$	$< CMAQ >$	δObs	$\delta CMAQ$	slope	int	RMSE	RMSEs	RMSEu	Index	MAE	NMAE	MBE	NMBE
-	#	ppb	ppb	ppb	ppb	-	ppb	ppb	ppb	ppb	-	ppb	ppb	ppb	ppb
T01	18	14.6	25.2	18.6	25.8	1.81	21.3	39.5	36.2	15.9	0.64	33.4	229.1	-33.1	-227.6
T02	96	16.9	29.7	18.9	26.5	1.06	12.2	21.8	13.1	17.4	0.78	13.9	82.3	-13.1	-77.3
T04	96	18.7	27.2	17.8	31.6	1.62	-2.8	19.0	14.1	12.8	0.85	13.9	74.3	-8.8	-47.1
T06	92	12.0	29.6	14.4	28.5	1.71	9.9	25.6	21.2	14.4	0.69	18.7	154.9	-18.5	-153.8
T09	95	20.6	36.4	22.7	31.5	1.26	10.9	22.0	17.2	13.8	0.84	17.4	84.4	-16.2	-78.5
T12	95	29.5	47.2	26.7	21.4	0.64	28.6	24.1	20.3	13.0	0.78	19.7	66.6	-17.8	-60.4
T13	96	22.0	33.9	19.3	29.1	1.37	3.9	18.6	14.1	12.1	0.86	14.5	65.9	-12.1	-55.1
T15	96	33.2	35.9	22.6	30.5	1.22	-4.5	14.3	5.8	13.1	0.92	11.9	35.8	-2.9	-8.7
T17	96	21.0	34.1	19.7	25.8	1.14	10.5	18.4	13.8	12.2	0.84	14.7	70.0	-13.5	-64.5
T18	96	19.9	30.1	17.5	30.1	1.54	-0.3	19.3	14.2	13.2	0.84	14.2	71.4	-10.5	-52.9
T20	96	25.7	32.4	26.4	35.5	1.30	-0.5	14.0	10.6	9.2	0.95	9.8	38.1	-7.1	-27.6
T26	96	18.7	33.2	21.6	24.0	1.01	14.6	17.8	14.8	9.9	0.86	14.9	79.7	-14.8	-79.2
T27	93	29.9	44.0	27.3	26.5	0.82	20.1	20.9	15.6	14.0	0.86	17.3	57.7	-14.8	-49.5
T29	96	32.6	45.8	25.6	14.2	0.34	35.0	24.3	21.5	11.2	0.66	20.5	62.9	-13.3	-40.9
T30	96	31.1	37.1	27.8	33.5	1.14	1.8	13.3	7.3	11.1	0.95	10.5	33.9	-6.2	-19.9
T31	95	20.1	33.3	18.0	28.1	1.45	4.6	19.2	15.8	10.9	0.84	14.3	71.1	-13.6	-67.8
T33	95	26.5	40.3	24.8	27.6	0.96	14.8	19.0	13.8	13.1	0.87	16.0	60.3	-13.8	-52.0
Vic	93	15.2	38.3	12.4	20.1	1.21	20.6	27.4	23.9	13.5	0.56	23.9	157.0	-23.7	-155.9
Nam	93	18.4	46.0	10.8	17.9	0.98	28.2	31.4	27.9	14.5	0.46	27.9	151.5	-27.9	-151.5
Sat	95	37.2	54.0	17.5	24.3	1.11	12.4	22.2	16.8	14.6	0.75	17.2	46.3	-16.6	-44.7

TABLE 40. CO time series statistics at various stations within the 4km domain for the 1995 event.

Stn	N	$< Obs >$	$< CMAQ >$	δObs	$\delta CMAQ$	slope	int	RMSE	RMSEs	RMSEu	Index	MAE	NMAE	MBE	NMBE
-	#	ppb	ppb	ppb	ppb	-	ppb	ppb	ppb	ppb	-	ppb	ppb	ppb	ppb
T01	44	904.5	866.5	380.3	784.1	0.07	455.6	564.3	521.7	215.2	0.41	430.7	47.6	386.8	42.8
T02	43	369.8	580.2	70.8	612.4	1.17	-58.3	273.2	13.0	272.9	0.55	148.2	40.1	-5.0	-1.4
T04	18	388.9	1056.1	118.3	835.8	2.86	-494.6	501.9	312.0	393.1	0.58	263.0	67.6	-227.6	-58.5
T06	44	470.5	897.4	76.5	783.3	6.07	-2197.1	710.0	428.4	566.2	0.27	350.1	74.4	-190.4	-40.5
T09	44	834.1	785.7	455.9	560.6	-0.08	707.0	774.6	525.5	569.0	0.30	549.1	65.8	195.6	23.5
T12	45	300.0	380.9	56.4	250.3	0.46	155.2	233.6	31.3	231.5	0.27	134.1	44.7	7.7	2.6
T15	45	340.0	826.2	91.5	710.5	5.42	-1215.3	758.1	492.0	576.7	0.22	329.4	96.9	-287.1	-84.4
T17	43	274.4	459.0	44.1	459.4	1.61	-74.3	421.4	97.6	409.9	0.12	169.7	61.8	-93.9	-34.2
T18	45	537.8	826.1	199.2	594.4	1.46	-273.1	342.6	94.3	329.4	0.77	216.9	40.3	24.0	4.5
T26	39	430.8	679.5	95.0	582.2	2.28	-485.7	485.3	137.6	465.4	0.37	244.8	56.8	-66.8	-15.5
T27	45	526.7	670.9	113.6	668.3	-1.51	1366.5	712.1	285.5	652.4	0.09	415.5	78.9	-44.9	-8.5
T33	45	822.2	421.5	386.6	210.9	0.12	207.1	638.6	615.0	172.1	-0.34	592.8	72.1	515.2	62.7

TABLE 41. NOx time series statistics at various stations within the 4km domain for the 1995 event.

Stn	N	$< Obs >$	$< CMAQ >$	δObs	$\delta CMAQ$	slope	int	RMSE	RMSEs	RMSEu	Index	MAE	NMAE	MBE	NMBE
-	#	ppb	ppb	ppb	ppb	-	ppb	ppb	ppb	ppb	-	ppb	ppb	ppb	ppb
T01	44	43.4	50.5	20.3	35.8	0.10	23.2	26.2	24.1	10.3	0.63	19.7	45.5	15.9	36.7
T02	43	13.2	36.5	6.3	31.3	1.26	3.8	10.5	7.4	7.5	0.81	7.8	58.7	-7.2	-54.3
T04	29	32.0	53.6	10.6	38.7	0.50	5.8	19.5	11.4	15.8	0.80	16.0	50.1	10.1	31.7
T06	44	53.7	45.4	24.3	35.2	0.77	-16.2	34.8	28.8	19.6	0.59	30.1	56.1	28.3	52.7
T09	44	34.5	37.8	17.9	29.4	0.68	-0.7	22.2	13.2	17.8	0.71	18.1	52.5	11.9	34.5
T12	45	11.1	14.5	3.9	11.3	1.18	-4.9	8.4	2.9	7.9	0.64	5.5	49.6	2.8	25.5
T13	43	30.2	35.3	13.4	25.0	0.47	0.3	19.9	17.3	9.9	0.67	17.1	56.4	15.8	52.3
T15	44	16.0	38.2	8.7	29.8	2.36	-18.2	22.3	12.1	18.8	0.70	12.0	74.9	-3.5	-21.8
T17	31	8.7	24.1	2.7	22.4	4.25	-20.8	20.3	11.6	16.7	0.27	9.4	108.3	-7.6	-86.7
T18	45	29.4	43.3	20.6	30.5	0.61	0.1	17.7	13.8	11.1	0.85	14.5	49.4	11.3	38.5
T26	38	24.2	34.2	12.6	27.2	1.01	-3.7	17.0	3.4	16.7	0.77	11.5	47.7	3.4	14.1
T27	45	13.6	27.3	6.4	26.7	2.81	-21.6	21.5	11.7	18.0	0.58	11.3	83.6	-2.9	-21.6
T33	45	21.2	20.0	8.3	14.7	0.56	-4.2	16.0	13.9	7.9	0.49	14.4	67.7	13.4	63.3
Vic	45	19.9	24.3	12.4	16.2	0.39	7.5	12.6	8.9	9.0	0.73	9.4	47.1	4.7	23.7

TABLE 42. Ozone time series statistics at various stations within the 4km domain for the 1995 event.

Stn	N	$< Obs >$	$< CMAQ >$	δObs	$\delta CMAQ$	slope	int	RMSE	RMSEs	RMSEu	Index	MAE	NMAE	MBE	NMBE
-	#	ppb	ppb	ppb	ppb	-	ppb	ppb	ppb	ppb	-	ppb	ppb	ppb	ppb
T01	94	7.0	18.1	5.2	17.6	2.46	1.2	18.4	13.8	12.2	0.45	12.6	179.4	-11.5	-163.4
T02	93	15.5	22.6	11.6	17.0	1.22	3.9	12.4	7.7	9.7	0.82	8.9	57.8	-7.3	-47.1
T04	92	13.8	21.3	13.4	21.9	1.48	1.5	14.4	10.3	10.1	0.84	10.3	74.7	-8.1	-58.6
T06	95	7.3	23.8	6.3	19.9	2.69	4.2	22.3	19.6	10.7	0.49	16.9	233.1	-16.4	-226.6
T09	95	16.9	26.9	17.7	21.7	1.11	8.3	14.2	10.3	9.8	0.88	10.7	63.2	-10.1	-59.6
T12	96	25.0	38.3	21.3	14.5	0.45	27.1	20.8	17.7	11.0	0.71	17.4	69.9	-13.3	-53.3
T13	94	12.9	26.3	11.7	24.5	1.80	3.8	21.1	16.9	12.7	0.69	14.5	112.6	-14.1	-109.1
T15	96	19.8	26.8	16.6	26.3	1.50	-2.6	13.8	11.0	8.4	0.90	9.5	48.3	-7.3	-36.8
T17	95	17.3	27.3	8.8	19.9	1.67	-1.6	17.8	11.7	13.4	0.66	12.8	73.9	-10.1	-58.0
T18	95	14.1	22.3	12.7	23.4	1.66	-1.0	15.8	11.9	10.5	0.81	10.8	76.7	-8.4	-59.2
T26	89	10.9	26.4	11.4	17.1	1.30	12.1	18.1	15.8	9.0	0.70	15.5	141.6	-15.4	-140.8
T27	96	22.2	32.4	19.3	23.5	1.04	9.6	16.1	10.4	12.3	0.86	11.7	52.8	-10.4	-46.9
T29	93	29.6	37.2	27.4	12.8	0.23	29.9	24.7	22.1	10.9	0.59	20.9	70.5	-7.2	-24.4
T33	96	22.1	33.4	19.5	23.6	1.01	11.5	17.4	11.7	12.8	0.84	12.9	58.4	-11.7	-53.1
Vic	93	20.4	35.7	12.3	18.9	1.11	14.1	20.6	16.4	12.5	0.65	17.0	83.2	-16.4	-80.3
Sat	89	23.8	36.7	10.6	18.2	1.48	0.6	16.1	13.1	9.4	0.73	12.6	53.0	-12.1	-50.9

TABLE 43. CO time series statistics at various stations within the 4km domain for the 1993 event.

Stn	N	$<Obs>$	$<CMAQ>$	δObs	$\delta CMAQ$	slope	int	RMSE	RMSEs	RMSEu	Index	MAE	NMAE	MBE	NMBE
-	#	ppb	ppb	ppb	ppb	-	ppb	ppb	ppb	ppb	-	ppb	ppb	ppb	ppb
T02	45	473.3	804.6	235.9	1028.4	1.26	29.7	919.5	164.5	904.6	0.30	333.2	70.4	-152.9	-32.3
T04	43	616.3	1136.2	236.0	1064.0	3.48	-1091.3	1196.9	727.2	950.6	0.31	615.1	99.8	-439.6	-71.3
T06	45	597.8	936.3	192.5	879.3	2.97	-848.6	1030.9	501.1	901.0	0.25	542.8	90.8	-331.6	-55.5
T09	44	818.2	698.6	302.1	603.0	0.62	145.1	702.9	204.5	672.5	0.37	492.0	60.1	169.3	20.7
T15	45	382.2	1133.4	143.5	1024.9	2.92	-391.0	994.6	438.6	892.7	0.28	530.6	138.8	-343.6	-89.9
T17	45	320.0	570.7	125.4	464.1	1.62	-125.6	278.2	105.3	257.4	0.62	135.2	42.2	-72.2	-22.6
T18	9	277.8	1276.1	66.7	1267.1	2.31	87.3	860.8	459.8	727.8	0.21	452.3	162.8	-452.3	-162.8
T26	43	488.4	710.3	241.2	768.6	2.50	-438.3	848.4	462.2	711.5	0.43	403.0	82.5	-293.3	-60.1
T27	43	474.4	659.4	160.5	622.1	-0.32	598.8	559.8	211.5	518.3	0.28	383.1	80.7	28.2	5.9
T33	45	733.3	411.9	447.2	340.8	0.10	203.3	658.3	601.8	267.0	0.07	597.9	81.5	453.2	61.8

TABLE 44. NOx time series statistics at various stations within the 4km domain for the 1993 event.

Stn	N	$< Obs >$	$< CMAQ >$	δObs	$\delta CMAQ$	slope	int	RMSE	RMSEs	RMSEu	Index	MAE	NMAE	MBE	NMBE
-	#	ppb	ppb	ppb	ppb	-	ppb	ppb	ppb	ppb	-	ppb	ppb	ppb	ppb
T02	39	27.8	42.5	21.1	35.9	0.38	21.9	35.8	13.7	33.1	0.46	20.3	72.8	-4.7	-16.9
T04	42	39.5	49.3	21.2	39.4	1.23	-10.1	33.2	4.9	32.8	0.70	24.4	61.8	0.9	2.3
T06	45	61.4	39.6	32.1	31.4	0.63	-5.4	42.5	30.3	29.9	0.56	34.3	55.8	27.9	45.5
T09	44	37.2	29.7	20.5	26.8	0.44	5.8	30.0	18.8	23.3	0.48	22.8	61.3	15.0	40.3
T13	43	35.6	48.9	16.1	38.8	0.95	-11.7	31.8	13.6	28.7	0.67	25.3	71.2	13.6	38.3
T15	45	18.9	49.0	8.2	41.7	1.94	-14.7	29.3	8.2	28.1	0.64	18.3	96.8	-3.1	-16.3
T17	45	12.9	28.1	11.1	22.9	0.74	4.8	10.0	3.2	9.5	0.86	6.4	50.0	-1.4	-11.2
T18	45	32.3	58.5	28.4	46.6	1.16	-10.1	26.8	6.7	25.9	0.88	18.9	58.5	5.1	15.7
T26	44	26.9	28.5	25.7	26.3	0.82	6.4	21.8	4.8	21.3	0.82	12.0	44.5	-1.7	-6.4
T27	43	17.2	25.7	11.6	26.0	0.11	10.7	20.8	11.2	17.5	0.52	15.1	88.0	4.6	26.7
T33	45	20.6	17.8	9.9	17.4	0.68	-6.4	16.2	13.3	9.2	0.53	14.4	69.9	12.9	62.5
Vic	45	27.7	22.8	16.0	17.1	0.07	11.8	26.4	20.3	16.9	0.29	19.9	71.7	14.0	50.5

TABLE 45. Ozone time series statistics at various stations within the 4km domain for the 1993 event.

Stn	N	$<Obs>$	$<CMAQ>$	δObs	$\delta CMAQ$	slope	int	RMSE	RMSEs	RMSEu	Index	MAE	NMAE	MBE	NMBE
-	#	ppb	ppb	ppb	ppb	-	ppb	ppb	ppb	ppb	-	ppb	ppb	ppb	ppb
T02	96	11.0	19.6	10.6	15.1	1.21	6.4	11.9	9.0	7.7	0.81	9.2	83.8	-8.8	-79.4
T04	92	15.0	21.1	9.8	17.6	1.29	1.8	13.4	6.7	11.6	0.75	10.9	72.9	-6.1	-40.5
T06	96	8.3	25.2	7.4	15.1	1.16	15.5	21.0	16.9	12.5	0.46	18.0	215.3	-16.8	-201.7
T09	95	17.8	26.6	19.7	16.2	0.59	15.9	16.2	11.7	11.2	0.80	13.5	75.6	-8.5	-47.6
T13	93	9.9	21.9	9.3	21.8	1.81	3.3	18.2	13.5	12.2	0.66	12.6	127.3	-11.3	-114.6
T15	96	20.0	21.1	16.2	21.2	1.08	-0.3	12.2	1.7	12.1	0.89	8.2	41.1	-1.2	-6.2
T17	96	13.2	24.0	11.2	17.1	1.26	7.7	14.9	11.4	9.6	0.76	11.6	88.1	-11.1	-83.9
T18	96	11.3	19.4	10.9	22.0	1.73	0.0	16.1	11.4	11.4	0.76	11.3	99.9	-8.3	-73.0
T26	95	12.6	28.1	10.8	14.0	0.92	16.3	18.2	15.3	9.8	0.63	16.3	129.1	-15.3	-121.7
T27	93	21.4	27.9	20.5	18.1	0.67	13.8	15.2	9.5	11.9	0.84	12.3	57.4	-6.6	-31.1
T29	56	8.3	32.2	15.4	8.0	0.00	28.9	26.4	25.6	6.5	0.41	24.5	295.1	-20.6	-248.9
T33	94	20.0	30.4	20.1	16.0	0.64	17.6	15.9	12.6	9.8	0.81	13.2	65.9	-10.4	-51.8
Vic	93	17.2	33.2	15.0	16.9	0.95	17.5	19.0	16.7	9.1	0.73	16.7	97.2	-16.6	-96.9

TABLE 46. CO time series statistics at various stations within the 4km domain for the 1987 event.

Stn	N	$<Obs>$	$<CMAQ>$	δObs	$\delta CMAQ$	slope	int	RMSE	RMSEs	RMSEu	Index	MAE	NMAE	MBE	NMBE
-	#	ppb	ppb	ppb	ppb	-	ppb	ppb	ppb	ppb	-	ppb	ppb	ppb	ppb
T04	37	1020.5	1741.3	449.6	966.4	0.21	1246.1	1198.3	561.6	1075.9	0.31	804.8	78.9	-404.4	-39.6
T06	35	528.6	1587.1	297.4	880.0	-0.25	1373.8	1221.5	800.7	902.3	-0.02	828.9	156.8	-721.6	-136.5
T09	38	164.4	1391.4	217.6	770.8	0.58	1066.1	1273.1	1001.5	786.2	-0.71	1002.2	609.4	-996.9	-606.2
T15	37	213.6	998.4	237.8	688.1	0.94	484.2	680.5	471.7	491.9	0.25	507.3	237.5	-469.9	-220.0
T17	38	371.1	824.9	196.1	541.3	0.77	329.1	616.0	247.4	566.3	0.33	342.5	92.3	-237.9	-64.1

TABLE 47. NOx time series statistics at various stations within the 4km domain for the 1987 event.

Stn	N	$< Obs >$	$< CMAQ >$	δObs	$\delta CMAQ$	slope	int	RMSE	RMSEs	RMSEu	Index	MAE	NMAE	MBE	NMBE
-	#	ppb	ppb	ppb	ppb	-	ppb	ppb	ppb	ppb	-	ppb	ppb	ppb	ppb
T04	4	37.3	87.6	20.6	50.5	1.48	-29.2	21.7	14.7	18.9	0.88	19.7	52.8	3.4	9.1
T09	31	59.6	68.5	18.0	42.6	0.28	20.1	37.2	25.8	24.9	0.53	32.2	54.0	24.2	40.6
T13	22	26.7	43.1	10.4	25.0	1.83	-22.2	20.2	8.4	19.1	0.69	13.9	52.2	1.5	5.5
T17	31	24.4	38.3	13.7	23.0	0.53	8.2	20.2	7.2	18.6	0.66	15.3	62.7	4.7	19.4

TABLE 48. Ozone time series statistics at various stations within the 4km domain for the 1987 event.

Stn	N	$<Obs>$	$<CMAQ>$	δObs	$\delta CMAQ$	slope	int	RMSE	RMSEs	RMSEu	Index	MAE	NMAE	MBE	NMBE
-	#	ppb	ppb	ppb	ppb	-	ppb	ppb	ppb	ppb	-	ppb	ppb	ppb	ppb
T04	86	16.3	11.7	16.3	16.2	0.72	-0.5	11.3	6.8	9.3	0.86	8.6	52.5	4.6	28.3
T06	46	11.1	13.9	11.8	16.8	1.21	-2.0	9.7	2.5	9.4	0.88	6.3	56.9	-0.4	-3.2
T09	74	18.2	14.4	20.0	18.4	0.86	3.5	11.3	3.0	10.9	0.90	8.1	44.7	-1.3	-7.2
T12	89	23.0	20.4	23.1	17.4	0.53	9.2	16.4	10.9	12.7	0.81	12.4	53.9	0.5	2.4
T13	89	10.6	17.2	7.8	18.0	1.58	1.2	15.4	8.6	13.0	0.62	10.7	101.7	-7.0	-66.1
T15	86	28.9	16.2	18.1	17.7	0.72	-4.1	17.7	13.1	12.1	0.78	14.5	50.1	11.9	41.1
T17	90	19.4	17.9	19.1	17.6	0.62	7.4	15.3	7.2	13.8	0.78	11.0	56.8	-0.9	-4.7
T27	90	22.5	21.5	22.3	16.9	0.64	8.3	12.2	7.9	9.4	0.89	9.3	41.5	-1.0	-4.6
Vic	82	13.9	19.4	8.2	14.7	1.08	5.5	14.1	6.7	12.5	0.58	10.8	77.4	-6.6	-47.2

TABLE 49. CO time series statistics at various stations within the 4km domain for the 1985 event.

Stn	N	$< Obs >$	$< CMAQ >$	δObs	$\delta CMAQ$	slope	int	RMSE	RMSEs	RMSEu	Index	MAE	NMAE	MBE	NMBE
-	#	ppb	ppb	ppb	ppb	-	ppb	ppb	ppb	ppb	-	ppb	ppb	ppb	ppb
T001	3	866.7	1655.2	230.9	1617.6	-0.22	535.3	587.0	573.6	124.7	0.85	525.2	60.6	525.2	60.6
T002	45	380.0	1092.4	214.9	1234.4	1.29	266.4	923.3	380.1	841.5	0.30	429.3	113.0	-375.2	-98.7
T003	45	788.9	1075.9	332.5	1103.3	-0.95	1329.8	899.8	672.8	597.5	0.36	655.9	83.1	206.6	26.2
T004	45	722.2	1536.7	352.2	1058.1	0.15	733.6	803.9	319.4	737.8	0.63	524.2	72.6	-118.4	-16.4
T006	29	327.6	1403.0	198.0	1025.3	0.36	644.2	853.8	452.7	724.0	0.42	468.8	143.1	-435.3	-132.9
T007	43	4.7	591.0	30.5	282.1	-1.68	495.4	540.0	489.6	227.7	-3.06	484.8	10423.2	-482.9	-10382.1
T009	45	211.1	1098.3	361.3	659.1	-0.35	737.2	834.3	660.6	509.5	0.28	622.8	295.0	-453.3	-214.7
T010	45	575.6	949.0	197.9	546.7	-0.73	1032.1	526.2	339.9	401.7	0.42	322.6	56.1	-39.0	-6.8
T015	45	240.0	842.8	358.3	729.6	0.31	469.5	722.4	390.0	608.0	0.42	483.4	201.4	-304.2	-126.7

TABLE 50. NOx time series statistics at various stations within the 4km domain for the 1985 event.

Stn	N	$< Obs >$	$< CMAQ >$	δObs	$\delta CMAQ$	slope	int	RMSE	RMSEs	RMSEu	Index	MAE	NMAE	MBE	NMBE
-	#	ppb	ppb	ppb	ppb	-	ppb	ppb	ppb	ppb	-	ppb	ppb	ppb	ppb
T002	14	37.9	58.2	6.3	53.5	0.57	-1.1	19.3	17.7	7.8	0.81	17.5	46.2	17.5	46.2
T003	20	23.9	54.1	8.2	52.1	1.03	-10.9	11.8	10.2	5.8	0.94	10.8	45.3	10.2	42.8
T004	17	45.1	75.7	16.0	55.7	1.69	-42.5	28.9	15.7	24.2	0.82	22.6	50.1	11.6	25.6
T005	20	56.0	77.1	22.3	59.4	0.90	-23.4	34.9	29.1	19.4	0.77	30.6	54.6	29.0	51.8
T007	20	24.0	23.9	9.1	17.0	-0.35	22.7	18.2	15.4	9.6	0.26	14.2	59.4	9.7	40.6
T010	20	30.6	43.1	9.6	30.6	-0.39	33.3	25.3	15.8	19.7	0.52	19.7	64.5	9.1	29.8
T014	20	31.1	73.2	12.0	53.7	-0.14	42.5	47.7	15.1	45.3	0.48	23.7	76.2	-7.0	-22.7
T015	20	27.3	37.8	12.4	32.6	1.05	-8.7	28.4	7.4	27.4	0.59	18.8	69.0	7.4	27.1
T016	10	31.3	44.4	18.0	35.5	0.28	5.8	22.7	20.7	9.5	0.76	17.7	56.4	16.7	53.2

TABLE 51. Ozone time series statistics at various stations within the 4km domain for the 1985 event.

Stn	N	$< Obs >$	$< CMAQ >$	δObs	$\delta CMAQ$	slope	int	RMSE	RMSEs	RMSEu	Index	MAE	NMAE	MBE	NMBE
-	#	ppb	ppb	ppb	ppb	-	ppb	ppb	ppb	ppb	-	ppb	ppb	ppb	ppb
T001	91	15.3	18.0	19.3	21.0	0.94	4.7	11.6	4.0	10.8	0.91	6.8	44.6	-3.9	-25.4
T002	95	18.0	20.8	20.6	18.4	0.71	8.3	13.2	6.7	11.4	0.88	10.1	56.5	-3.1	-17.1
T003	38	16.8	22.2	17.8	22.5	1.21	7.0	14.3	11.2	8.8	0.88	10.6	62.9	-10.6	-62.9
T004	97	24.0	20.6	20.0	23.4	1.08	-5.3	9.7	3.7	8.9	0.95	7.7	32.3	3.4	14.1
T005	97	28.4	20.7	24.7	23.5	0.87	-3.9	12.7	8.3	9.6	0.93	9.7	34.2	7.7	27.1
T006	70	17.4	22.6	16.9	23.4	1.17	2.0	15.1	5.7	14.0	0.86	10.7	61.5	-4.9	-28.4
T007	97	39.9	35.4	25.8	19.3	0.64	9.9	14.3	10.3	10.0	0.89	10.8	27.1	4.5	11.2
T009	97	32.8	24.1	31.9	24.9	0.73	0.1	14.8	12.2	8.5	0.93	10.7	32.5	8.7	26.5
T010	59	29.0	25.1	24.2	25.0	0.88	-2.8	13.6	6.9	11.7	0.92	10.8	37.1	6.3	21.6
T012	97	36.3	37.9	32.2	18.7	0.47	20.8	20.2	17.0	10.9	0.83	16.1	44.3	-1.6	-4.3
T015	97	46.2	25.5	28.4	25.1	0.79	-10.8	24.6	21.6	11.6	0.81	20.9	45.3	20.8	44.9
T016	74	33.3	25.2	30.9	26.2	0.86	-2.7	12.7	8.8	9.1	0.95	9.6	28.8	7.6	22.7
T025	97	36.3	45.6	20.8	15.0	0.51	27.0	17.3	13.7	10.5	0.78	15.0	41.3	-9.3	-25.7

TABLE 52. MAE (in ppb), RMSE (in ppb) and IOA for the CMAQ, CALGRID and UAM model simulations over the July 18 0400 (PST) to July 20 2300 (PST) 1985 period.

Station	CMAQ			CALGRID			UAM		
	MAE	RMSE	IOA	MAE	RMSE	IOA	MAE	RMSE	IOA
T02	12.6	15.7	0.85	10.2	18.8	0.65	15.5	17.5	0.73
T07	11.1	14.9	0.88	20.1	25.1	0.53	20.5	26.7	0.53
T11	13.1	17.0	0.91	22.6	27.8	0.63	26.6	31.0	0.59
T12	20.0	23.7	0.79	25.0	29.5	0.57	28.2	33.1	0.44

Table 53. Ozone performance statistics for daily peak ozone concentrations.

Statistic	2006	2001	1998	1995	1993	1987	1985	NRC
n (data points)	71	72	65	56	48	30	27	270
Model mean (ppb)	50.6	61.3	75.3	59.9	51.5	45.5	64.7	41.9
Obs mean (ppb)	44.5	53.1	56.6	41.7	35.6	48.1	68.9	42.8
MB (ppb)	6.1	8.2	18.7	18.2	15.8	-2.6	-4.2	-0.9
NMB (%)	13.6	15.5	33.1	43.7	44.4	-5.4	-6.1	-2.2
ME (ppb)	10.8	13.6	20.5	23.5	19.5	17.6	15.9	10.4
NME (%)	24.2	25.6	36.3	56.3	54.6	36.6	23.1	24.3
% within factor of 2	98.6	97.2	98.2	75.0	72.9	86.7	100.0	95.9

List of Figures

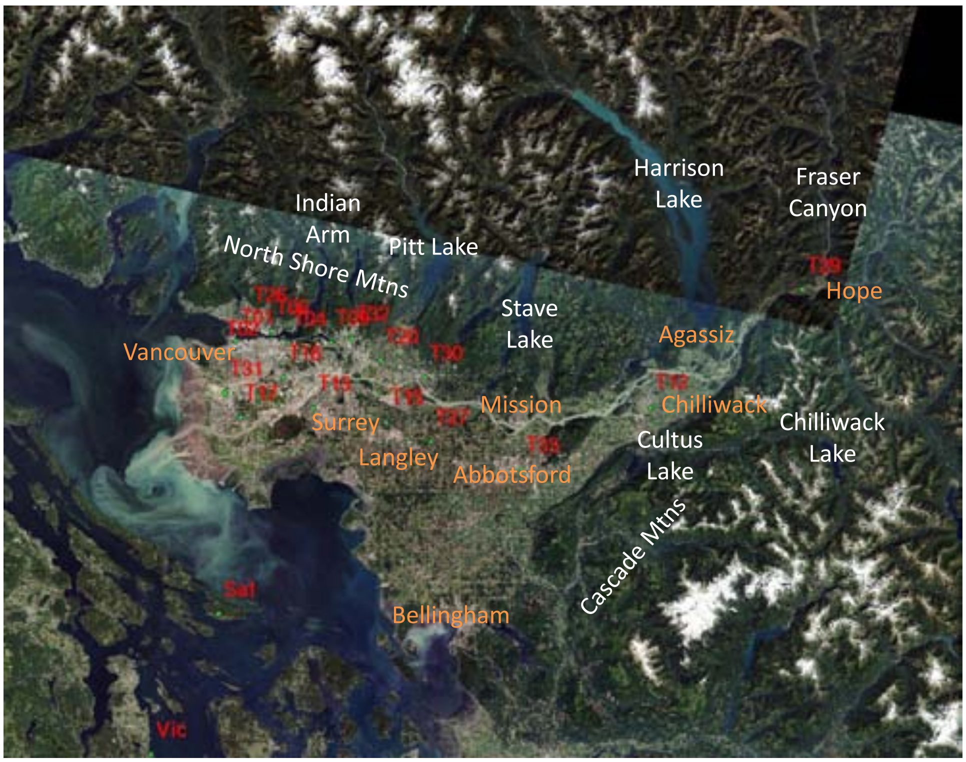

Fig. 1. Composite LANDSAT images showing MV monitoring station locations (red), urban areas of note (orange) and select geographic locations (white).

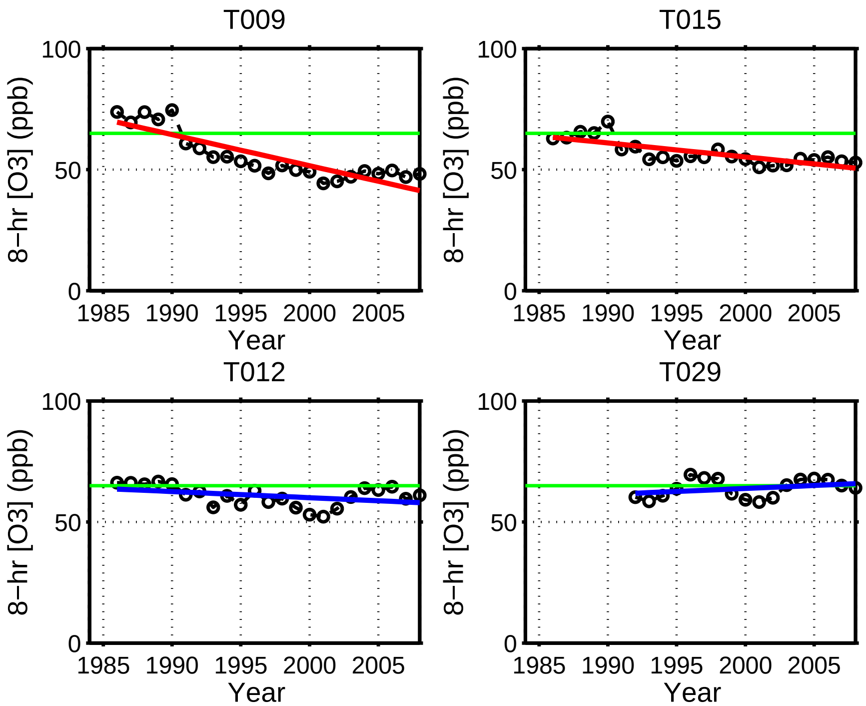

FIG. 2. Timeseries plots of the 3-year running average of the 4th highest 8-hour averaged ozone concentration (open circles) at T09 (Rocky Point Park), T15 (Surrey East), T12 (Chilliwack) and T29 (Hope). The green line in each plot is the CWS of 65 ppb. Also include are trend lines. Red lines indicated statistically significant trends while blue lines are not statistically significant.

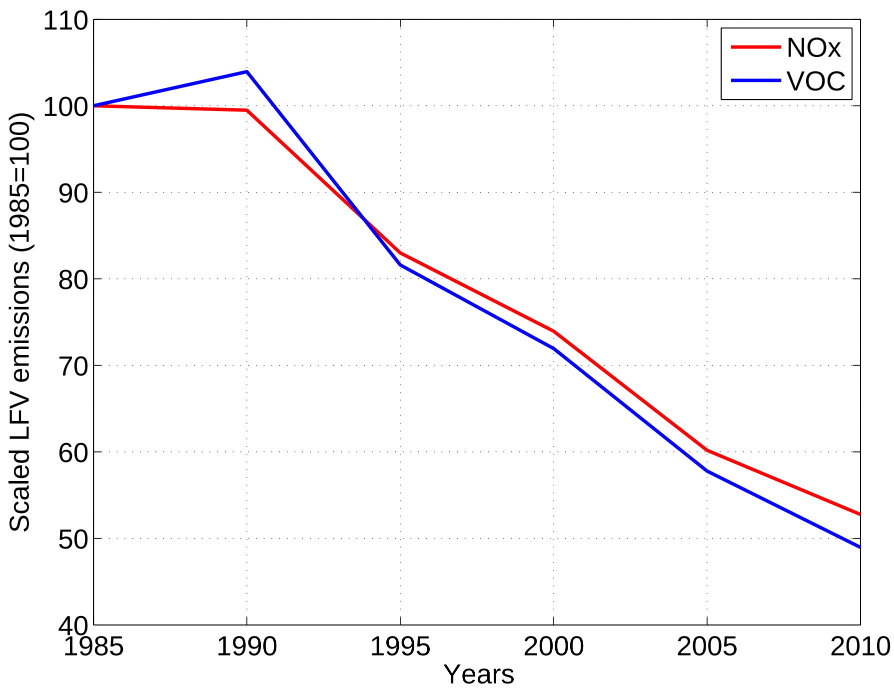

FIG. 3. Timeseries plot of total NOx (red) and anthropogenic VOC (blue) emissions over the LFV. Both the NOx and VOC emissions totals have been scaled so that their 1985 values equal 100.

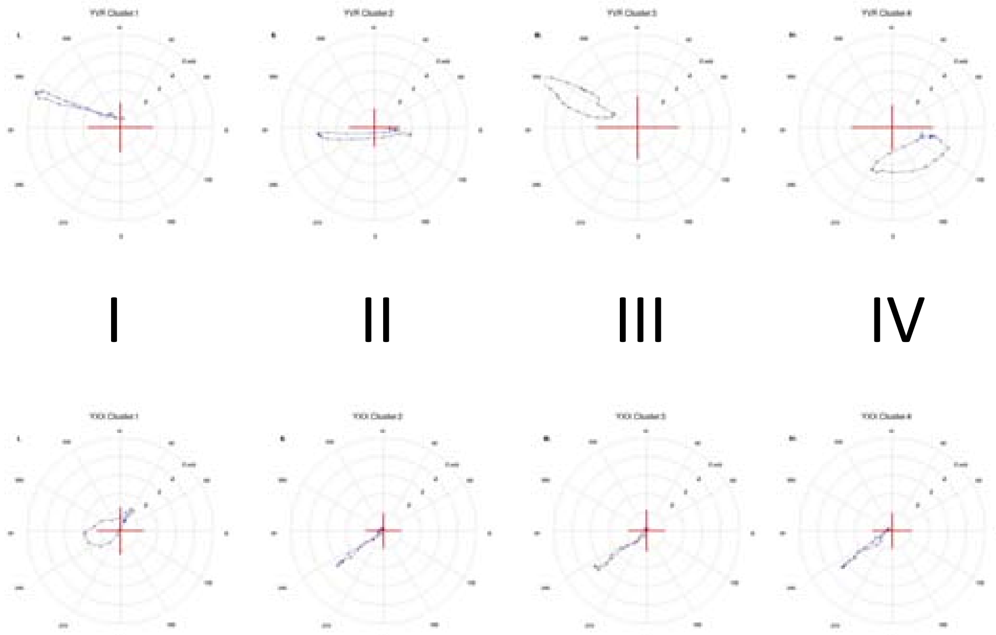

Fig. 4. Mean daily hodographs at YVR (top row) and YXX (bottom row) for the 4 meso-scale circulation regimes identified in Ainslie and Steyn (2007). On each plot are the 24-hourly wind speed and directions averaged over each day have the same circulation type. The azimuthal scale gives wind direction in degrees and the range rings give wind speeds in m/s. The arms on the red crosses at the center of each hodograph give the size of the standard deviation of the u and v wind components.

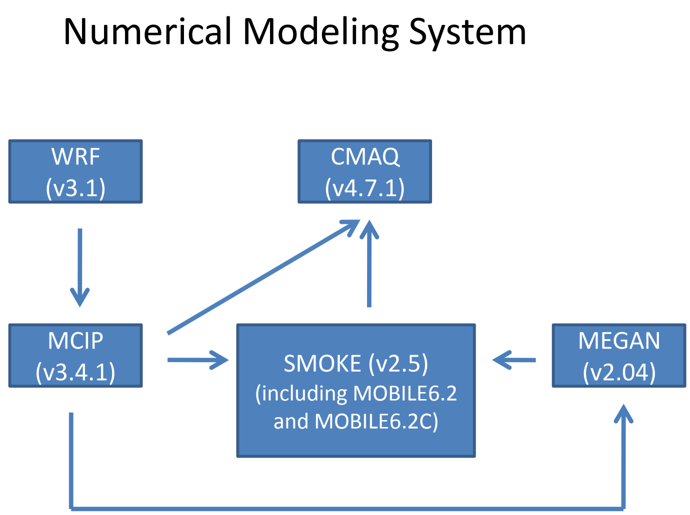

FIG. 5. Flowchart showing linkages between the major modeling components.

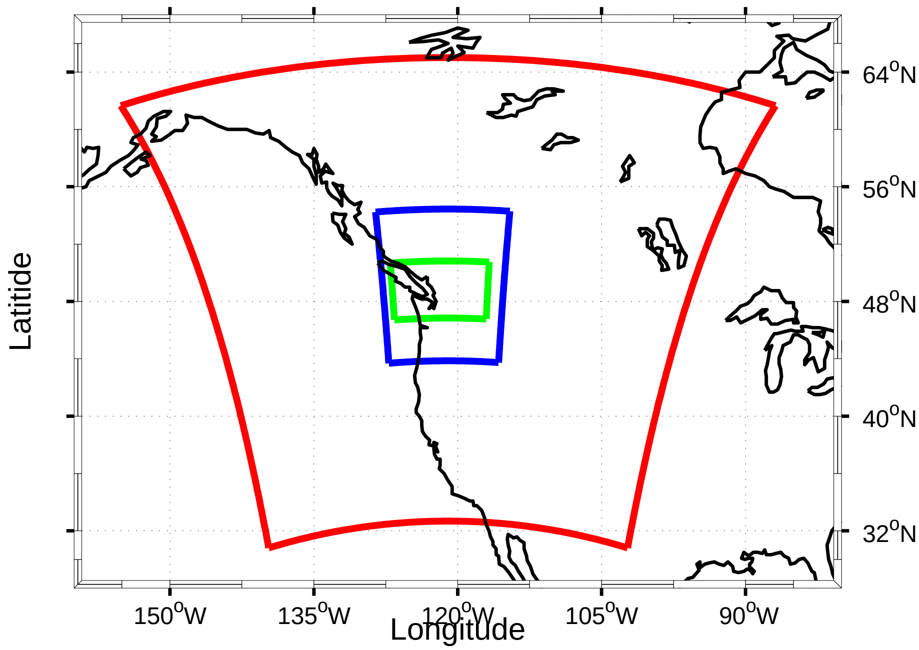

FIG. 6. Plot of the 36 km (red), 12 km (blue) and 4 km (green) computational modeling domains.

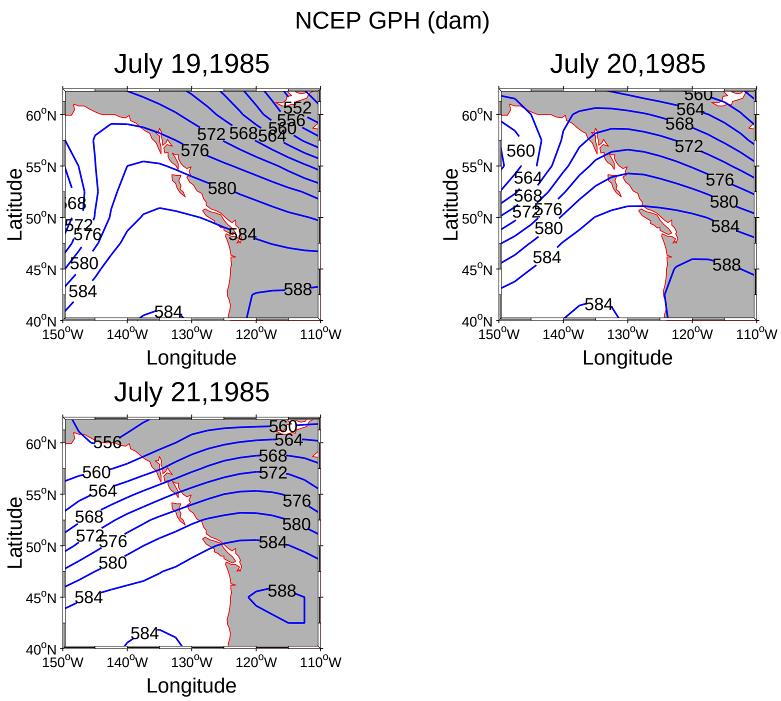

Fig. 7. Daily average 500mb geopotential height (in dam) over the Pacific Northwest during each day of the the July 1985 episode.

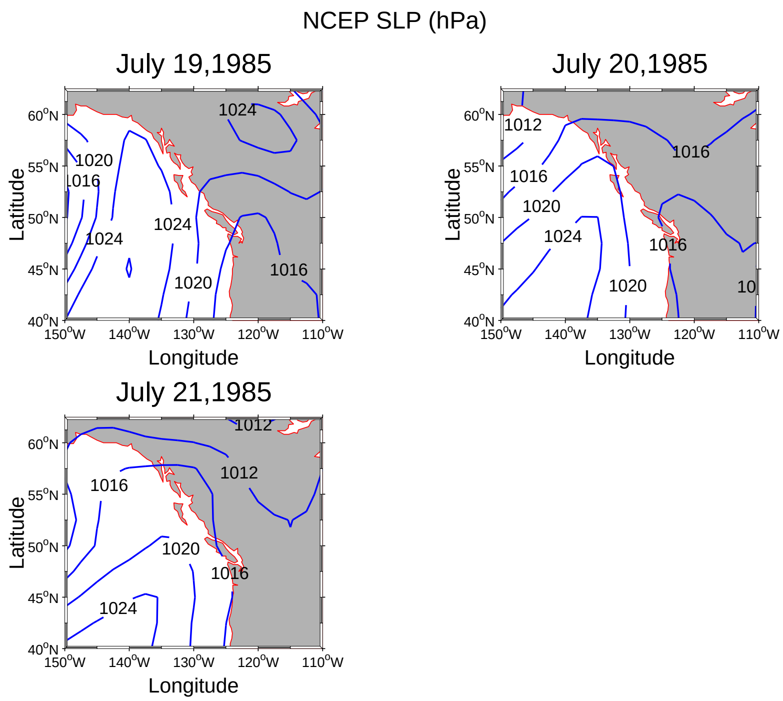

FIG. 8. Daily average sea-level pressure (in hPa) over the Pacific Northwest during each day of the the July 1985 episode.

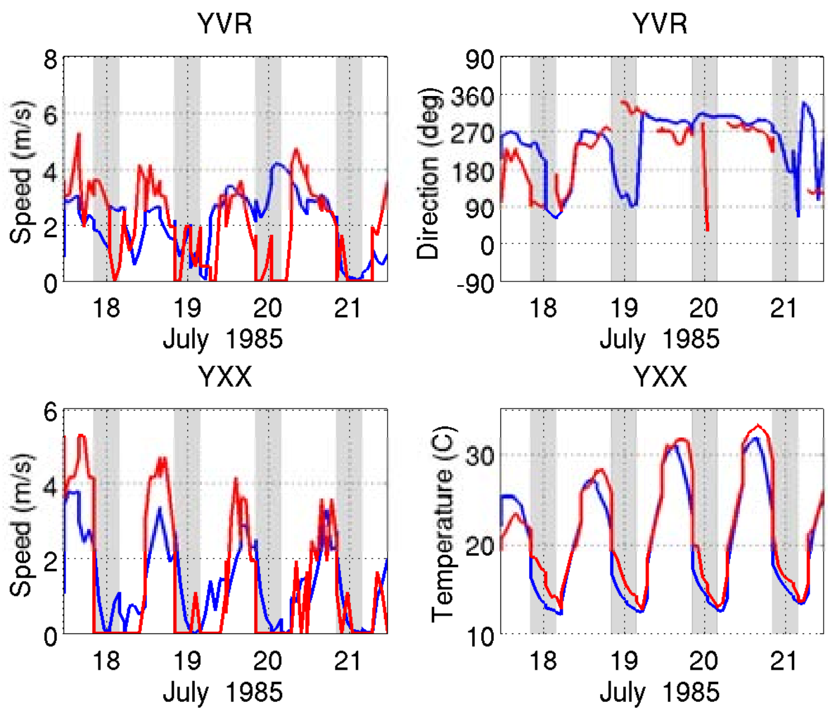

FIG. 9. Timeseries plots of WRF modeled (blue) and observed (red) wind speed (in m/s) at YVR (upper left), YVR wind direction (upper right), YXX wind speed (lower left) and YXX temperature (^{o}C, lower right) during the July 1985 episode.

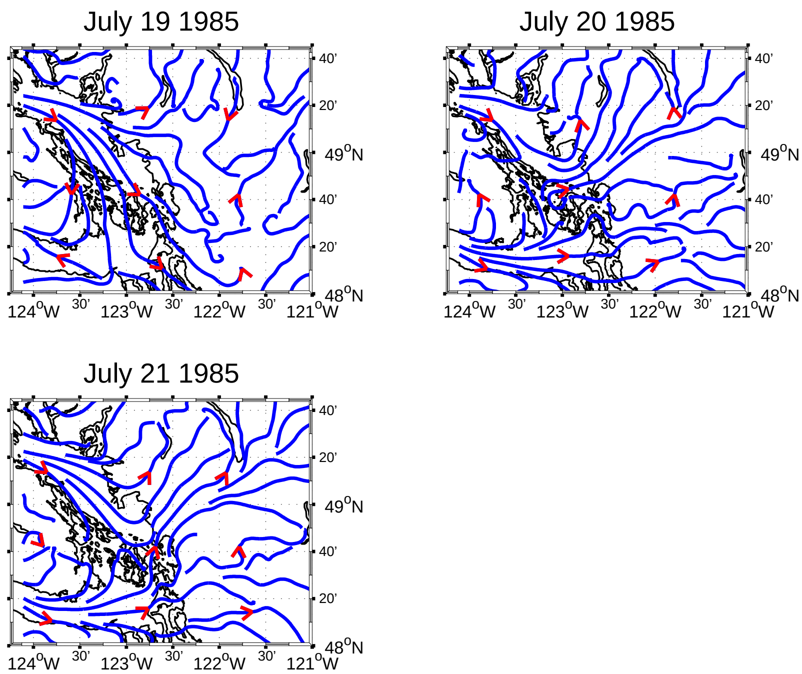

Fig. 10. Streamlines (blue) based on 0700-1500 (PST) average WRF surface wind field over the Georgia Basin for each day of the July 1985 episode. For clarity, the arrow heads indicating flow direction have been coloured red.

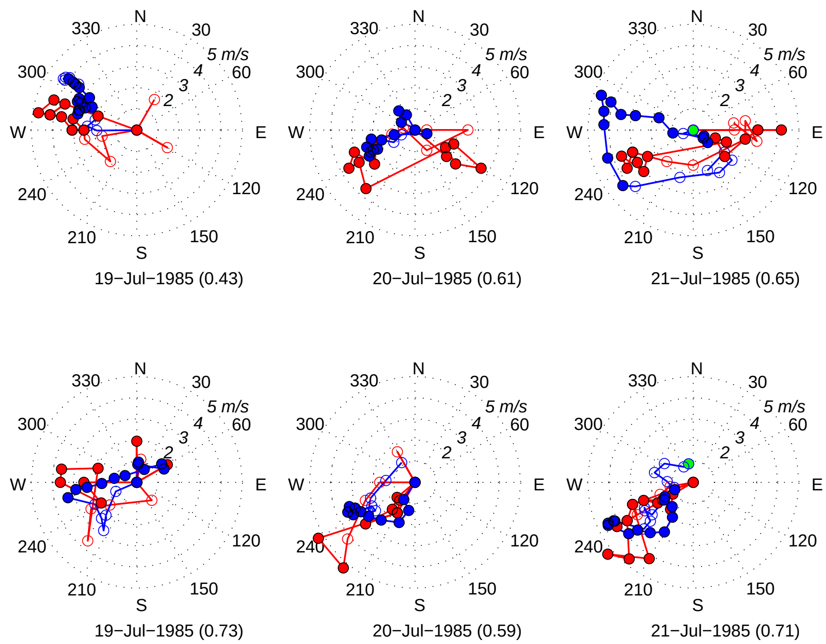

FIG. 11. Daily YVR (top row) and YXX (bottom row) hodograph plots of observed (red) and modeled (blue) winds. Solid circles are daytime values and open circles are nighttime. The number in parentheses by each date gives the vector correlation coefficient between the observed and modeled winds.

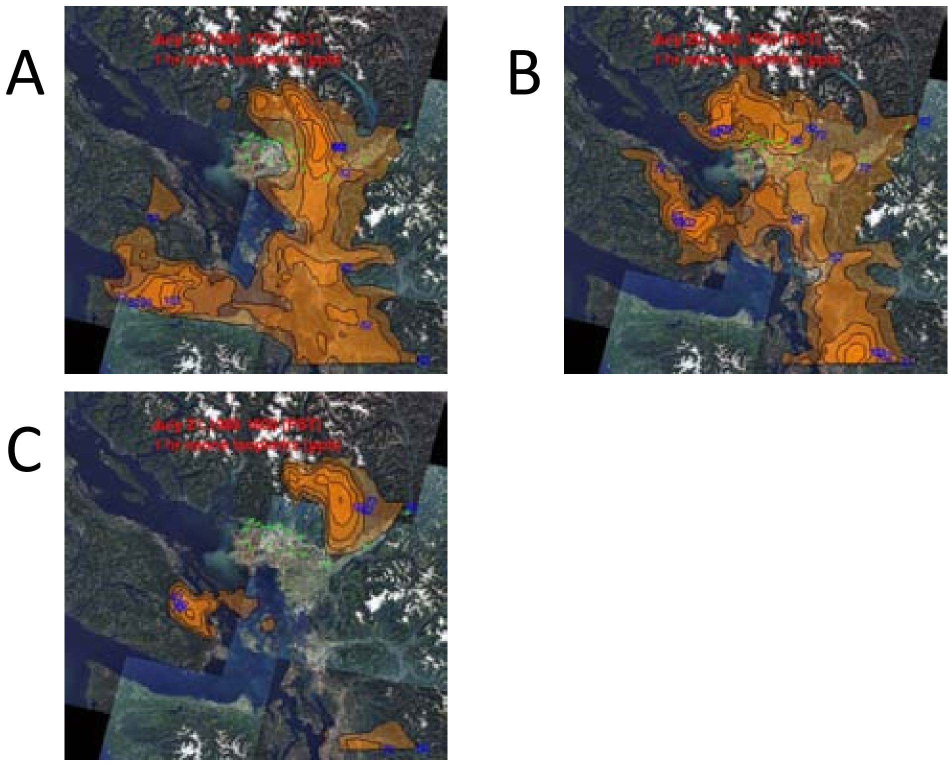

Fig. 12. Surface ozone concentrations contours (in 10 ppb increments) over the Georgia Basin at time of maximum modeled concentration for (A) July 19th, 1985 at 1700 (PST), (B) July 20th, 1985 at 1500 (PST) and (C) July 21st, 1985 at 1600 (PST). Also shown are the fixed monitoring network station locations (+). Concentrations below 62 ppb have not been contoured.

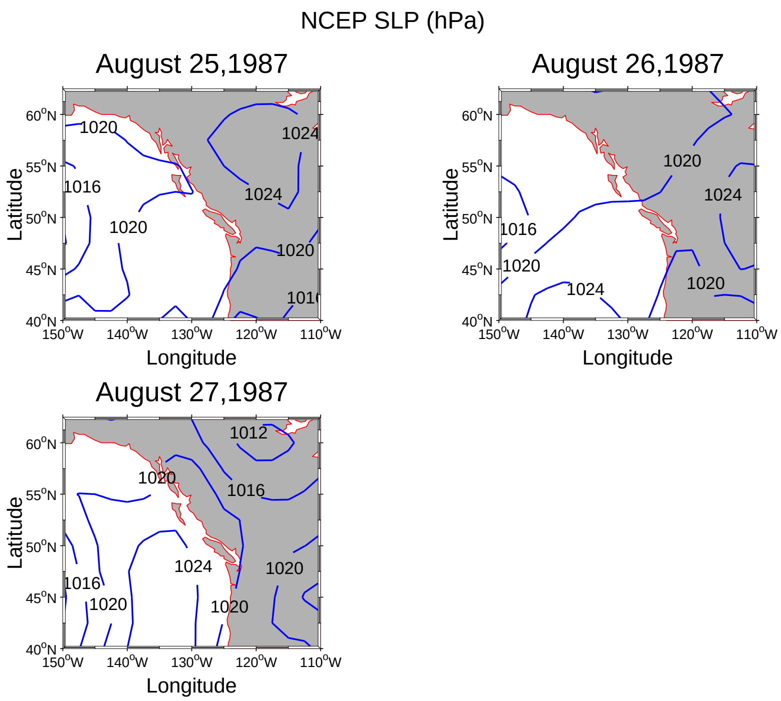

FIG. 13. Daily average sea-level pressure (in hPa) over the Pacific Northwest during each day of the the August 1987 episode.

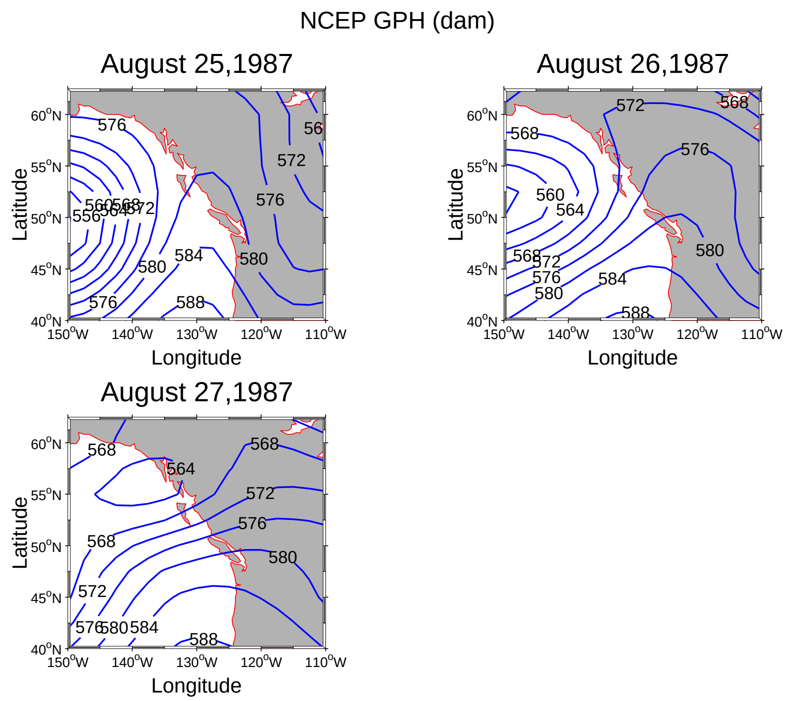

Fig. 14. Daily average 500mb geopotential height (in dam) over the Pacific Northwest during each day of the the August 1987 episode.

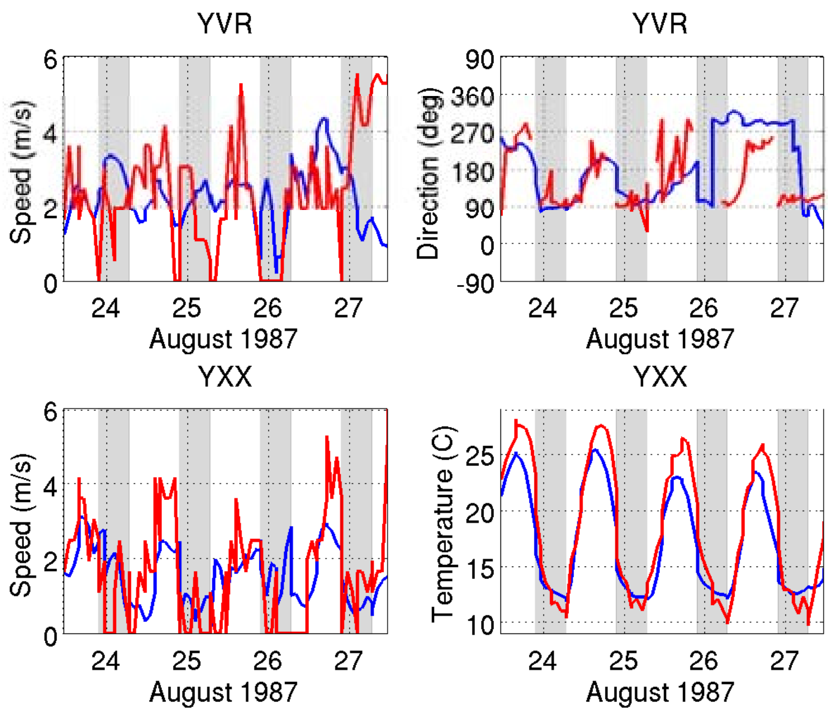

FIG. 15. Timeseries plots of WRF modeled (blue) and observed (red) wind speed (in m/s) at YVR (upper left), YVR wind direction (upper right), YXX wind speed (lower left) and YXX temperature (^{o}C, lower right) during the August 1987 episode.

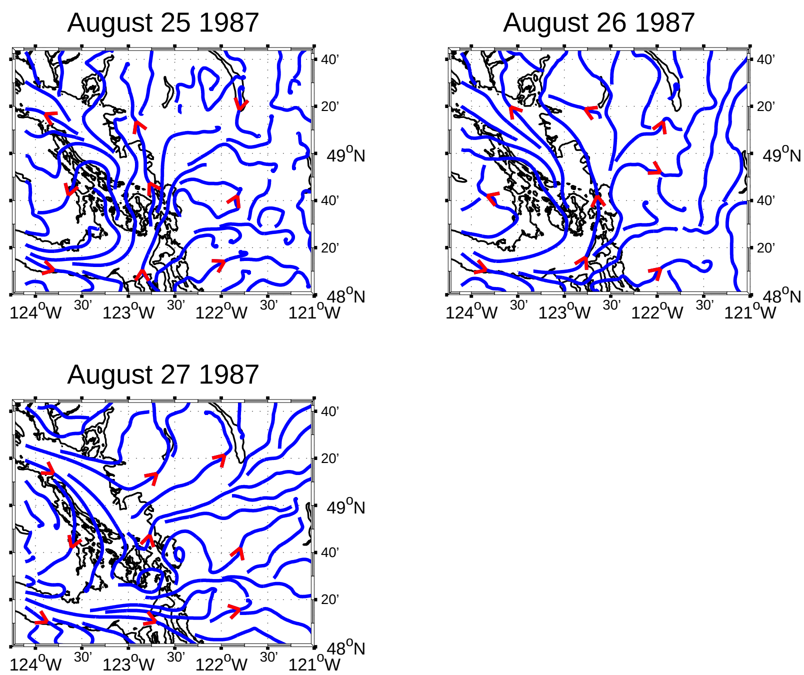

FIG. 16. Streamlines (blue) based on 0700-1500 (PST) average WRF surface wind field over the Georgia Basin for each day of the August 1987 episode. For clarity, the arrow heads indicating flow direction have been coloured red.

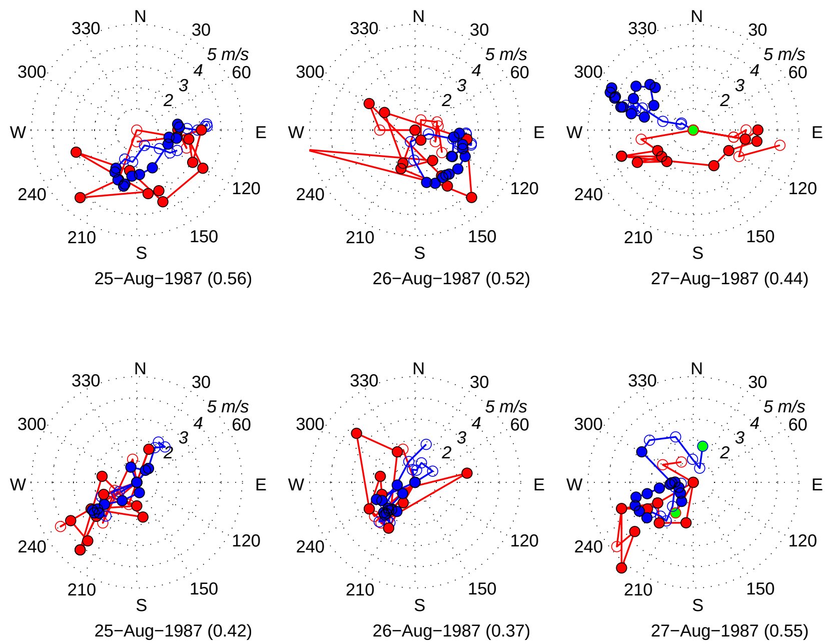

Fig. 17. Daily YVR (top row) and YXX (bottom row) hodograph plots of observed (red) and modeled (blue) winds. Solid circles are daytime values and open circles are nighttime. The number in parentheses by each date gives the vector correlation coefficient between the observed and modeled winds.

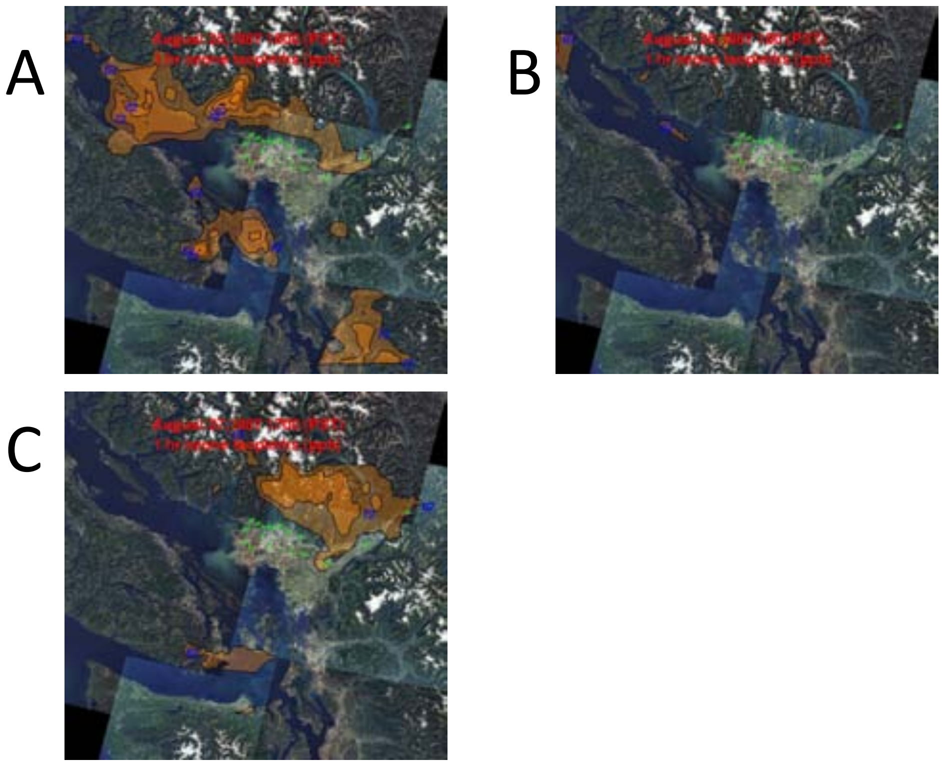

FIG. 18. Surface ozone concentrations contours (in 10 ppb increments) over the Georgia Basin at time of maximum modeled concentration for (A) August 25th, 1987 at 1600 (PST), (B) August 26th, 1987 at 0100 (PST) and (C) August 27th, 1987 at 1700 (PST). Also shown are the fixed monitoring network station locations (+). Concentrations below 62 ppb have not been contoured.

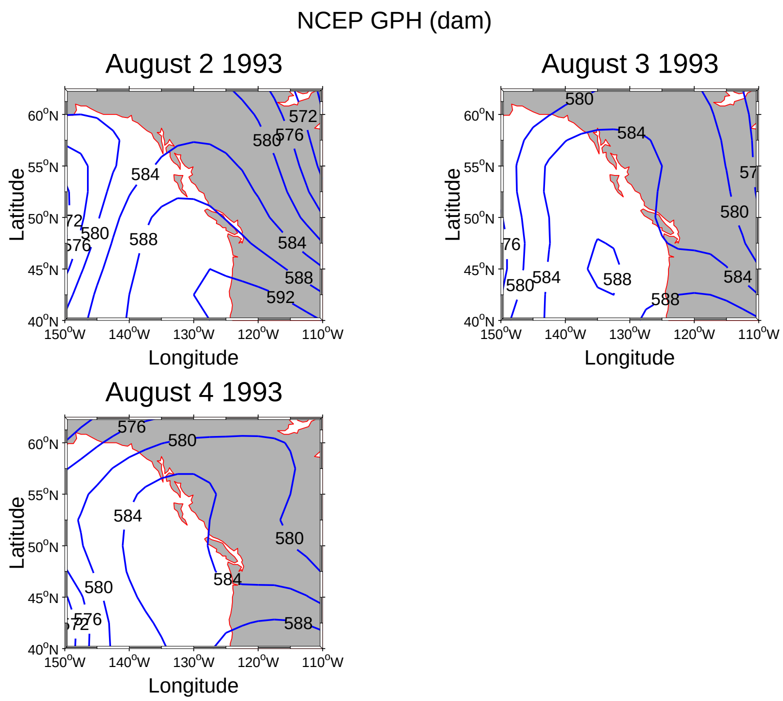

FIG. 19. Daily average 500mb geopotential height (in dam) over the Pacific Northwest during each day of the the August 1993 episode.

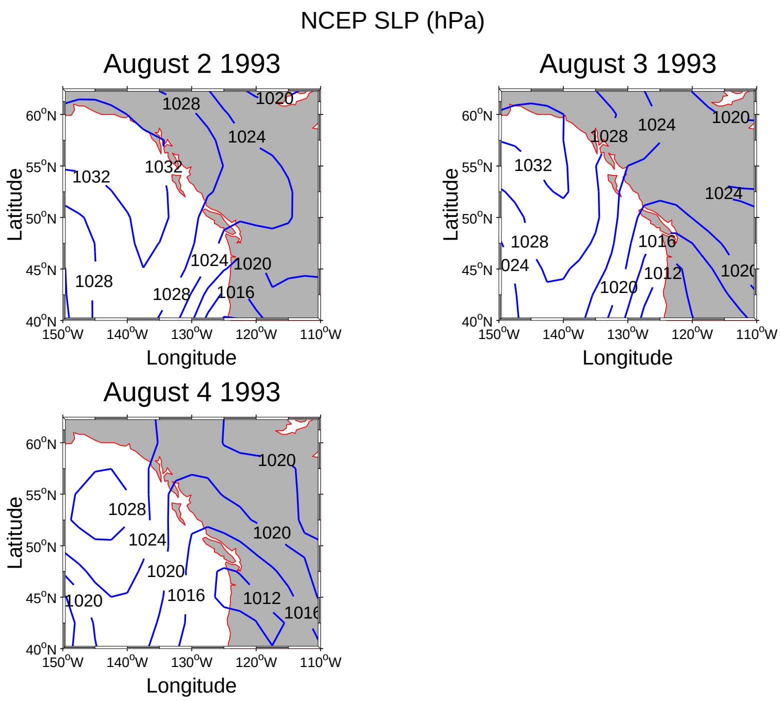

FIG. 20. Daily average sea-level pressure (in hPa) over the Pacific Northwest during each day of the the August 1993 episode.

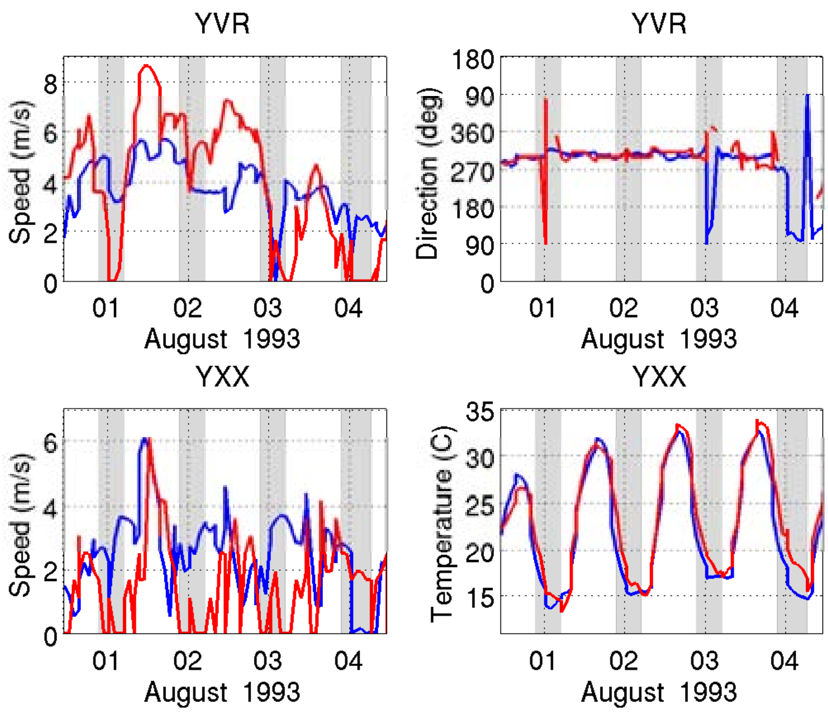

FIG. 21. Timeseries plots of WRF modeled (blue) and observed (red) wind speed (in m/s) at YVR (upper left), YVR wind direction (upper right), YXX wind speed (lower left) and YXX temperature (^{o}C, lower right) during the August 1993 episode.

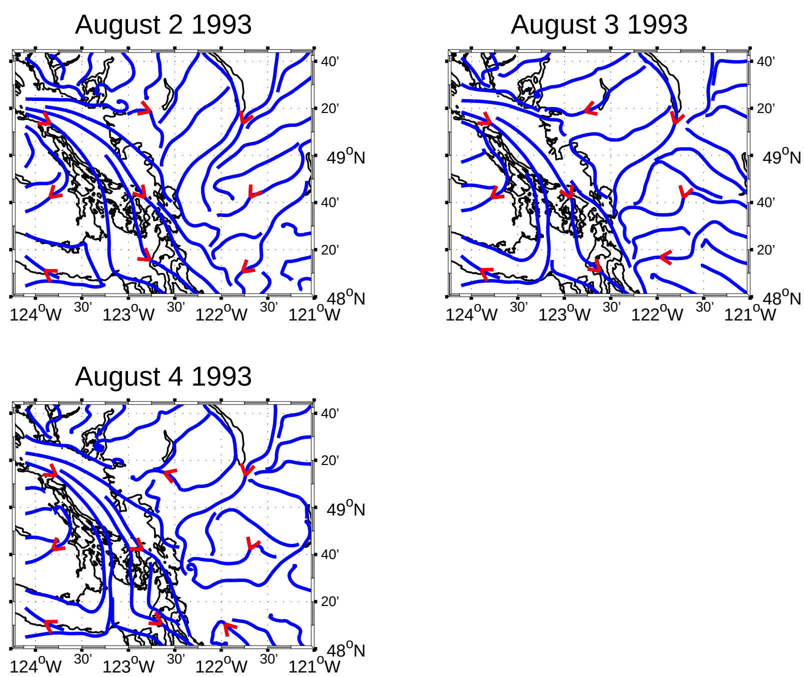

Fig. 22. Streamlines (blue) based on 0700-1500 (PST) average WRF surface wind field over the Georgia Basin for each day of the August 1993 episode. For clarity, the arrow heads indicating flow direction have been coloured red.

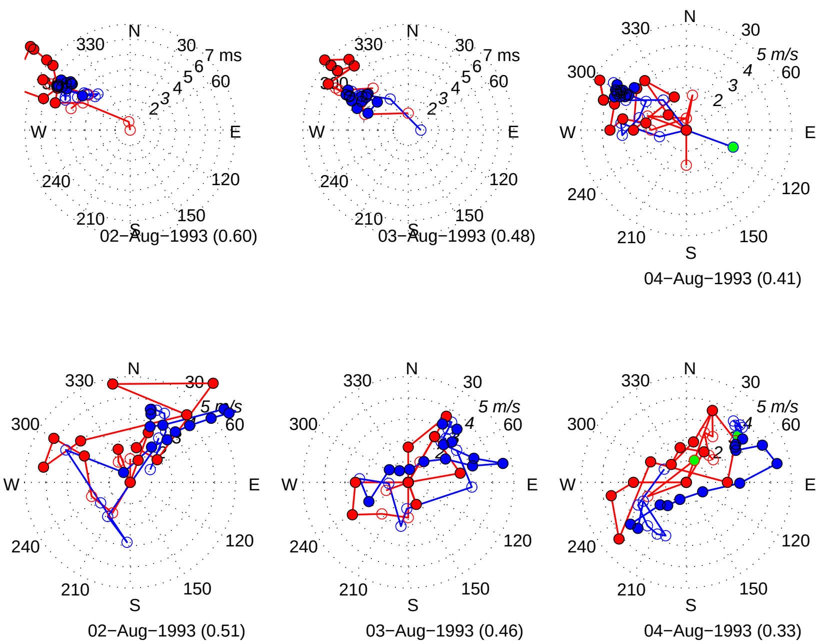

FIG. 23. Daily YVR (top row) and YXX (bottom row) hodograph plots of observed (red) and modeled (blue) winds. Solid circles are daytime values and open circles are nighttime. The number in parentheses by each date gives the vector correlation coefficient between the observed and modeled winds.

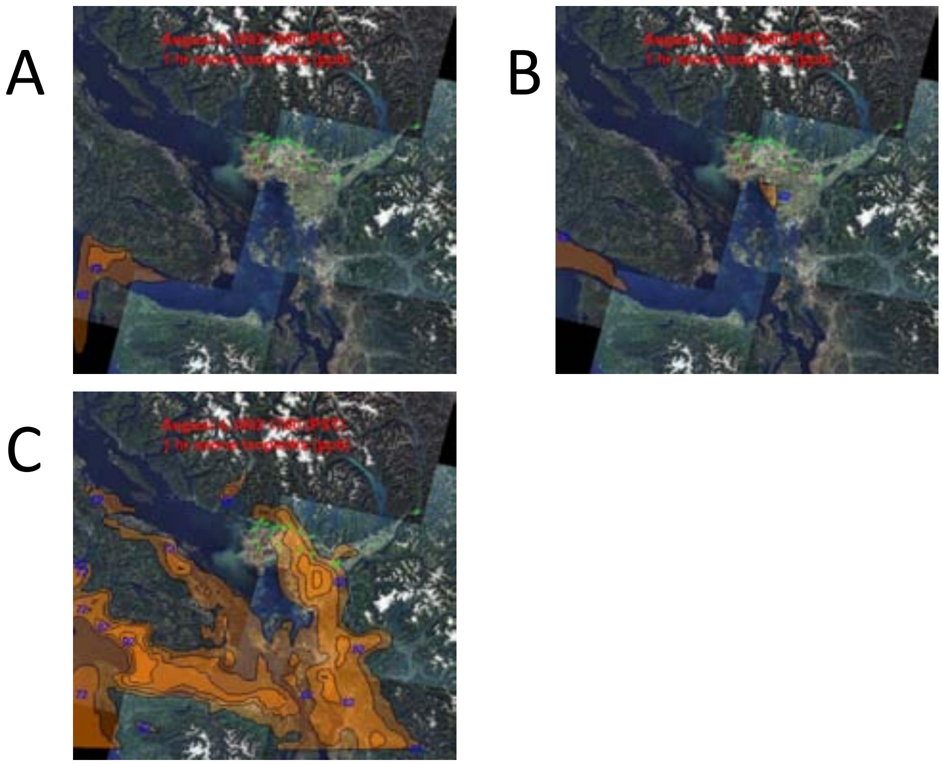

Fig. 24. Surface ozone concentrations contours (in 10 ppb increments) over the Georgia Basin at time of maximum modeled concentration for (A) August 2nd, 1993 at 1500 (PST), (B) August 3rd, 1993 at 1300 (PST) and (C) August 4th, 1993 at 1700 (PST). Also shown are the fixed monitoring network station locations (+). Concentrations below 62 ppb have not been contoured.

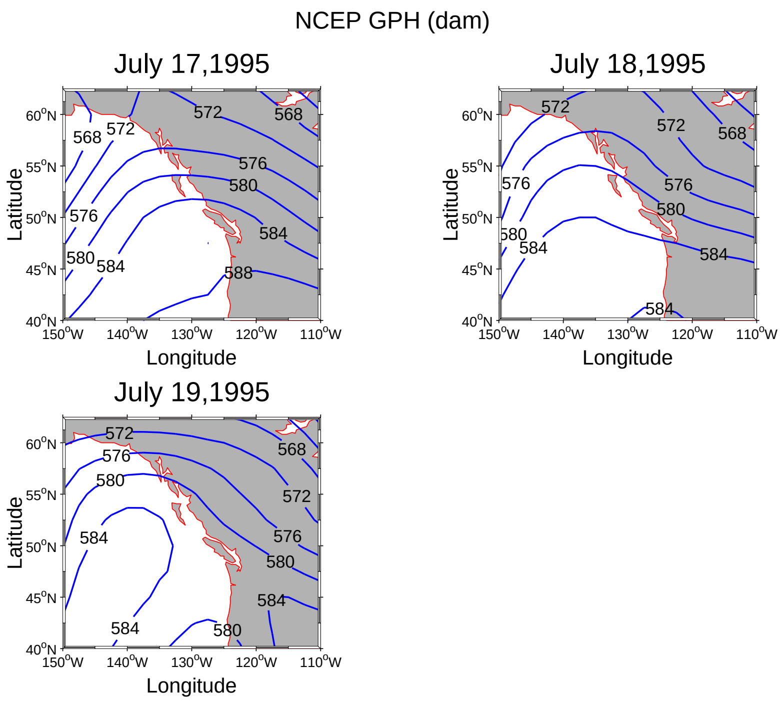

FIG. 25. Daily average 500mb geopotential height (in dam) over the Pacific Northwest during each day of the the July 1995 episode.

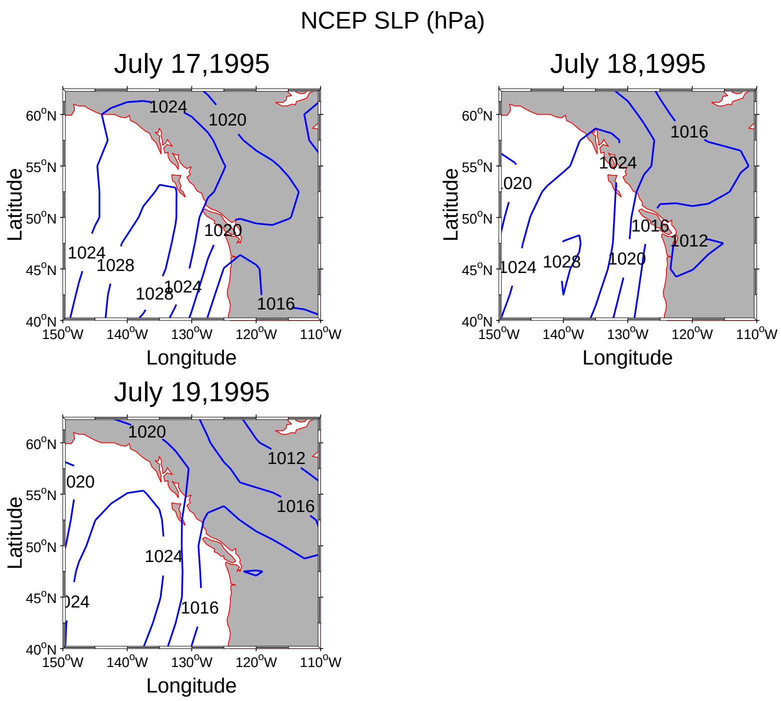

FIG. 26. Daily average sea-level pressure (in hPa) over the Pacific Northwest during each day of the the July 1995 episode.

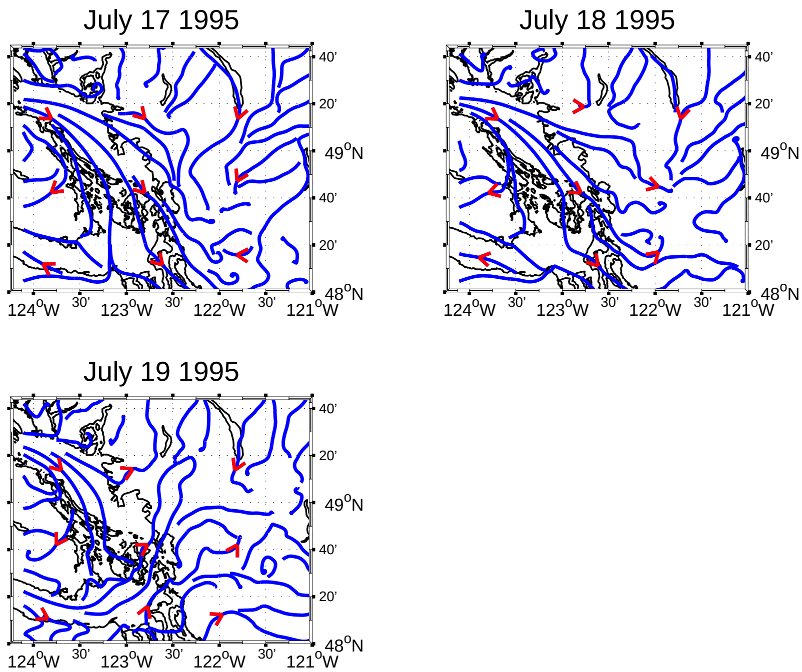

FIG. 27. Streamlines (blue) based on 0700-1500 (PST) average WRF surface wind field over the Georgia Basin for each day of the July 1995 episode. For clarity, the arrow heads indicating flow direction have been coloured red.

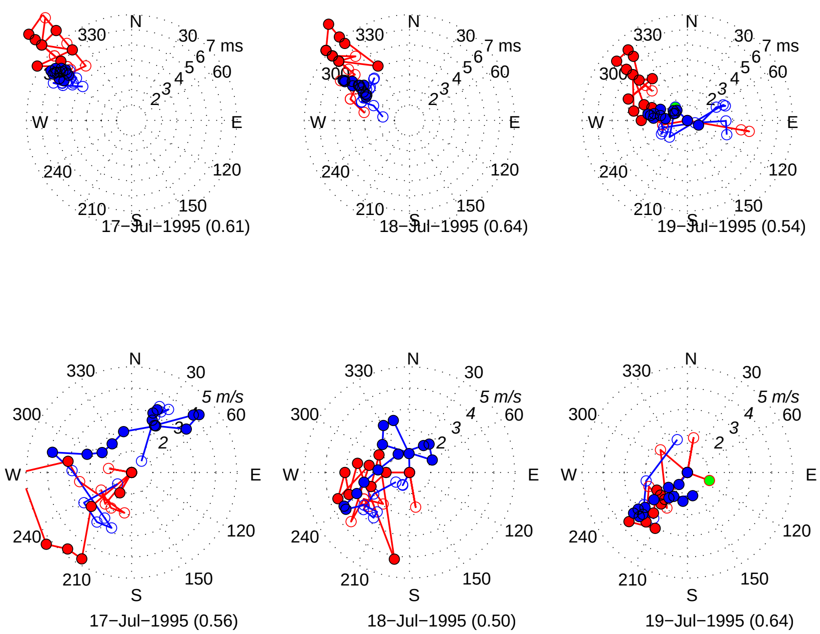

Fig. 28. Daily YVR (top row) and YXX (bottom row) hodograph plots of observed (red) and modeled (blue) winds. Solid circles are daytime values and open circles are nighttime. The number in parentheses by each date gives the vector correlation coefficient between the observed and modeled winds.

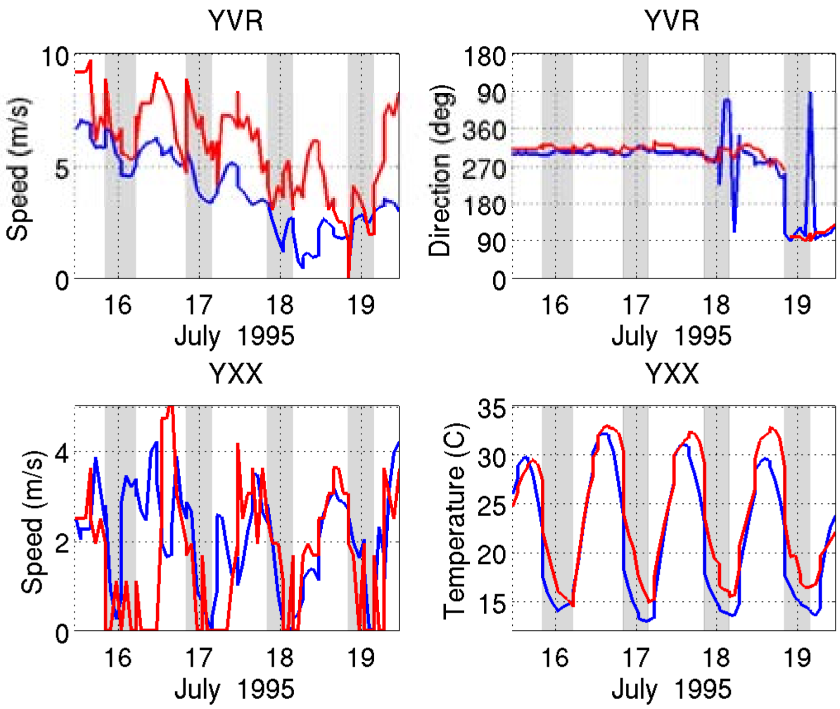

FIG. 29. Timeseries plots of WRF modeled (blue) and observed (red) wind speed (in m/s) at YVR (upper left), YVR wind direction (upper right), YXX wind speed (lower left) and YXX temperature (^{o}C, lower right) during the July 1995 episode.

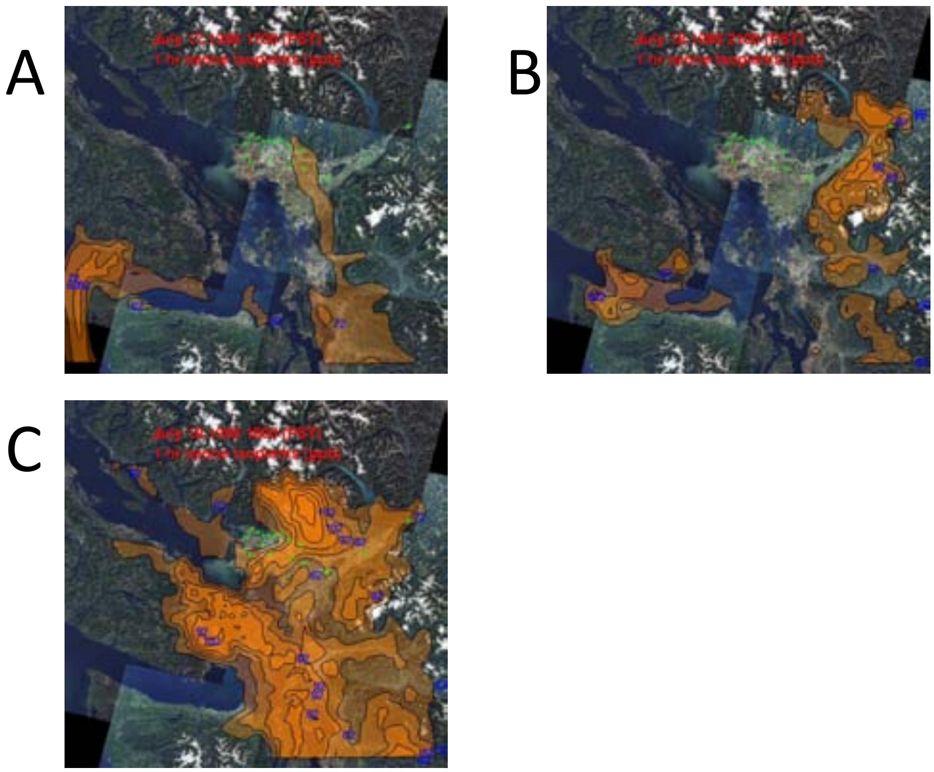

Fig. 30. Surface ozone concentrations contours (in 10 ppb increments) over the Georgia Basin at time of maximum modeled concentration for (A) July 17th, 1995 at 1700 (PST), (B) July 18th, 1995 at 2100 (PST) and (C) July 19th, 1995 at 1800 (PST). Also shown are the fixed monitoring network station locations (+). Concentrations below 62 ppb have not been contoured.

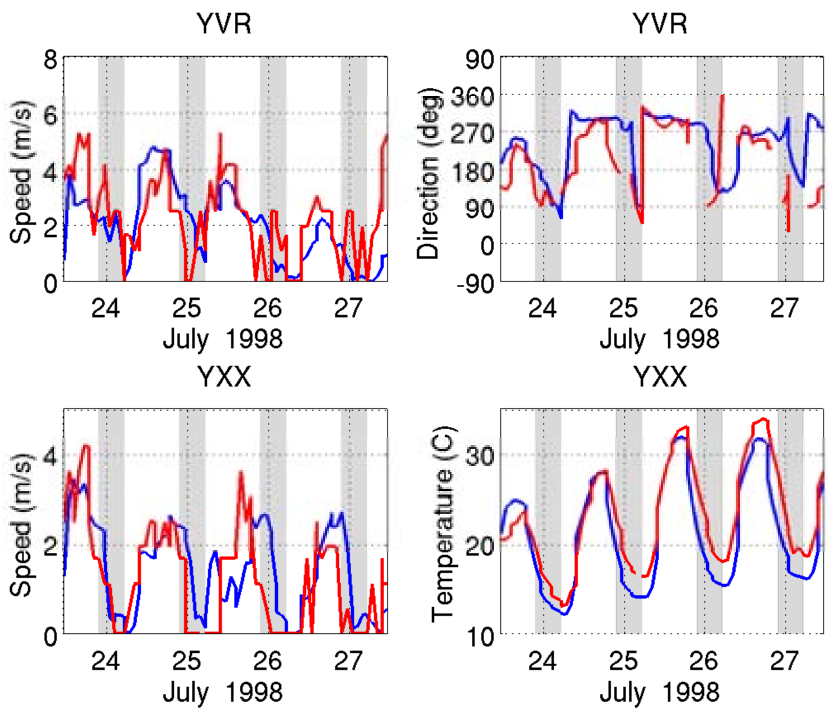

FIG. 31. Timeseries plots of WRF modeled (blue) and observed (red) wind speed (in m/s) at YVR (upper left), YVR wind direction (upper right), YXX wind speed (lower left) and YXX temperature (^{o}C, lower right) during the July 1998 episode.

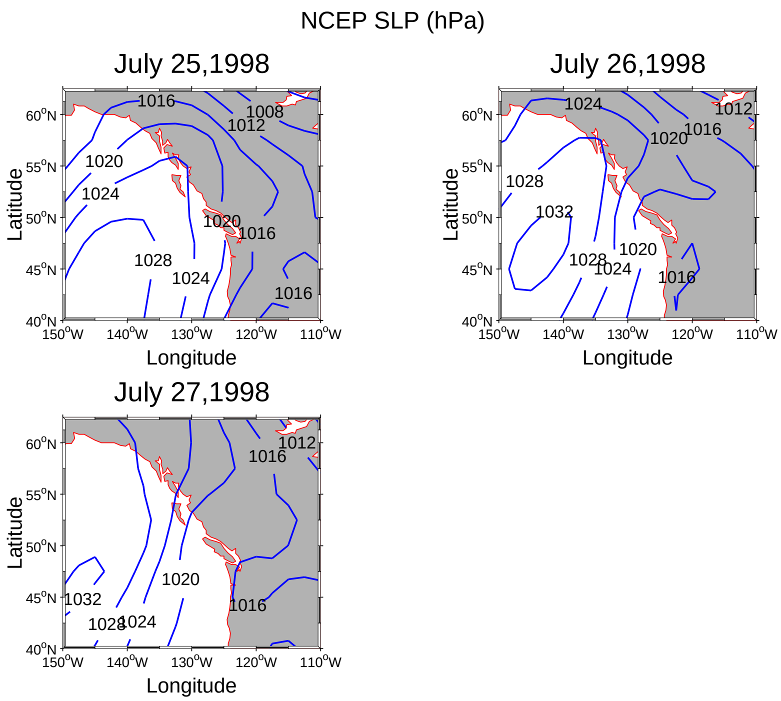

Fig. 32. Daily average sea-level pressure (in hPa) over the Pacific Northwest during each day of the the July 1998 episode.

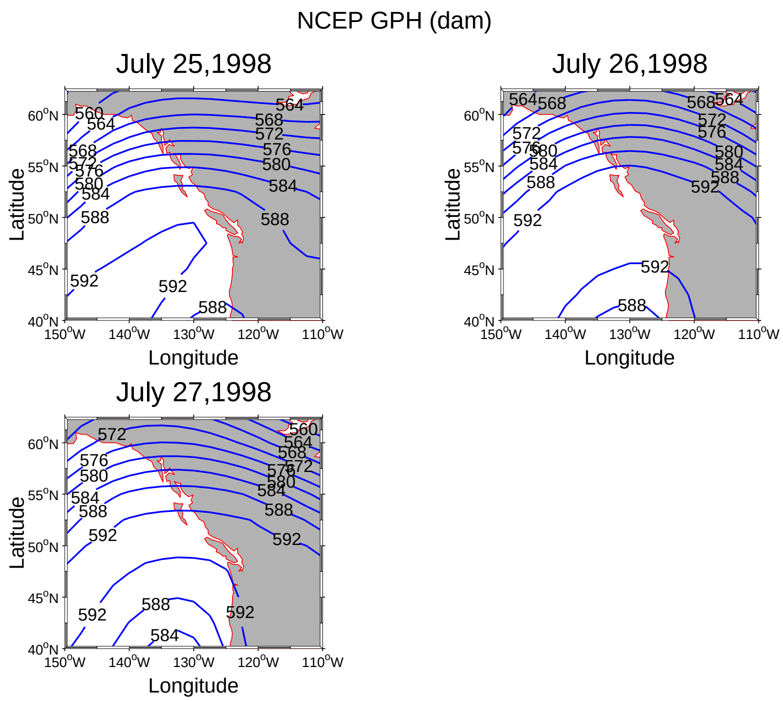

FIG. 33. Daily average 500mb geopotential height (in dam) over the Pacific Northwest during each day of the the July 1998 episode.

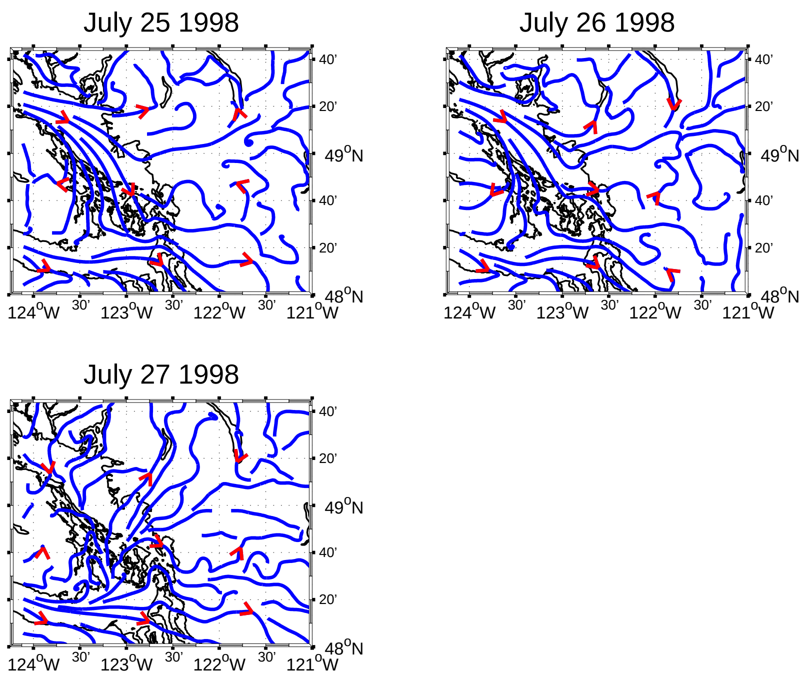

Fig. 34. Streamlines (blue) based on 0700-1500 (PST) average WRF surface wind field over the Georgia Basin for each day of the July 1998 episode. For clarity, the arrow heads indicating flow direction have been coloured red.

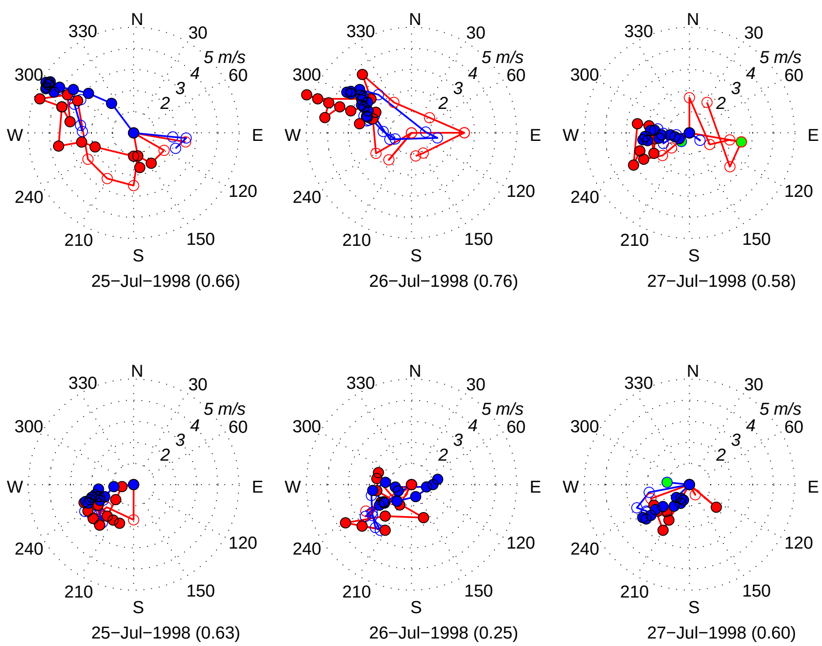

FIG. 35. Daily YVR (top row) and YXX (bottom row) hodograph plots of observed (red) and modeled (blue) winds. Solid circles are daytime values and open circles are nighttime. The number in parentheses by each date gives the vector correlation coefficient between the observed and modeled winds.

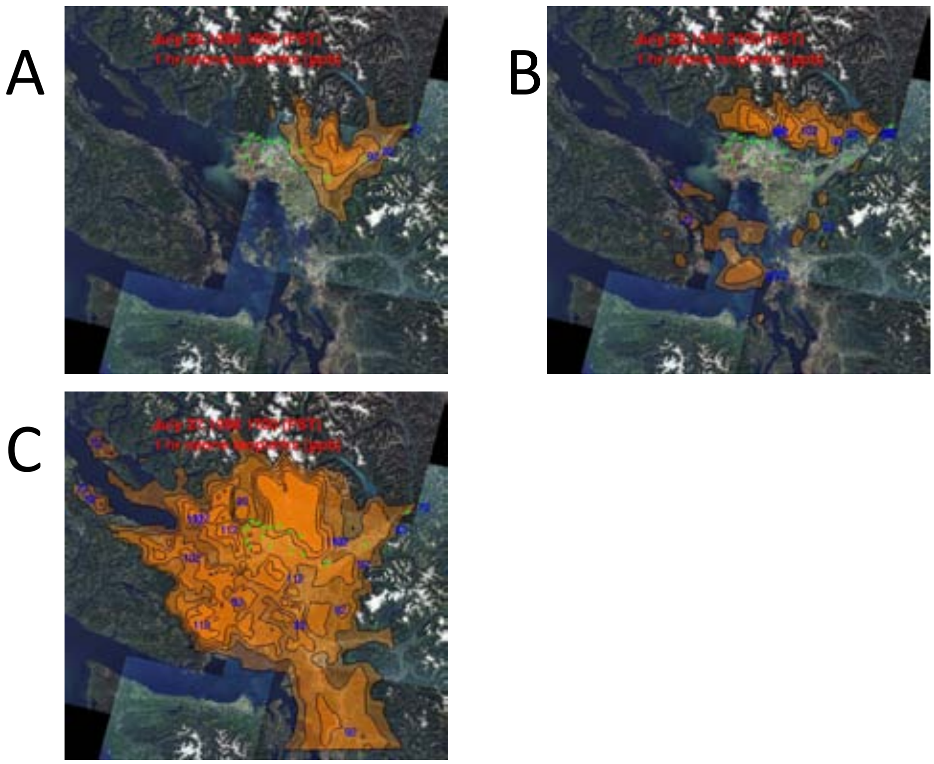

Fig. 36. Surface ozone concentrations contours (in 10 ppb increments) over the Georgia Basin at time of maximum modeled concentration for (A) July 25th, 1998 at 1600 (PST), (B) July 26th, 1998 at 2100 (PST) and (C) July 27th, 1998 at 1700 (PST). Also shown are the fixed monitoring network station locations (+). Concentrations below 72 ppb have not been contoured.

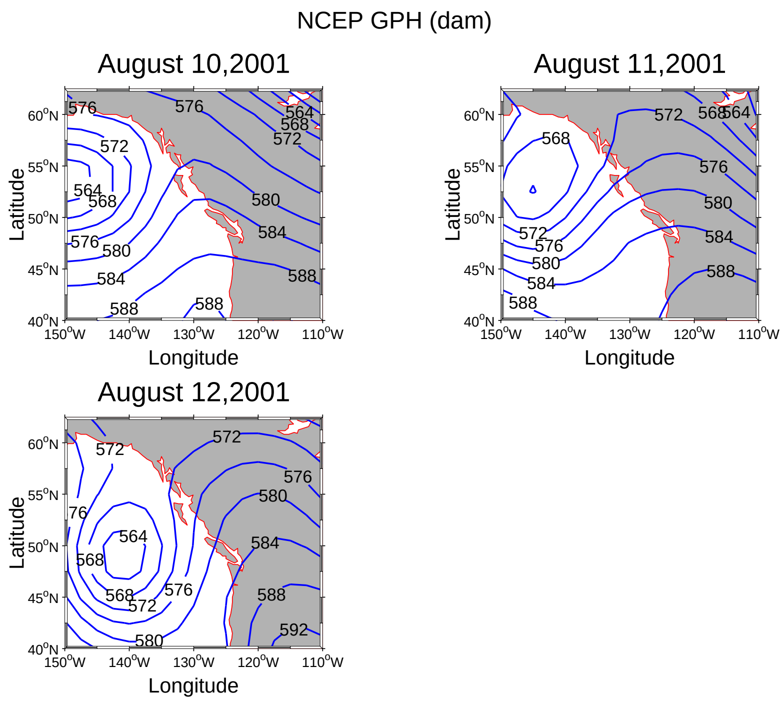

Fig. 37. Daily average 500mb geopotential height (in dam) over the Pacific Northwest during each day of the the August 2001 episode.

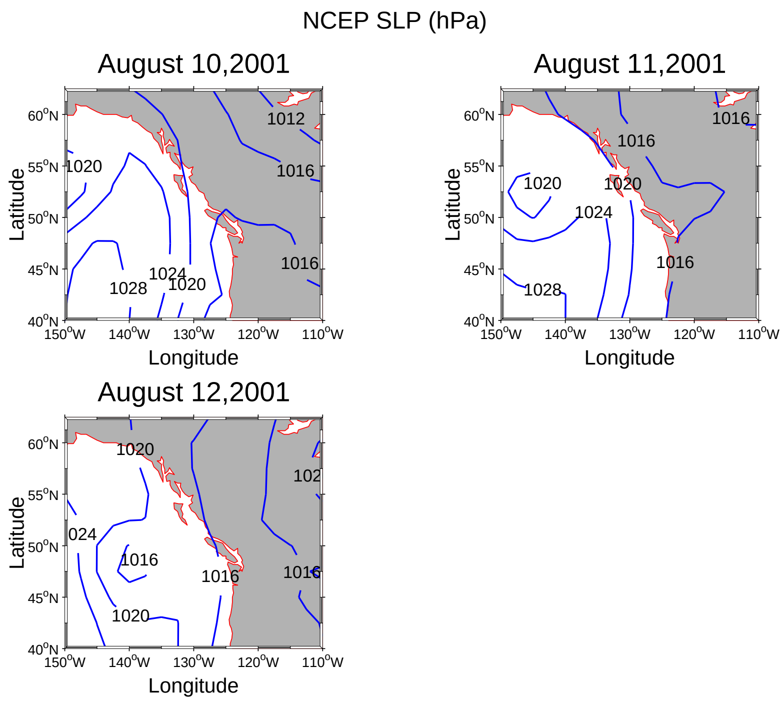

Fig. 38. Daily average sea-level pressure (in hPa) over the Pacific Northwest during each day of the the August 2001 episode.

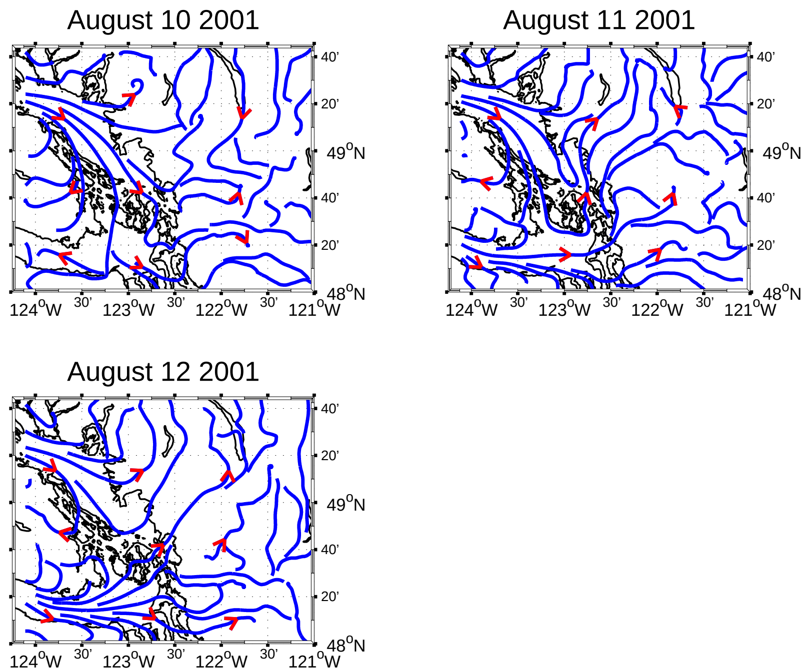

Fig. 39. Streamlines (blue) based on 0700-1500 (PST) average WRF surface wind field over the Georgia Basin for each day of the August 2001 episode. For clarity, the arrow heads indicating flow direction have been coloured red.

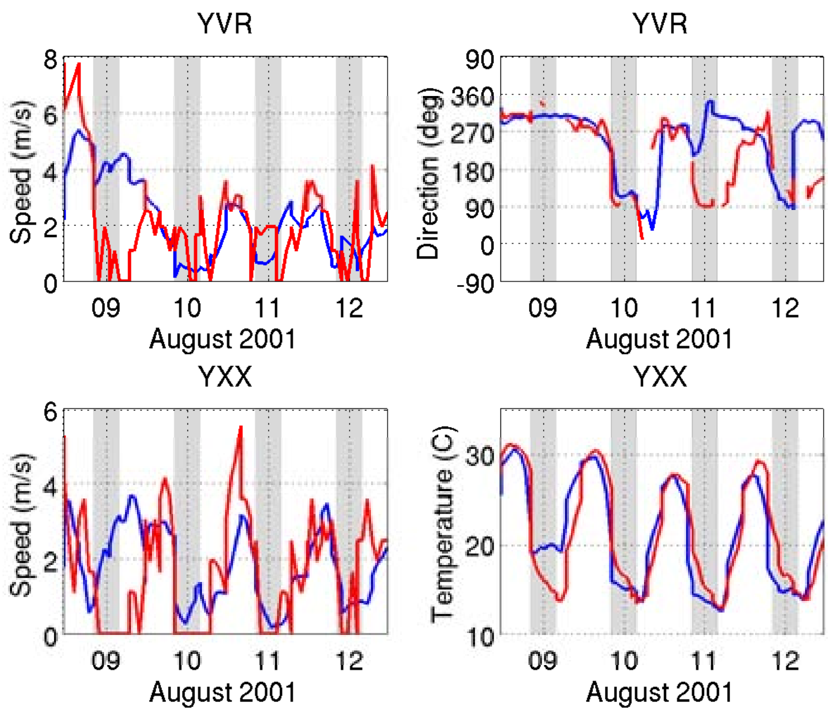

FIG. 40. Timeseries plots of WRF modeled (blue) and observed (red) wind speed (in m/s) at YVR (upper left), YVR wind direction (upper right), YXX wind speed (lower left) and YXX temperature (^{o}C, lower right) during the August 2001 episode.

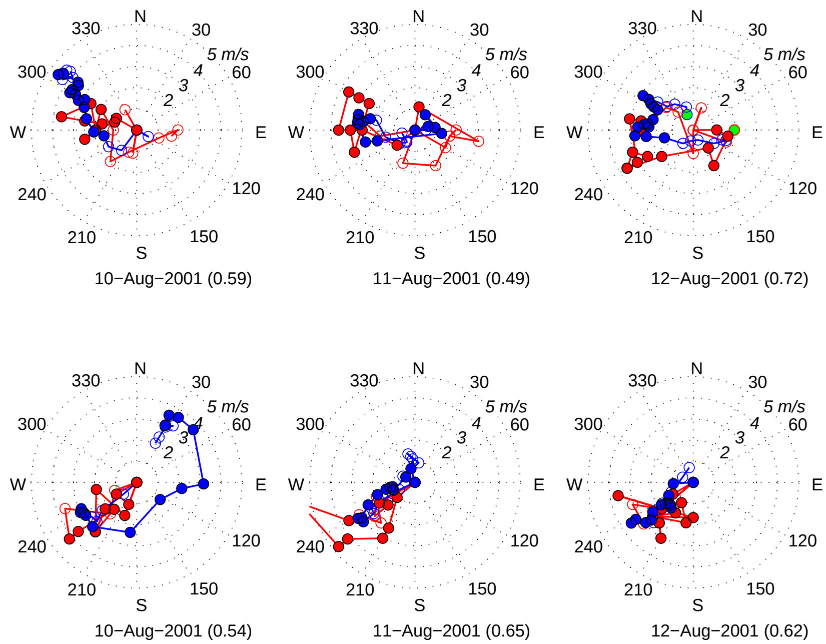

FIG. 41. Daily YVR (top row) and YXX (bottom row) hodograph plots of observed (red) and modeled (blue) winds. Solid circles are daytime values and open circles are nighttime. The number in parentheses by each date gives the vector correlation coefficient between the observed and modeled winds.

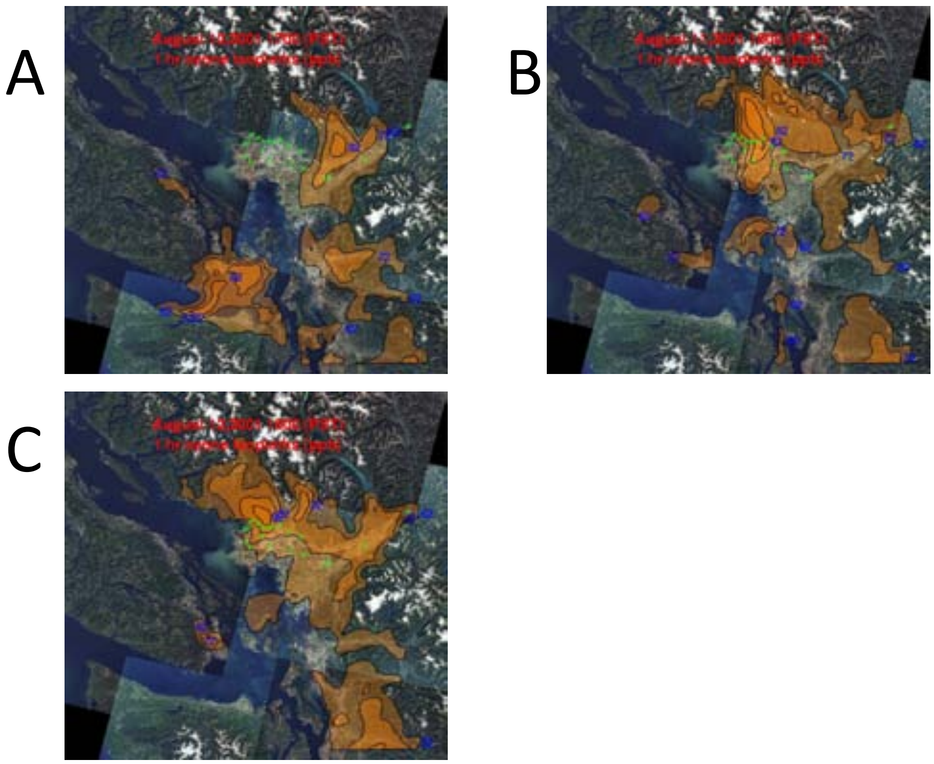

Fig. 42. Surface ozone concentrations contours (in 10 ppb increments) over the Georgia Basin at time of maximum modeled concentration for (A) August 10th, 2001 at 1700 (PST), (B) August 11th, 2001 at 1800 (PST) and (C) August 12th, 2001 at 1600 (PST). Also shown are the fixed monitoring network station locations (+). Concentrations below 62 ppb have not been contoured.

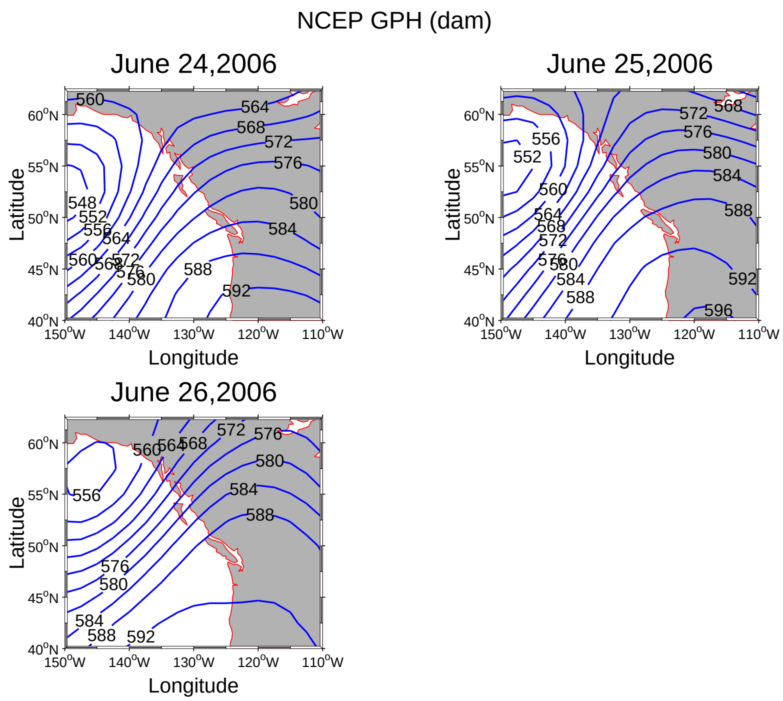

FIG. 43. Daily average 500mb geopotential height (in dam) over the Pacific Northwest during each day of the the June 2006 episode.

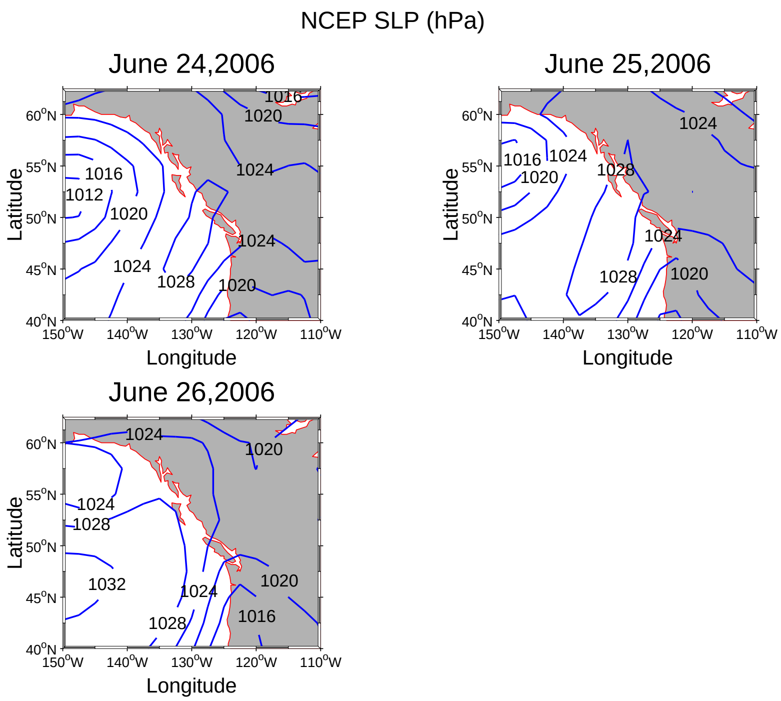

FIG. 44. Daily average sea-level pressure (in hPa) over the Pacific Northwest during each day of the the June 2006 episode.

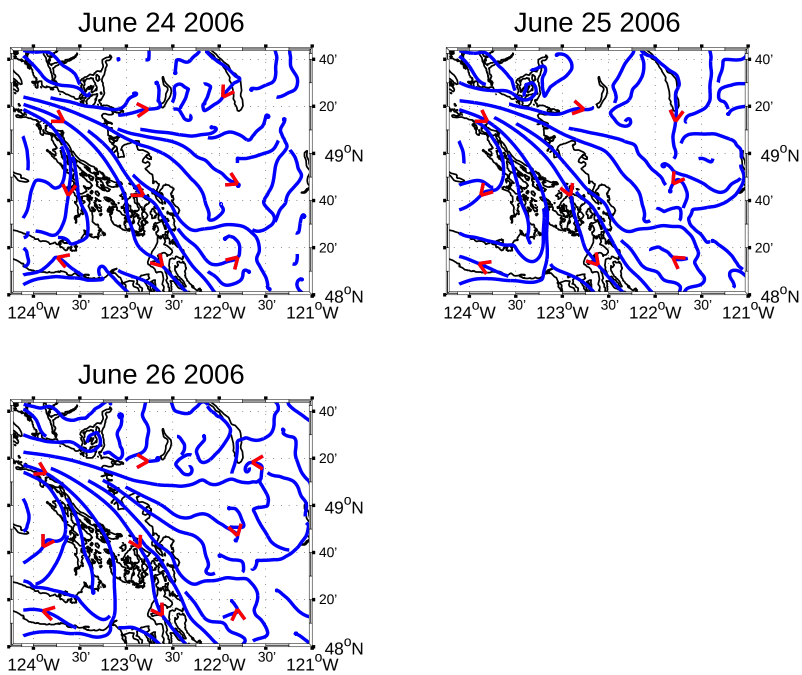

Fig. 45. Streamlines (blue) based on 0700-1500 (PST) average WRF surface wind field over the Georgia Basin for each day of the June 2006 episode. For clarity, the arrow heads indicating flow direction have been coloured red.

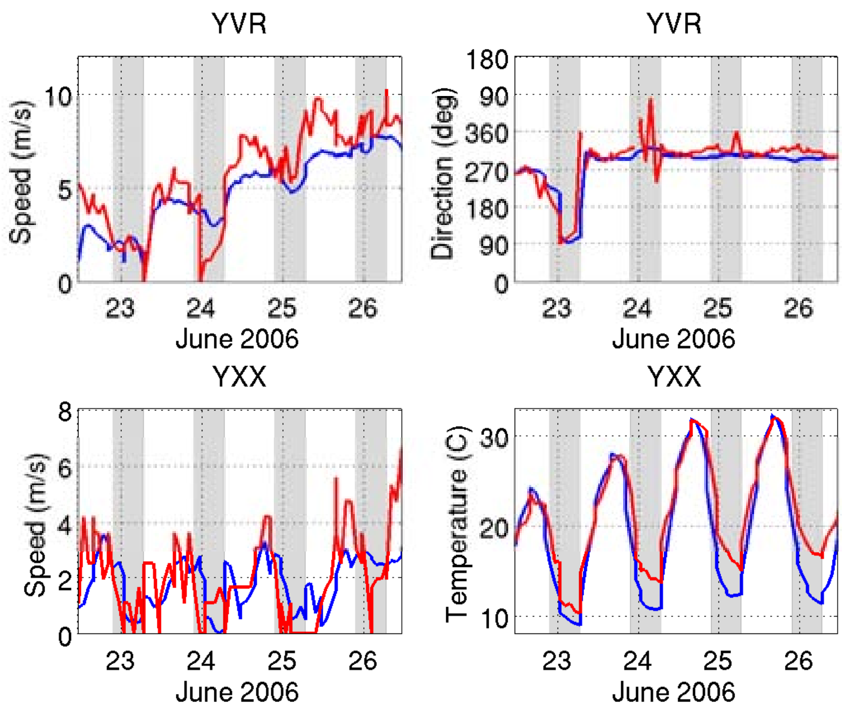

FIG. 46. Timeseries plots of WRF modeled (blue) and observed (red) wind speed (in m/s) at YVR (upper left), YVR wind direction (upper right), YXX wind speed (lower left) and YXX temperature (^{o}C, lower right) during the June 2006 episode.

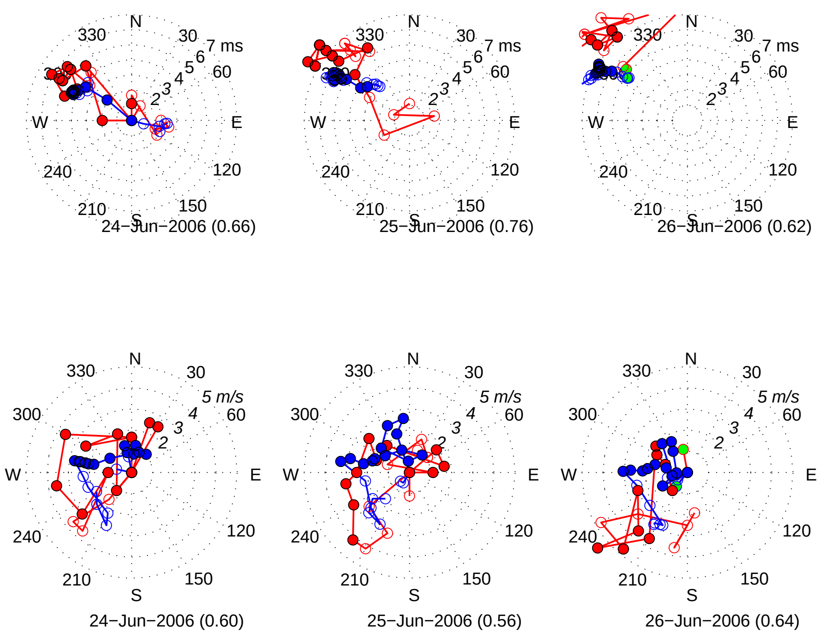

Fig. 47. Daily YVR (top row) and YXX (bottom row) hodograph plots of observed (red) and modeled (blue) winds. Solid circles are daytime values and open circles are nighttime. The number in parentheses by each date gives the vector correlation coefficient between the observed and modeled winds.

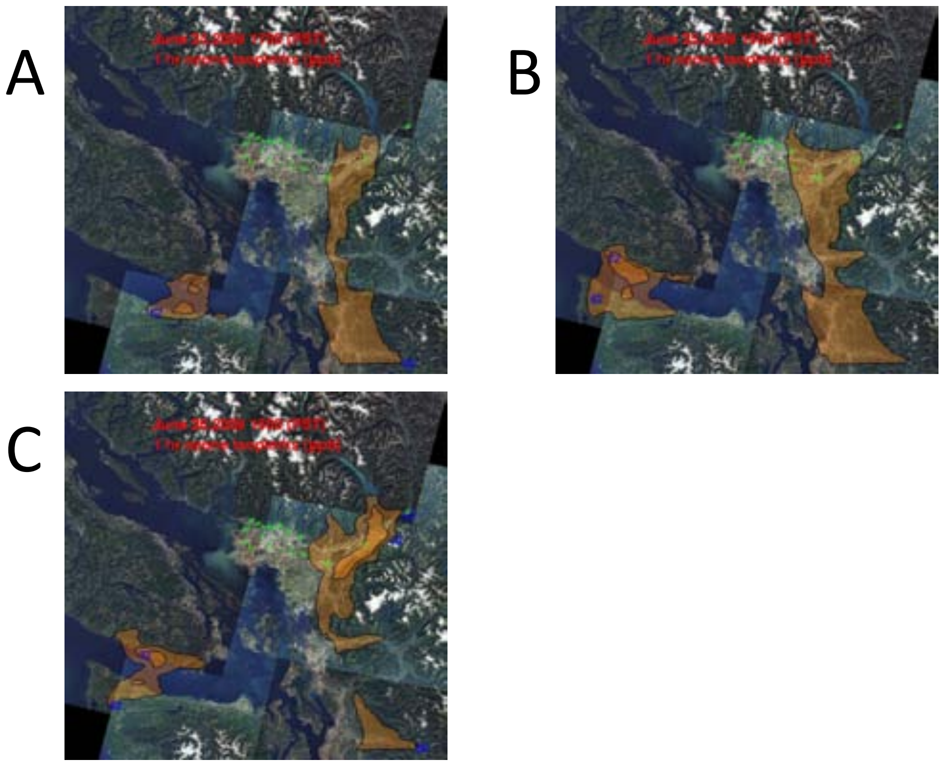

Fig. 48. Surface ozone concentrations contours (in 10 ppb increments) over the Georgia Basin at time of maximum modeled concentration for (A) June 24th, 2006 at 1700 (PST), (B) June 25th, 2006 at 1600 (PST) and (C) June 26th, 2006 at 1600 (PST). Also shown are the fixed monitoring network station locations (+). Concentrations below 62 ppb have not been contoured.

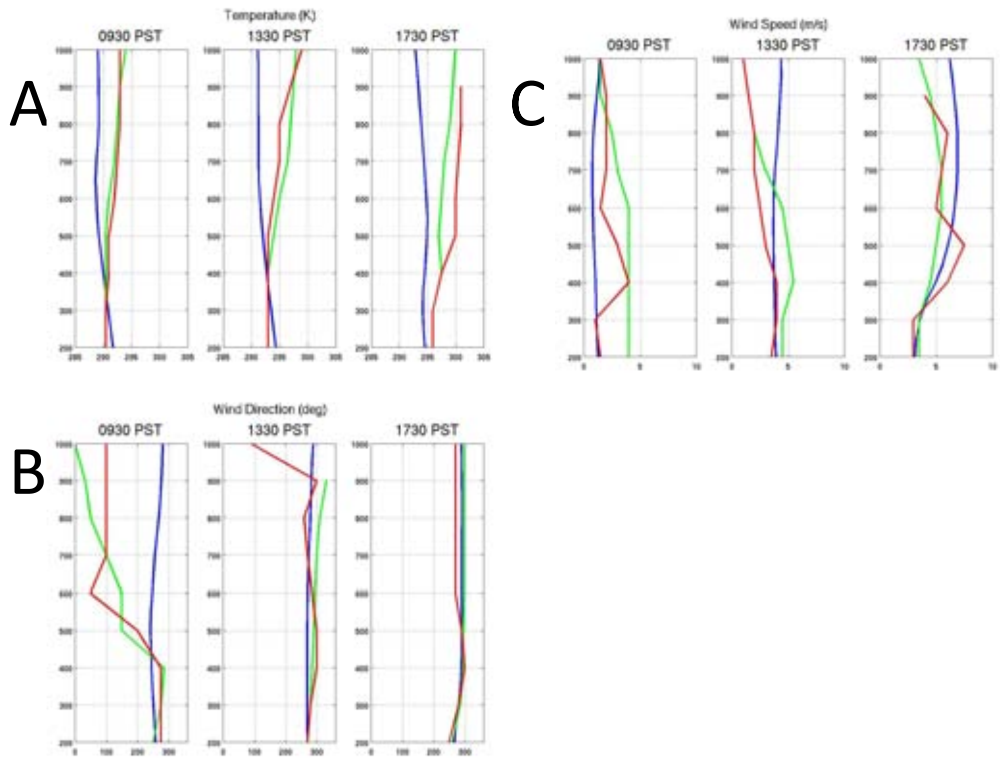

FIG. 49. Profiles of observed (red), WRF-modeled (blue) and RAMS-modeled (green) temperatures (A), wind speeds (B) and wind directions (C) on July 17th 1985 at Queen Elizabeth Park, Vancouver, B.C. Each plot has results for 0930, 1330 and 1730 PST. The observed and RAMS results have been manually extracted from Figures 6-8 in Cai and Steyn (2000) at 100 m intervals from 200 m to 1000 m and appear smoother than shown in the original figures.

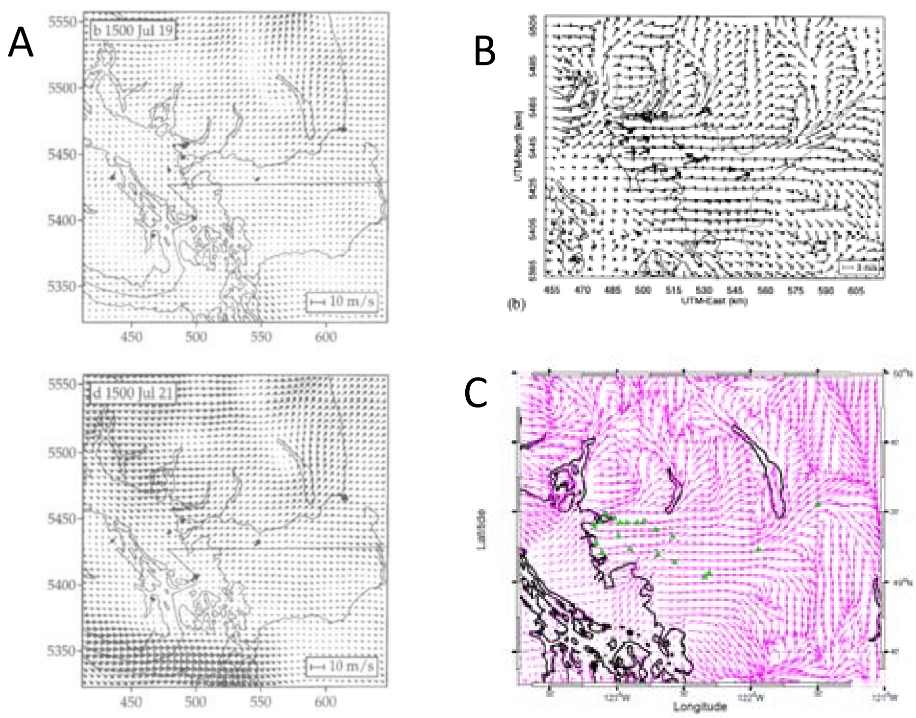

Fig. 50. Surface (10m) wind fields (a) from Hedley and Singleton (1997) valid 1500 (PST) July 19 (upper) and 1500 (PST) July 20, 1985 (lower), (b) from Cai and Steyn (2000) valid 1600 (PST) July 17th, 1985 and (c) from the present WRF simulations valid 1600 (PST) July 17th, 1985.

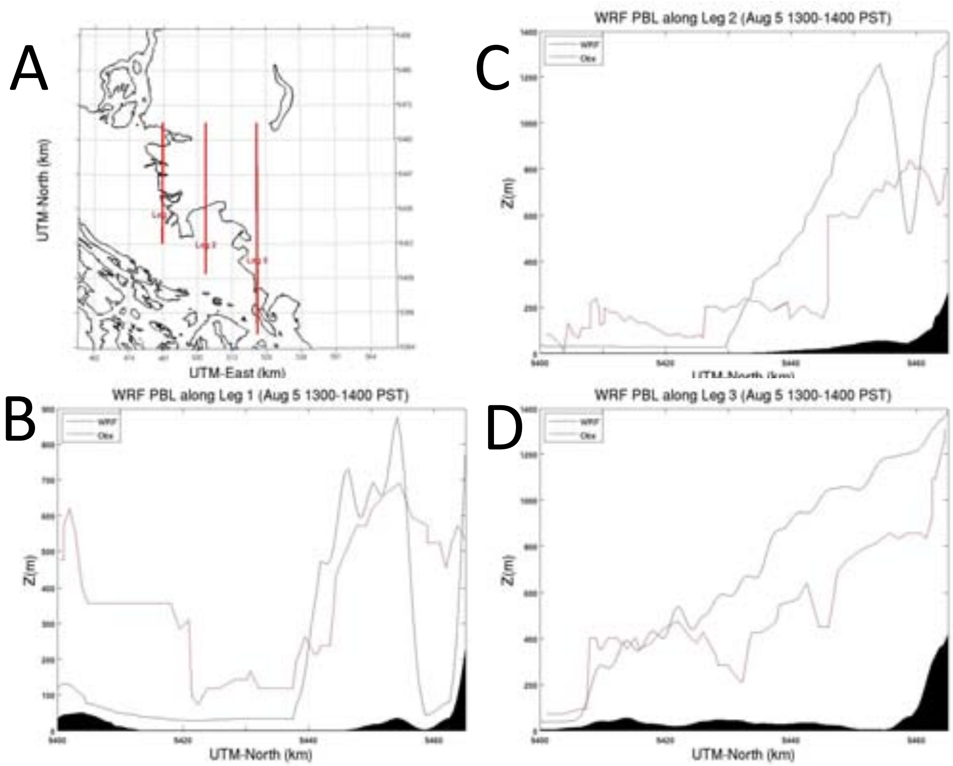

FIG. 51. Aircraft LIDAR observed (red) and WRF-modeled (blue) MLD along the 3 transects (from Batchvarova et al. (1999)). Panel (A) shows the flight paths over the LFV while panels B,C, and D show MLD along with surface topography (dark shaded areas) with north to the right.

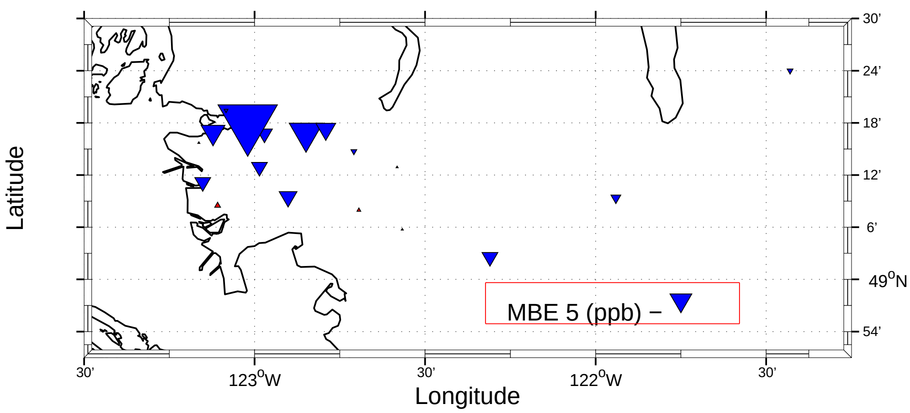

FIG. 52. Proportional symbol plot showing modeled daytime MBE (in ppb) at the MV monitoring station locations averaged over the 7 episodes. Blue triangles pointing down represent CMAQ under-predictions. Red upward pointing triangles are CMAQ over-predictions.

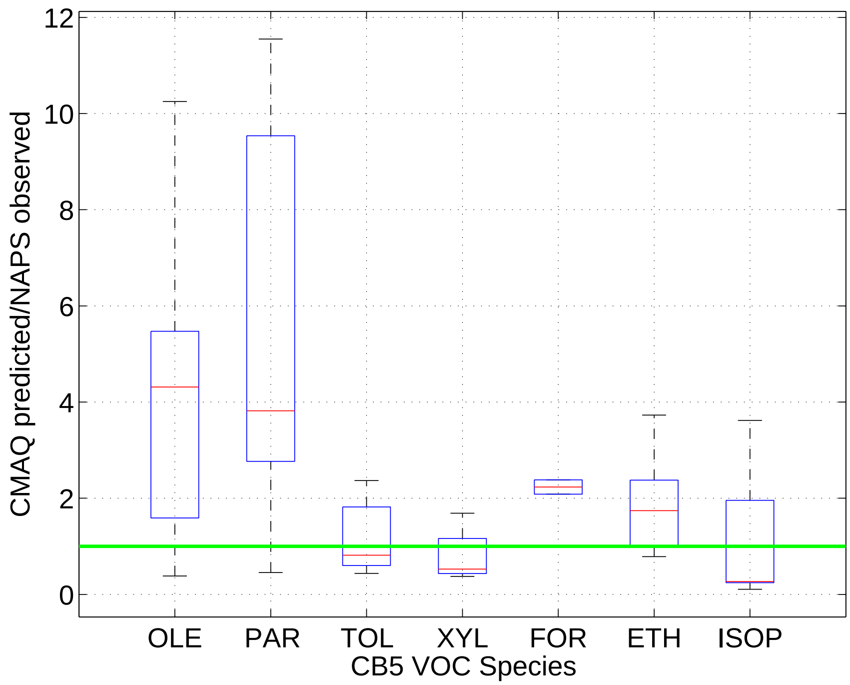

FIG. 53. Box and whisker plots of ratio of observed to predicted VOC concentrations by CB5 VOC class. Solid green line is at the ratio value of 1.0. For each CB5 class, box indicates 25th, 50th and 75th percentiles. The upper (lower) whisker represents the largest (lowest) data value less (greater) than 1.5 times the inter-quartile range plus (minus) the 75th (25th) percentile.

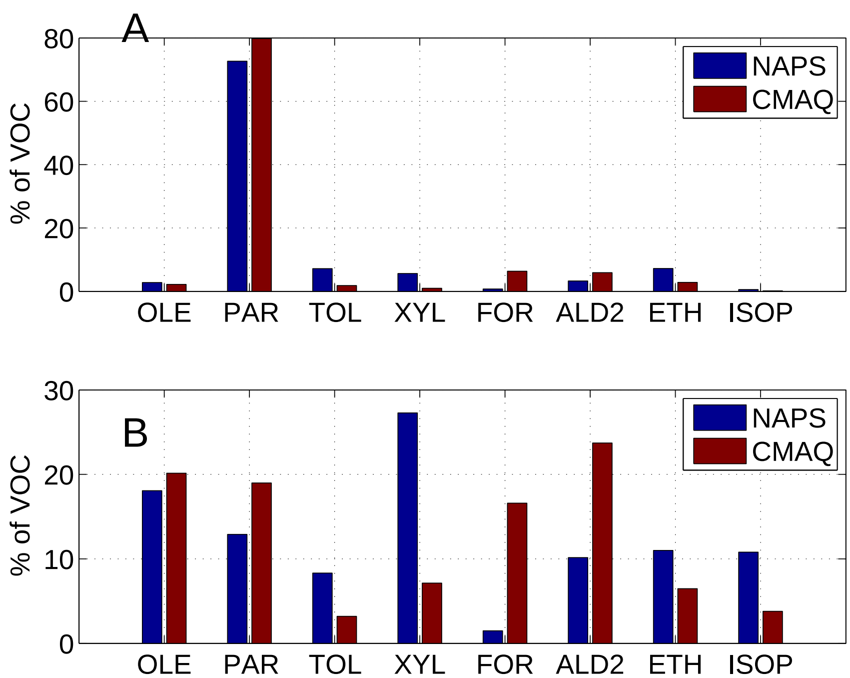

FIG. 54. A. Mean VOC speciation (in percent by concentration) broken down by CB5 class, based the CMAQ modeled and NAPS observed concentrations averaged over all years and stations. B. Same as (A) but VOC concentrations weighted by kOH reactivity.

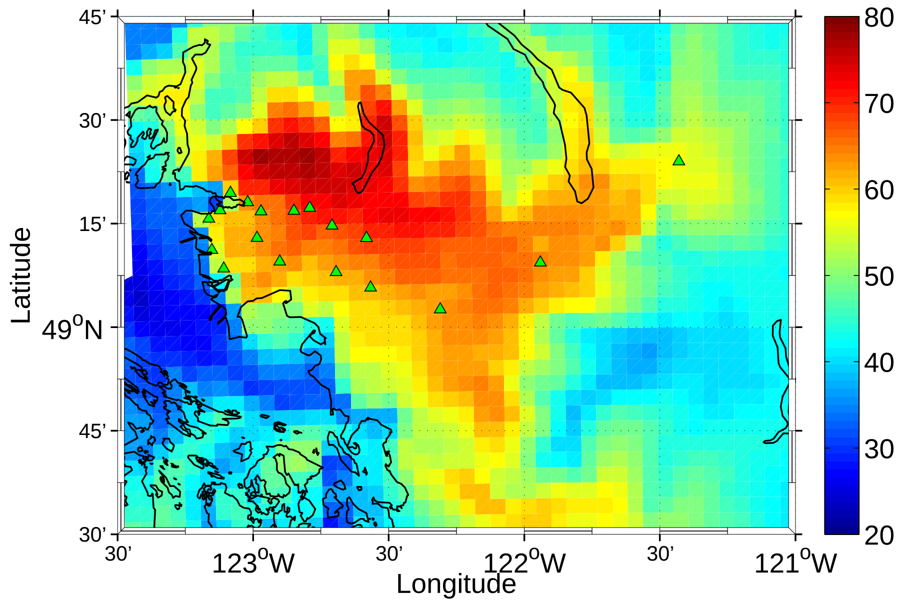

Fig. 55. Modeled 1300-1800 (PST) average ozone concentration (in ppb) valid August 11th, 2001 (A) over the LFV using from 100% VOC and NOx anthropogenic emissions.

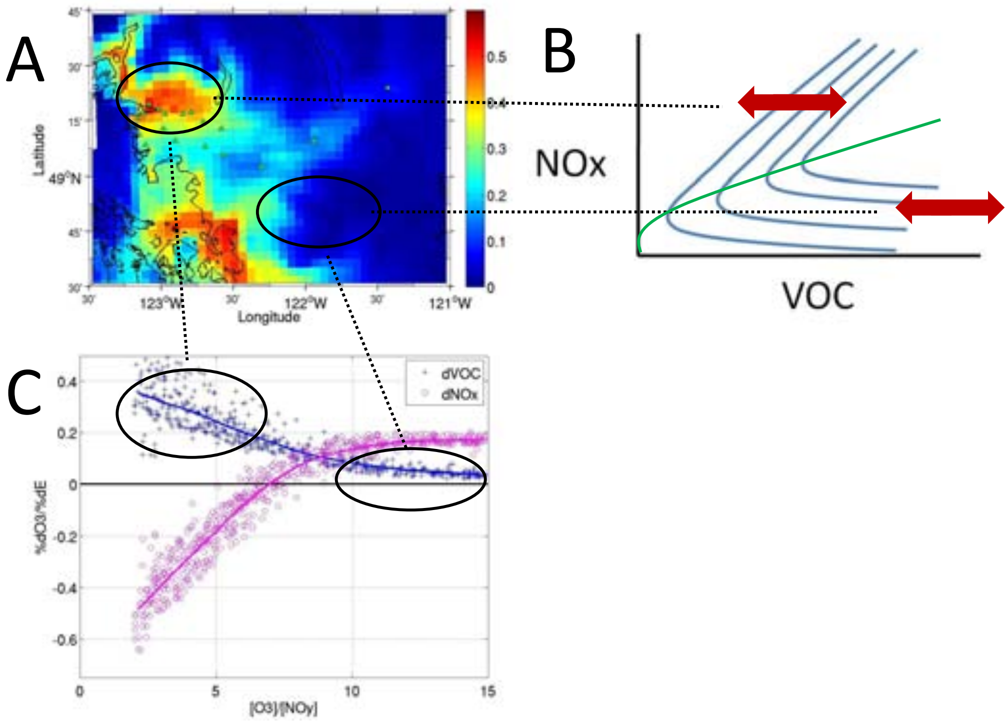

FIG. 56. Spatial plot of modeled ozone sensitivity (%change in ozone/% change in emissions) to changing anthropogenic VOC emissions (A). The warm coloured areas indicate regions of high sensitivity. Figure B gives a schematic of an ozone isopleth diagram. The solid blue lines are lines of constant ozone concentration (isopleths) that represent the final ozone concentration arising from different mixtures of VOC and NOx emissions. Isopleth magnitudes increase further from the origin. The green line is the ridgeline separating the plot into a VOC-limited region (above) and a NOx-limited region below. The red arrow above the ridgeline shows how the sensitivity of the ozone response surface to changing VOC emissions: ozone concentrations increase with increasing VOC emissions and decrease with decreasing VOC emissions (while NOx emissions are held constant). Below the ridgeline ozone is relatively insensitive to changing VOC emissions. The warm coloured regions in A are representative of points lying above the ridgeline and the cooler coloured regions below the ridgeline. This is highlighted by the 2 circled regions in A. In C, the modeled ozone sensitivity values used to create the spatial plot in (A) are plotted as a function of the modeled ratio of $[O_3]/[NOy]$ (blue crosses). The circled regions in this plot show how the warm and cold regions in (A) get represented in (C).

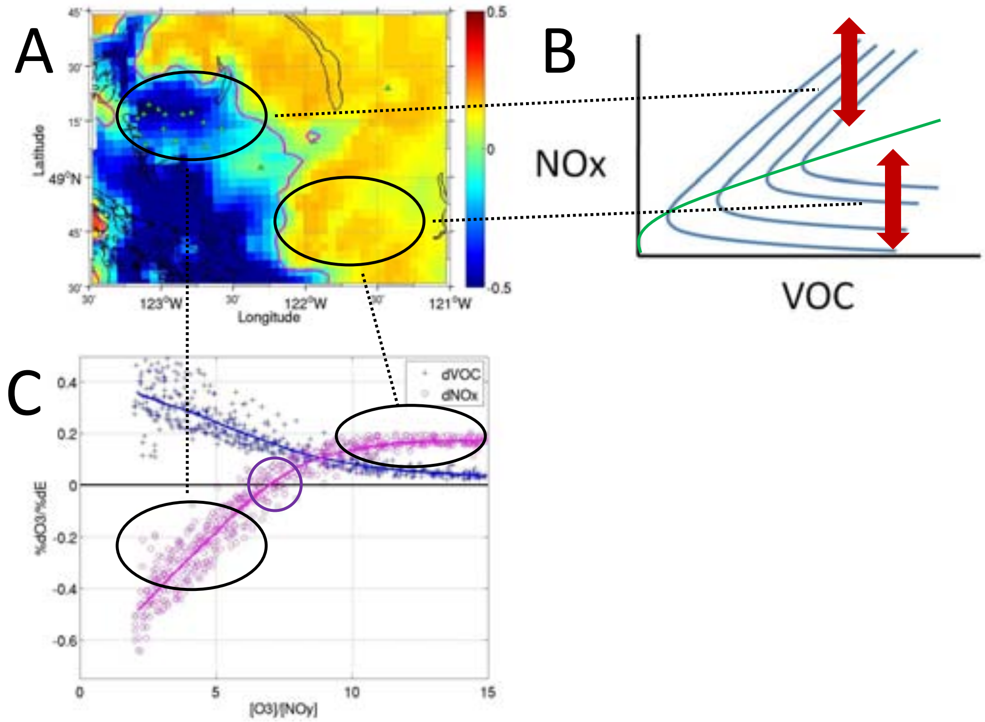

FIG. 57. Spatial plot of modeled ozone sensitivity (%change in ozone/% change in emissions) to changing NOx emissions (A). The warm coloured areas indicate regions of positive sensitivity. Figure B is as in Fig 56 except the red arrows now indicate ozone response to changing NOx emissions: above the ridgeline ozone concentrations *decrease with increasing NOx emissions and* increase with decreasing NOx emissions (while VOC emissions are held constant). Below the ridgeline ozone the opposite holds: ozone concentrations *increase with increasing NOx emissions and* decrease with decreasing NOx emissions. The cool coloured regions in A are representative of points lying above the ridgeline and the warmer coloured regions below the ridgeline. This is highlighted by the 2 circled regions in A. In C, the modeled ozone sensitivity values used to create the spatial plot in (A) are plotted as a function of the modeled ratio of $[O_3]/[NOy]$ (purple circles). The circled regions in this plot show how the warm and cool regions in (A) get represented in (C). Also shown in C is the region where the purple circles change from negative to positive sensitivity (small circled region). This corresponds to a $[O_3]/[NOy]$ ratio of approximately 7.0 and identifies the ridgeline. The $[O_3]/[NOy]$ threshold has been used to plot the ridgeline location in A (purple line).

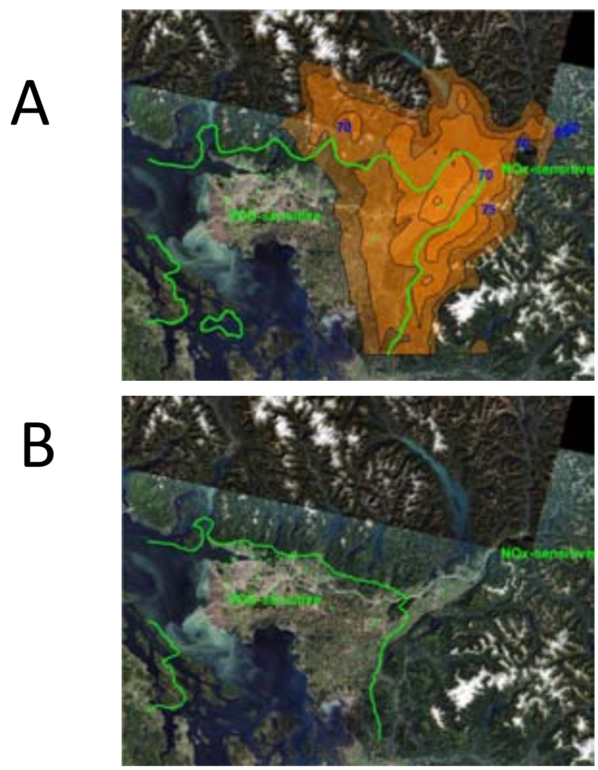

Fig. 58. Modeled maximum 8-hr average ozone exposure contours (in 5 ppb increments) over day 1 using cluster I meteorology for (A) 1985 emissions and (B) 2005 emissions. Also shown is the predicted VOC/NOx ridgeline based on the $[O_3]/[NOy]$ ratio (green line) and the fixed monitoring network station locations (+).

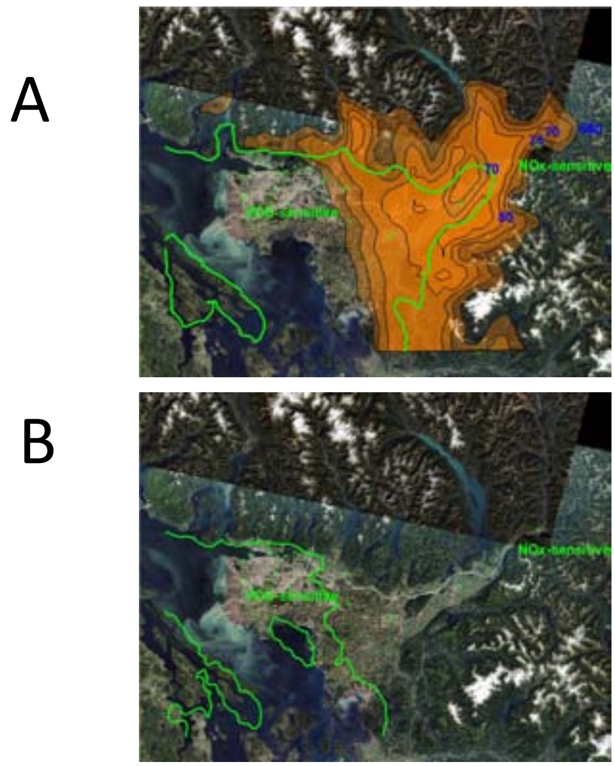

Fig. 59. Modeled maximum 8-hr average ozone exposure contours (in 5 ppb increments) over day 2 using cluster I meteorology for (A) 1985 emissions and (B) 2005 emissions. Also shown is the predicted VOC/NOx ridgeline based on the $[O_3]/[NOy]$ ratio (green line) and the fixed monitoring network station locations (+).

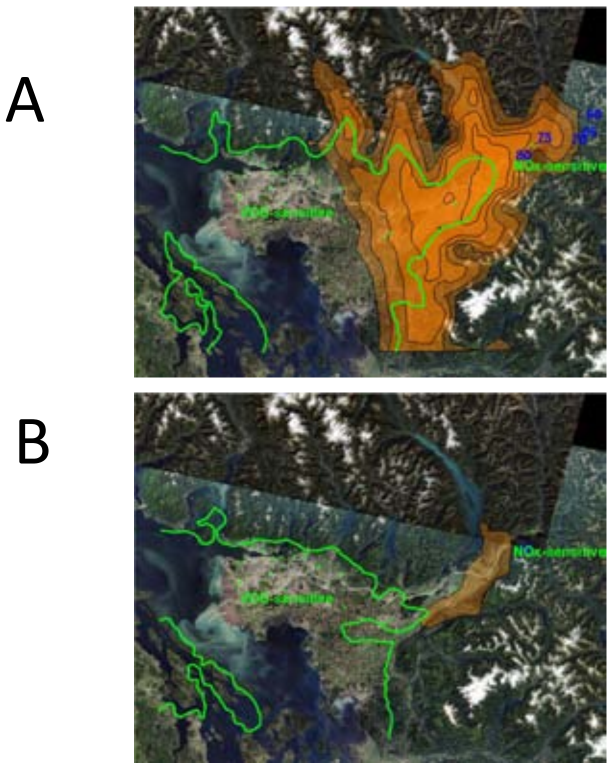

Fig. 60. Modeled maximum 8-hr average ozone exposure contours (in 5 ppb increments) over day 3 using cluster I meteorology for (A) 1985 emissions and (B) 2005 emissions. Also shown is the predicted VOC/NOx ridgeline based on the $[O_3]/[NOy]$ ratio (green line) and the fixed monitoring network station locations (+).

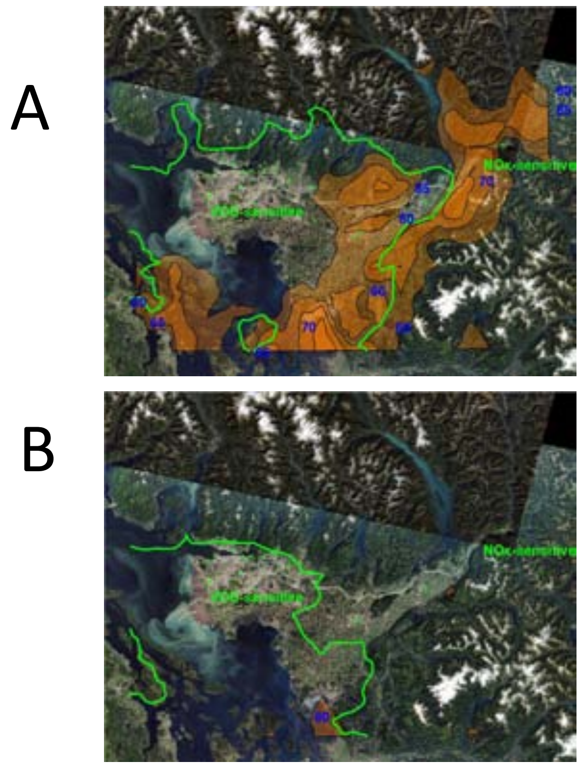

FIG. 61. Modeled maximum 8-hr average ozone exposure contours (in 5 ppb increments) over day 1 using cluster II meteorology for (A) 1985 emissions and (B) 2005 emissions. Also shown is the predicted VOC/NOx ridgeline based on the $[O_3]/[NOy]$ ratio (green line) and the fixed monitoring network station locations (+).

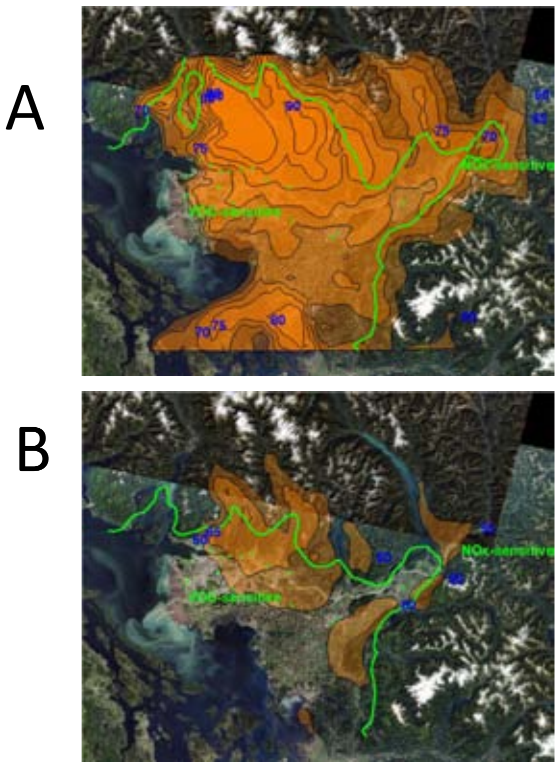

Fig. 62. Modeled maximum 8-hr average ozone exposure contours (in 5 ppb increments) over day 2 using cluster II meteorology for (A) 1985 emissions and (B) 2005 emissions. Also shown is the predicted VOC/NOx ridgeline based on the $[O_3]/[NOy]$ ratio (green line) and the fixed monitoring network station locations (+).

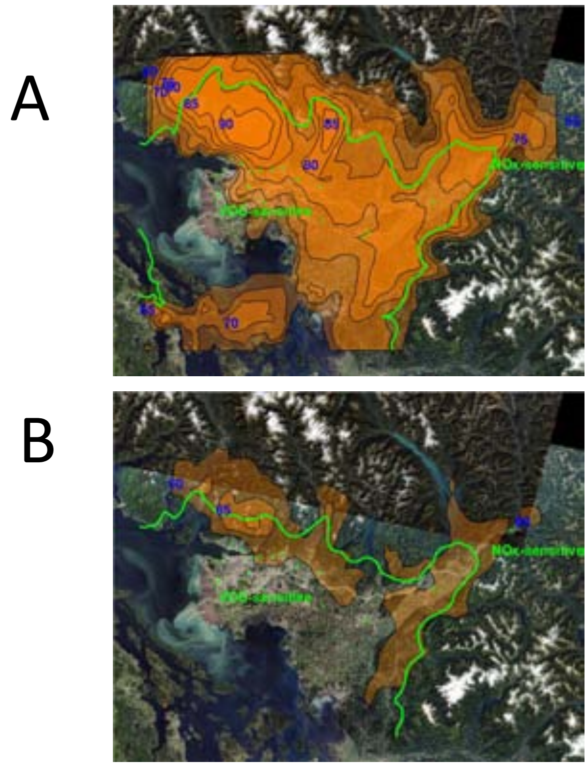

FIG. 63. Modeled maximum 8-hr average ozone exposure contours (in 5 ppb increments) over day 3 using cluster II meteorology for (A) 1985 emissions and (B) 2005 emissions. Also shown is the predicted VOC/NOx ridgeline based on the $[O_3]/[NOy]$ ratio (green line) and the fixed monitoring network station locations (+).

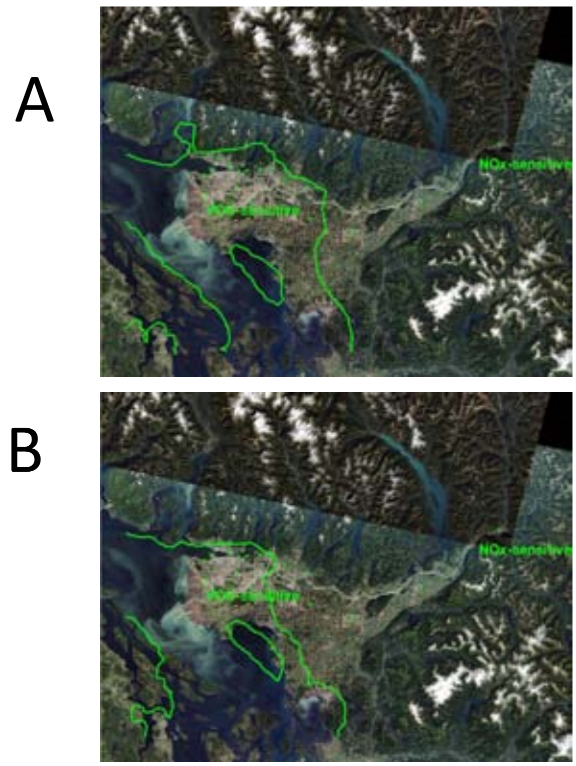

Fig. 64. Modeled maximum 8-hr average ozone exposure contours (in 5 ppb increments) over day 1 using cluster III meteorology for (A) 1985 emissions and (B) 2005 emissions. Also shown is the predicted VOC/NOx ridgeline based on the $[O_3]/[NOy]$ ratio (green line) and the fixed monitoring network station locations (+).

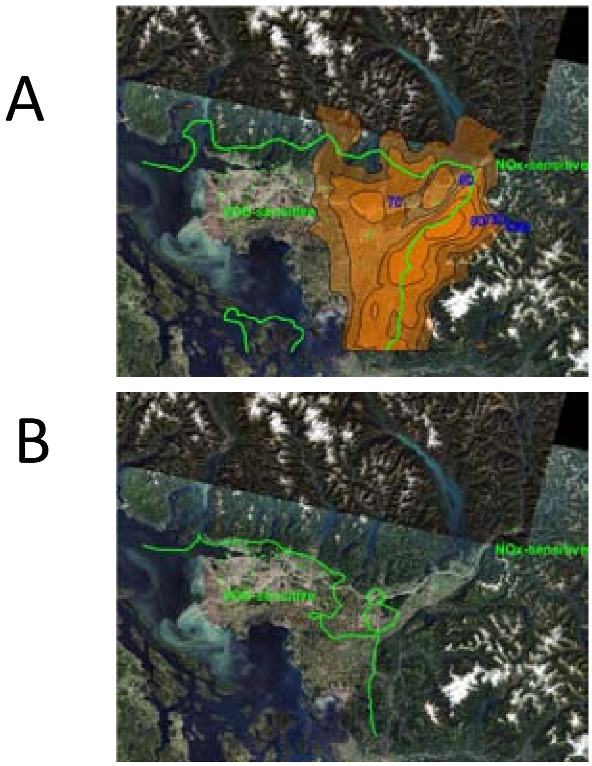

Fig. 65. Modeled maximum 8-hr average ozone exposure contours (in 5 ppb increments) over day 2 using cluster III meteorology for (A) 1985 emissions and (B) 2005 emissions. Also shown is the predicted VOC/NOx ridgeline based on the $[O_3]/[NOy]$ ratio (green line) and the fixed monitoring network station locations (+).

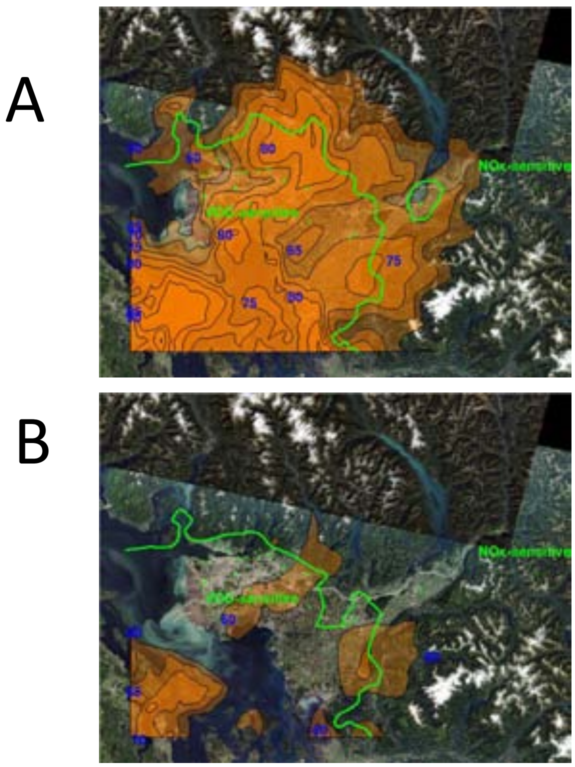

FIG. 66. Modeled maximum 8-hr average ozone exposure contours (in 5 ppb increments) over day 3 using cluster III meteorology for (A) 1985 emissions and (B) 2005 emissions. Also shown is the predicted VOC/NOx ridgeline based on the $[O_3]/[NOy]$ ratio (green line) and the fixed monitoring network station locations (+).

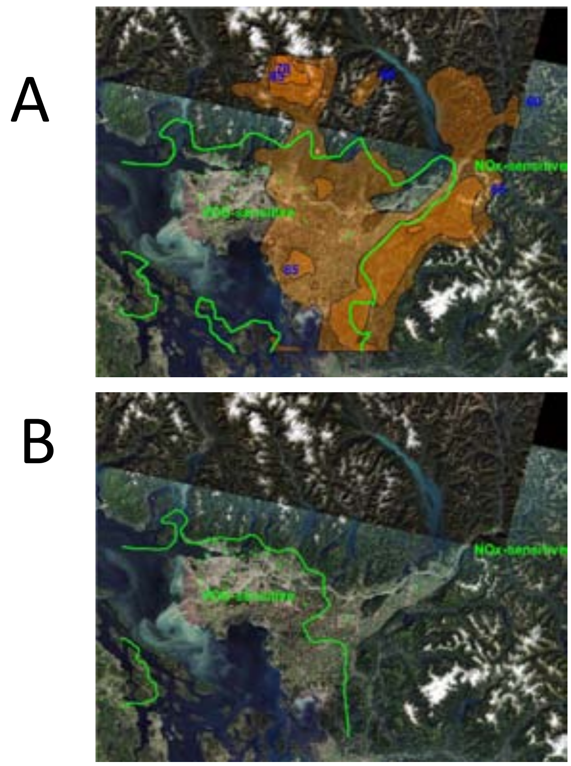

FIG. 67. Modeled maximum 8-hr average ozone exposure contours (in 5 ppb increments) over day 1 using cluster IIII meteorology for (A) 1985 emissions and (B) 2005 emissions. Also shown is the predicted VOC/NOx ridgeline based on the $[O_3]/[NOy]$ ratio (green line) and the fixed monitoring network station locations (+).

A

B

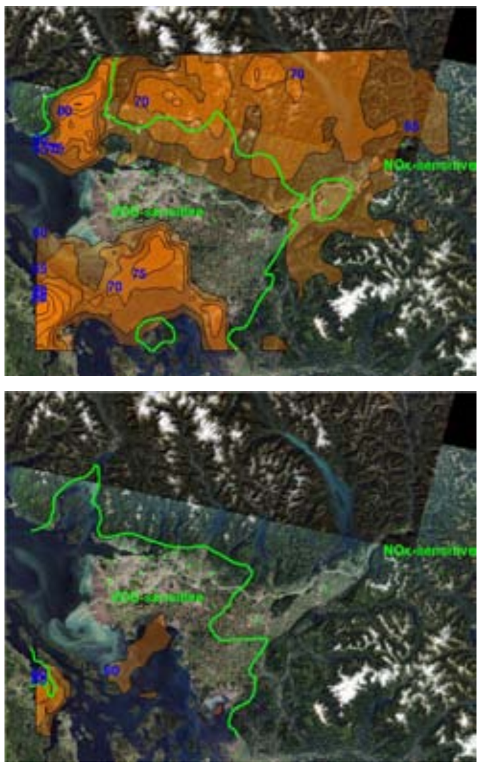

FIG. 68. Modeled maximum 8-hr average ozone exposure contours (in 5 ppb increments) over day 2 using cluster IIII meteorology for (A) 1985 emissions and (B) 2005 emissions. Also shown is the predicted VOC/NOx ridgeline based on the $[O_3]/[NOy]$ ratio (green line) and the fixed monitoring network station locations (+).

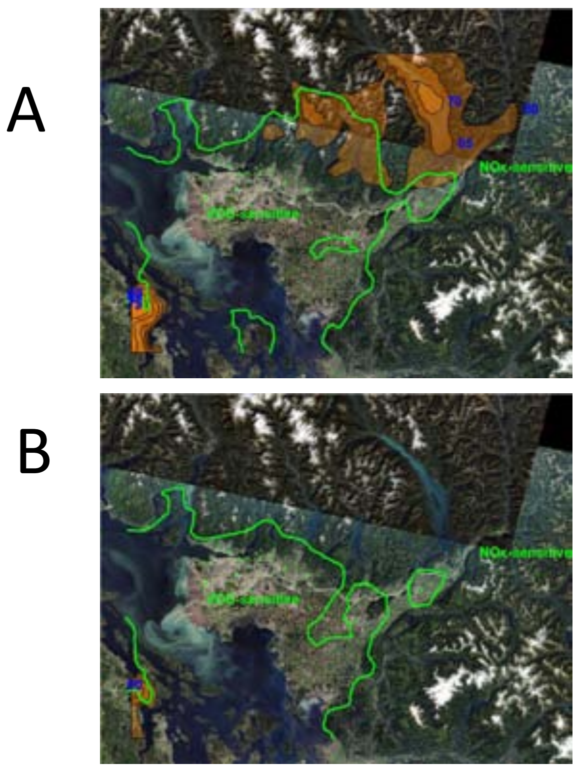

FIG. 69. Modeled maximum 8-hr average ozone exposure contours (in 5 ppb increments) over day 3 using cluster IIII meteorology for (A) 1985 emissions and (B) 2005 emissions. Also shown is the predicted VOC/NOx ridgeline based on the $[O_3]/[NOy]$ ratio (green line) and the fixed monitoring network station locations (+).

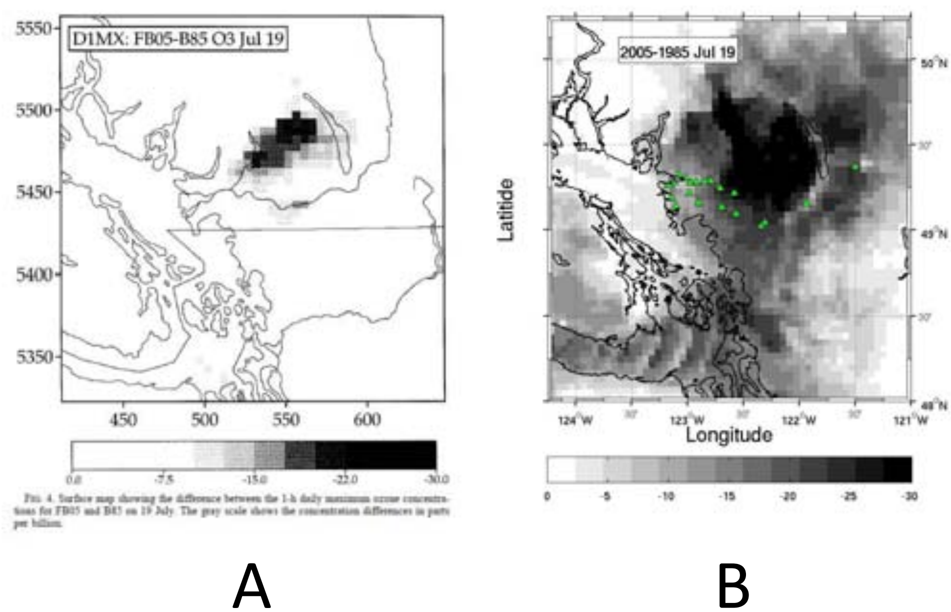

FIG. 70. Surface map for July 19th, 1995 showing the difference in 1-hr average ozone exposures between the 2005 and 1985 emissions inventories based on (A) the Hedley et al. (1998) CALGRID and (B) the present CMAQ simulations. MV monitoring station locations (green triangles) are also plotted in (B). The gray scales below each plot give the concentration differences in ppb. Figure (A) is a reproduction of Figure 4 in Hedley et al. (1998).

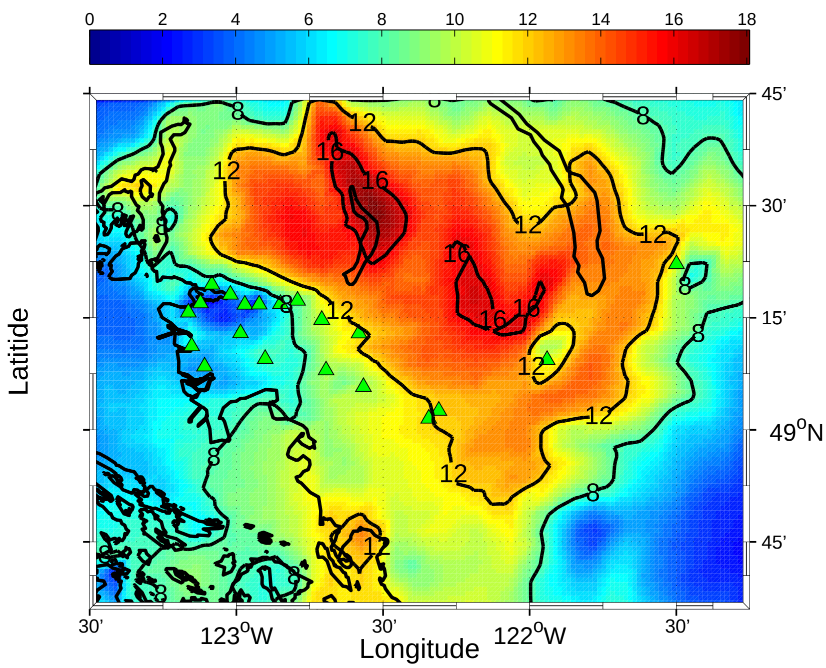

FIG. 71. Spatial plot of the average change (in ppb) between 1985 and 2005 in the modeled 8-hr averaged ozone exposure. The 8-hr exposure field has been averaged over each of the 3 days in each of the 4 exploration runs. Also shown are the monitoring network station locations (green triangles) and contours at 8, 12 and 16 ppb (thin black lines).

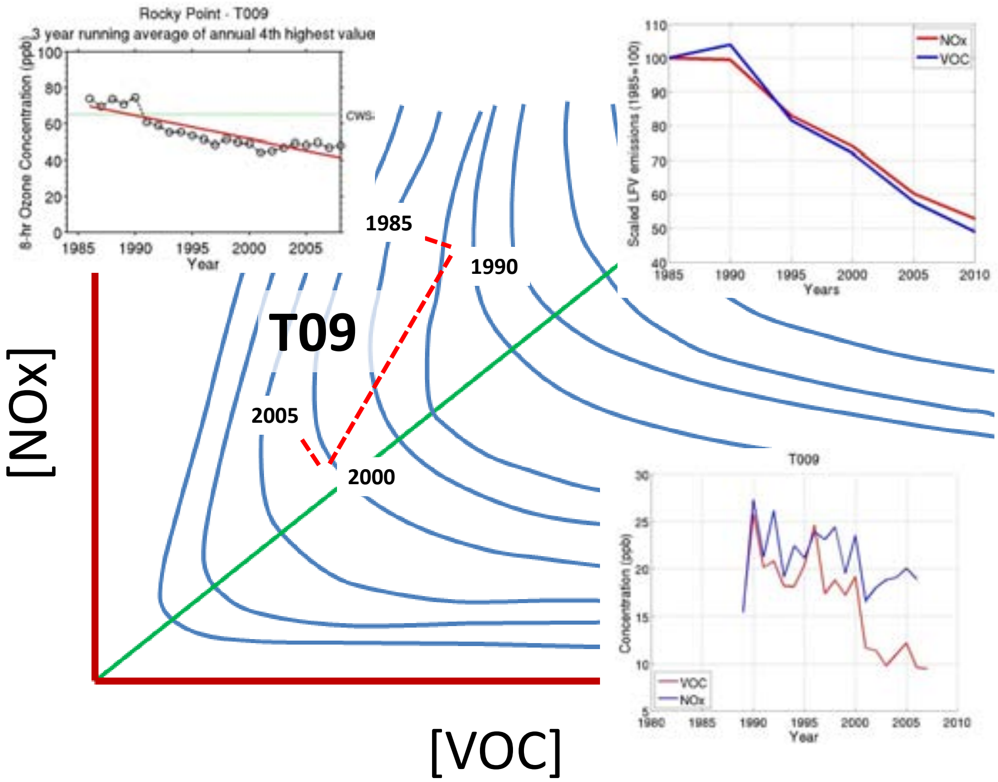

FIG. 72. Ozone isopleth schematic showing ozone response surface (blue lines) as a function if VOC and NOx concentrations. The green line represents the ridgeline. Also shown is the CWS ozone timeseries for T09 (upper left), the scaled timeseries plot of LFV VOC and NOx emissions (upper right), and yearly mean 8-average summertime VOC and NOx concentrations (restricted to days with VOC measurements) observed at T09 (lower right). Overlaid on top of the isopleth diagram is an estimate of how the ozone response to precursor emissions at T09 has changed over the 1985-2005 period (dashed red lines).

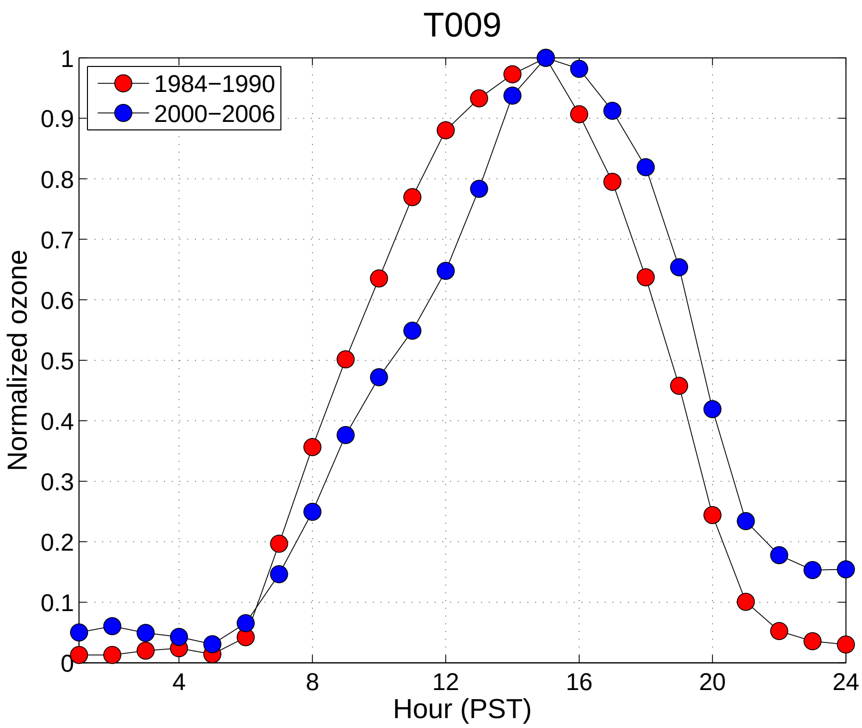

Fig. 73. Average diurnal ozone concentration profile from the 1985-1990 (red) and 2000-2006 (blue) periods. Each curve has been normalized to better highlight the temporal evolution of the diurnal profile.

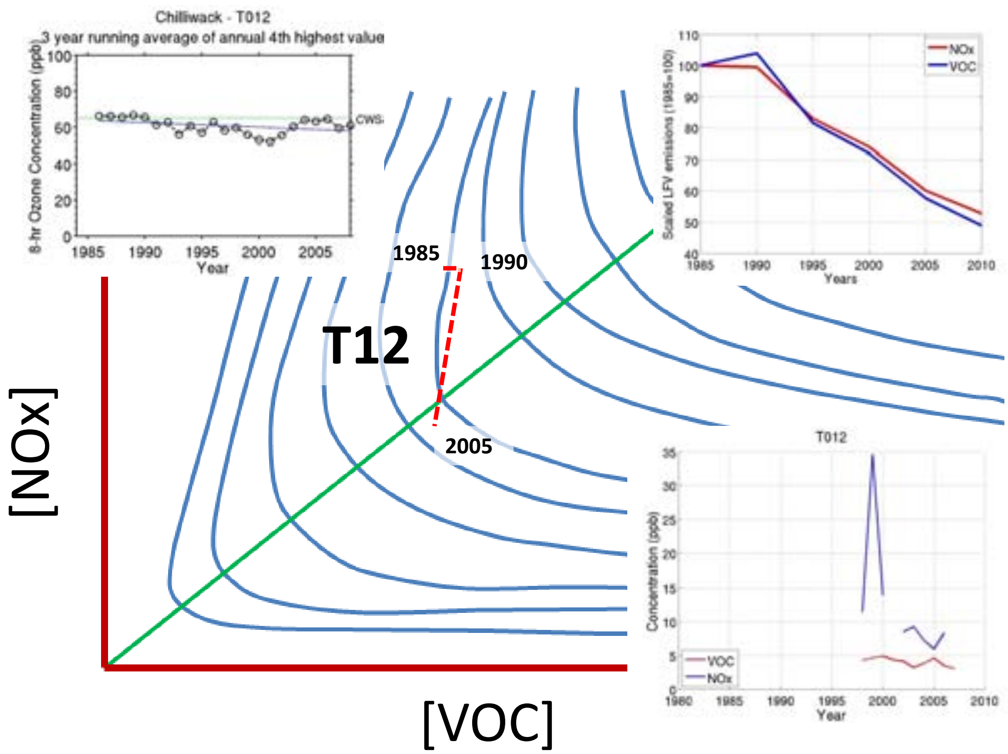

FIG. 74. Ozone isopleth schematic showing ozone response surface (blue lines) as a function if VOC and NOx concentrations. The green line represents the ridgeline. Also shown is the CWS ozone timeseries for T12 (upper left), the scaled timeseries plot of LFV VOC and NOx emissions (upper right), and yearly mean 8-average summertime VOC and NOx concentrations (restricted to days with VOC measurements) observed at T12 (lower right). Overlaid on top of the isopleth diagram is an estimate of how the ozone response to precursor emissions at T12 has changed over the 1985-2005 period (dashed red lines).

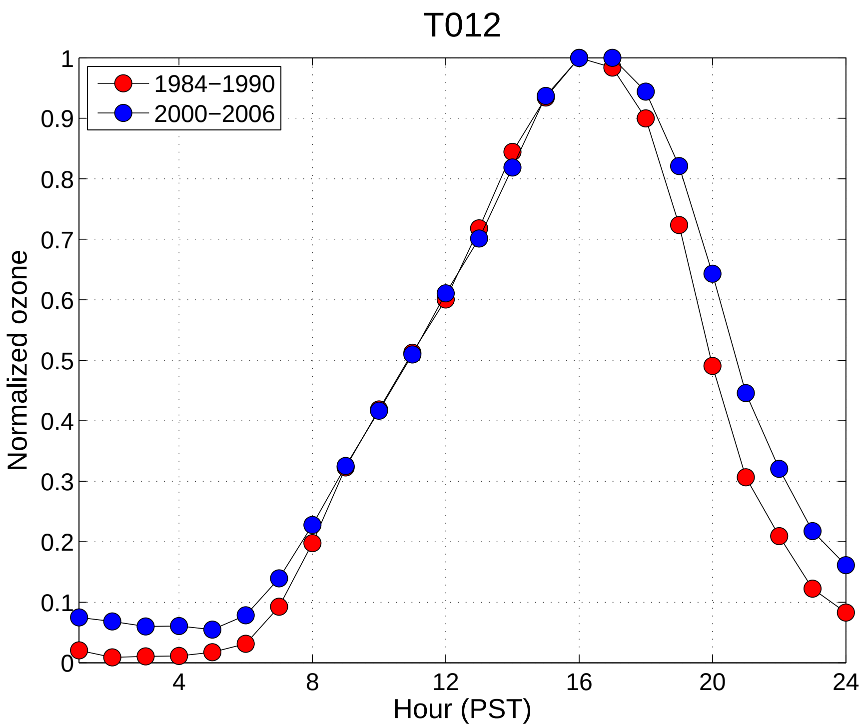

FIG. 75. Average diurnal ozone concentration profile from the 1985-1990 (red) and 2000-2006 (blue) periods. Each curve has been normalized to better highlight the temporal evolution of the diurnal profile.

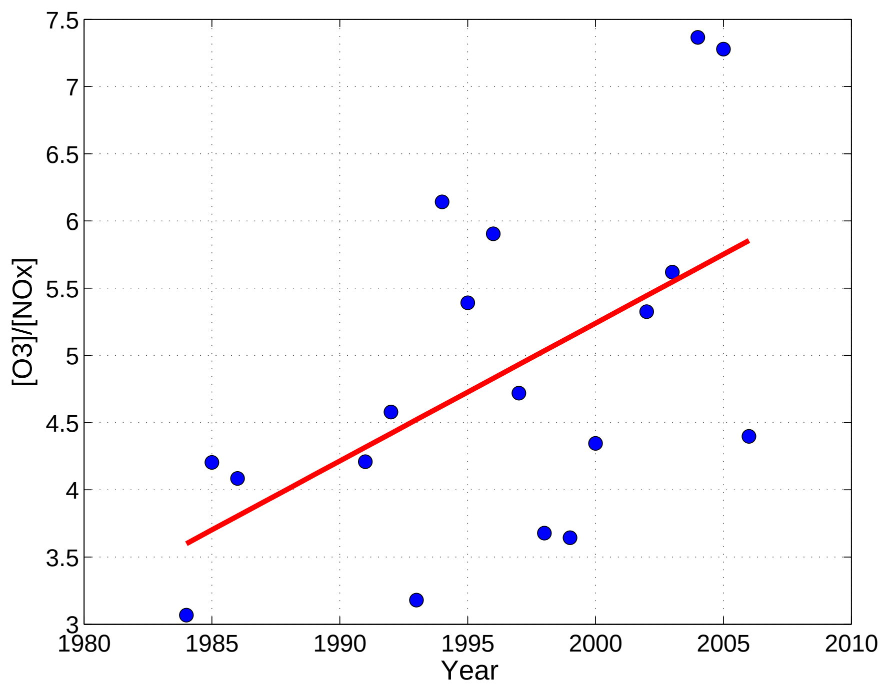

Fig. 76. Ratio of 8-hr average ozone to 8-hr average NOx concentrations between 1984 and 2006 (blue dots) along with trend line (red line). Yearly values based on 8-hr averages of the 7 days with the highest hourly ozone concentrations.

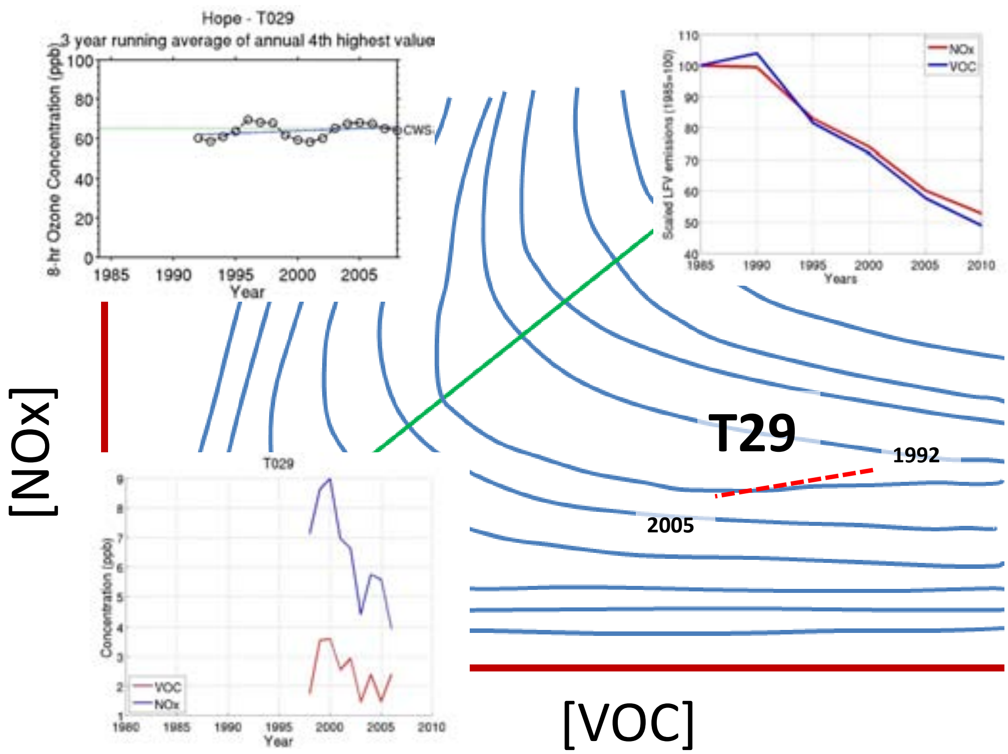

Fig. 77. Ozone isopleth schematic showing ozone response surface (blue lines) as a function if VOC and NOx concentrations. The green line represents the ridgeline. Also shown is the CWS ozone timeseries for T29 (upper left), the scaled timeseries plot of LFV VOC and NOx emissions (upper right), and yearly mean 8-average summertime VOC and NOx concentrations (restricted to days with VOC measurements) observed at T12 (lower left). Overlaid on top of the isopleth diagram is an estimate of how the ozone response to precursor emissions at T29 has changed over the 1985-2005 period (dashed red lines).

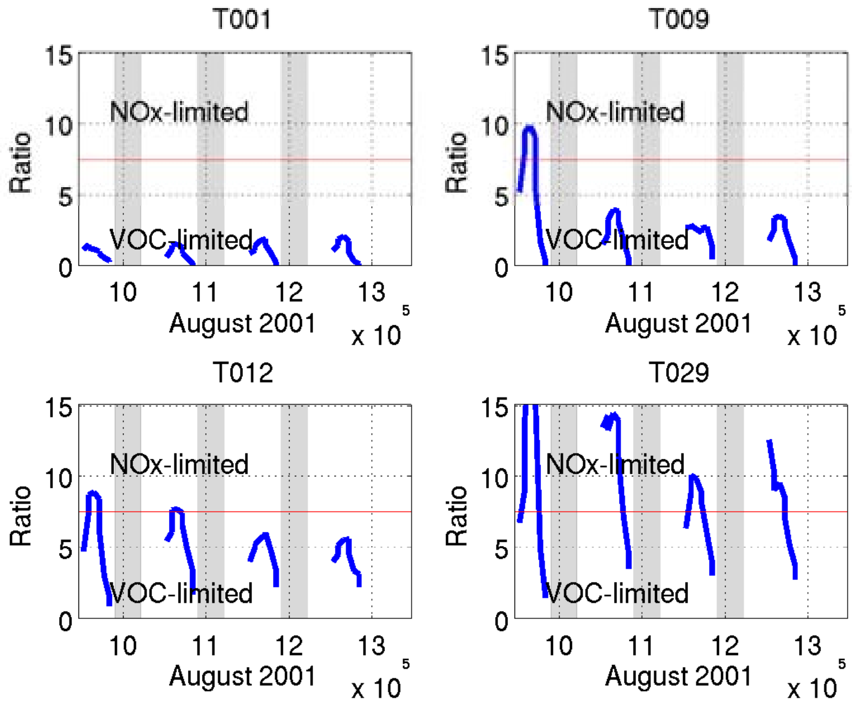

FIG. 78. Timeseries plots of $[O_3]/[NOy]$ throughout the 2001 simulation at the T01, T09, T12 and T29 stations (blue lines). The timeseries have only been plotted between the hours of 1000 and 2000 PST because the early morning and nighttime values of $[O_3]$ and $[NOy]$ are indicative of local ozone titration and NOx emissions and not ozone production under fair weather conditions. Also shown in each plot is the critical $[O_3]/NOy$ threshold (red line) indicating VOC-limited conditions below and NOx-limited conditions above the red line.

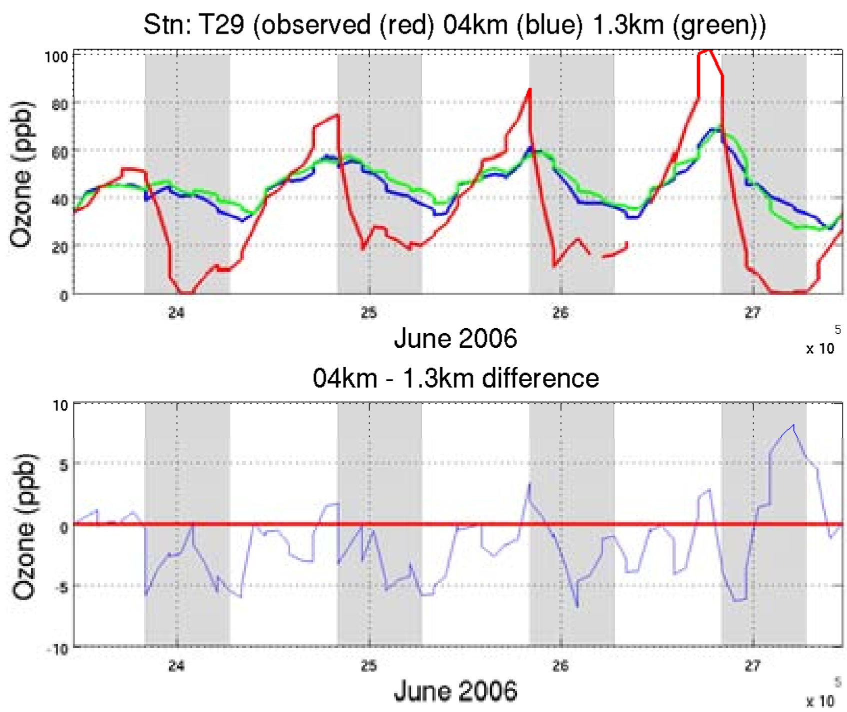

FIG. 79. Timeseries of observed (red) CMAQ model output at 4 km (blue) and 1.33 km (green) during the 2006 episode at T29 (upper plot). Timeseries (in ppb) of the difference between the 4 and 1.33 km runs at T29 during the same episode (lower plot). The nighttime hours are shaded gray.

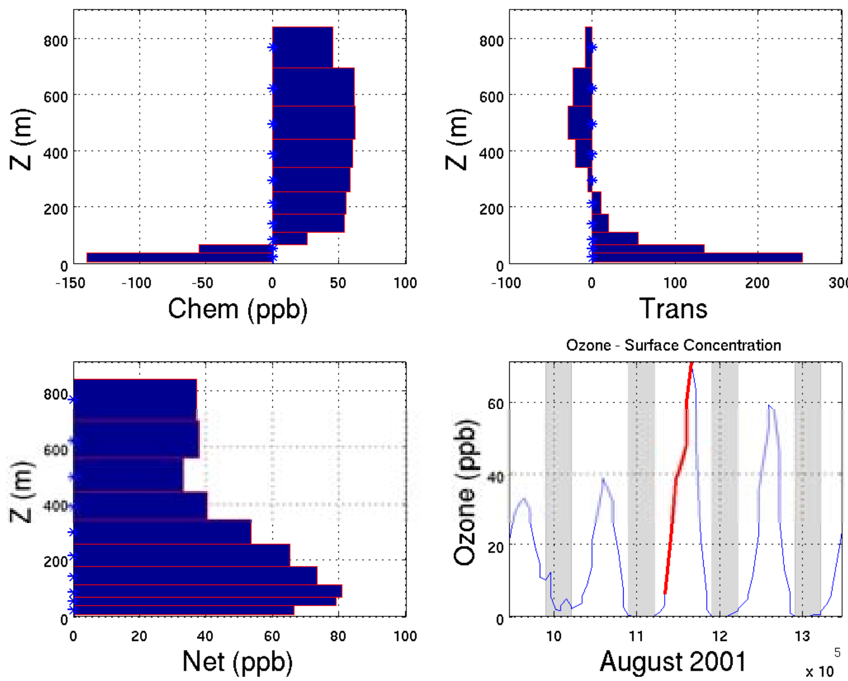

Fig. 80. Total ozone production (in ppb) as a function of height (m agl) due to chemical processes over the 8-hour period leading up to the peak ozone concentration modeled on August 11th at T01 (upper left panel). The upper right panel gives total ozone production due to horizontal and vertical transportation processes (advection and turbulent diffusion) while the lower left panel gives the net (chemical + transport - deposition) 8-hour production (in ppb). Not shown is the 47 ppb loss due to deposition which only occurs at the lowest model level. The lower right plot shows the modeled ozone timeseries with the red segment highlighting the 8-hour averaging period leading up to the peak modeled ozone concentration. In the 3 bar plots, bar heights are not uniform due to the varying thicknesses of the vertical levels and only model output from the lowest 10 vertical levels is presented.

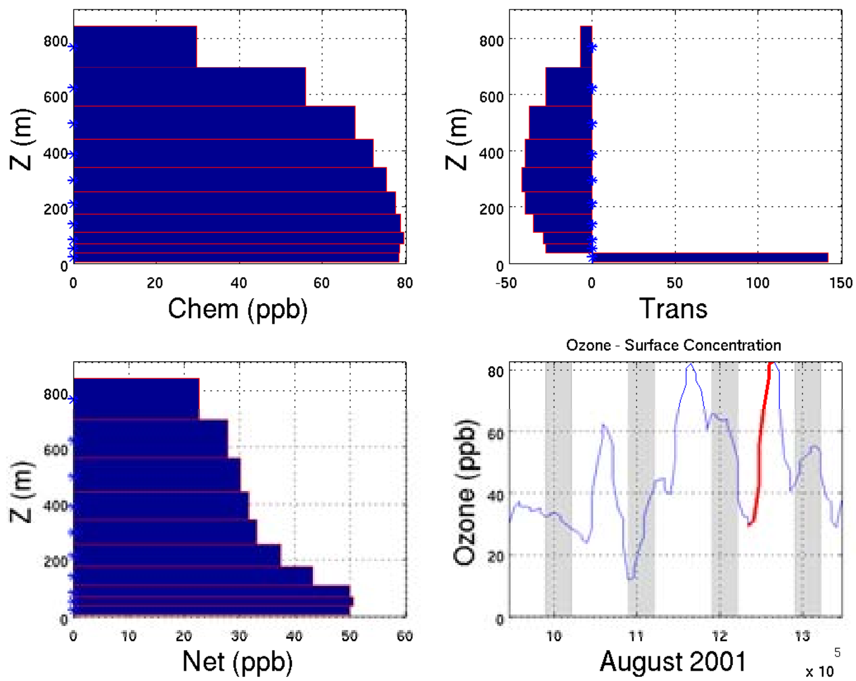

FIG. 81. Total ozone production (in ppb) as a function of height (m agl) due to chemical processes over the 8-hour period leading up to the peak ozone concentration modeled on August 11th at Pitt Lake (upper left panel). The upper right panel gives total ozone production due to horizontal and vertical transportation processes (advection and turbulent diffusion) while the lower left panel gives the net (chemical + transport - deposition) 8-hour production (in ppb). Not shown is the 47 ppb loss due to deposition which only occurs at the lowest model level. The lower right plot shows the modeled ozone timeseries with the red segment highlighting the 8-hour averaging period leading up to the peak modeled ozone concentration. In the 3 bar plots, bar heights are not uniform due to the varying thicknesses of the vertical levels and only model output from the lowest 10 vertical levels is presented.

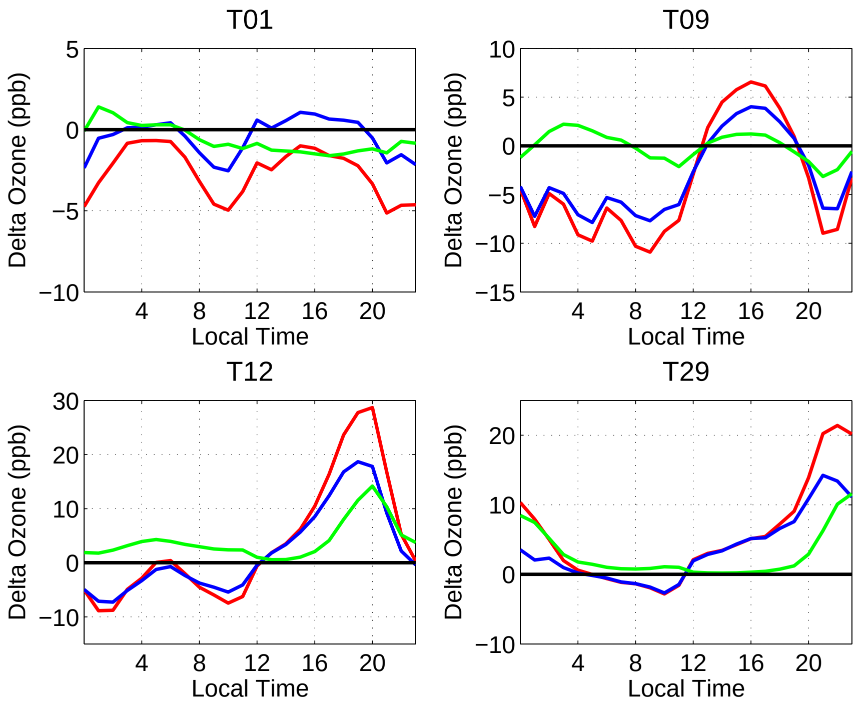

Fig. 82. Timeseries plots of the modeled difference in the average diurnal ozone concentrations (ppb) at T01, T09, T12 and T29 between runs with: 1985 emissions/1985 spatial surrogates and 2005 emissions/2005 spatial surrogates (red curves); 1985 emissions/2005 spatial surrogates and 2005 emissions/2005 spatial surrogates (blue curves); 2005 emissions/1985 spatial surrogates and 2005 emissions/2005 spatial surrogates (green curves).

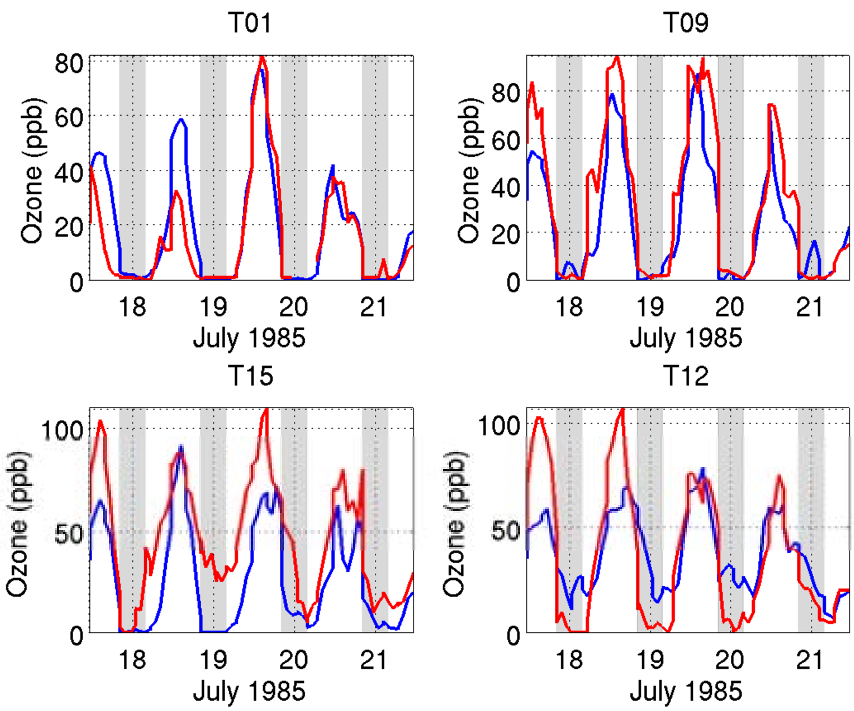

Fig. 83. Timeseries plot of observed (red) and CMAQ modeled (blue) surface ozone concentrations (in ppb) at T01, T09, T15 and T12 during the July 1985 episode. Night time hours are shaded.

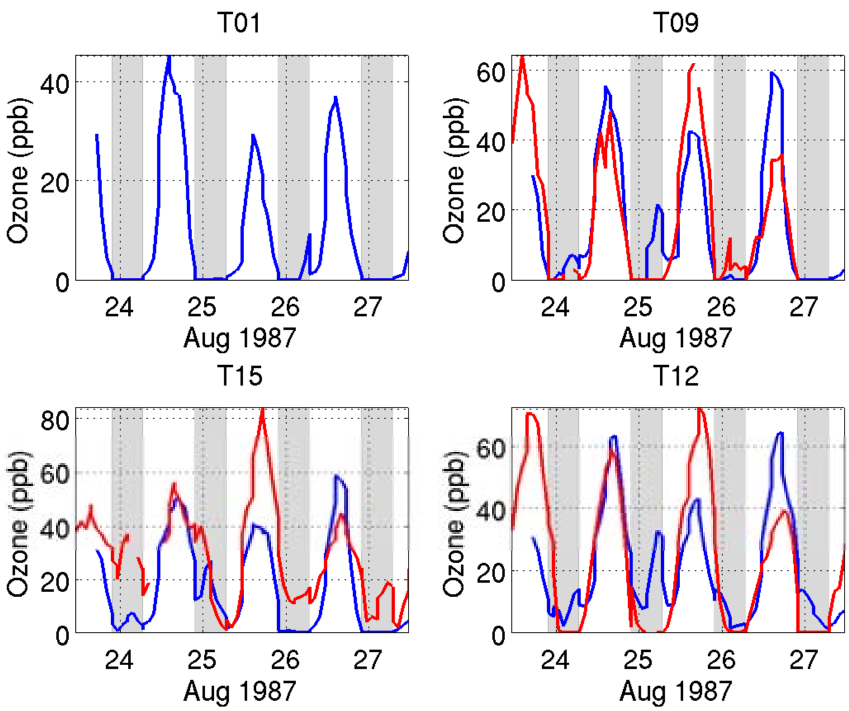

FIG. 84. Timeseries plot of observed (red) and CMAQ modeled (blue) surface ozone concentrations (in ppb) at T01, T09, T15 and T12 during the August 1987 episode. Night time hours are shaded.

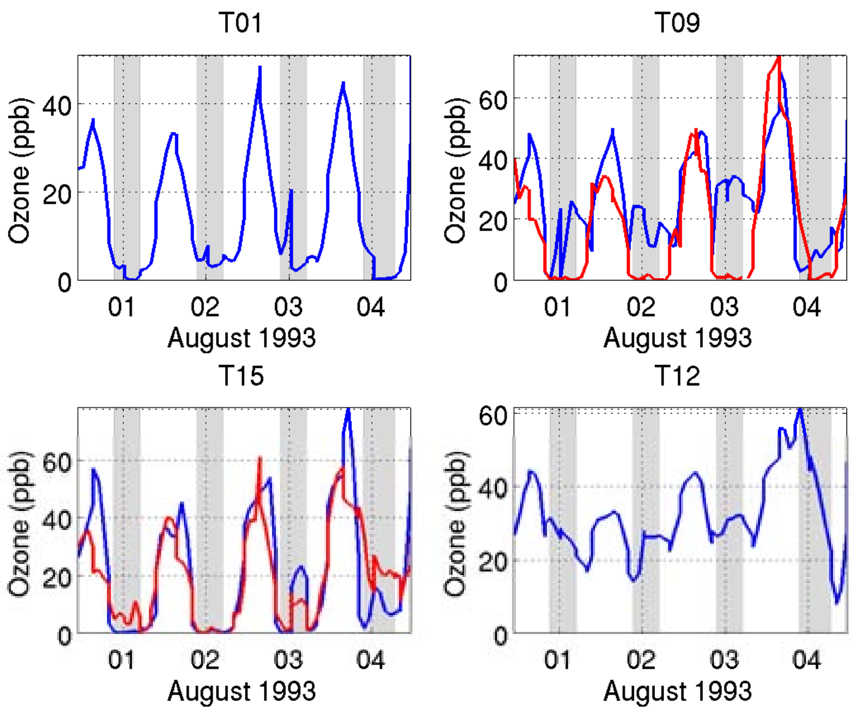

FIG. 85. Timeseries plot of observed (red) and CMAQ modeled (blue) surface ozone concentrations (in ppb) at T01, T09, T15 and T12 during the August 1993 episode. Night time hours are shaded.

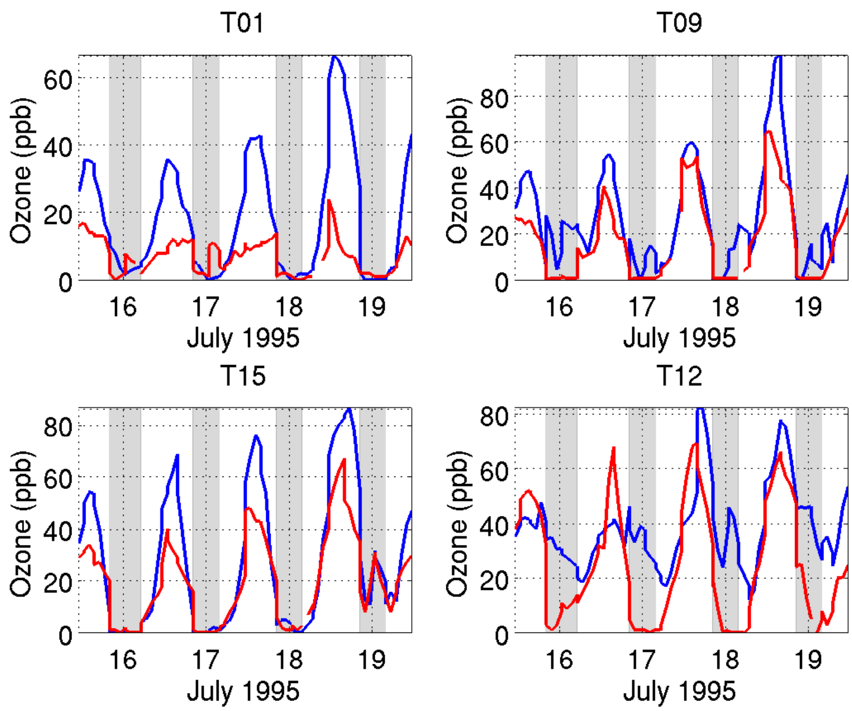

FIG. 86. Timeseries plot of observed (red) and CMAQ modeled (blue) surface ozone concentrations (in ppb) at T01, T09, T15 and T12 during the July 1995 episode. Night time hours are shaded.

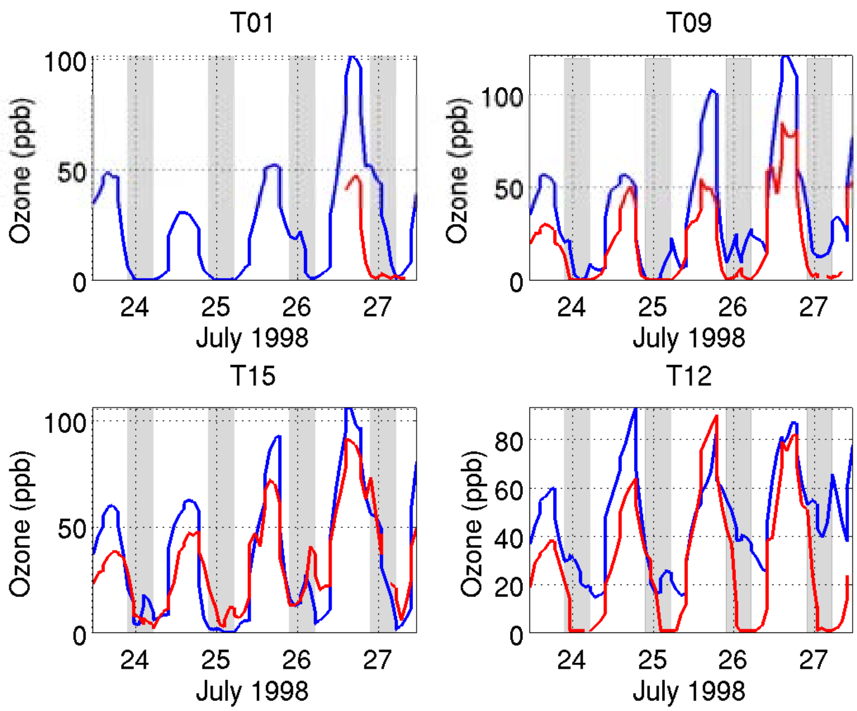

FIG. 87. Timeseries plot of observed (red) and CMAQ modeled (blue) surface ozone concentrations (in ppb) at T01, T09, T15 and T12 during the July 1998 episode. Night time hours are shaded.

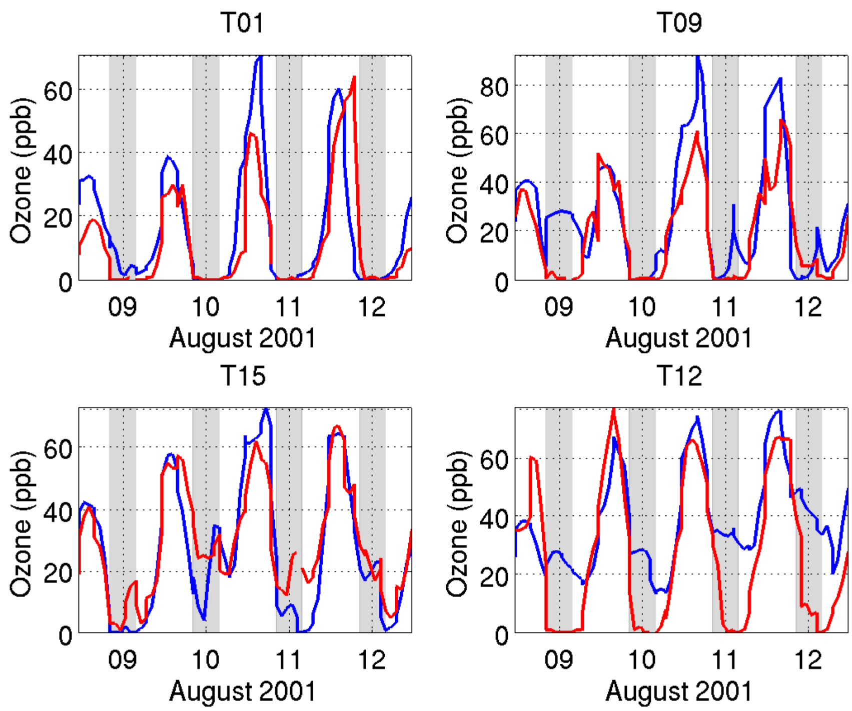

FIG. 88. Timeseries plot of observed (red) and CMAQ modeled (blue) surface ozone concentrations (in ppb) at T01, T09, T15 and T12 during the August 2001 episode. Night time hours are shaded.

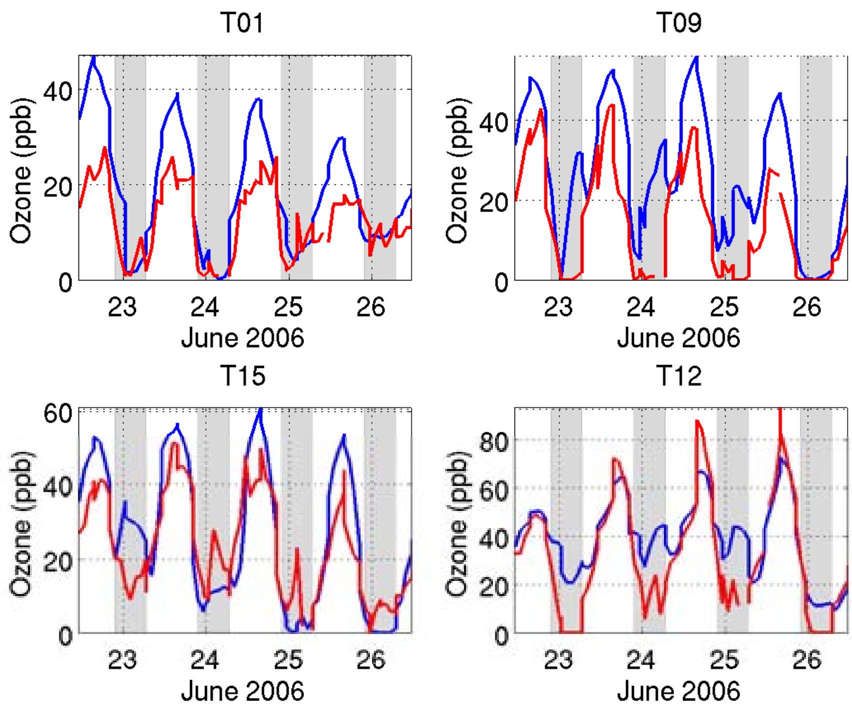

Fig. 89. Timeseries plot of observed (red) and CMAQ modeled (blue) surface ozone concentrations (in ppb) at T01, T09, T15 and T12 during the June 2006 episode. Night time hours are shaded.

Table 4. Ozone time series statistics[a]

Station	n	$\langle c_o \rangle$	$\langle c_p \rangle$	δ_o	δ_p	b	a	E	E_S	E_U	d
T01	109	14.3	11.6	18.3	8.8	0.34	6.8	13.9	12.4	6.3	0.70
T02	114	17.4	14.2	19.8	11.4	0.47	6.1	12.8	10.9	6.6	0.82
T03	67	14.5	17.6	16.0	14.7	0.85	5.2	6.6	3.8	5.4	0.95
T04	92	24.8	20.9	20.3	11.0	0.44	9.9	13.5	11.9	6.3	0.80
T05	115	27.5	17.9	23.4	10.6	0.35	8.1	19.0	17.9	6.6	0.70
T06	59	19.2	17.8	17.7	10.4	0.42	9.8	12.6	10.4	7.2	0.78
T07	116	38.4	26.4	25.1	13.2	0.39	11.3	21.3	19.4	8.7	0.70
T09	116	32.6	27.0	30.5	13.0	0.30	17.1	23.7	21.9	9.1	0.68
T10	48	33.7	30.0	24.5	12.7	0.25	21.5	21.5	18.4	11.0	0.60
T11	116	32.0	45.3	29.8	16.7	0.43	31.5	24.1	21.5	10.8	0.76
T12	114	35.5	46.9	32.0	13.4	0.30	36.1	26.6	24.9	9.2	0.69
T13	55	28.1	23.0	12.8	12.0	0.66	4.6	10.9	6.7	8.6	0.79
T15	115	44.5	34.3	27.7	16.8	0.43	15.2	22.2	18.8	11.8	0.74
T16	93	31.3	31.0	30.1	16.3	0.40	18.5	20.9	17.9	10.8	0.78

[a] The terms n, b and d are dimensionless. All other terms have dimension ppb. The o and p subscripts refer to observed and predicted values, respectively. The standard deviations are represented by δ. The time-averaged species mixing ratios are denoted by $\langle c \rangle$.

FIG. 90. Table 4 from Hedley et al. (1997) showing ozone timeseries statistics at Metro Vancouver monitoring stations over the July 17-22, 1985 MC2/CALGRID simulation.

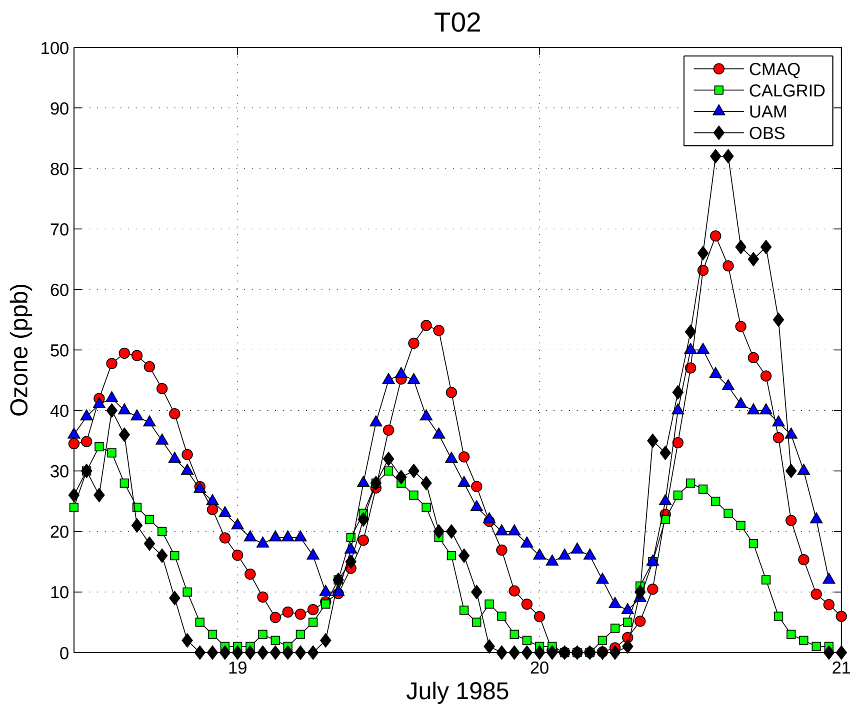

FIG. 91. Timeseries plot of observed, CMAQ modeled, CALGRID-modeled and UAM-modeled surface ozone concentrations between 0400 (PST) July 18th and 2300 (PST) July 2300, 1985 at T02 (Kitslano).

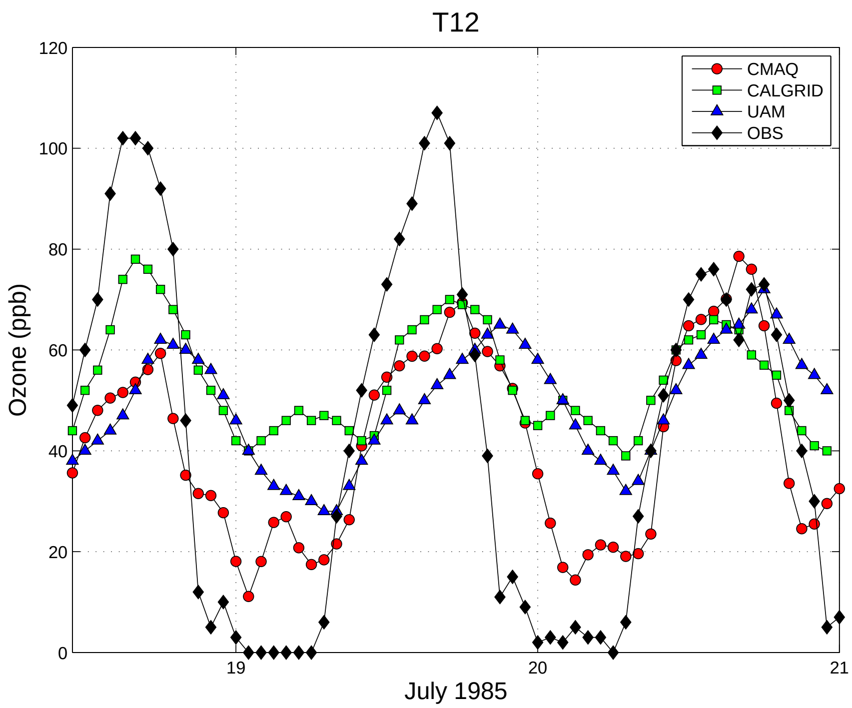

Fig. 92. Timeseries plot of observed, CMAQ modeled, CALGRID-modeled and UAM-modeled surface ozone concentrations between 0400 (PST) July 18th and 2300 (PST) July 2300, 1985 at T12 (Chilliwack).

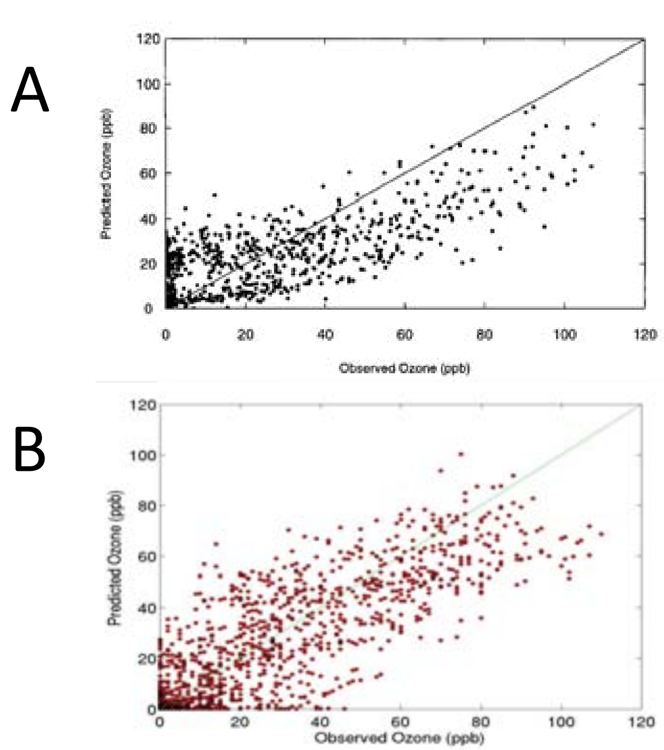

FIG. 93. Scatter plot of predicted versus observed ozone concentrations based on the RAMS/UAM-V simulations of Suzuki (1997) (A) and the present WRF/CMAQ simulations (B). The RAMS/UAM-V simulations span the July 17-19, 1985 timeframe while the WRF/CMAQ span July 18-22, 1985.

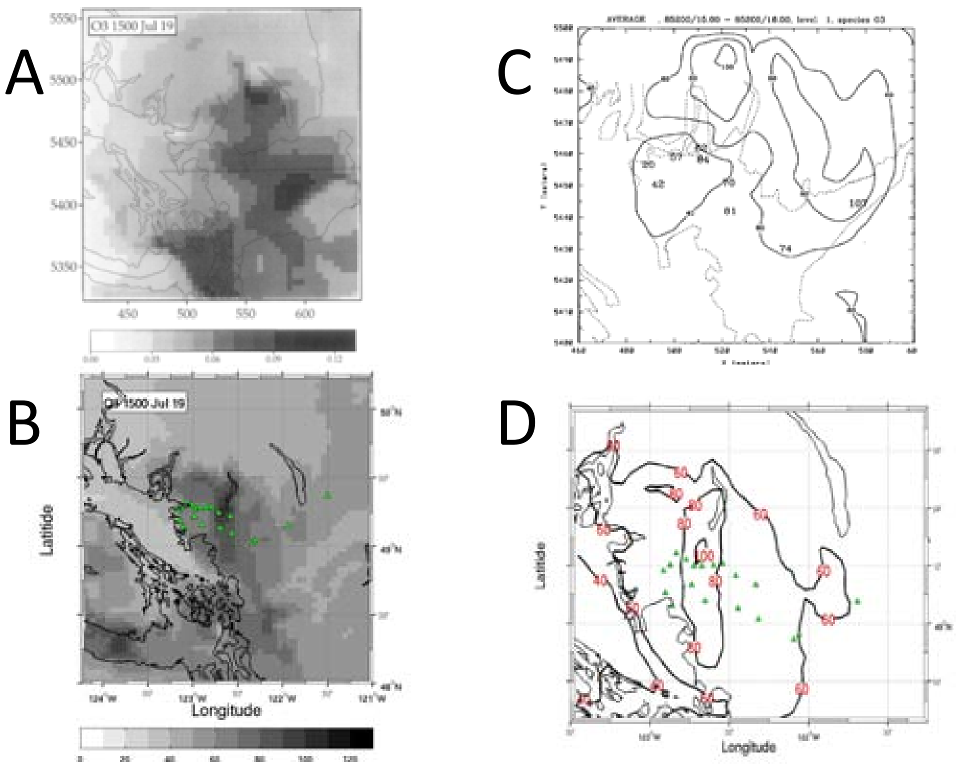

Fig. 94. Surface ozone concentrations over LFV valid July 19th, 1985 at 1500 (PST) based on the Hedley et al. (1997) MC2/CALGRID simulations (A) and the present WRF/CMAQ simulations (B and D) and the RAMS/UAM-V modeling of Suzuki (1997) (C). The WRF/CMAQ presented in B and D are from the same time but have been presented differently in order to facilitate comparisons with A and C. Concentrations are in ppm in A and ppb in B, C and D.

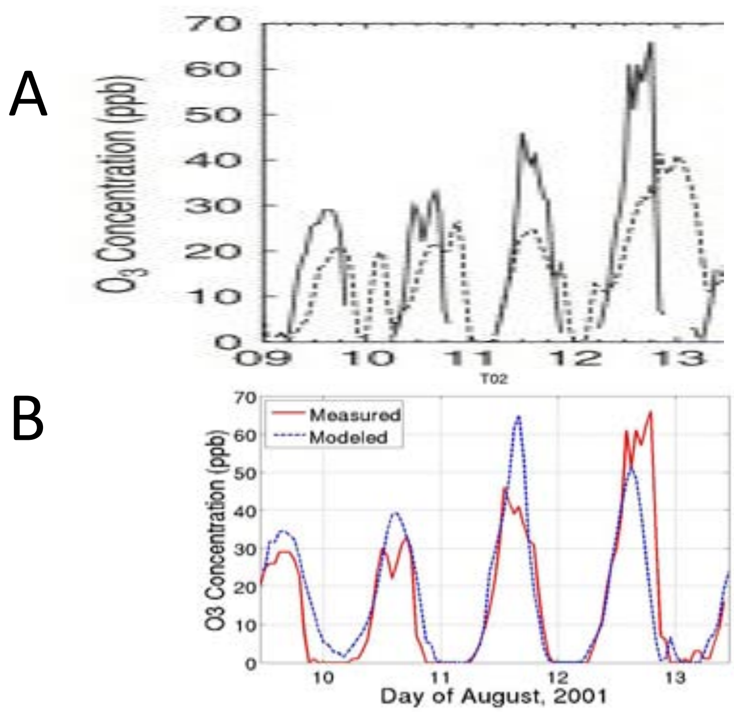

FIG. 95. Timeseries plot of observed (solid) and modeled (dashed) surface ozone concentrations between August 9th and August 13th 1000 (PST) 2001 at T02. Upper panel (A) gives the MM5-CMAQ results based on Smyth et al. (2006) and the lower panel (B) shows the WRF-CMAQ results from the present analysis.

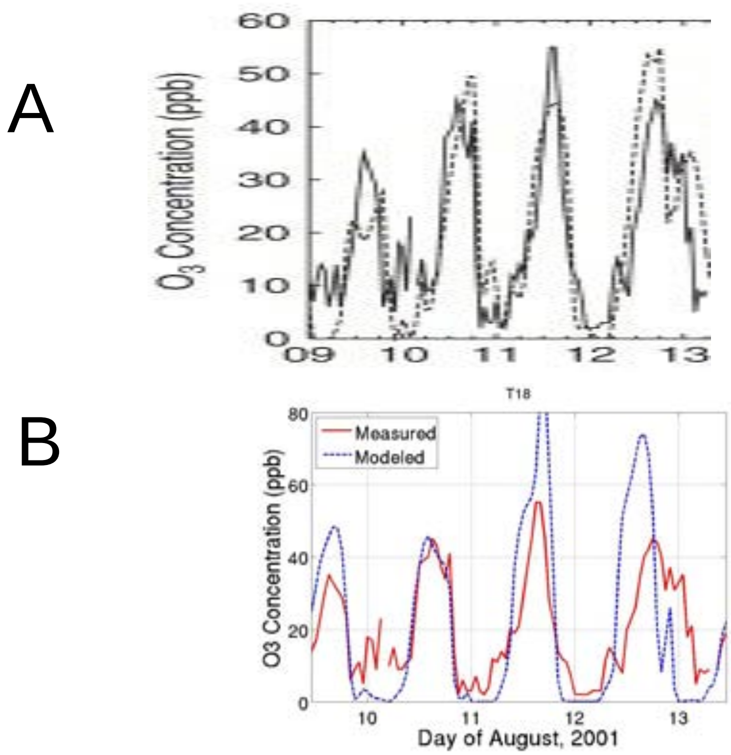

FIG. 96. Timeseries plot of observed (solid) and modeled (dashed) surface ozone concentrations between August 9th and August 13th 1000 (PST) 2001 at T18. Upper panel (A) gives the MM5-CMAQ results based on Smyth et al. (2006) and the lower panel (B) shows the WRF-CMAQ results from the present analysis.

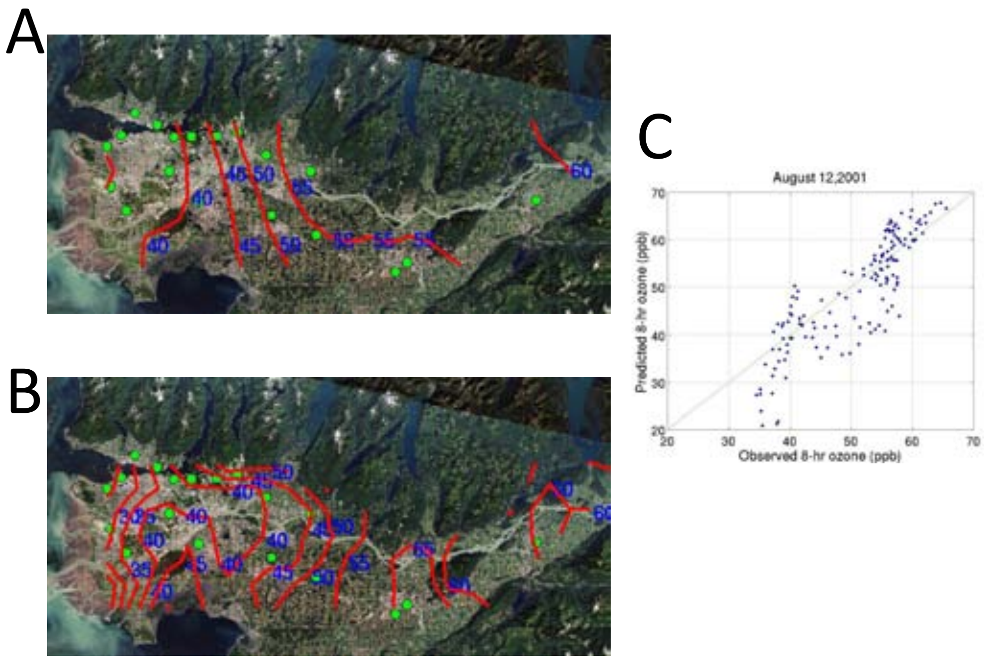

FIG. 97. Ozone isopleths (ppb) at time of maximum 8-hr averaged concentration on August 12, 2001 based on interpolated station data (A) and CMAQ model output (B). The contouring in both plots has been restricted to locations over the valley. Figure C shows a scatter plot of the interpolated and modeled values used in the contouring.

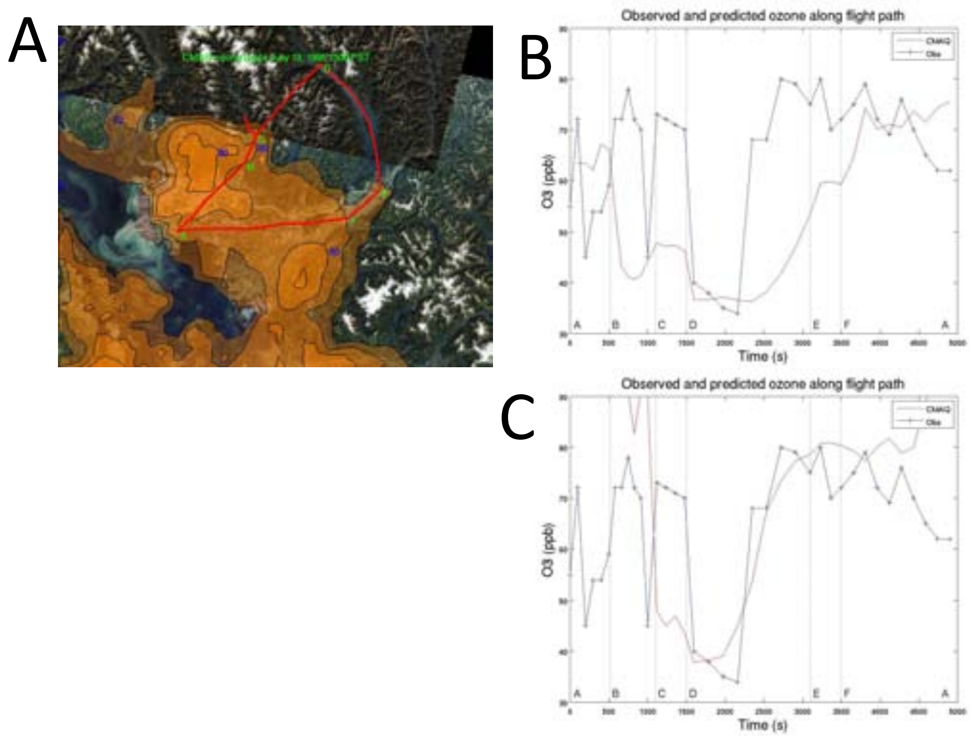

Fig. 98. A) Flight path and 1500 (PST) ozone isopleths (ppb) based on CMAQ output (after Figure 3a in McKendry et al. (1998b)). B) Aircraft observed and 1500 (PST) CMAQ predicted ozone concentrations along flight path (after Figure 3b in McKendry et al. (1998b)). C) Same as B but using the CMAQ 1800 (PST) ozone field.

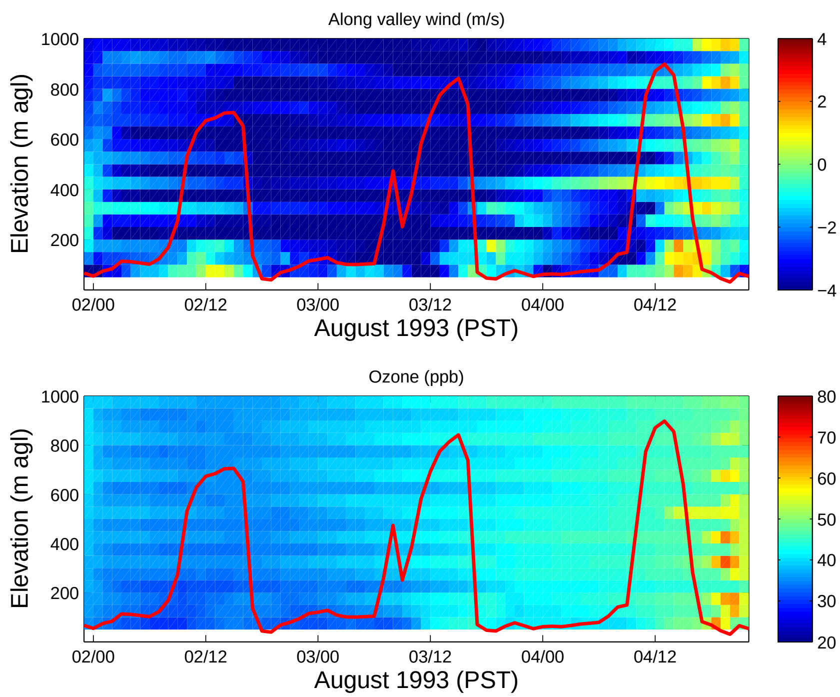

Fig. 99. Time-height cross-section of CMAQ modeled up-valley flow (A) and ozone concentration (B) at the entrance to the Pitt River valley during Pacific 1993. Up-valley flows are represented by the warm (red) colours and down-valley by the cooler (blue) colours. The solid red line in each figure is the modeled MLD.

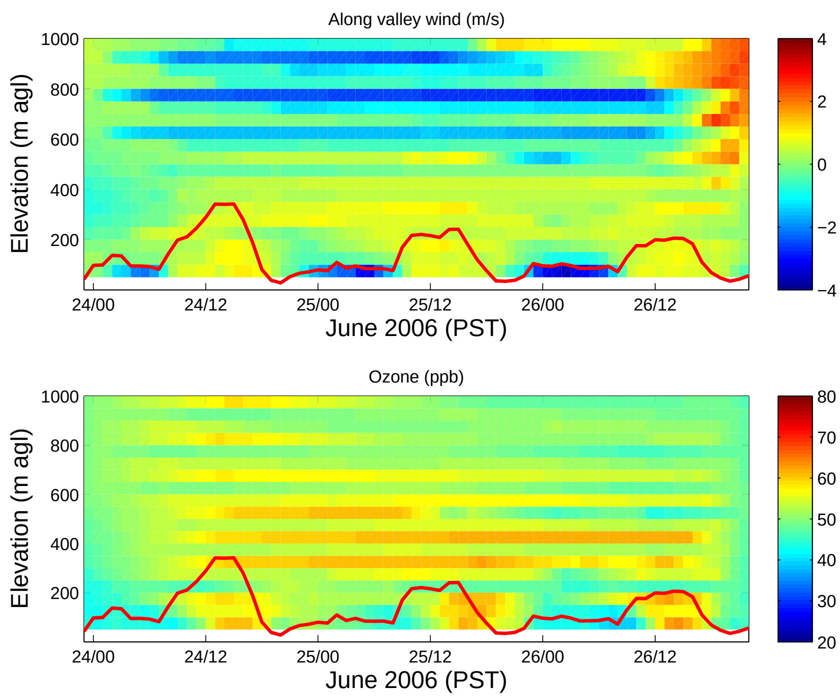

FIG. 100. Time-height cross-section of CMAQ modeled up-valley flow (A) and ozone concentration (B) at the entrance to the Pitt River valley during the June 2006 episode. Up-valley flows are represented by the warm (red) colours and down-valley by the cooler (blue) colours. The solid red line in each figure is the modeled MLD.

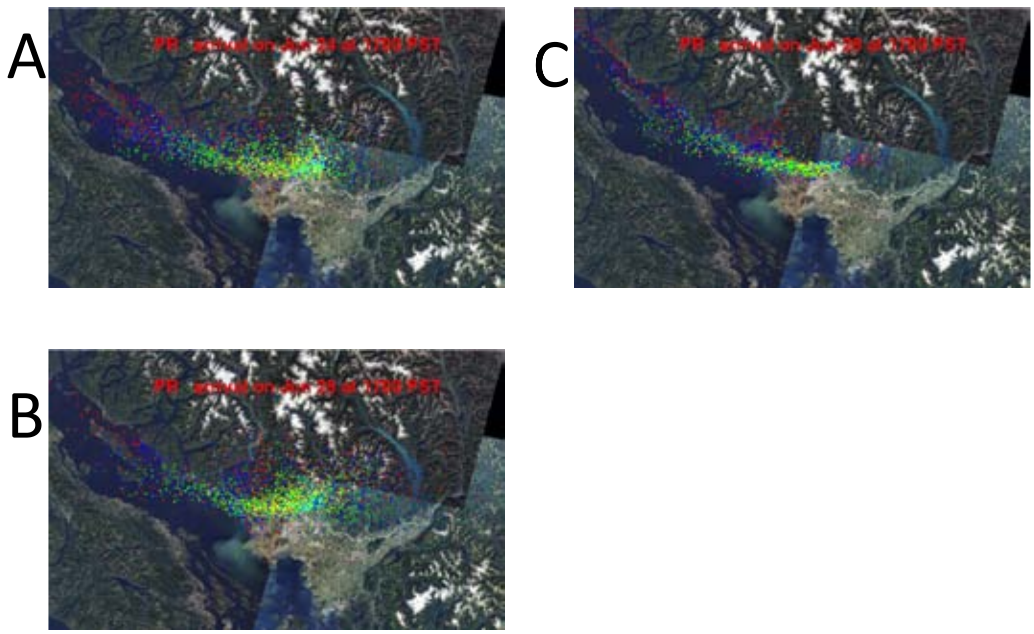

Fig. 101. HYSPLIT simulated backward particle releases from the entrance to the Pitt River valley for June 24th (A), June 25th (B) and June 26th 2006 (C).

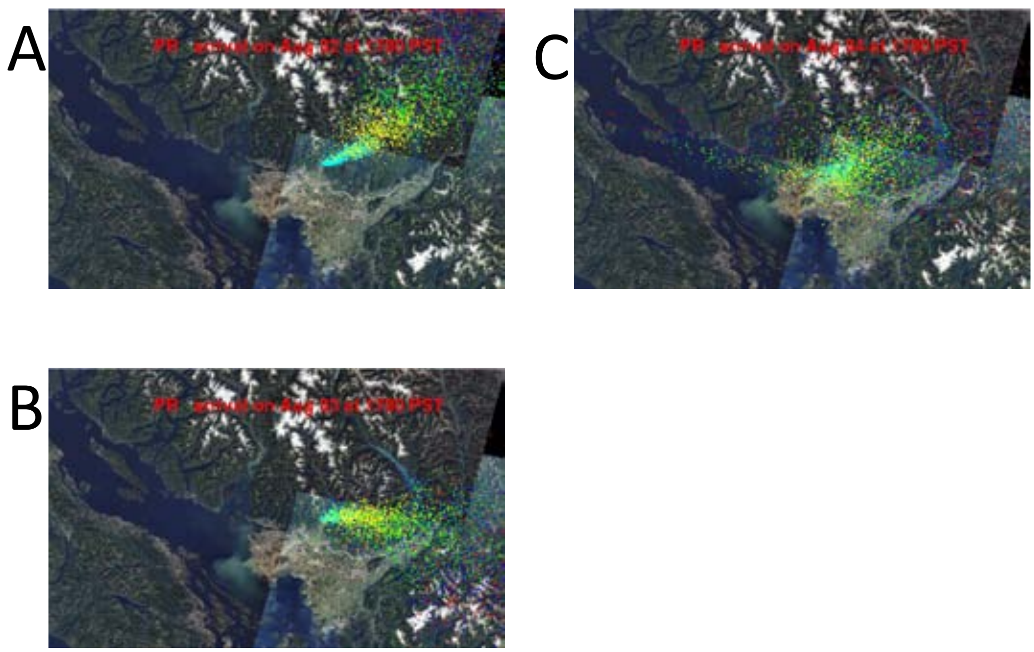

Fig. 102. HYSPLIT simulated backward particle releases from the entrance to the Pitt River valley for August 2nd (A), August 3rd (B) and August 4th 1993 (C).